NA62H-973

NORTH AMERICAN AVIATION, INC.

COLUMBUS DIVISION COLUMBUS 16, OHIO

ENGINEERING DEPARTMENT

A FEASIBILITY STUDY OF APPLIED LOAD RATIOS TO SIMULATE ELEVATED TEMPERATURE STATIC TESTS AT ROOM TEMPERATURE

Prepared Under Department of the Navy, Bureau of Naval Weapons
Contract NOw 61-0963-d

PREPARED BY R. W. Gehring
R. W. Gehring
Structural Analysis Group

R. L. Engle
R. L. Engle
Structures Laboratory

APPROVED BY C. W. Annis
C. W. Annis, Chief
Structural Mechanics & Computing

V. L. Beals
Director
Research and Development

No. of Pages 248

Date May 1963

ABSTRACT

This study was performed under Bureau of Naval Weapons Contract NOw 61-0963-d.

The primary objective of this study was to determine the feasibility of performing elevated temperature structural tests at room temperature by modifying the applied loads. Since this amounts to increasing the applied loads by some factor, the basis for defining this factor for a given cross-section and temperature environment could be questionable. A number of tests have been performed in this manner when moderate temperatures and temperature distributions were involved.

Therefore, it was the purpose of this study to investigate, both analytically and experimentally, some means whereby applied load ratios at room temperature could be used to satisfactorily verify strength and permanent set characteristics of the structure in any elevated temperature environment. The cross-section strain design procedures which provide the load-deformation curve of the cross-section seem to provide a rational means to establish the applied load ratios for a given structure for any temperature environment. The advantage of this type of procedure is that it allows for the following factors which must be allowed for in any simulation factor or applied load ratio.

1. Variation of material properties through the cross-section is allowed for, including the effects of previous complex temperature exposure histories.

2. The effects of thermal stresses on the load-deformation characteristics are included and the temperature-load sequence is considered.

3. Inelastic stress-strain relationships are allowed for by the Ramberg-Osgood stress-strain curve.

4. Creep effects can be allowed for by using an isochronous stress-strain curve represented by the Ramberg-Osgood equation.

5. The non-linear effects of element buckling are included.

6. Any combination of materials in the cross-section is allowed for.

Structural tests of bending, short column (crippling), long column, and thermal cycling (bending) specimens were performed under a number of non-uniform temperature distributions. Experimental load-deformation

curves were obtained and compared with calculated curves. Applied load ratios showed generally good agreement, with the calculated ratios being slightly conservative. Comparison is also made with some simple ratios which illustrates the strong influence of material properties and the over-emphasis which might be placed on the thermal stresses.

The strain design procedures shown provide not only a rational means to define the test applied load ratio for room temperature simulation, but the analytical means for structural analysis and design as well.

Acknowledgements

Dr. B. E. Gatewood, Consultant — For the original derivation and development of the strain design procedures and for helpful criticisms and suggestions during the performance of this study.

J. E. Wilson, Sr. Engineer, Structural Test Laboratory — For all temperature, strain, and deflection instrumentation, calibration of equipment, data correction and evaluation, and tabulation of all test data.

H. W. Brehm, Sr. Engineer, Structural Test Laboratory — For instrumentation and data evaluation.

TABLE OF CONTENTS

LIST OF FIGURES

LIST OF FIGURES (CONT'D)

LIST OF FIGURES (CONT'D)

LIST OF FIGURES (CONT'D)

LIST OF FIGURES (CONT'D)

LIST OF FIGURES (CONT'D)

LIST OF FIGURES (CONT'D)

LIST OF FIGURES (CONT'D)

SYMBOLS

α	=	coefficient of linear thermal expansion, in./in./^{o}F
ρ	=	radius of gyration, in.
A_n	=	area of element n, in.^{2}
b	=	distance from centroid of cross section to extreme fiber in x-direction, in.
b_n	=	width of plate element number n, in.
b_{n_e}	=	effective width of plate element, number n, in.
c	=	distance from centroid of cross section to extreme fiber in x-direction, in.
C_n	=	effective-area factor for buckling of element number n
Cl_x	=	deflection coefficient for beam column with compression applied load
e_{ap}	=	elastic applied-axial-load strain, in./in.
e_{crn}	=	critical compression buckling strain of element number n, in./in.
e_m	=	critical element strain, in./in.
e_n	=	strain associated with the stress at centroid of element number n, in./in.
e_{no}	=	shift of origin of stress-strain curve for element n, in./in.
e_p	=	nonlinear part of the axial strain, in./in.
e_{pn}	=	nonlinear part of the strain of element number n, in./in.

SYMBOLS (Con't.)

e_{ps} = permanent-set strain after load and temperature are removed, in./in.

e_T = elastic thermal axial strain, in./in.

e_{Tn} = elastic thermal strain on element number n, in./in.

E = modulus of elasticity, lbs./in.^{2}

E_n = modulus of elasticity for element number n, lbs./in.^{2}

F_{apn} = elastic applied stress on element number n, lbs./in.^{2}

F_n = stress on element number n, lbs./in.^{2}

F_{yn} = yield stress of element number n at temperature of element n, lbs./in.^{2}

I = moment of inertia, in.^{4}

K = compression buckling coefficient

K_{ax} = net bending moment strain, in./in.

K_{apx}, K_{apy} = elastic rotation angles produced by applied bending moments about coordinate axes x and y, in./in.

K_{ix} = moment strain term for initial deflection or eccentricity, in./in.

K_{px}, K_{py} = rotation angles produced by nonlinear effects about coordinate axes x and y, in./in.

K_{Tx}, K_{Ty} = elastic rotation angles produced by temperature distribution about coordinate axes x and y, in./in.

K_{wx} = deflection moment strain, in./in.

L = effective column length, in.

SYMBOLS (Con't.)

m	=	exponent for Ramberg-Osgood stress-strain curve depending upon material and temperature
M_{apx}	=	applied bending moment about the x-axis, in.-lbs.
M_{Tx}, M_{Ty}	=	temperature moments about coordinate axes x and y, in.-lbs.
M_x, M_y	=	bending moments about coordinate axes x and y, in.-lbs.
P	=	applied axial load, lbs.
T	=	temperature, ^oF
t_n	=	thickness of plate element number n, in.
w	=	deflection, in.
x_n	=	distance from centroid of cross section to centroid of element number n in x-direction, in.
x_{nR}	=	distance from y reference axis to centroid of element number n, in.
y_n	=	distance from centroid of cross section to centroid of element number n in y direction, in.
y_{nR}	=	distance from x reference axis to centroid of element number n, in.

Subscripts

ap	=	applied load or moment
j	=	step in temperature-load sequence
m	=	element with maximum strain
n	=	number of the element on the cross section
p	=	nonlinear effects (buckling, inelastic portion of stress-strain curve, change in elastic modulus due to temperature)

Subscripts (Con't.)

ps	=	permanent set after load and temperature removal
r	=	iteration step
T	=	thermal load or moment
x,y	=	about corresponding coordinate axes x and y
z	=	in the direction of the length of the column

REFERENCES

(a) Gatewood, B. E., Thermal Stresses, McGraw-Hill Book Co., Inc., New York, 1957

(b) Gatewood, B. E., The Problem of Strain Accumulation Under Thermal Cycling, Journal of the Aero/Space Sciences, Vol. 27, No. 6, June 1960

(c) Gatewood, B. E., and Gehring, R. W., Allowable Axial Loads and Bending Moments for Inelastic Structures Under Nonuniform Temperature Distribution, Journal of the Aero/Space Sciences, Vol. 29, No. 5, May 1962

(d) MIL-HDBK-5, Strength of Metal Aircraft Elements, March 1961

(e) Apodaca, D. R., Design Curves for Effects of Complex Thermal Exposures on Aluminum Alloys, General Materials Information - Phase III, Final Progress Report, Northrop Corporation (Norair) Report No. NOR62-17, Contract AF33(616)-8140, Project Nr: 1(8-7381), Task Nr: 73812, 15 February 1962

(f) Ramberg, W., and Osgood, W. R., Description of Stress-Strain Curves by Three Parameters, NACA T.N. 902, July 1943

(g) Hackman, L. E., Generalized Honeycomb Thermal Stress Study, North American Aviation, Inc. Report No. NA61H-755, Bureau of Naval Weapons Contract NOw 61-0355-d, November 1962

(h) Gatewood, B. E., and Gehring, R. W., Inelastic Redundant Analysis and Test Data Comparison for a Heated Ring Frame, Journal of the Aero/Space Sciences, Vol. 29, No. 3, March 1962

(i) Peery, D. J., Aircraft Structures, McGraw-Hill Book Co., Inc., New York, 1950

(j) Breitenbach, M. J., The Buckling and Ultimate Strength of Structural Shapes in Compression, Proceedings of the AEROSPACE FORUM I SESSION, Sherman M. Fairchild Fund Paper No. FF-30, Presented at the IAS 30th Annual Meeting, New York, N. Y., January 22-24, 1962

1.0 INTRODUCTION

The static test of aircraft and missile components has two specific functions; first, to determine load-deformation and permanent set characteristics, and second, to determine the ultimate load carrying capacity of a structural component. For aircraft and missiles operating essentially in a room temperature environment, the loads on the various components are applied by some external source and consequently may be duplicated satisfactorily in the structures laboratory. However, those vehicles operating in Mach No. - altitude regions where aerodynamic heating produces severe structural temperatures and non-uniform temperature distributions present an entirely different problem of static test. Considering that the critical flight conditions have been established using the Mach No. - altitude - load factor histories of the vehicle, the static tests must allow for the structural temperatures as well as the external applied loads. These structural temperatures produce material properties reduction on many of the major elements of a structural cross-section in addition to an internal load system produced by a non-uniform temperature distribution through the cross-section. The question then arises as to whether it is necessary to duplicate as closely as possible not only the applied loads but the temperature environment as well during static test of airframe components. An alternative, which has been used by some contractors, is to increase the applied loads by some specified amount to account for reduced material properties and thermal stresses and perform the static tests at room temperature. It is the purpose of this study to determine, in part, the feasibility of room temperature simulation and the validity of applied load ratios.

The duplication of the true applied loads and temperature environment for a static test condition on any component is extremely difficult and complex and requires consideration of three particularly critical items. The first two items are the additional time required to perform static tests in an elevated temperature environment and the increased expenses incurred by the increase in engineering man-hours and additional equipment required due to the elevated temperatures. The question also arises as to whether the exact load and temperature environment can be duplicated accurately enough to justify the additional time and expense. On large airplane or missile components the accurate duplication of load and temperature environment may be quite difficult to achieve for the following reasons. First, the temperature and load applications must be made either sequentially or simultaneously; in either case this necessitates the presence of heating and loading devices in the same area simultaneously. Even assuming that this can be accomplished satisfactorily,

the loading devices (pads, formers, etc.) represent local heat sinks of high heat capacity, making it virtually impossible to duplicate the structural temperature distributions as accurately as would be required. Since the data obtained from the test is of primary importance the complexity of the elevated temperature static test is expanded considerably by the amount, type, and doubtful accuracy of the instrumentation required in such a test. To determine the temperature distributions throughout the structure vast numbers of thermocouples would be required and this data must be monitored during the test as a constant check on the local temperatures and temperature distributions. Futhermore, strain measurements must be taken at many locations throughout the structure requiring the use of elevated temperature strain gages since the use of electro-mechanical extensometers presents installation and accessibility problems. The additional expense of elevated temperature strain gages in sufficient quantity may not be warranted when the accuracy of the data is questionable because of the inability to maintain desired temperature distributions. The present state-of-the-art requires specific installation techniques for elevated temperature strain gages. These techniques require temperature-time curing histories which not only add to complexity and test phase time, but may, in some cases with aluminum alloy, produce permanent losses of material properties which must be accounted for in the analysis of test data and results. Overall structural deflections would also present a serious problem when rods, wires and other equipment may be in close proximity to the heat lamps. In addition, the effects of thermal cycling could only be determined by the expensive, time-consuming procedure of sequentially heating and cooling the structure. This procedure requires that strain data be monitored in addition to temperature data to determine when, and if, elastic shakedown has occurred. Remote and/or automatic testing and data recording equipment is required due to the particularly hazardous nature of elevated temperature tests.

It is also doubtful if a single contractor would have the full capability of testing large components at elevated temperature for some time. The establishment and maintenance of complete elevated temperature testing facilities by each contractor must be absorbed in the cost of future vehicles and the duplication of complete facilities may be quite inefficient since some may remain idle for long periods.

Since some contractors have performed simulated elevated temperature tests at room temperature using additional factors on the applied loads, it is essential that the validity of these factors be determined. If room temperature simulation of elevated

temperature static tests is considered feasible, it is equally essential that the applied load ratios be established by some rational procedure which allows for material property variation and the presence of temperature induced loads (thermal stresses) for any structure in any temperature-load environment. The use of these applied load ratios must allow sufficiently accurate room temperature static tests to be performed to prove the structural integrity of an airfame in an elevated temperature environment.

2.0 OBJECTIVES

The primary objective of this study was to investigate the feasibility of simulating elevated temperature static tests at room temperature and the use of applied load ratio procedures presently being used. A secondary objective was to investigate some rational means of establishing applied load factors which would account for the various factors affecting both the elevated temperature and room temperature strength and deformation. It was also necessary to establish what additional problems might be encountered in performing the elevated temperature tests and evaluating data from those tests. With 7075-T6 aluminum alloy selected as the material for the test specimens the material properties variation became a significant factor as higher test temperatures and complex temperature exposure histories affected the recovery of the basic material properties. Therefore, an important secondary objective was to investigate the difficulties of data evaluation and theoretical analysis when severe temperature-time environments are present.

Since the majority of static test failures occur in compression members the study was restricted to bending and axial load where the failures would be precipitated by local instability. Furthermore, compression failures are affected to a greater degree by the presence of thermal stresses than a straight tension failure, particularly when local buckling is involved. The test specimens selected for the experimental portion of the program were built-up box specimens using plate element b/t values within the range of present aircraft wing and empennage structures. Bending, crippling, and long column specimens were tested to obtain load-deformation data based on extreme fiber strain data, and overall foreshortening data in the case of the long columns.

It was also questionable whether the effects of strain accumulation produced by temperature cycling at high loads could be adequately represented by a single static test at room temperature. This type of environment is generally representative of pressurized fuselages at high Mach numbers.

Essentially, then, the combined analytical-experimental program performed during this study was to investigate applied load ratio simulation at room temperature by considering the critical factors affecting the applied load ratio at any desired offset strain (permanent set), maximum desired strain, or at ultimate (failure). The major factors affecting the definition of any applied load ratio are:

1. Variation of material properties through the cross-section where the reduction of material properties on any structural element must, in some cases, allow for the effects of previous complex temperature exposure histories.

2. The effects of thermal stresses.

3. Inelastic stress-strain relationships.

4. Buckling.

5. Possible use of mixed materials.

The strain design procedures described in Section 3.0 allow for these factors and constitute the major analytical effort in this study. The significance in the use of strain design procedures, aside from allowing for inelastic effects, etc., lies in the fact that the elevated temperature and room temperature load-deformation curves are defined on a single, compatible basis.

Some simulation testing has been performed using applied load ratios based on material properties reduction at elevated temperature. For some of the more severe temperature environments producing significant thermal stresses some additional factors have been included in the applied load ratio to account for the elastic thermal stresses. Therefore, it was also the objective of this program to investigate the validity of these simplified ratios.

3.0 THEORETICAL ANALYSIS

For the assumption that a cross-section of a structural component remains plane at all times except near cut-outs or near the ends of a beam, the strain equations may be written for the structural elements in the cross-section for any combination of temperature and load or for any temperature-load sequence. These strains and the associated stresses obtained from the Ramberg-Osgood representation of the stress-strain curve for each element provide the data for constructing the load-deformation curve of the entire cross-section. The procedures shown include temperature variation through the cross-section, mixed materials, material property variation, local instability, column instability (including any local instability effects), and inelastic stress-strain relationships. The load-deformation curves of Section 4.0 which are constructed for the entire cross-section reflect the presence of the aforementioned effects on each element in the cross-section. The following procedure is basically that shown in References (a) and (c) with minor modifications.

3.1 STRAIN EQUATIONS

The strain of any element in the cross-section consists of the sum of the elastic thermal strain, the elastic applied axial load and bending moment strains, and a correcting linear strain term to account for all inelastic effects as shown in Eq. (3.1.1).

$$\left.\begin{aligned} e_n &= e_{T_n} + \frac{F_{ap_n}}{E_n} + e_{p_n} \\ \text{where,} \quad \frac{F_{ap_n}}{E_n} &= e_{ap} + K_{ap_x}\frac{y_n}{c} + K_{ap_y}\frac{x_n}{b} \\ \text{and,} \quad e_{p_n} &= e_p + K_{p_x}\frac{y_n}{c} + K_{ap_y}\frac{x_n}{b} \end{aligned}\right\} \quad (3.1.1)$$

e_{T_n} is the elastic thermal strain, F_{ap_n}/E_n is the elastic applied axial load and bending moment strain, and e_{p_n} is the correcting term for all inelastic effects. e_{ap} is an elastic applied axial load strain and K_{ap_x} and K_{ap_y} are elastic applied bending moment strains about orthogonal axes x and y, respectively. e_p, K_{px}, and K_{p_y} are the correcting axial and bending strains for inelastic effects. x_n and y_n are distances from the elastic centroid of the cross-section to the centroid of element n, and b and c are the maximum values of x and y, respectively.

The elastic thermal strain in Eq. (3.1.1) is

$$\left.\begin{aligned} e_{T_n} &= -(\alpha T)_n + e_T + K_{T_x}\frac{y_n}{c} + K_{T_y}\frac{x_n}{b} \\ \text{where,} \\ e_T &= \frac{\sum E_n (\alpha T)_n A_n}{\sum E_n A_n} \\ K_{T_x} &= c\left[\frac{M_{T_x}(EI_y) - M_{T_y}(EI_{xy})}{(EI_x)(EI_y) - (EI_{xy})^2}\right] \\ K_{T_y} &= b\left[\frac{M_{T_y}(EI_x) - M_{T_x}(EI_{xy})}{(EI_x)(EI_y) - (EI_{xy})^2}\right] \end{aligned}\right\} \quad (3.1.2)$$

In Eq. (3.1.2) the thermal moments and the elastic bending stiffness parameters are

$$\left.\begin{aligned} M_{T_x} &= \sum E_n (\alpha T)_n A_n y_n \quad , \quad M_{T_y} = \sum E_n (\alpha T)_n A_n x_n \\ (EI_x) &= \sum E_n A_n y_n^2 \quad , \quad (EI_y) = \sum E_n A_n x_n^2 \\ (EI_{xy}) &= \sum E_n A_n x_n y_n \end{aligned}\right\} (3.1.3)$$

The values of x_n and y_n are calculated from reference axes x_R and y_R by

$$x_n = x_{n_R} - \frac{\sum E_n A_n x_{n_R}}{\sum E_n A_n} \quad , \quad y_n = y_{n_R} - \frac{\sum E_n A_n y_{n_R}}{\sum E_n A_n} \qquad (3.1.4)$$

The axial load and bending moment strains in Eq. (3.1.1) can be obtained from the applied load P and the applied bending moments M_x and M_y by

$$\left.\begin{aligned} e_{ap} &= \frac{P}{E_n A_n} \\ K_{ap_x} &= c\left[\frac{M_x(EI_y) - M_y(EI_{xy})}{(EI_x)(EI_y) - (EI_{xy})^2}\right] \\ K_{ap_y} &= b\left[\frac{M_y(EI_x) - M_x(EI_{xy})}{(EI_x)(EI_y) - (EI_{xy})^2}\right] \end{aligned}\right\} \qquad (3.1.5)$$

The values of the inelastic correcting strains e_p, K_{p_x}, and K_{p_y} must be determined by the iteration procedures of Sec. 3.6 to satisfy the conditions of axial load and bending moment equilibrium on the cross-section with the stresses obtained from Sec. 3.3.

3.2 SEQUENCE LOADING

The general element strain equation of Sec. 3.1 is directly applicable only to the very specific case of simultaneous application of temperature and load and does not allow for any previous temperature - load history. Eq. (3.1.1) can be written in terms of any previous step j-1 in the temperature-load sequence and the load or temperature application or removal at step j as

$$\begin{aligned} e_{n_j} &= \frac{F_n}{E_n} - (\alpha T)_{n_j} + (e_T + e_{ap} + e_p)_j + (K_{T_x} + K_{ap_x} + K_{p_x})_j \frac{x_n}{c} \\ &\quad + (K_{T_y} + K_{ap_y} + K_{p_y})_j \frac{x_n}{b} \\ &= \left(\frac{F_n}{E_n}\right)_{j-1} + \Delta e_{n_j} \end{aligned} \qquad (3.2.1)$$

In Eq. (3.2.1) the term $\left(\frac{F_n}{E_n}\right)_{j-1}$ is the elastic strain from the previous step assuming that the strain e_{n_j} starts from a new origin. Δe_{n_j} is the incremental strain for a temperature or load application or removal step. The values of Δe_{n_j} for temperature and load application and removal steps are shown in Eq. (3.2.2).

APPLY TEMPERATURE (+T)

$$\Delta e_{n_j} = -(\alpha T)_{n_j} + (e_T+e_p)_j + (K_{T_x}+K_{p_x})_j \frac{y_n}{c} + (K_{T_y}+K_{p_y})_j \frac{x_n}{b}$$

APPLY LOAD (+P)

$$\Delta e_{n_j} = (e_{ap} + e_p)_j + (K_{ap_x}+K_{p_x})_j \frac{y_n}{c} + (K_{ap_y}+K_{p_y})_j \frac{x_n}{b} \qquad (3.2.2)$$

REMOVE LOAD (-P)

$$\Delta e_{n_j} = (-e_{ap}+e_p)_j + (-K_{ap_x}+K_{p_x})_j \frac{y_n}{c} + (-K_{ap_y} + K_{p_y})_j \frac{x_n}{B}$$

REMOVE TEMPERATURE (-T)

$$\Delta e_{n_j} = (\alpha T)_{n_j} + (-e_T+e_p)_j + (-K_{T_x}+K_{p_x})_j \frac{y_n}{c} + (-K_{T_y}+K_{p_y})_j \frac{x_n}{b}$$

3.3 STRESS EQUATIONS

In order to obtain the element stresses from the element strains calculated by Eq. (3.2.1) for a particular load or temperature step, the non-dimensional Ramberg-Osgood equation is used. The general form from References (a) and (f) is

$$\frac{E_n e_n}{F_{y_n}} = \frac{F_n}{F_{y_n}}\left[1 + \frac{3}{7}\left(\frac{F_n}{F_{y_n}}\right)^{m-1}\right] \qquad (3.3.1)$$

The strain e_{n_j} associated with the stress is completely defined by Eq. (3.2.1) except for the case where unloading from the original stress-strain curve has occurred and subsequent reloading returns the element to the old stress-strain curve. In this case, the strain associated with the stress is expressed as

$$(e_{n_j} + q_{n_j}) \text{ with } q_{n_j} = \sum_{i=k}^{j-1} e_{n_{oi}} \qquad (3.3.2)$$

where $e_{n_{oi}}$ is determined by

$$e_{n_o} = e_n - \frac{F_n}{E_n} \qquad (3.3.3)$$

and k is the step at which the last sign reversal of $e_{n_{oi}}$ occurred.
Eq. (3.3.3) is not included in the sum of Eq. (3.3.2) unless it satisfies the equation

$$e_{n_o} \geq 0.046\left(\frac{F_{y_n}}{E_n}\right) \tag{3.3.4}$$

which corresponds to a point on the stress-strain curve where

$$\frac{F_n}{F_{y_n}} \geq 0.80 \tag{3.3.5}$$

for the particular case with a Ramberg-Osgood exponent m=10. Eq. (3.3.5) is an arbitrarily selected point on the stress-strain curve which defines an effective elastic limit. A new stress-strain curve is assumed to arise whenever unloading occurs from a point on the stress-strain curve which satisfies Eq. (3.3.5).

To determine the element stresses at any step in the temperature-load sequence corresponding to the strains in Eq's. (3.2.1) and (3.3.2), Eq. (3.3.1) is modified to

$$\frac{E_{n_j}}{F_{y_{n_j}}}\left(e_{n_j}+q_{n_j}\right) = \frac{F_{n_j}}{F_{y_{n_j}}}\left[1 + \frac{3}{7}\, r_{n_j}\left(\frac{F_{n_j}}{F_{y_{n_j}}}\right)^{m-1}\right] \tag{3.3.6}$$

where

$$r_{n_j} = 0\ ,\ 1$$
$$q_{n_j} = 0\ ,\ \sum_{i=k}^{j-m} e_{n_{o_i}} \tag{3.3.7}$$

The values of r_{n_j} and q_{n_j} to be used at any temperature or load step depend upon the previous steps, the signs of Δe_{n_j} and e_{n_j} in Eq. (3.2.1), and the sum of all $e_{n_{oi}}$ values satisfying Eq. (3.3.4) and occurring after $e_{n_{oi}}$ reverses sign at step k. Step j-m in Eq. 3.3.7 is the last step at which $e_{n_{oi}}$ satisfies Eq. (3.3.4). The values of r_{n_j} and q_{n_j} to use in Eq. (3.3.6) are defined at any step in the temperature-load sequence by the logic table of Fig. 3.1.

FIGURE 3.1

LOGIC TABLE FOR DEFINITION OF ELEMENT STRESS - STRAIN CURVE

$r_{n_{j-1}}$	$\frac{F_{nj-1}}{E_{nj-1}}$	Δe_{n_j}	e_{n_j}	$s_{n_j} = e_{n_j} + \sum_{i=k}^{j-m} e_{no_i}$				$(e_{n_o})_{j-m}$ $\geqq .046 \left(\frac{F_{yn}}{E_n}\right)_{j-m}$	r_{n_j}	q_{n_j}
				$> s_{n_{j-m}}$	$= s_{n_{j-m}}$	$< s_{n_{j-m}}$	$\gtrless s_{n_{j-m}}$			
1	+	+	+				X	+,0	1	$\sum_{i=k}^{j-m} e_{no_i}$
0	+	+	+		X	X		+	0	0
0	+	+	+	X				+	1	$\sum_{i=k}^{j-m} e_{no_i}$
0	+	+	+				X	-,0	1	0
1	-	-	-				X	-,0	1	$\sum_{i=k}^{j-m} e_{no_i}$
0	-	-	-	X	X			-	0	0
0	-	-	-			X		-	1	$\sum_{i=k}^{j-m} e_{no_i}$
0	-	-	-				X	+,0	1	0
1,0	+	-	+				X	$\pm$,0	0	0
1,0	-	+	-				X	$\pm$,0	0	0
1,0	+	-	-				X	+,0	1	0
1,0	+	-	-	X	X			-	0	0
1,0	+	-	-			X		-	1	$\sum_{i=k}^{j-m} e_{no_i}$
1,0	-	+	+				X	-,0	1	0

FIGURE 3.1
LOGIC TABLE FOR DEFINITION OF ELEMENT STRESS - STRAIN CURVE

$r_{n_{j-1}}$	$\frac{Fnj-1}{Enj-1}$	Δe_{n_j}	e_{n_j}	$s_{n_j} = e_{n_j} + \sum_{i=k}^{j-m} e_{n_{o_i}}$				$(e_{n_o})_{j-m} \geq .046 \left(\frac{Fy_n}{E_n}\right)_{j-m}$	r_{n_j}	q_{n_j}
				$> s_{n_{j-m}}$	$= s_{n_{j-m}}$	$< s_{n_{j-m}}$	$\gtrless s_{n_{j-m}}$			
1,0	-	+	+		X	X		+	0	0
1,0	-	+	+	X				+	1	$\sum_{i=k}^{j-m} e_{n_{o_i}}$
1	+	+	+				X	-	1	0
1	-	-	-				X	+	1	0

3.4 SIGN CONVENTION

The use of the equations of Section 3.0 to define the load-deformation curves of Section 4.0 requires that certain definite sign conventions be established for compatibility in any temperature - load sequence. The following table outlines the required sign convention.

FIGURE 3.2

SIGN CONVENTION

Equation Term	Algebraic Sign
T	(+) if temperature increases from datum (-) if temperature decreases from datum
x_n , y_n	(+) dimension toward the extreme fiber element having the highest positive value of (αT). In the case of symmetrical temperature distribution and geometry any convenient sign convention may be selected if the applied moment values have consistent signs.
F_n , F_m	(+) tension (-) compression
c,b	(+)
e_{ap}	(+) tension (-) compression
K_{ap_x}	(+) if the applied bending moment M_x puts compression on elements having $-y_n$ values. (-) if the applied bending moment M_x puts compression on elements having $+y_n$ values.
K_{ap_y}	(+) if the applied bending moment M_y puts compression on elements having $-x_n$ values. (-) if the applied bending moment M_y puts compression on elements having $+x_n$ values.

Equation Term	Algebraic Sign
P	(+) tension (-) compression
M_x	(+) if moment produces compression on elements having $-y_n$ values. (-) if moment produces compression on elements having $+y_n$ values.
M_y	(+) if moment produces compression on elements having $-x_n$ values. (-) if moment produces compression on elements having $+x_n$ values.
e_n , e_m	(+) tension (-) compression
e_{cr} , e_{cr_n}	(-)

3.5 BUCKLING

For stable elements in the structure or for those elements with stresses below the local buckling stresses the stress-strain relationship is adequately defined by the non-dimensional Ramberg-Osgood stress-strain curve of Sec. 3.3. Since some elements may buckle at any step in the temperature-load sequence the stress and strain distribution on these elements changes due to the change in length of the buckled element from the deflection. Also, since some part of the buckled element (one or more edges) does not deflect, the strain in this undeflected portion is taken as the reference strain for the element. This reference strain is also the strain to be associated with the strains of the other elements in the structural cross-section.

The critical buckling strain of any element in the cross-section is:

$$e_{cr_n} = -K \left(\frac{t_n}{b_n}\right)^2 \qquad (3.5.1)$$

where the buckling coefficient K depends upon the edge conditions. For the usual effective-area case for compression, an effective width is defined as in Ref. (a) where

$$\frac{b_{n_e}}{b_n} = \left(\frac{e_{cr_n}}{e_n}\right)^{1/2} \qquad (3.5.2)$$

and b_{n_e} is the effective width of element n after the critical buckling strain has been reached. Since e_n is the strain associated with the stress except for unloading and subsequent reloading to the old stress-strain curve Eq. (3.5.2) must be modified to:

$$\frac{b_{n_e}}{b_n} = \left(\frac{e_{cr_n}}{e_{n_j} + q_{n_j}}\right)^{1/2} \qquad (3.5.3)$$

where the correcting strain q_{n_j} is defined at each step j in the temperature-load sequence by the methods and logic table of Sec. 3.3.

The effective area coefficients for elements subject to local instability are then defined at any temperature or load step and any iteration step by

$$C_n = 1, \ (e_{n_j} + q_{n_j}) \leq e_{cr_n}$$
$$C_n = \left(\frac{e_{cr_n}}{e_{n_j} + q_{n_j}}\right)^{1/2}, \ (e_{n_j} + q_{n_j}) > e_{cr_n} \qquad (3.5.4)$$

If q_{n_j} is always defined as $q_{n_j} = \sum_{i=k}^{j-m} e_{no_i}$ then the values of q_{n_j} shown in the effective area factors of Equation 3.5.4 are adequately defined. In the digital computer program which uses the logic table of Figure 3.1, q_{n_j} may be defined as either

$$q_{n_j} = \sum_{i=k}^{j-m} e_{no_i} \quad \text{or} \quad q_{n_j} = 0$$

depending upon whether the element strain is on an elastic line, a new stress-strain curve, or has returned to the original stress-strain. In any case the value of q_{n_j} in Equations 3.5.3 and 3.5.4 is always defined by

$$q_{n_j} = \sum_{i=k}^{j-m} e_{no_i}$$

3.6 ITERATION EQUATIONS

The first approximation of the element strains at any step in the temperature-load sequence is made by solving Equation 3.2.1 using the applicable Δe_{n_j} from Equation 3.2.2 with e_p, K_{p_x}, and K_{p_y} as zero. The stresses associated with these strains are calculated using the modified Ramberg-Osgood Equation 3.3.6 and the logic table of Figure 3.1 . The second approximations for the values of e_p, K_{p_x}, and K_{p_y} are given by the general iteration equations

$$\left.\begin{aligned} (e_{p_j})_r &= (e_{p_j})_{r-1} - (e_{ap_j})_{r-1} + e_{ap} \\ (K_{p_{x_j}})_r &= (K_{p_{x_j}})_{r-1} - (K_{ap_{x_j}})_{r-1} + K_{ap_x} \\ (K_{p_{y_j}})_r &= (K_{p_{y_j}})_{r-1} - (K_{ap_{y_j}})_{r-1} + K_{ap_y} \end{aligned}\right\} \quad (3.6.1)$$

where,

$$(e_{ap_j})_{r-1} = \frac{\sum (F_{n_j})_{r-1} A_n (C_{n_j})_{r-1}}{\sum E_n A_n}$$

$$(K_{ap_{x_j}})_{r-1} = -\left[\frac{\left[\sum(F_{n_j})_{r-1} A_n (C_{n_j})_{r-1} (\frac{x_n}{b})\right]\left[\sum E_n A_n (\frac{y_n}{c})(\frac{x_n}{b})\right]}{\left[\sum E_n A_n (\frac{y_n}{c})^2\right]\left[\sum E_n A_n (\frac{x_n}{b})^2\right] - \left[\sum E_n A_n (\frac{y_n}{c})(\frac{x_n}{b})\right]^2} - \frac{\left[\sum(F_{n_j})_{r-1} A_n (C_{n_j})_{r-1} (\frac{y_n}{c})\right]\left[\sum E_n A_n (\frac{x_n}{b})^2\right]}{\left[\sum E_n A_n (\frac{y_n}{c})^2\right]\left[\sum E_n A_n (\frac{x_n}{b})^2\right] - \left[\sum E_n A_n (\frac{y_n}{c})(\frac{x_n}{b})\right]^2}\right]$$

$$(K_{ap_{y_j}})_{r-1} = -\left[\frac{\left[\sum(F_{n_j})_{r-1} A_n (C_{n_j})_{r-1} (\frac{y_n}{c})\right]\left[\sum E_n A_n (\frac{y_n}{c})(\frac{x_n}{b})\right]}{\left[\sum E_n A_n (\frac{y_n}{c})^2\right]\left[\sum E_n A_n (\frac{x_n}{b})^2\right] - \left[\sum E_n A_n (\frac{y_n}{c})(\frac{x_n}{b})\right]^2} - \frac{\left[\sum(F_{n_j})_{r-1} A_n (C_{n_j})_{r-1} (\frac{x_n}{b})\right]\left[\sum E_n A_n (\frac{y_n}{c})^2\right]}{\left[\sum E_n A_n (\frac{y_n}{c})^2\right]\left[\sum E_n A_n (\frac{x_n}{b})^2\right] - \left[\sum E_n A_n (\frac{y_n}{c})(\frac{x_n}{b})\right]^2}\right] \quad (3.6.2)$$

For bending about one axis only, the internal bending moments at the r-1 iteration step are simplified to

$$(K_{ap_{x_j}})_{r-1} = \frac{\sum(F_{n_j})_{r-1} A_n (C_{n_j})_{r-1} (\frac{y_n}{c})}{\sum E_n A_n (\frac{y_n}{c})^2}$$

or,

$$(K_{ap_{y_j}})_{r-1} = \frac{\sum(F_{n_j})_{r-1} A_n (C_{n_j})_{r-1} (\frac{x_n}{b})}{\sum E_n A_n (\frac{x_n}{b})^2}$$

e_{ap}, K_{ap_x}, and K_{ap_y} in Equation 3.6.1 are defined by Equation 3.1.5.

New strains and stresses are obtained from Equations 3.2.1 and 3.3.6 using the successive approximations of Equation 3.6.1. The iteration is continued until $e_{p_j} = (e_{p_j})_r = (e_{p_j})_{r-1}$, $K_{p_{x_j}} = (K_{p_{x_j}})_r = (K_{p_{x_j}})_{r-1}$, and $K_{p_{y_j}} = (K_{p_{y_j}})_r = (K_{p_{y_j}})_{r-1}$ within a

specified tolerance. An acceptable tolerance range has been found to be $\pm$ 0.00003 in./in. to $\pm$ 0.00006 in./in. depending upon the type of problem where the smaller tolerance is required in strain accumulation problems such as thermal cycling. For most static (+T, +P, -P, -T) problems a realistic tolerance is $\pm$ 0.00005 in./in.

3.7 COLUMN PROCEDURES
Reference (g)

Columns may have an unsymmetrical temperature distribution through the cross-section or a secondary bending moment may be acting on the column producing deflections normal to the neutral plane of the column. An axial load acting on the column element will affect these deflections by producing a bending moment due to the deflections. If symmetrical bending only is considered, the net bending moment strain consists of two parts, one due to applied secondary bending moments and one due to deflection.

$$K_{a_x} = K_{ap_x} + K_{w_x} \tag{3.7.1}$$

The deflection moment strain may be described in terms of e_{ap} and the deflection W as follows:

$$K_{w_x} = \frac{W}{c}\, e_{ap}\, \frac{\sum E_M A_M}{\sum E_M A_M \left(\frac{y_M}{c}\right)^2} = \frac{W}{c}\, e_{ap}\, \left(\frac{c}{\rho}\right)^2 \tag{3.7.2}$$

where M is an element in the column cross-section. In many problems the applied secondary bending moment may be related to the applied axial load as

$$M_{ap_x} = p\, P_{ap} \tag{3.7.3}$$

In this case Equation (3.7.2) may also be written

$$\frac{K_{ax}}{e_{ap}} = \frac{W + P}{c}\, \left(\frac{c}{\rho}\right)^2 \tag{3.7.4}$$

If z is the variable along the length of the structure, then W depends on z and the end conditions, while p may depend on z if the applied moment is variable. For simple beams

$$\frac{d^2W}{dz^2} = \frac{M}{EI} = \frac{K_x}{c} \tag{3.7.5}$$

The net rotational strain of any cross-section through the column may be written

$$K_x = K_{i_x} + K_{w_x} + K_{ap_x} + K_{T_x} + K_{p_x} + \sum_{j=1}^{j-1} K_{px_j} \qquad (3.7.6)$$

for the temperature-load sequence +T, +P where K_i represents the initial deflection or eccentricity of the load. In Equation (3.7.6) K_{p_x} is a function of z depending upon the amount of inelastic action of the various cross-sections throughout the span or length of the column. Equation (3.7.5) can be written

$$\frac{d^2K_{w_x}}{dz^2} = \left(\frac{e_{ap}}{\rho^2}\right) K_x \qquad (3.7.7)$$

where, with K as a table of values for selected values of z, then K_{w_x} can be obtained from Equation (3.7.7) by an area-moment numerical integration or by a double summation.

If K_{ap_x}, K_{T_x} and K_{i_x} are constant along the beam, then K_{p_x} will be constant except for the effect of W. Assume K_{p_x} is constant along the span so that Equation (3.7.7) can be integrated to give

$$\left.\begin{aligned} K_{w_x} &= (K_{i_x} + K_{ap_x} + K_{T_x} + \textstyle\sum K_{p_{x_j}} + K_{p_x}) f(z) \\ f(z) &= \frac{\cos q\,(1 - \frac{2z}{L}) - \cos q}{\cos q} \quad \text{(compression)} \\ &= \frac{\cosh q\,(1 - \frac{2z}{L}) - \cosh q}{\cosh q} \quad \text{(tension)} \end{aligned}\right\} \qquad (3.7.8)$$

where

$$q^2 = -\frac{e_{ap} L^2}{4\rho^2} \qquad (3.7.9)$$

For a simply supported beam-column

$$\text{let} \quad e_{cr} = -\frac{\pi^2 \rho^2}{L^2}, \quad q^2 = \frac{\pi^2}{4}\left(\frac{e_{ap}}{e_{cr}}\right) \tag{3.7.10}$$

so that the maximum deflection in Equation (3.7.8) at $z = \frac{L}{2}$ is

$$(K_{w_x})_{max.} = \left(K_{i_x} + K_{ap_x} + K_{T_x} + \sum_{j=1}^{j-1} K_{p_{x_j}} + K_{p_x}\right) f_{max.}\left(\frac{e_{ap}}{e_{cr}}\right) \tag{3.7.11}$$

Equation (3.7.6) may be written

$$K_x = \left[1 + f_{max.}\left(\frac{e_{ap}}{e_{cr}}\right)\right]\left(K_{i_x} + K_{ap_x} + K_{T_x} + \sum_{j=1}^{j-1} K_{p_x} + K_{p_x}\right) \tag{3.7.12}$$

The temperature-load sequence of primary importance for defining the column load-deformation curve is apply temperature (+T), then apply load (+P). For any given temperature distribution through the column cross-section a range of loads is applied to establish the shape and the peak of the column load-deformation curve.

The strain equation for the temperature application step for the column is essentially that shown by Equations (3.2.1) and (3.2.2). For the applied load step in the temperature-load sequence +T, +P the element strains are found by the following equation

$$e_{M_j} = \frac{F_{M_{j-1}}}{E_{M_{j-1}}} + (e_{ap} + e_p)_j + (K_{ap_x} + K_{w_x} + K_{p_x})_j \frac{y_M}{c} \tag{3.7.13}$$

where

$$K_{w_{x_j}} = (K_{i_{m_j}} + (K_{T_x})_{j-1} + K_{ap_{x_j}} + K_{p_{x_j}} + \sum_{j=1}^{j-1} K_{p_{x_j}})\ C_{l_x}$$

and

$$C_{l_x} = \frac{1 - \cos \pi/2 \left(\frac{e_{ap}}{e_{cr}}\right)}{\cos \pi/2 \ (e_{ap}/e_{cr})}$$

when a compression load is acting.

e_{p_j} and K_{px_j} must be determined by an iterative procedure to satisfy the following equilibrium conditions.

$$\left.\begin{aligned} e_{ap_j} &= \frac{\sum F_{M_j} A_M}{\sum E_M A_M} \\ (K_{apx_j} + K_{w_{x_j}}) &= \frac{\sum\limits_M F_{M_j} A_M \left(\frac{y_M}{c}\right)}{\sum\limits_M E_M A_M \left(\frac{y_M}{c}\right)^2} \end{aligned}\right\} \quad (3.7.14)$$

In Equation (3.7.12) the stresses F_{M_j} are determined by the procedures of Section 3.3. The iteration equations for the equilibrium condition are:

$$\left.\begin{aligned} (e_{p_j}) &= (e_{p_j})_{r-1} + e_{ap_j} - \frac{\sum (F_{M_j})_{r-1} A_M \ (C_{M_j})_{r-1}}{\sum E_M A_M} \\ (K_{px_j})_r &= (K_{px_j})_{r-1} \pm \left[K_{ap_{x_j}} + (K_{wx_j})_{r-1} \right. \\ &\qquad \left. - \frac{\sum\limits_M (F_{M_j})_{r-1} A_M \ (C_{M_j})_{r-1} \ (\frac{y_M}{c})}{\sum\limits_M E_M A_M \ (\frac{y_M}{c})^2} \right] \end{aligned}\right\} \quad (3.7.15)$$

Two sets of answers are provided at convergence of the iteration equations (3.7.15) with the second set defining a post-buckling point on the column load-deformation curve.

The column procedures presented in this section are based on constant moments and a maximum value of K_{wxj}. Further column studies have shown this approximation to be quite accurate for practical design use. Comparisons of column load-deformation curves using the approximate procedures of this section and by integrating the inelastic effects along the length of the column show good correlation between the two methods with the approximate procedures being slightly conservative.

3.8 ELEMENT FAILURE CRITERIA

Since the Ramberg-Osgood equation representing the element stress-strain curve is a continually rising function, stresses could be calculated which are beyond the tensile ultimate strength of the material. Therefore, it is necessary to provide an upper limit stress cut-off when using the Ramberg-Osgood equation. This cut-off would be either the tensile ultimate strength (F_{tu}) or the compressive yield strength (F_{cy}) depending upon the loading and geometry of the structure. Generally, for tension elements and those compression elements not affected by local instability even at high strains the stress cut-off may be taken as F_{tu}. For those compression elements subject to local instability (typical of most airframe compression structures) the stress cut-off is more realistically taken as F_{cy}. In either case, however, an element reaching this stress cut-off does not necessarily indicate failure of the cross-section since the element strain can still increase with the increase in load being carried by lower stressed elements in the cross-section. Essentially, then, a single critically loaded element reaching a stress cut-off on the stress-strain curve may have little relationship to the load-carrying capacity of the cross-section. Although the element strains are allowed to increase beyond the point of stress cut-off the stresses used in the equilibrium iteration equations of Section 3.6 are the cut-off stresses.

Coupled with the element stress cut-off to define failure of the entire cross-section is the value of element strain at any step in the temperature-load sequence. A more realistic criterion for defining element failure compatible with the failing load of the entire cross-section is a given strain which is generally the tensile elongation of the material. For most test comparisons and studies made to date, favorable agreement on load carrying capacity has been obtained using the tensile elongation strain cut-off on <u>all</u> tension and compression elements.

In addition to the necessary failure criteria the strain accumulation or thermal cycling problem may reach an elastic shakedown state where no further strain

accumulation occurs and the strain cut-off may never be reached by any element in the cross-section. Therefore, some criterion is necessary to define when, and if, elastic shakedown has occurred. For thermal cycling the criterion for elastic shakedown is defined by each element in the cross-section satisfying the equation

$$\left.\begin{aligned} &\sum_{i=j-4}^{i=j} e_{no_i} = 0 \\ &\text{where} \\ &e_{no_i} = 0, \text{ if } e_{no_i} \leq 0.046 \left(\frac{F_{y_n}}{E_n}\right) \end{aligned}\right\} \quad (3.8.1)$$

3.9 IBM PROGRAM

The allowable loads and load-deformation curves presented in this study were determined by the use of the IBM 709 digital computer. The IBM program used was identical to that described in Appendix C of Reference (g) which includes a complete FORTRAN listing and block diagram of the program.

4.0 LOAD-DEFORMATION CURVES

In order to obtain the applied load ratios it is first necessary to obtain the load-deformation curves for the structural cross-section in the design temperature environment and a room temperature environment. For a static test two temperature-load sequences will be of particular importance. These are +T, +P for data comparison with temperature and load acting on the structure and for defining the ultimate load; and, +T, +P, -P, -T for any comparison involving permanent set characteristics such as the applied load ratios for defining yield load. This temperature-load sequence may, in some cases, be quite different where the sequence is defined by the particular critical design condition.

The solution of the equations of Sections 3.1 through 3.6 or Section 3.7 gives the strains and stresses on each element of the cross-section at each step of the temperature-load sequence, and also gives the values of the inelastic strains e_{p_j}, $K_{p_{x_j}}$, and $K_{p_{y_j}}$ for each step in the sequence. After a finite number of steps the net inelastic effect on any element n is given by

$$e_{p_{s_n}} = \sum_j e_{p_j} + \left(\sum_j K_{p_{x_j}}\right) \frac{y_n}{c} + \left(\sum_j K_{p_{y_j}}\right) \frac{x_n}{b} \qquad (4.0.1)$$

The inelastic strain represented by $e_{p_{s_n}}$ represents the net inelastic effect with reference to the origin of the original stress-strain curve for element n. $\sum e_{p_j}$ represents the inelastic axial strain while $\sum K_{p_{x_j}}$ and $\sum K_{p_{y_j}}$ represent the inelastic rotation of the cross-section. If the inelastic strain represented by $e_{p_{s_n}}$ is calculated after temperature and load are applied and then removed (+T, +P, -P, -T) then $e_{p_{s_n}}$ represents the permanent set strain on the element.

The calculations are performed for a particular cross-section, material or material combinations, temperature distribution and temperature-load cycle for a range of values of the applied loads and/or moments. The load-deformation curves for the cross-section are then constructed where the ordinate may be in terms of an elastic applied stress defined by

$$F_{ap_m} = \left[e_{ap} + K_{ap_x}\left(\frac{y_m}{c}\right) + K_{ap_y}\left(\frac{x_m}{b}\right) \right] E_m \qquad (4.0.2)$$

or, the ordinate may be taken as the applied load or moment (P or M) in the case of applied loads for structural testing. The critical element strain on the abscissa is defined by $F_{ap_m}/E_m + e_{ps_m}$ where the subscript m denotes the element with the maximum inelastic or permanent set strain. This curve is equivalent to an applied stress-strain curve for the critical element m and includes temperature effects on material properties, thermal stresses, and inelastic effects on the entire cross-section.

The load-deformation curves represent the load-carrying capacity of the entire cross-section and not that of the highest stressed element. Although the allowable stress for the highest stressed element may have little relationship to the actual load-carrying capacity of the structure, the element with the largest inelastic or permanent set strain is important to determine the shape of the load-deformation curve.

For long columns (or beam-columns) the foreshortening strain on the abscissa is $e_{ap} + e_p + \frac{\Delta L}{L}$ where $\frac{\Delta L}{L}$ is the foreshortening due to bending deflection and is defined by

$$\frac{\Delta L}{L} = -\frac{\pi^2 W_m^2}{4 L^2} \qquad (4.0.3)$$

In Eq. 4.0.2 the maximum deflection W_m is defined by

$$\left.\begin{aligned} W_m &= \frac{\rho^2 K}{c\, e_{ap}}\left[\frac{\cos q\,(1 - \frac{2z}{L}) - \cos q}{\cos q}\right], \text{ compression} \\ &= \frac{\rho^2 K}{c\, e_{ap}}\left[\frac{\cosh q\,(1 - \frac{2z}{L}) - \cosh q}{\cosh q}\right], \text{ tension} \end{aligned}\right\} \qquad (4.0.4)$$

where,

$$q^2 = \frac{-e_{ap} L^2}{4\rho^2} = \frac{\pi^2}{4}\left(\frac{e_{ap}}{e_{cr}}\right), \quad e_{cr} = -\frac{\pi^2 \rho^2}{L^2} \qquad (4.0.5)$$

In Eq. 4.0.4 the general rotational strain term is

$$K = K_{i_m} + K_{T_x} + K_{ap_x} + \sum_j K_{p_{x_j}} \qquad (4.0.6)$$

The calculated and experimental load-deformation curves for the specimens tested during this study are explained and plotted in Sec. 8.0.

5.0 TEST PROGRAMS

The purpose of the test program was to test three typical aircraft components under a variety of time-temperature histories in order to obtain as many data points as possible to use in the development and refinement of the mathematical analysis of these same components.

5.1 TEST SPECIMENS

A total of twenty-eight specimens were tested in this program, consisting of sixteen bending beams, six short columns and six long columns. Part of the specimens were assembled with close tolerance bolts and the remainder with high shear rivets in order to ascertain if the type of fastener would make any detectable difference in the test results. Sketches of each type of specimen are shown in Figures 5.1, 5.2 and 5.3.

5.1.1 SPECIMEN IDENTIFICATION

Each specimen was identified according to the following code:

A-1 through A-6 were short columns
B-1 through B-17 were bending beams
C-1 through C-6 were long columns

In addition, each cover plate and channel of each specimen was identified as to which sheet of material it was from and the location on that sheet. This was for correlating material properties of each specimen with tensile coupons taken from each sheet of material.

5.1.2 FASTENERS

Three short columns, eight bending beams and all long columns were assembled with NAS464-4-6 high strength close tolerance bolts, NAS679A4 self-locking high temperature nuts and ZW17-416 washers as required.

The remainder of the specimens were assembled with high shear rivets consisting of HS52P-8-9 pins, HS32-8 collars and ZW17-416 washers.

5.1.3 SPECIMEN FABRICATION

After detail parts were formed for each specimen, the assemblies were clamped together and pilot drilled. Each hole was then brought up in steps to the correct size, with reaming the hole to the correct tolerance being the final step.

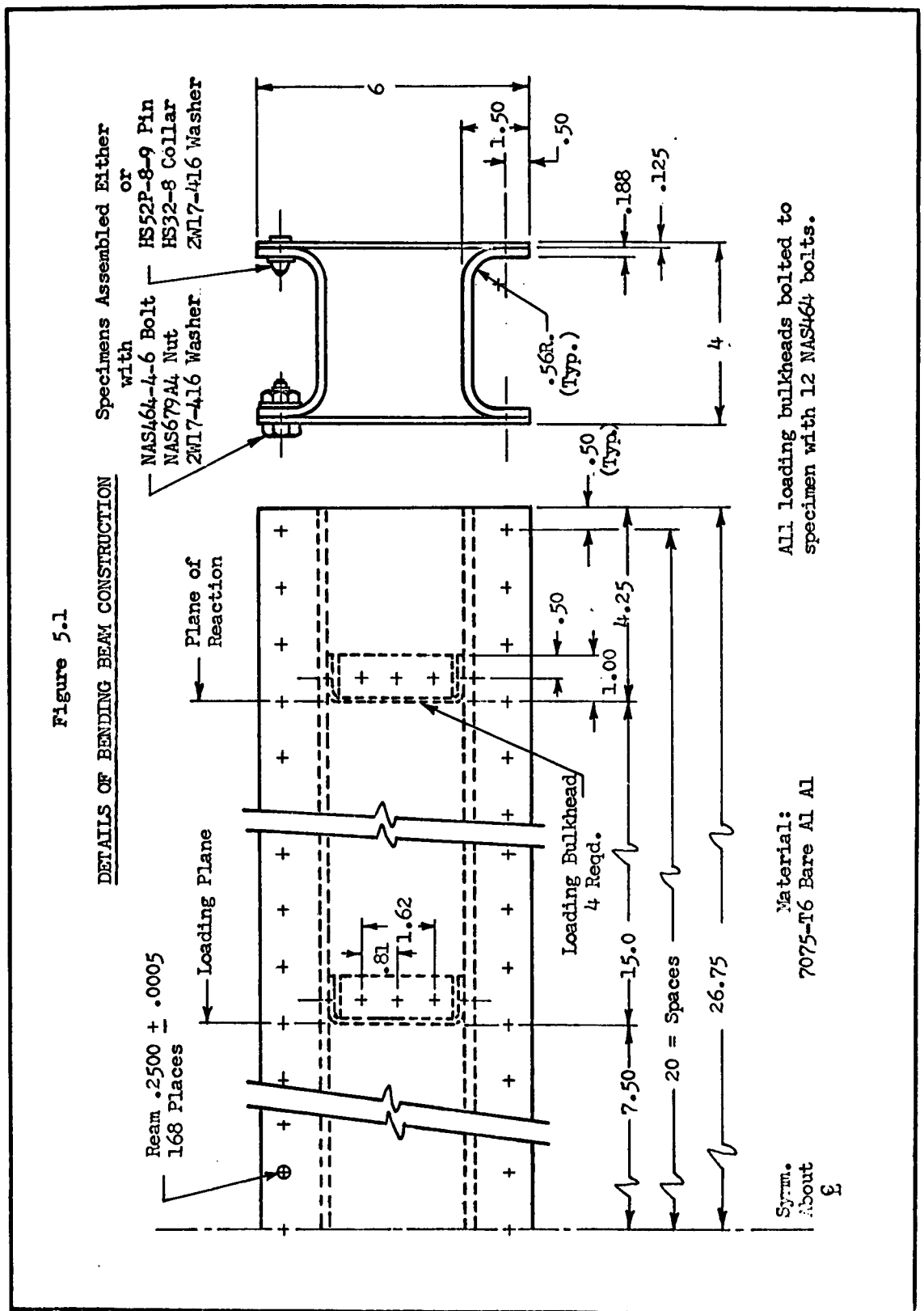

Figure 5.1

DETAILS OF BENDING BEAM CONSTRUCTION

H-18-G-1

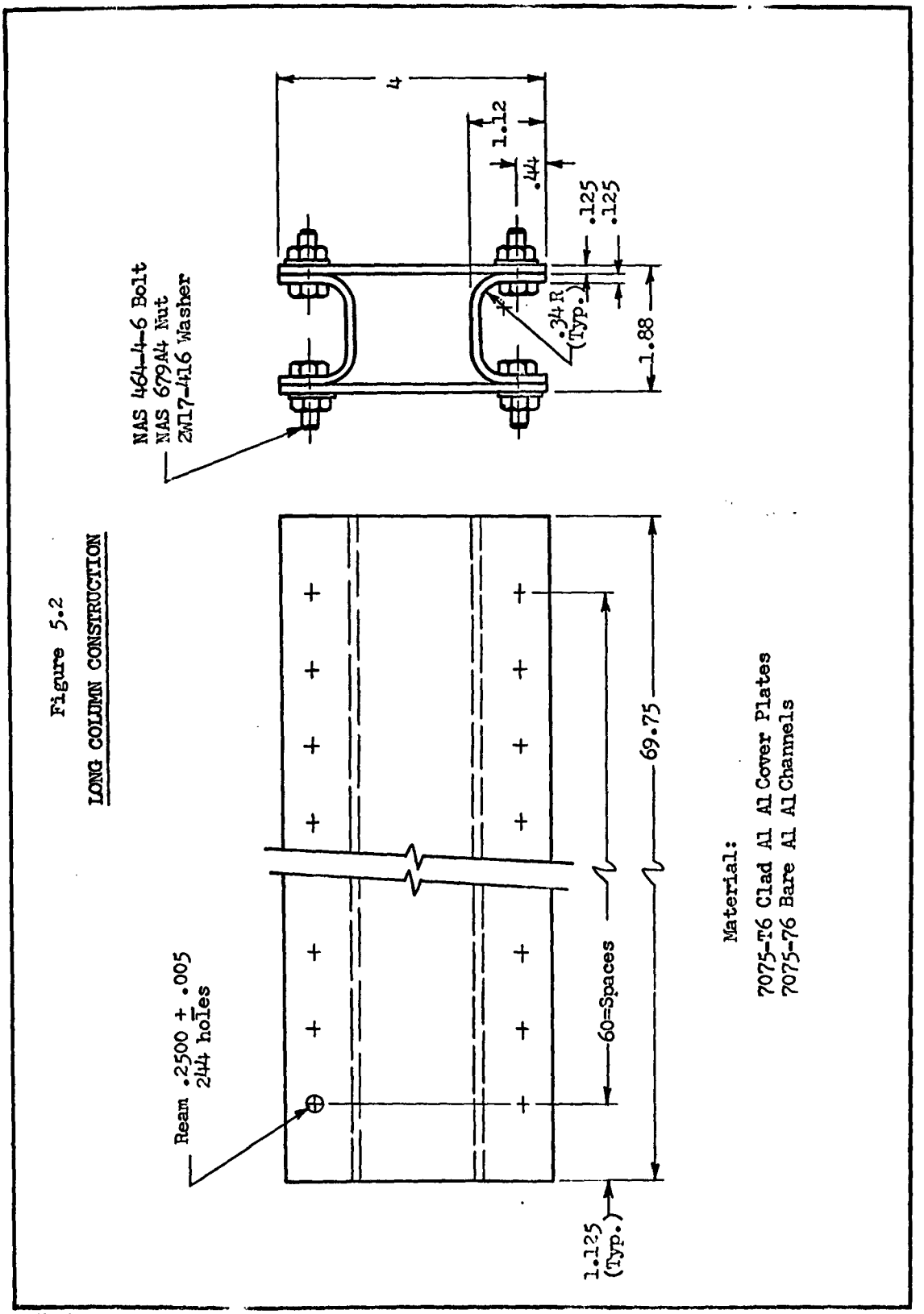

Figure 5.2

LONG COLUMN CONSTRUCTION

H-18-G-1

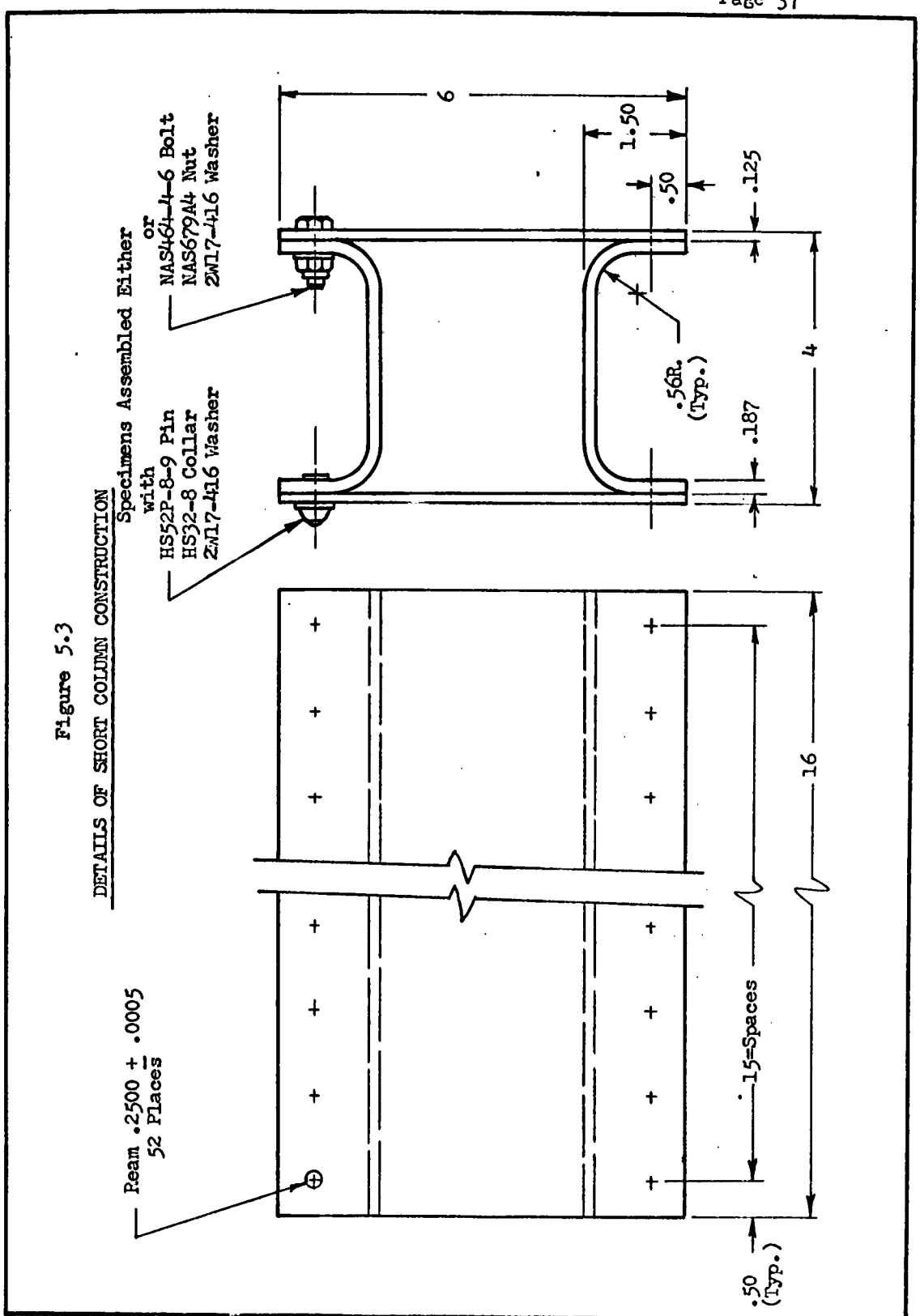

Figure 5.3

DETAILS OF SHORT COLUMN CONSTRUCTION

H-18-G-1

The fasteners were inserted in the holes and the parts drawn together tightly by either torquing the bolts to eighty inch-pounds or driving the rivets, depending upon the type of fasteners used in the specimen.

5.2 INSTRUMENTATION

5.2.1 EXTENSOMETER

An attempt was made to buy some type of transducer which would read post yield strains both at ambient temperature and elevated temperatures. No commercial device was found to do this. After considering several mechanical-type devices to read strains it was decided to fabricate bent-type extensometers incorporating four temperature compensated foil strain gages arranged in a Wheatstone bridge configuration sensitive to bending strains. These instruments were used on all specimens tested. Figure 5.4 shows the details of the extensometer.

5.2.1.1 EXTENSOMETER CALIBRATION

The extensometers were calibrated using fixture shown in Figure B.1. The dial indicator was used to set predetermined deflections in the extensometer and this deflection was checked by the Starrett dial indicator. The output from the Wheatstone bridge on the extensometer for all deflections set in the extensometer was read by a Baldwin-Lima-Hamilton a-c powered Model N portable strain recorder. A plot of this calibration is shown in Figure 5.5.

5.2.1.2 CHECKS OF EXTENSOMETER MEASUREMENTS

Three checks were made of extensometer measurements at elevated temperatures. The first consisted of fastening the extensometer to a quartz rod, inserting the assembly in an oven, and reading the output of the extensometer at various temperatures up to 400°F. The extensometer showed negligible output at this temperature range. Since the theoretical linear coefficient of linear expansion of quartz is $.277 \times 10^{-6}$ $\frac{\text{inches}}{\text{inch } ^\circ\text{F}}$ and the gage length of the extensometer is 1.00 inches, the theoretical output of the extensometer would be $\frac{(400 - 80) \times .28 \times 10^{-6}}{13.457} = 6.6$ microinches, and this can be considered negligible.

The second check consisted of fastening the extensometer to a short bar of 2024 aluminum alloy and inserting the assembly in an oven. In this manner the coefficient of expansion of the 2024 aluminum alloy bar could be measured directly since the gage length of the extensometer is 1.00 inches. The results of these measurements are shown in Figure 5.6.

The third check consisted of using a high elongation strain gage of Tatnall Type HE-181-E fastened to a standard tension specimen with C-2 cement. The extensometer was also fastened to the tension specimen and the entire assembly loaded in tension. The results of this check are shown in Figure 5.7.

The results of these checks were felt to be of sufficient accuracy to warrant their use in the test program.

5.2.2. STRAIN GAGES

5.2.2.1 HIGH TEMPERATURE GAGES

The Tatnall Measuring Systems Type C-12-142B strain gage employed in these tests are self temperature compensating "advance" metal film strain gages. The term "self temperature compensated" refers to a strain gage intended for use on material having a certain therral coefficient of expansion. The temperature coefficient of resistance of the gage alloy and the thermal coefficient of expansion of the mounting surface combine so as to produce a minimum resistance change in the strain gage output with changing temperature. This results in a very low value of apparent strain or temperature induced strain. Practical considerations limit this particular strain gage to 500°F for short term static testing.

In addition to self temperature compensation the amount of apparent strain is also minimized through consideration of bridge configurations, lead wire hook up, and type of read out instrumentation.

The manufacturer of these gages packages, along with the strain gage, a curve of apparent strain versus temperature. Prior laboratory tests have served to verify this information.

Gage Installation procedures are those recommended by the manufacturer utilizing TMS Type GA 50 epoxy cement with a curing cycle of two hours at 350°F followed by one half hour at 450°F.

5.2.2.2 HIGH ELONGATION GAGES

The Tatnall Measuring Systems Type HE-181-E high elongation strain gages employed in these tests are considered to be a relatively new item entering the strain gage field. Their use is primarily advantageous for post yield work. No particular temperature compensation is attempted and due to the nature of transferring post yield strains from the material to the gage, an Armstrong C-2, an unfilled resin cement with 2 hours at 200°F cure was used.

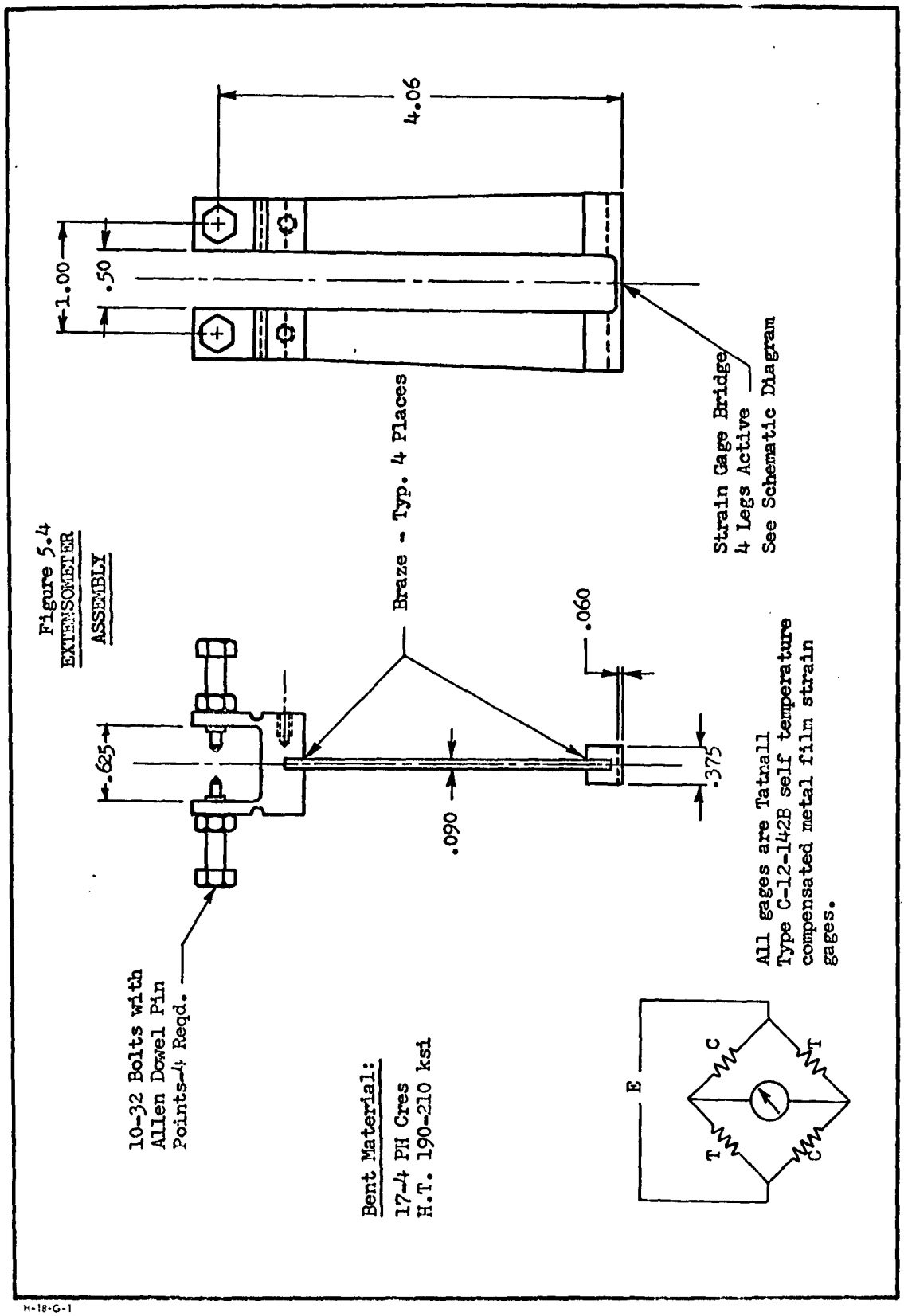

Figure 5.4
EXTENSOMETER
ASSEMBLY

H-18-G-1

Figure 5.5

EXTENSOMETER CALIBRATION

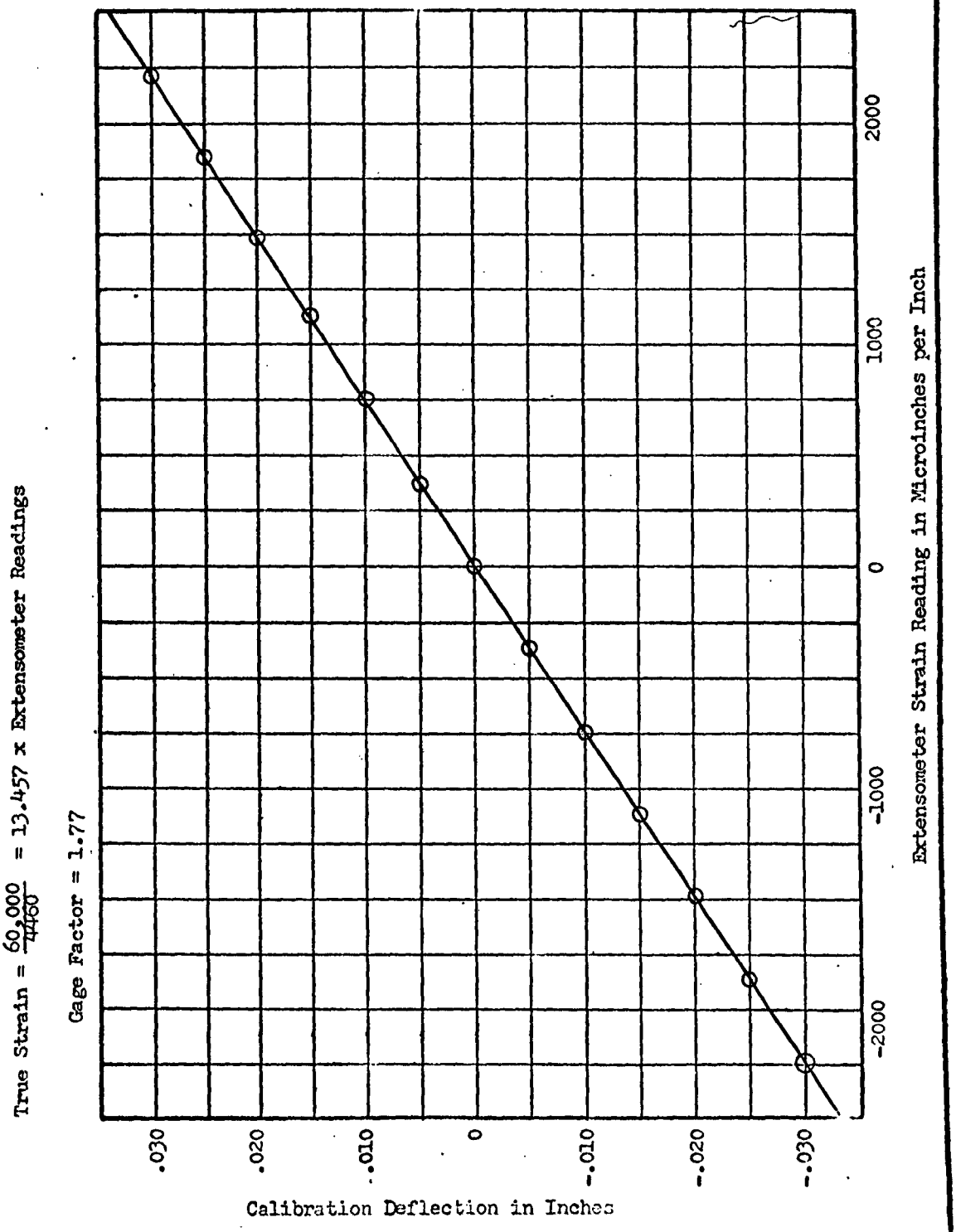

FORM H-18-8-1

Figure 5.6

CALIBRATION CHECK OF EXTENSOMETER
USING 2024 ALUMINUM ALLOY ROD

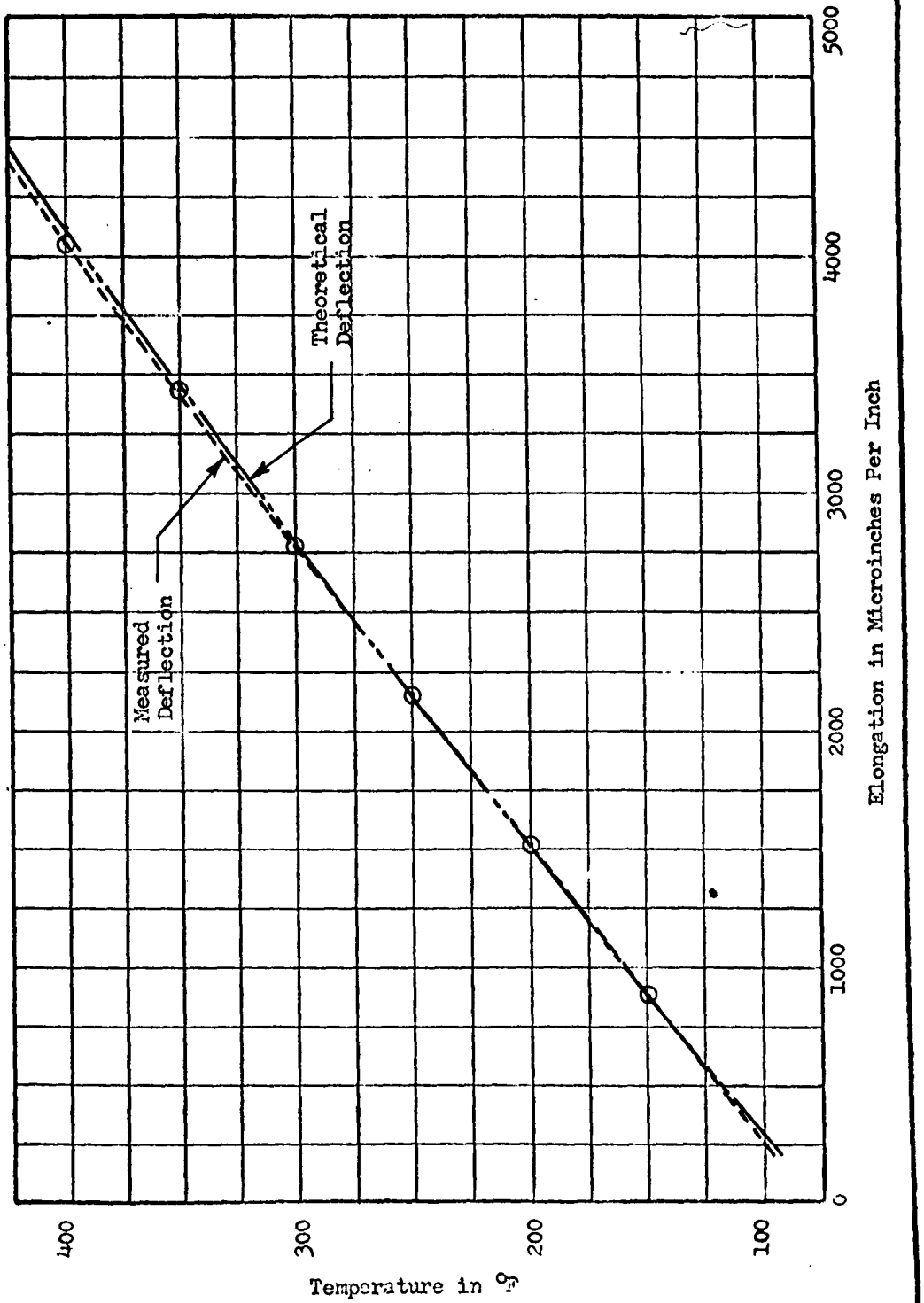

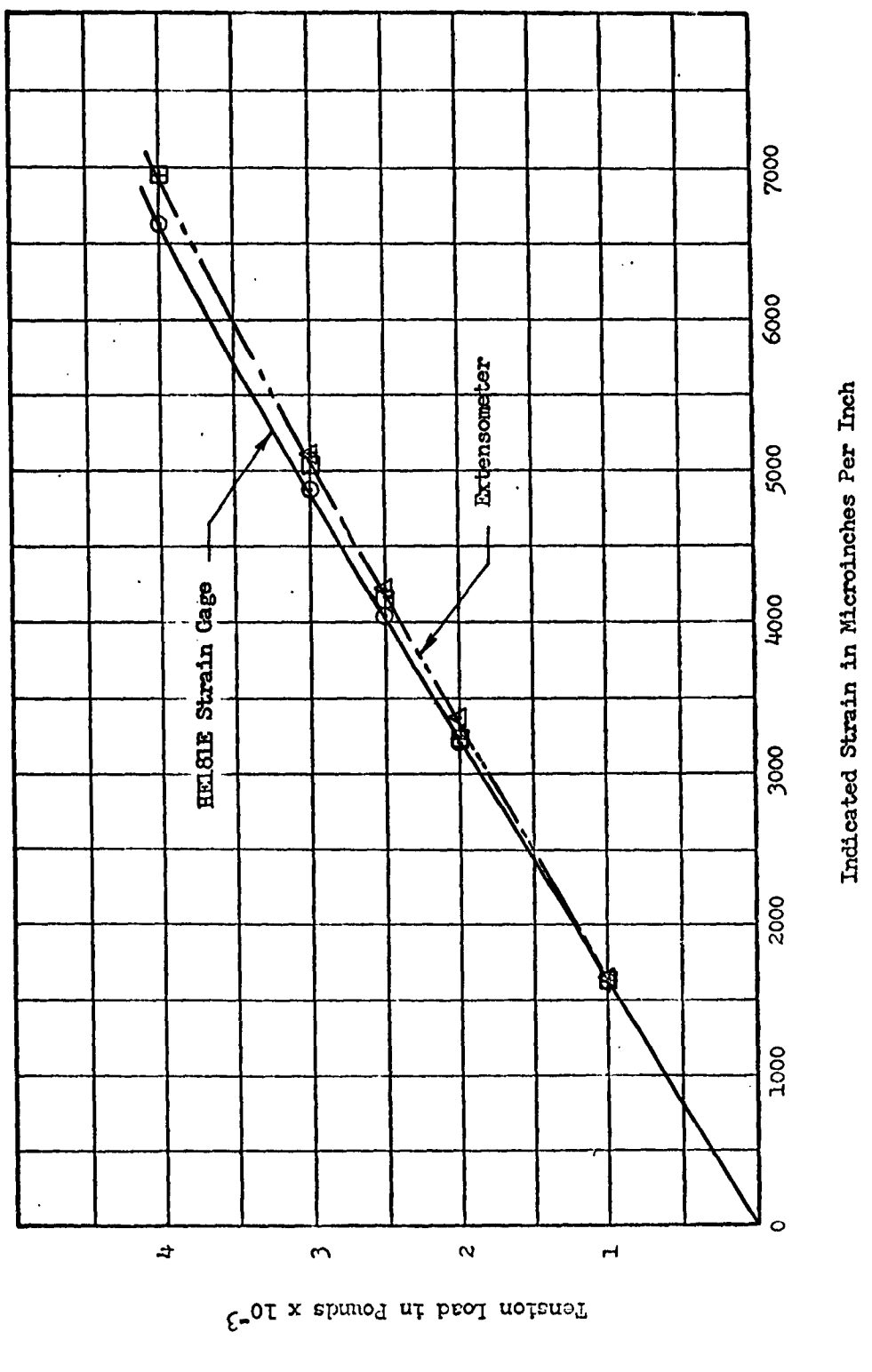

Figure 5.7
LOAD VS. STRAIN FOR EXTENSOMETER AND HEISIE STRAIN GAGE ON STANDARD TENSION COUPON

Figure 5.7 shows the curves comparing the use of the high elongation strain gage and the extensometer on the same tensile coupon.

5.2.3 INSTRUMENTATION LOCATION

5.2.3.1 SPECIMEN INSTRUMENTATION

The instrumentation for measuring strain and temperature were located on a cross-section at the centerline of each specimen. The location and identification of this instrumentation is shown in Figure 5.8.

The room temperature specimens had no thermocouples, and the strain gages were of the high elongation type (Tatnall HE-181-E).

All specimens tested to failure at elevated temperatures had iron-constantan thermocouples and high temperature strain gages (Tatnall C-12-142B) as shown in Figure 5.8. All specimens thermal cycled had iron-constantan thermocouples, but no strain gages.

All specimens were tested using extensometers located as shown in Figure 5.8.

5.2.3.2 COLUMN DEFLECTION MEASUREMENTS

All column deflections were obtained by measuring the movement between the heads of the Universal testing machine used for all column tests. This movement was measured by means of a deflection transducer.

The input from the deflection transducer and the input from a load cell incorporated in the load-measuring system of the Universal testing machine were combined by an X-Y plotter to give a load-deflection curve for each column tested. A curve being drawn by the X-Y plotter is shown in Figure B.2.

All tension coupons were tested in the Universal testing machine using the X-Y plotter with an extensometer furnishing the deflection input and a strain gaged calibrated load link furnishing the load input.

5.2.4 DATA RECORDING DEVICES

Thermocouple data was recorded on the Gilmore Model 179 data logger, while strain gage and transducer data was recorded manually using Baldwin Type L or N portable strain indicators. During certain test runs a multiplexing switch was employed with the portable strain indicators to increase channel capacity.

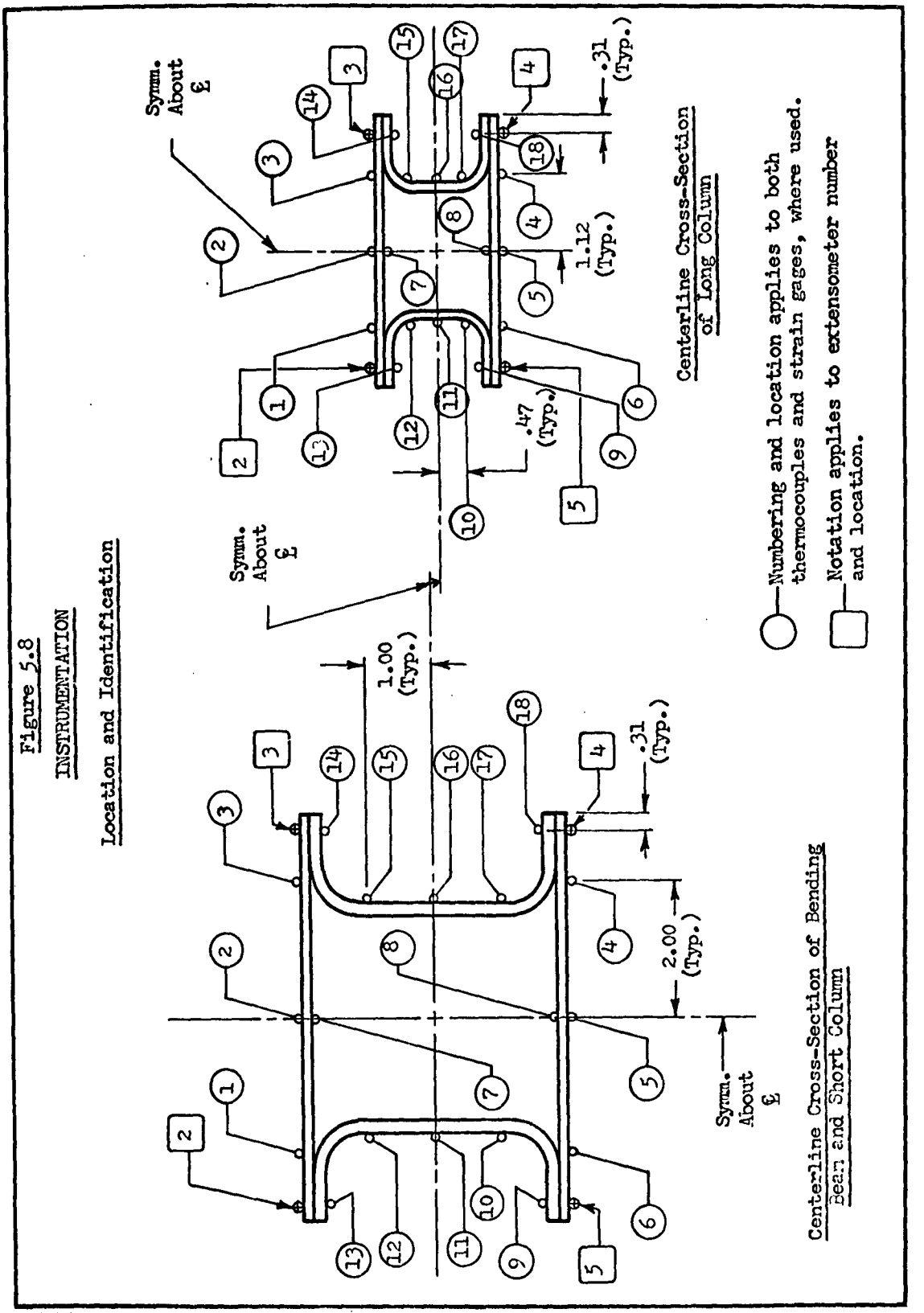

Figure 5.8
INSTRUMENTATION
Location and Identification

H-18-G-1

5.2.4.1 DATA LOGGER

The Gilmore Model 179 data logger is a medium speed instrumentation system which prints out in decimal notation 100 channels of strain gage (microinch per inch at ±0.5% full scale), thermocouple (degrees Fahrenheit at ±1% full scale), and millivolt data (millivolts at ±0.5% full scale). This system may be used with full or partial strain gage bridge circuits, any of three types of thermocouples or with any D.C. millivolt input of suitable amplitude. In addition, an automatic alarm function is provided which accepts a preset value of calculated strain for each channel and compares this value for each increment of load on the test specimen. Both a visual and printed alarm signal is provided if the measured strain exceeds the preset strain for a particular load condition. The range of the instrument is ±10,000 microinches per inch, 0° to 3000°F, or ±100 millivolts.

5.2.4.2 X-Y PLOTTER

The Moseley Autograph, Model 2A, is a two-axis, flat-bed, graphic millivolt recorder, utilizing standard 11" x 16½" graph paper and recording ink. The two axes correspond to the pen and the carriage. The basic voltage range is 0 to 5 millivolts for the Y axis and 0 to 7.5 millivolts for the X axis for full scale travel. The position of the balance circuit potentiometer and the pen and carriage, to which they are coupled, are always directly proportional to the amplitudes of the D.C. signal at the respective input terminals.

5.3 TEST PROCEDURES

5.3.1 METHOD OF TESTING

Prior to the running of each specimen a probable failing load for that particular specimen was computed, based on past time-temperature history, temperature at which the test was to be run, and material properties of the specimen as they were known to be at the time. From the predicted failing load a series of loading increments was decided upon which would give several data points in the elastic range and many points in the plastic range in order to obtain the desired information to use in the mathematical analysis.

A conventional procedure was used for the ambient temperature specimens. Zero strain gage, extensometer and deflection readings were taken before load was applied, a loading increment was applied and maintained, the instrumentation readings were taken, the next loading increment applied and the process repeated until failure of the specimen occurred.

For specimens tested under a constant temperature, a full set of instrumentation readings were taken at ambient temperature and then the banks of lamps were turned on. When the proper cover temperature had been reached and the temperature gradient across the specimen had been stabilized, another set of readings was taken and the remainder of the test conducted in the same manner as the ambient tests.

For specimens to be thermal cycled, a load was applied to the specimen which was well into the plastic range of the bending beam. Ambient temperature data was taken to insure that the plastic range had been reached. The load was then held constant while heat was applied to the specimen. When the temperature gradient across the specimen had stabilized, a set of extensometer readings was taken and the heat turned off. After the specimen temperature had reached about 120°F, the heat was reapplied and the procedure repeated until failure occurred or no more yield was indicated by the data.

5.3.2 SHORT COLUMNS

A total of six short columns was tested in the Baldwin-Southwark Universal testing machine. Each specimen had its ends milled flat and parallel and mounted between the compression heads of the testing machine with no extra loading plate either top or bottom. This permitted the measurement of head to head movement of the machine for use as deflection data for the short columns.

Strain gages and/or extensometers were read using portable strain indicators with a multiplexing switch. At each increment of applied load, strains were recorded manually and thermocouple data was recorded with a Gilmore Model 179 data logger. At the same time, a continuous load-deflection curve was being recorded on the X-Y plotter. Strain gage and extensometer data are shown in Figures A.3.9 through A.3.14.

5.3.3 LONG COLUMNS

A total of six long columns was tested in the Baldwin-Southwark Universal testing machine. Each specimen had a spherical ball fixture in each end which in turn rested on matching plates in the test machine. These fixtures and plates had two side effects on the testing. First, the spherical ball did not provide a completely pinned end condition for the column since the spherical ball had to slide relative to its matching plate rather than rotating freely as it would on a flat plate. This provided some small end fixity which was not desirable.

Second, the spherical ball and plate deflected a small amount under load which gave an indication of excessive column deflection, since the deflection was measured between the heads of the testing machine. When the deflection of the ball and plate at each end of the column was

calculated and deducted from the deflection between the heads of the test machine, very good agreement between calculated and measured column deflection was obtained.

Strain gages and/or extensometers were read using portable strain indicators with a multiplexing switch. At each increment of load, strains were recorded manually and thermocouple data was recorded with a Gilmore Model 179 data logger. At the same time, a continuous load-deflection curve was being recorded on the X-Y plotter. Strain gage and extensometer data are shown in Figures A.3.15 through A.3.19. A typical test setup is shown in Figure B.4.

5.3.4 BENDING BEAMS

A total of sixteen bending beams was tested in this program. Eight specimens were held at a constant temperature and loaded to failure, and the remaining eight were held at a constant load and the temperature cycled until the specimen either failed or reached elastic shakedown.

The load was applied at the third points of the beams by means of steel plates and linkage which in turn were loaded by means of hydraulic struts. The load was monitored by means of a strain gaged calibrated load link placed between the hydraulic struts and the steel linkage. The correct load was obtained by presetting the correct value on the portable strain indicator and applying hydraulic pressure to the struts until the null indicator was zeroed. During the thermal cycling testing it was necessary to watch the null indicator closely in order to hold the applied load constant, since the change in specimen temperature produced sizable load changes unless hydraulic fluid was added or removed from the struts.

Strain gages and/or extensometers were read using portable strain indicators with a multiplexing switch. At each increment of applied load, strains were recorded manually and thermocouple data was recorded with a Gilmore Model 179 data logger. Strain gage and extensometer data are shown in Figures A.3.1 through A.3.1 for the constant temperature specimens, and tabulated in Tables A.2.1 through A.2.8 for the thermal cycling specimens.

5.3.5 TEMPERATURE CONTROL

Temperature control for this test was accomplished through utilization of Research, Inc. ignitron power temperature controllers and General Electric 1000 T3 quartz infrared lamp banks (see Figures B.4 and B.8).

Accurate temperature control of the Research, Inc. units is achieved by use of precision potentiometric circuitry wherein a feedback from a specimen chromel-alumel thermocouple output is compared against a signal representing desired specimen temperature. The resulting error

signal is amplified and used to control the output of an ignitron power regulator. The ignitron power regulator controls the voltage impressed on infrared quartz lamp banks directed on specific specimen areas. Specimen temperature is thus brought to match the desired pre-established temperature set point value. The ignitron power regulator responds to control signals within one cycle of power line frequency (60 cps).

Circuit features of the Research, Inc. units also include continuous standard cell calibration, automatic thermocouple reference junction compensation, proportional band adjustment and limiter (rate) control which indirectly controls the time required to reach the desired set point temperature.

Each specimen had a control thermocouple located on the center of each cover (numbers (2) and (5) on Figure 5.8). These control thermocouples controlled each bank of lamps independently such that any change in temperature on one cover did not affect the bank of lamps heating the opposite cover.

5.4 TENSILE COUPONS

A total of twenty five tensile coupons was tested during this program. The primary purpose of these coupon tests was to provide material properties information for use in the mathematical analysis of test specimens.

5.4.1 DESCRIPTION OF COUPONS

The coupons were cut from the six sheets of 7075 aluminum from which all test specimens were fabricated. The sheets were laid out, each part identified, and the entire sheet photographed. The coupons were selected such that each sheet had coupons made from widely scattered spots. The identification of each coupon was stamped on its large end to preclude loss and mix-ups.

5.4.2 TEST PROGRAM

Coupons were machined to shape and divided into groups so that each group was subjected to a time-temperature history identical to that given the test beams and columns. Any beam or column tested had coupons made from the same sheets of material and subjected to an identical time temperature history so that the coupon test results could be used to predict yield and failing loads for the beam and column test specimens.

5.4.3 TEST SETUP

Coupons were machined to a constant .500 width for a length of 2.25 inches. The extensometer was fastened to the center one inch of this constant section, and the entire assembly placed in the Baldwin-Southwark Universal testing machine. Using the extensometer to drive one axis and a strain gaged calibrated load link to drive the other axis, a continuous curve was drawn by the X-Y plotter for each coupon tested.

Some tests were conducted at elevated temperature on the coupons, and for this purpose a small, four-sided oven was placed around the coupon and the heat provided by quartz lamps. A thermocouple located at the center of the coupon regulated the temperature of the coupon. The X-Y plotter was used to plot load strain curves for these coupons, also.

All coupon data is presented in Section A.1.

6.0 ANALYTICAL REPRESENTATION OF CROSS-SECTION

For the strain analysis procedures of Sec. 3.0 to define the load-deformation curves described in Sec. 4.0, the cross-section to be investigated must be defined by a finite number of structural elements. Specific information regarding each of these structural elements as to geometry, temperature, material properties and local buckling is required to perform the strain analysis. The geometry data includes the cross-sectional area of the element and coordinates x and y of the element centroid from orthogonal references axes X and Y. The temperature data includes the element temperature to define material properties and the temperature change from datum to define the thermal strains (and stresses) at any temperature step in the temperature-load sequence.

The material properties are more complex and may depend upon the temperature-time history of each element in the cross-section. The coefficient of thermal expansion is readily obtained from Ref. (a) for the commonly used aircraft materials. The use of the Ramberg-Osgood equation to define the stress-strain relationship of each element in the cross-section requires three parameters for description. These are the elastic modulus (E), the tension or compression yield stress (F_{ty} or F_{cy}) at 0.7E, and the shape factor m. For normal design use, this data should be taken from Ref. (d) or may be obtained from tension and/or compression test coupon stress-strain curves. In addition, the ultimate tension stress (F_{tu}) is used as a stress cut-off on tension stress-strain curves and the compression yield stress cut-off is used on compression elements. In many cases the only yield stress available may be the 0.002 in./in. offset yield. The 0.7E yield stress for the Ramberg-Osgood equation may be obtained by

$$(F_y)_{0.7E} = \frac{(F_y)_{0.002}}{\left[.004677 \frac{E}{(F_y)_{0.002}}\right]^{\frac{1}{m-1}}} \qquad \text{Ref. (j)}$$

where $(F_y)_{0.7E}$ is the 0.7E yield stress to define the Ramberg-Osgood equation and $(F_y)_{0.002}$ is the appropriate value of 0.002 in./in. offset yield stress from Ref. (d).

For local instability produced by compression buckling, the plate element width b and thickness t and the buckling coefficient K are required to define the critical compression buckling strain as shown in Sec. 3.5. However, strain forms of other buckling equations for curved sheet, inter-rivet buckling, etc., may be used.

For an analytical representation of the specimen cross-sections the following sections show the cross-section element breakdown, element areas, centroidal distances from the reference axis, buckling coefficients as

defined in Sec. 8.1 by strain gage data, element temperature data obtained by thermocouples during the tests, and applicable temperature exposure histories which would affect the material properties data of Sec. 7.0. The buckling coefficients, temperature distribution, and temperature exposure history were taken from test data to establish compatibility between the test and analysis conditions.

Note that the temperature exposure history curves of Fig.6.6 also include the temperature-time curve for the tensile coupons.

6.1 ELEMENT GEOMETRY AND BUCKLING DATA

The following diagrams and tables summarize the geometry and buckling data for the various types of test specimens. The element areas shown in the tables are based on nominal dimensions. For buckling modes other than the flat plate buckling, the following equations were used. For the attached edges of the cover plates, experience has shown the assumption of inter-rivet buckling to work quite well, in which case

$$e_{c_r} = K\left(\frac{t}{s}\right)^2, \text{ Reference (i)}$$

where s is the distance between fasteners and K = 3.62, as shown in the tables. For outstanding legs of the channel sections Eq. (3.5.1) is used with K = 0.385 for one side free, one side and ends simply supported. The radius sections of the channels were considered as curved plates where

$$e_{c_r} = 0.3\left(\frac{t}{R}\right), \text{ Reference (i)}$$

with R the mean radius of curvature. Flat sections of the channel webs were treated as flat plates in compression using Eq. (3.5.1) with K = 3.62 for simply supported sides and ends.

For bending specimens B-1, B-17, B-3, B-4, B-5, B-6, B-7, and B-8 and thermal cycling specimens B-13, B-11, B-16, B-12, B-10, B-15, B-9, and B-14 the geometry and buckling data are shown in Figures 6.1 and 6.2.

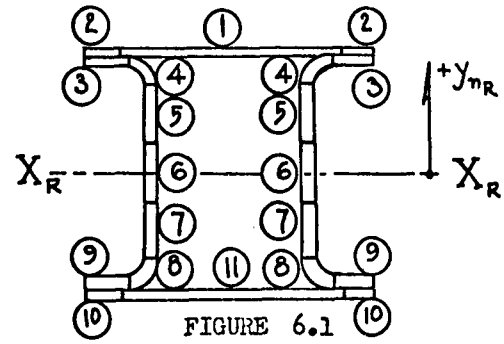

FIGURE 6.1
CROSS-SECTION ELEMENT BREAKDOWN
BENDING AND CRIPPLING SPECIMENS

ELEMENT NO.	AREA, A_n, in.^{2}	Y_{n_r}, inches	b_n, inches	t_n, inches	K_{cr_n}	BUCKLING MODE
1	0.625	1.9375	5	0.125	4.325	Flat Plate
2	0.0625 (2)	1.9375	s=1.25	0.125	3.62	Inter-Rivet
3	0.1403 (2)	1.782	0.75	0.187	0.385	Flat Plate
4	0.193 (2)	1.5875	R=0.655	0.187	0.3	Curved Plate
5	0.1402 (2)	0.75	2.25*	0.187	3.62	Flat Plate
6	0.1402 (2)	0	2.25*	0.187	3.62	Flat Plate
7	0.1402 (2)	-0.75	2.25*	0.187	3.62	Flat Plate
8	0.193 (2)	-1.5875	R=0.655	0.187	0.3	Curved Plate
9	0.1403 (2)	-1.782	0.75	0.187	0.385	Flat Plate
10	0.0625 (2)	-1.9375	s=1.25	0.125	3.62	Inter-Rivet
11	0.625	-1.9375	5	0.125	4.325	Flat Plate

*Total flat plate width used to define e_{cr} for elements 5, 6 and 7.

FIGURE 6.2
SUMMARY TABLE - BENDING SPECIMEN GEOMETRY AND BUCKLING DATA

The value of K_{cr_n} = 4.325 in Fig.6.2 for elements 1 and 11 was defined by test data as shown in Section 8.1.1.

For crippling specimens A-1, A-2, A-3, A-4, A-5, and A-6, the geometry and buckling data are shown in Figures 6.1 and 6.3.

ELEMENT NO.	AREA A_n, in.^{2}	Y_{n_r}, inches	b_n, inches	t_n, inches	K_{cr_n}	BUCKLING MODE
1	0.625	1.9375	5	0.125	4.985	Flat Plate
2	0.0625 (2)	1.9375	s=1.25	0.125	3.62	Inter Rivet
3	0.1403 (2)	1.782	0.75	0.187	0.385	Flat Plate
4	0.193 (2)	1.5875	R=0.655	0.187	0.3	Curved Plate
5	0.1402 (2)	0.75	2.25*	0.187	3.62	Flat Plate
6	0.1402 (2)	0	2.25*	0.187	3.62	Flat Plate
7	0.1402 (2)	-0.75	2.25*	0.187	3.72	Flat Plate
8	0.193 (2)	-1.5875	R=0.655	0.187	0.3	Curved Plate
9	0.1403 (2)	-1.782	0.75	0.187	0.385	Flat Plate
10	0.0625 (2)	-1.9375	s=1.25	0.125	3.62	Inter-Rivet
11	0.625	-1.9375	5	0.125	4.985	Flat Plate

* Total flat plate width used to define e_{cr} for elements 5, 6 and 7.

FIGURE 6.3
SUMMARY TABLE - CRIPPLING SPECIMEN GEOMETRY AND BUCKLING DATA

The value of K_{cr_n} = 4.985 in Fig.6.3 for elements 1 and 11 was defined by test data as shown in Section 8.1.2.

For column specimens C-1, C-2, C-3, C-4, C-5 and C-6 the geometry and buckling data are shown in Figures 6.4 and 6.5.

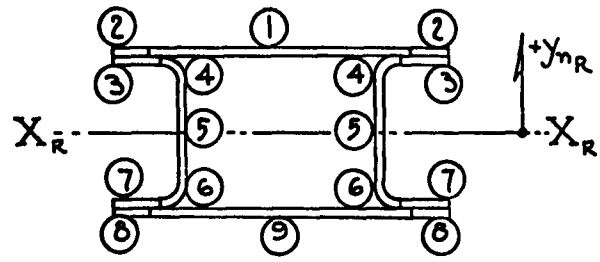

FIGURE 6.4

CROSS-SECTION ELEMENT BREAKDOWN
LONG COLUMN SPECIMENS

ELEMENT NO.	AREA A_n, in.^{2}	Y_{n_R}, inches	b_n, inches	t_n, inches	K_{cr_n}	BUCKLING MODE
1	0.3905	0.875	3.125	0.125	4.325	Flat Plate
2	0.0547 (2)	0.875	s=1.125	0.125	3.62	Inter-Rivet
3	0.0822 (2)	0.750	0.657	0.125	0.385	Flat Plate
4	0.08 (2)	0.6295	R=0.405	0.125	0.3	Curved Plate
5	0.0861 (2)	0	0.689	0.125	3.62	Flat Plate
6	0.08 (2)	-0.6295	R=0.405	0.125	0.3	Curved Plate
7	0.0822 (2)	-0.750	0.657	0.125	0.385	Flat Plate
8	0.0547 (2)	-0.875	s=1.125	0.125	3.62	Inter-Rivet
9	0.3905	-0.875	3.125	0.125	4.325	Flat Plate

FIGURE 6.5

SUMMARY TABLE - LONG COLUMN SPECIMEN GEOMETRY AND BUCKLING DATA

The value of K_{cr_n} = 4.325 in Fig.6.5 for elements 1 and 9 is defined as shown in Section 8.1.3. For the critical column buckling strain defined by the Euler equation refer to the discussion of end restraint conditions in Section 8.2.2.

6.2 TEMPERATURE DATA

The temperature data shown in this section is composed of three distinct parts required to define the thermal strains in Eq. (3.1.2)

the material properties of Section 7.0. For all static load-temperature test specimens using elevated temperature strain gages, the temperature exposure histories are shown since the recovery of 7075-T6 material properties is severely affected by the time at temperature necessary for curing the strain gage cement. Temperature exposure history diagrams are shown for the duration of the tests for those specimens with maximum test temperatures over 250°F. The temperature-time histories shown in these diagrams are significant in that they affect the recovery of material properties. The steady-state temperature distributions through the cross-section are shown where these diagrams define the particular element temperatures for calculating the thermal strains in Eq.(3.1.2) and for selecting the final values of F_y, F_u, E and m for the Ramberg-Osgood representation of the element stress-strain curve. The selection of material properties data for all test specimens is described fully in Section 7.0.

6.2.1 STRAIN GAGE CURING TEMPERATURE EXPOSURE HISTORY

Since the instrumentation on many of the test specimens included bonded foil-type elevated temperature strain gages, the entire specimen was soaked in a convection type furnace (Ref. Section 5.0) to cure the strain gage cement. Theoretically, the temperature-time soaking history should be two hours at 350°F. and one-half hour at 450°F. Thermocouples at the middle of the cover plates indicated the temperature exposure histories for the elevated temperature bending and crippling specimens to be as shown in Figure 6.6. The temperature exposure histories shown in Figure 6.6 are particularly important for the definition of element material properties in Section 7.0 for several reasons. First, the tensile coupon data did not accurately define the material properties of the box specimens due to the critical nature of the variation in temperature exposure histories as shown in the curves of Figure 6.6. Second, the material properties for 7075-T6 aluminum alloy were found to be extremely sensitive to the exact time at the maximum soaking temperature. In addition, this history constitutes the first increment of the entire temperature-time soaking history above the aging temperature of the material. For these test specimens, the initial soaking time at temperatures $>$ 400°F. was found to be most critical for defining material properties after exposure to elevated temperatures for various times.

No temperature exposure history is shown for the elevated temperature long column specimens or the thermal cycling specimens, since no elevated temperature strain gages were used and no bond curing was required.

6.2.2 TEST TEMPERATURE EXPOSURE HISTORY

The figures in this section summarize the test temperature exposure histories for those test specimens having test temperatures $>$ 250°F. (aging temperature of 7075-T6). For those specimens with maximum test temperatures of 250°F. the effect of the short time at 250°F. was negligible. The effect of these temperature exposure histories on the material properties is significant due to the high temperatures involved, the cumulative effect of

these histories with those of Section 6.2.1, and the variation in total test time required for each individual specimen. Figure 6.7 shows the temperature-time curves for bending specimens B-3, B-6, and B-7 for the cover plate (or plates) at 450°F. during the test. This temperature was recorded at the middle of the heated cover plates.

Figure 6.8 gives the total test temperature exposure history for crippling specimen A-3 and shows the temperature at the middle and at the cooler edges of the cover plates. This diagram applies to both heated cover plates since the temperature gradient was symmetrical. Note that two peak temperature (425°F.) areas occur. The first attempt to perform the test showed some necessary modifications to the test set up and the lamps were shut off to effect the modification. The second attempt at t = 29 minutes was successful, and the duration of the test was approximately 20 minutes. The total diagram is important, however, in that the cumulative time at temperature affects the material properties recovery, as shown in Section 7.0. Figure 6.9 shows the temperature-time diagram for specimen A-6. Equipment difficulties again necessitated a shutdown, and the total temperature-time diagram is very similar to that for specimen A-3. As with specimen A-3, the total time at temperature is important to define the recovery of material properties.

Figure 6.10 shows the test temperature exposure history for long column specimens C-5 and C-6. Lamp circuit difficulties were encountered with C-5 at about 340°F. necessitating a temporary shutdown of the test. For the long column specimens, Figure 6.10 constitutes the entire temperature exposure history, since no elevated temperature strain gages were used and no bond curing was required.

Figure 6.11 shows the test temperature exposure histories for all thermal cycling specimens except those tested in the 250°F. environment. Specimen B-16 had a longer history than the other specimens since temperature cycling was performed at several fixed bending moments on this specimen. This practice was discontinued on later specimens since data evaluation becomes unnecessarily difficult. Note in Figure 6.11 that the temperature exposure histories for specimens B-10, B-15, B-9, and B-14 were identical. These four specimens represented the 450°F. unsymmetrical temperature gradient tests, and since the time at temperature was relatively easy to control it was decided to eliminate that variable from the problem. With only a limited amount of test data available from the four specimens, more efficient use could be made of the combined strain data by eliminating the time variable. The time-temperature curves in Figure 6.11 constitute the entire temperature exposure history for the thermal cycling specimens since no elevated temperature strain gages were used and no bond curing was necessary.

6.2.3 CROSS-SECTION TEMPERATURE DISTRIBUTIONS

The steady state cross-section temperature distributions for elevated temperature bending specimens B-3 through B-8 are shown in Figure 6.12. The individual data points are from thermocouples located as shown in

Figure 5.8. The maximum temperatures of 250°F. and 450°F. are not shown, since these were control thermocouples at the middle of the cover plates. The curves of Figure 6.12 are used in conjunction with those of Figures 6.6 and 6.7 to define the element material properties of Section 7.0, and also provide the data for the determination of the thermal strains in Equation (3.1.2). The two curves for each specimen represent the distribution on each side of the box beam. For purposes of analysis, the average value is used for both material properties evaluation and for calculating the thermal strains. For the analysis this assumes temperature and material property symmetry about the Y-axis.

The steady state cross-section temperature distributions for crippling specimens A-3 through A-6 are shown in Figure 6.13. Thermocouples on these specimens are located identically to those on the bending specimens as shown in Figure 5.8. The maximum cover plate temperatures of 250°F. and 450°F. are not shown in Figure 6.13 since these were the control thermocouple temperatures. Figure 6.13 is used in conjunction with Figures 6.6, 6.8 and 6.9 to define the element material properties of Section 7.0 and provide temperature data for Equation (3.1.2). The assumption of temperature and material property symmetry about the Y-axis is maintained for purposes of analysis by using the average temperature between the two sides of the specimen.

Steady state temperature distributions for long column specimens C-3 thru C-6 are shown in Figure 6.14. Thermocouples were located as shown in Figure 5.8 with the control thermocouples located in the middle of the cover plates to record the maximum temperature of 250°F. or 450°F. and control the heat input. Figure 6.14 is used in conjunction with Figure 6.10 to define the element material properties of Section 7.0 and provide temperature data for Equation (3.1.2). As with the bending and crippling specimens, symmetry about the Y-axis is maintained by using the average temperature between the two sides of the specimen.

The steady state cross-section temperature distributions for all thermal cycling specimens are shown in Figures 6.15 and 6.16. Thermocouples were located as for the bending specimens shown in Figure 5.8 with the 250°F. or 450°F. control thermocouples located in the middle of the cover plates. These figures are used in conjunction with Figure 6.11 to define the element material properties shown in Section 7.0 and to provide temperature data for Equation (3.1.2). As with the bending specimens, symmetry about the Y-axis is assumed for calculation purposes by using the average temperature between the two sides of the specimen.

Figure 6.6
Strain Gage Curing Temperature Exposure Histories
Tensile Coupons
Crippling Specimens A-3 through A-6
Bending Specimens B-3 through B-8

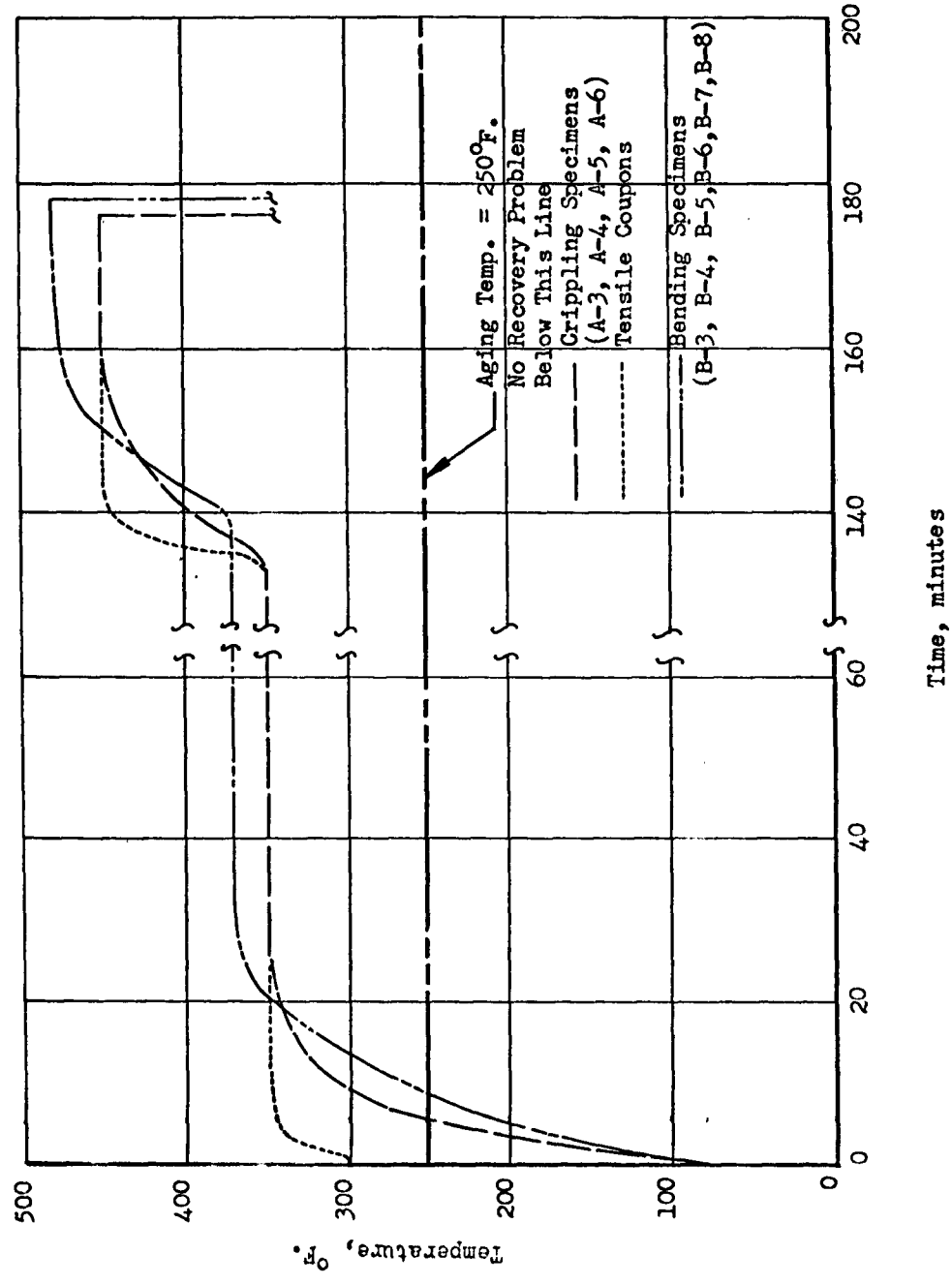

FIGURE 6.7
TEST TEMPERATURE EXPOSURE HISTORY
BENDING SPECIMENS B-3, B-6, and B-7

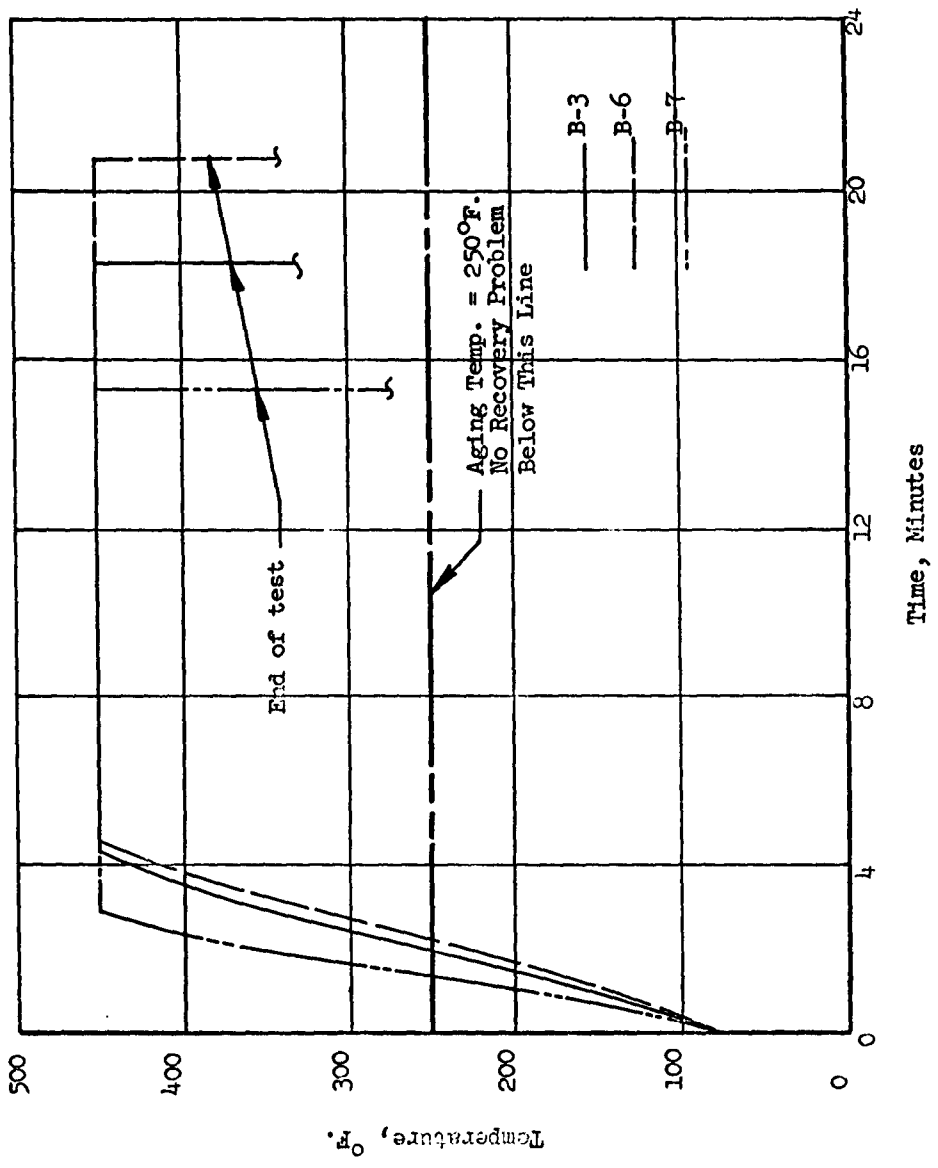

H-16-C-1

Figure 6.8
Test Temperature Exposure History
Crippling Specimen A-3

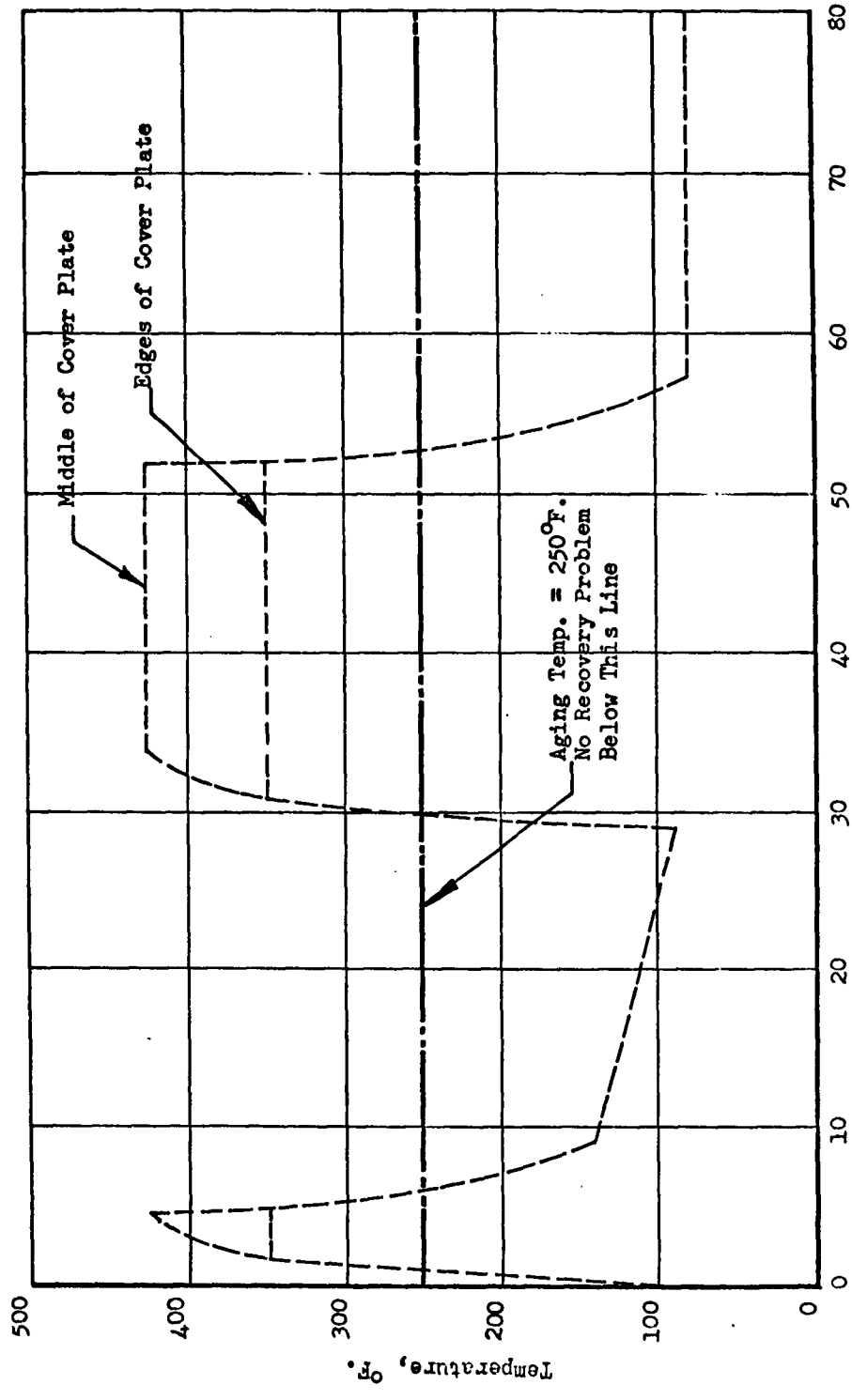

Figure 6.9

Test Temperature Exposure History
Crippling Specimen A-6

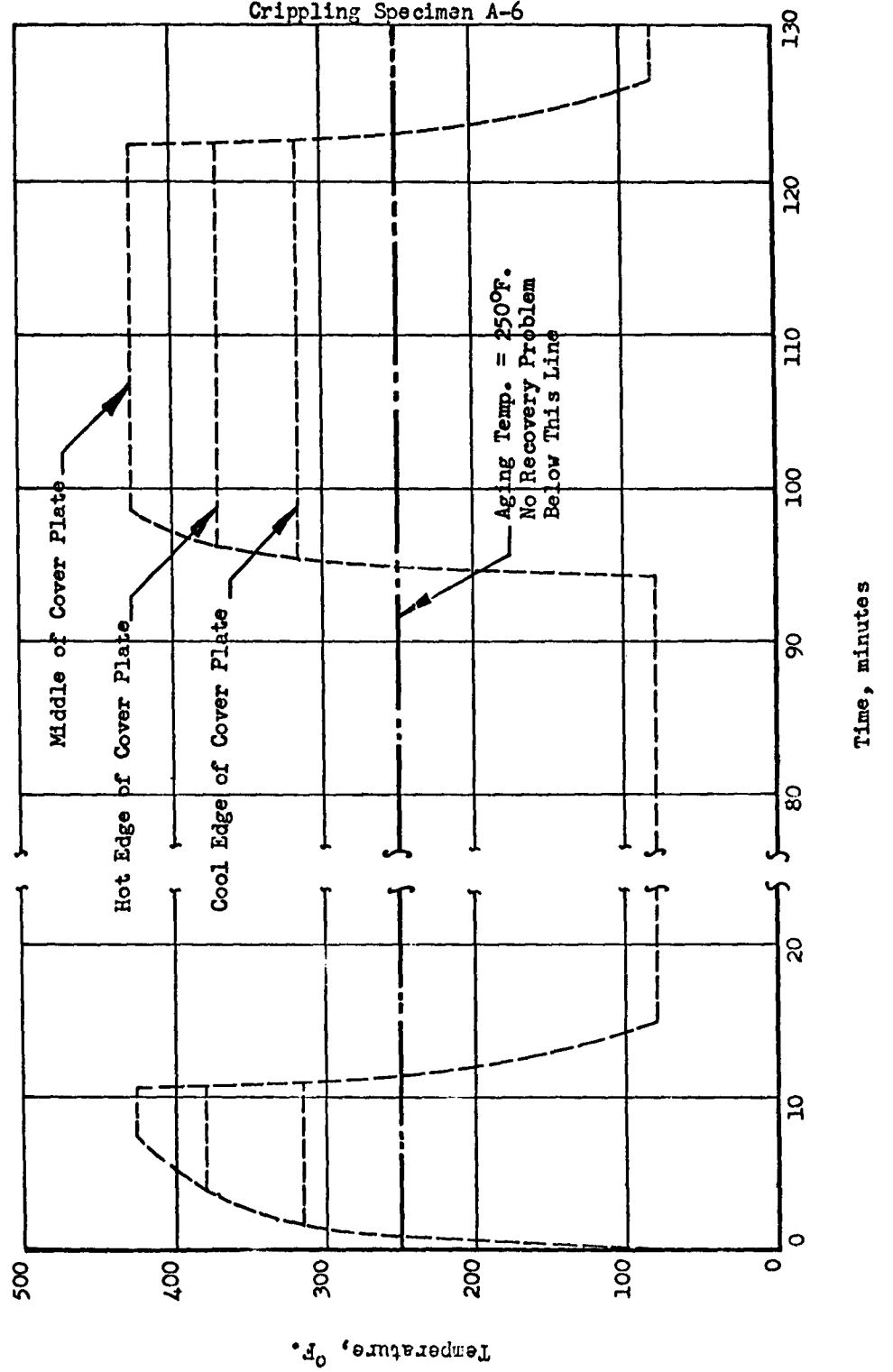

Figure 6.10
Test Temperature Exposure History
Long Column Specimens C-5 and C-6

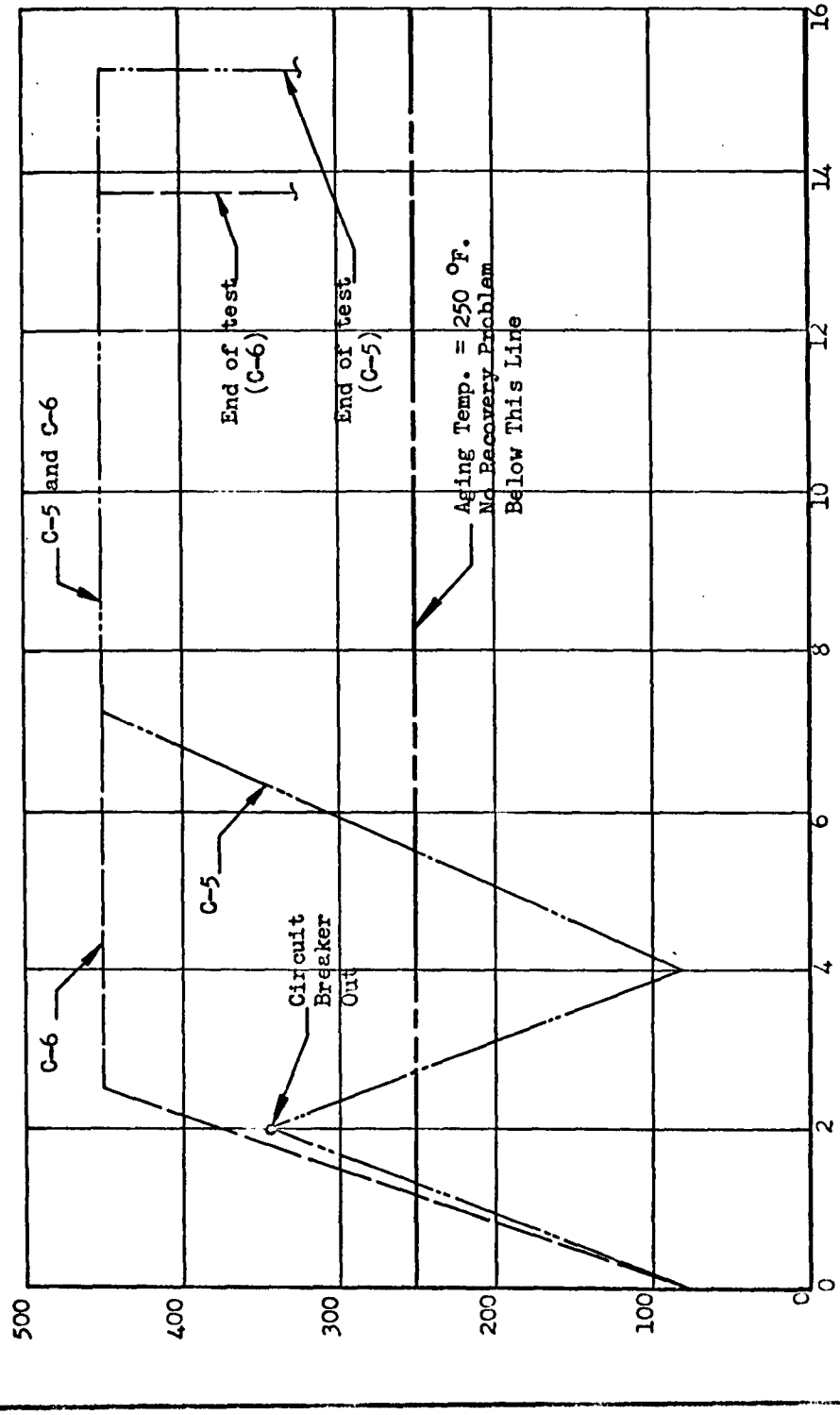

H-18-G-1

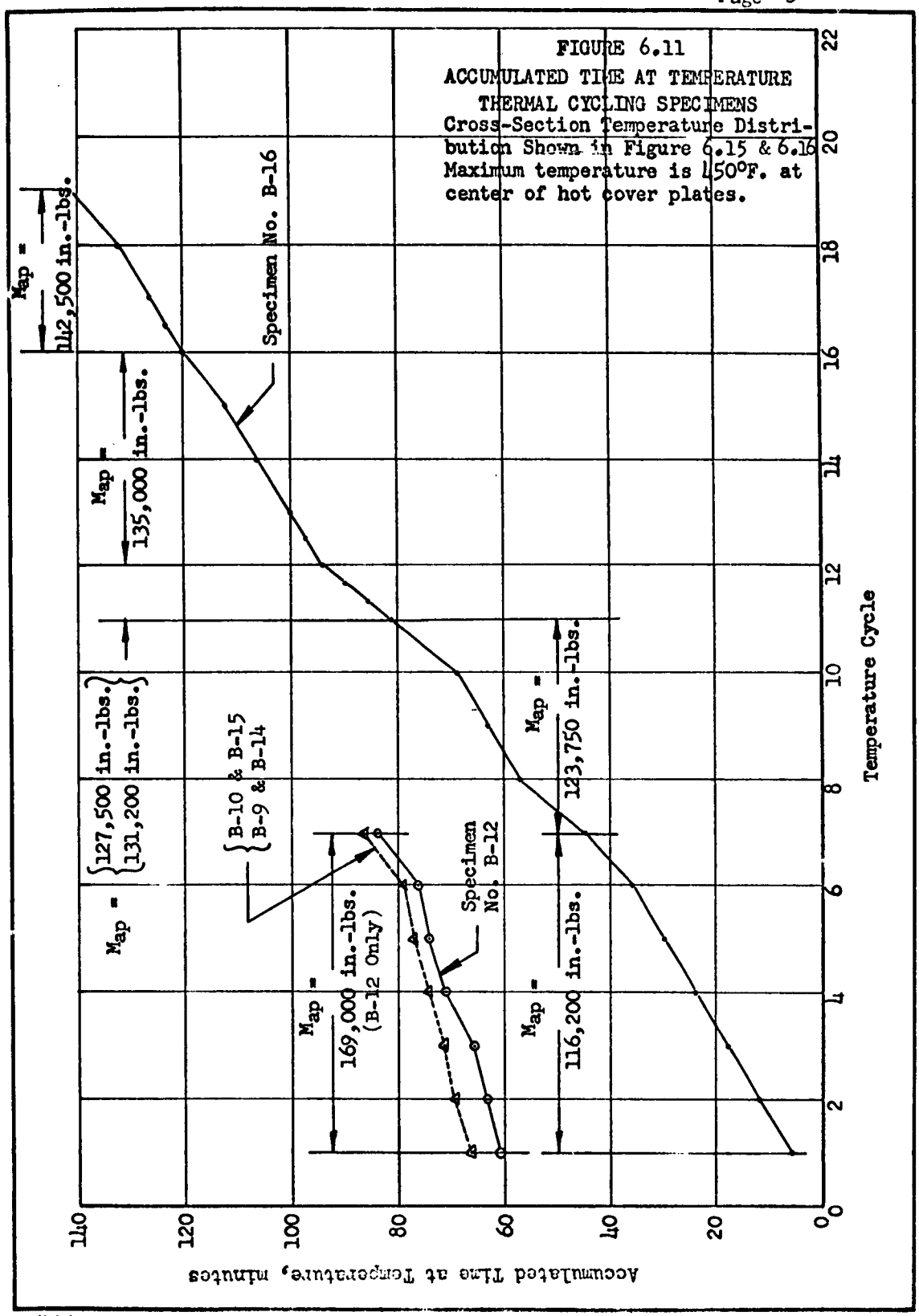

FIGURE 6.11
ACCUMULATED TIME AT TEMPERATURE
THERMAL CYCLING SPECIMENS
Cross-Section Temperature Distribution Shown in Figure 6.15 & 6.16
Maximum temperature is 1450°F. at center of hot cover plates.

H-18-G-1

Figure 6.12
Cross-Section Temperature Distribution (Steady State)
Bending Specimens (Reference Fig. 5.8)

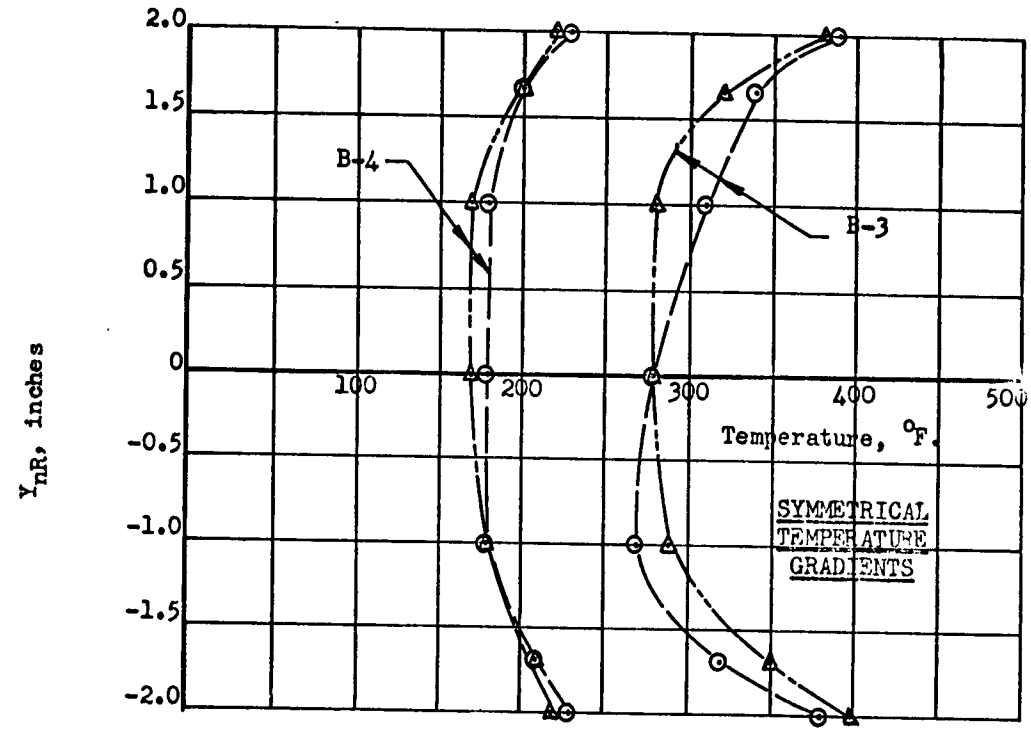

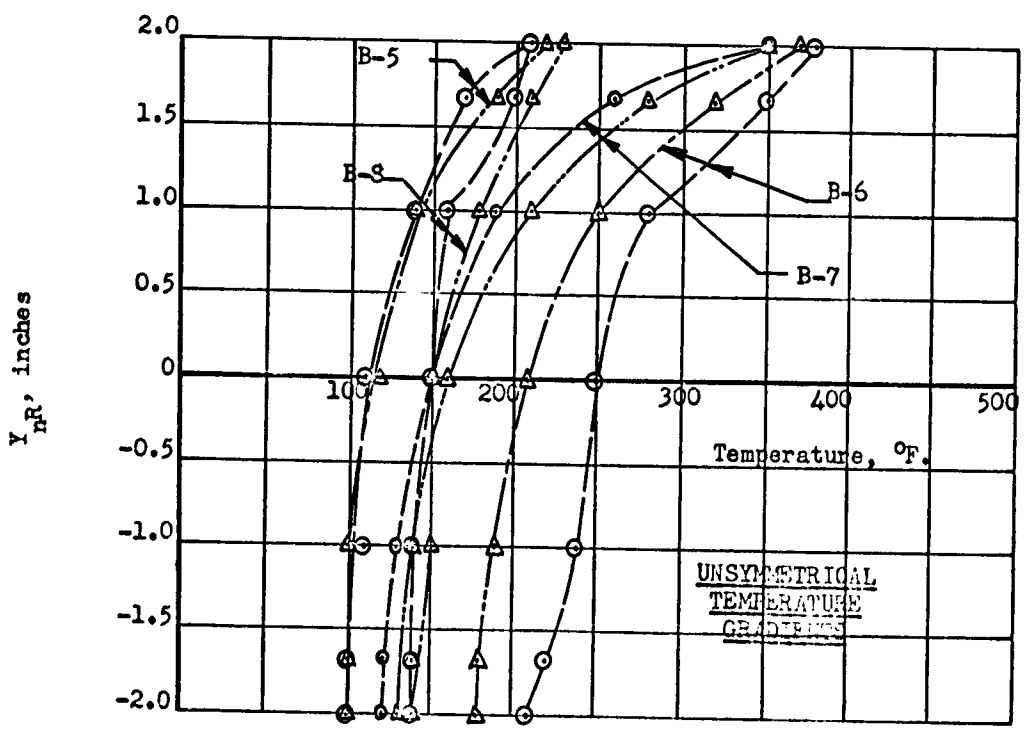

Figure 6.13
Cross-Section Temperature Distribution (Steady State)
Crippling Specimens (Reference Fig. 5.8)

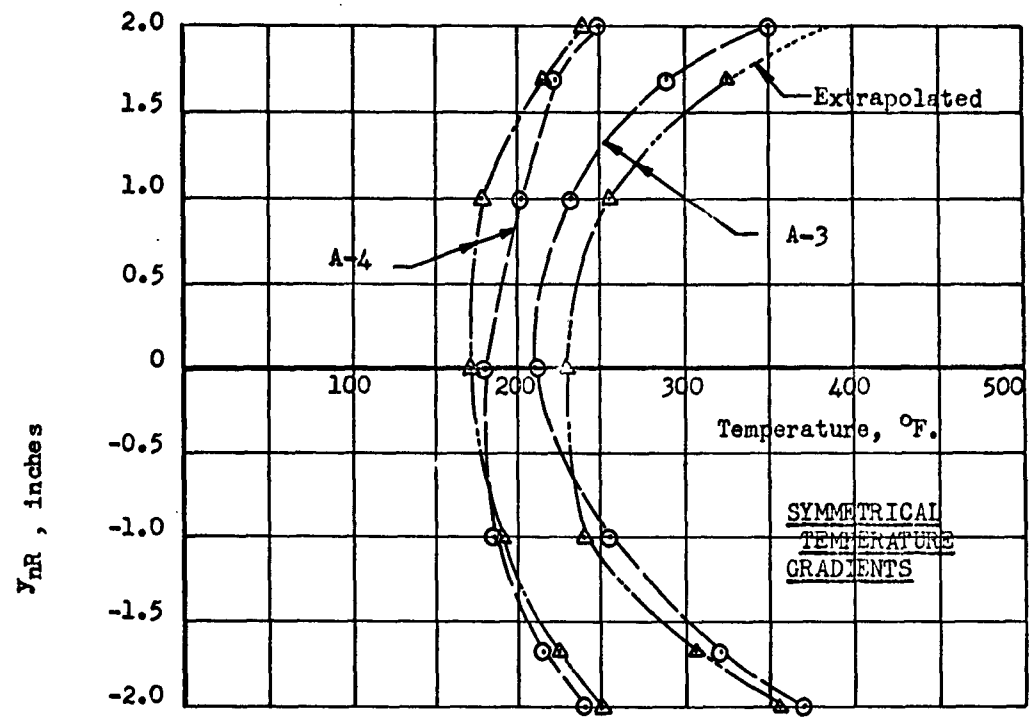

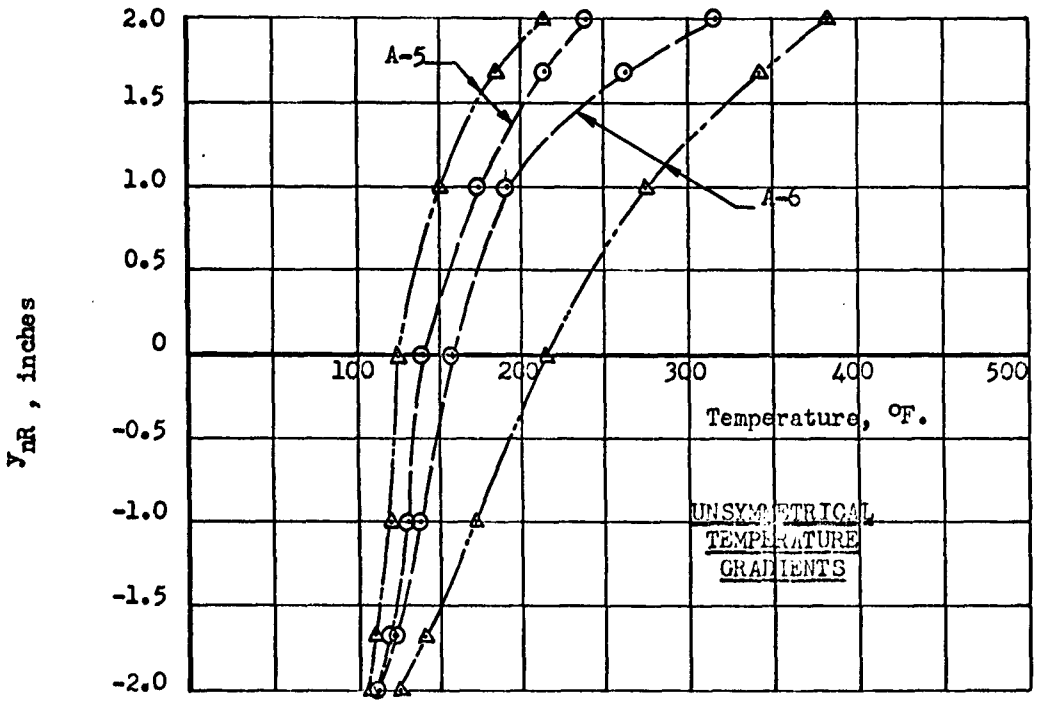

FIGURE 6.14

CROSS-SECTION TEMPERATURE DISTRIBUTION (STEADY STATE)
LONG COLUMN SPECIMENS (REFERENCE FIG. 5.8)

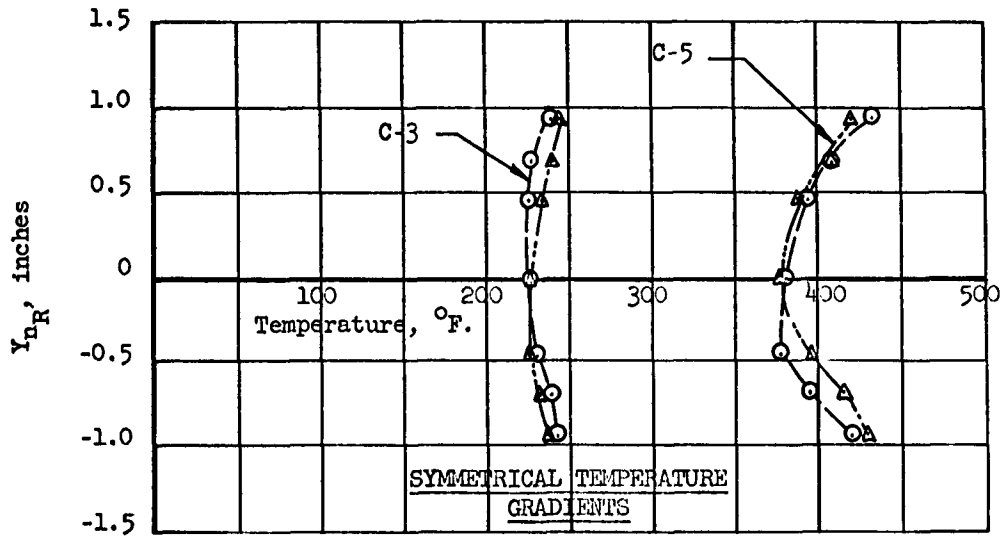

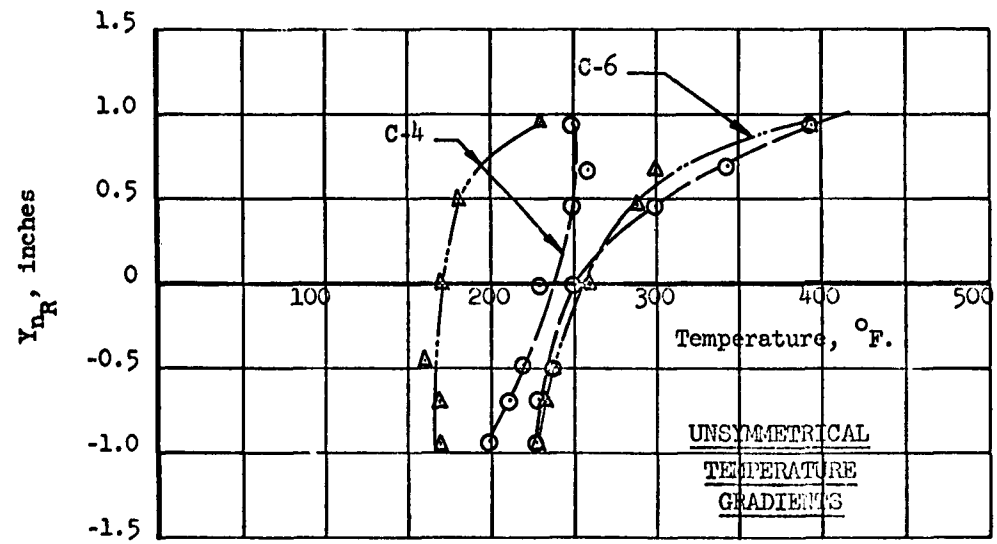

H-18-G-1

Figure 6.15
Cross-Section Temperature Distribution (Steady State)
Thermal Cycling Specimens (Reference Fig. 5.8)

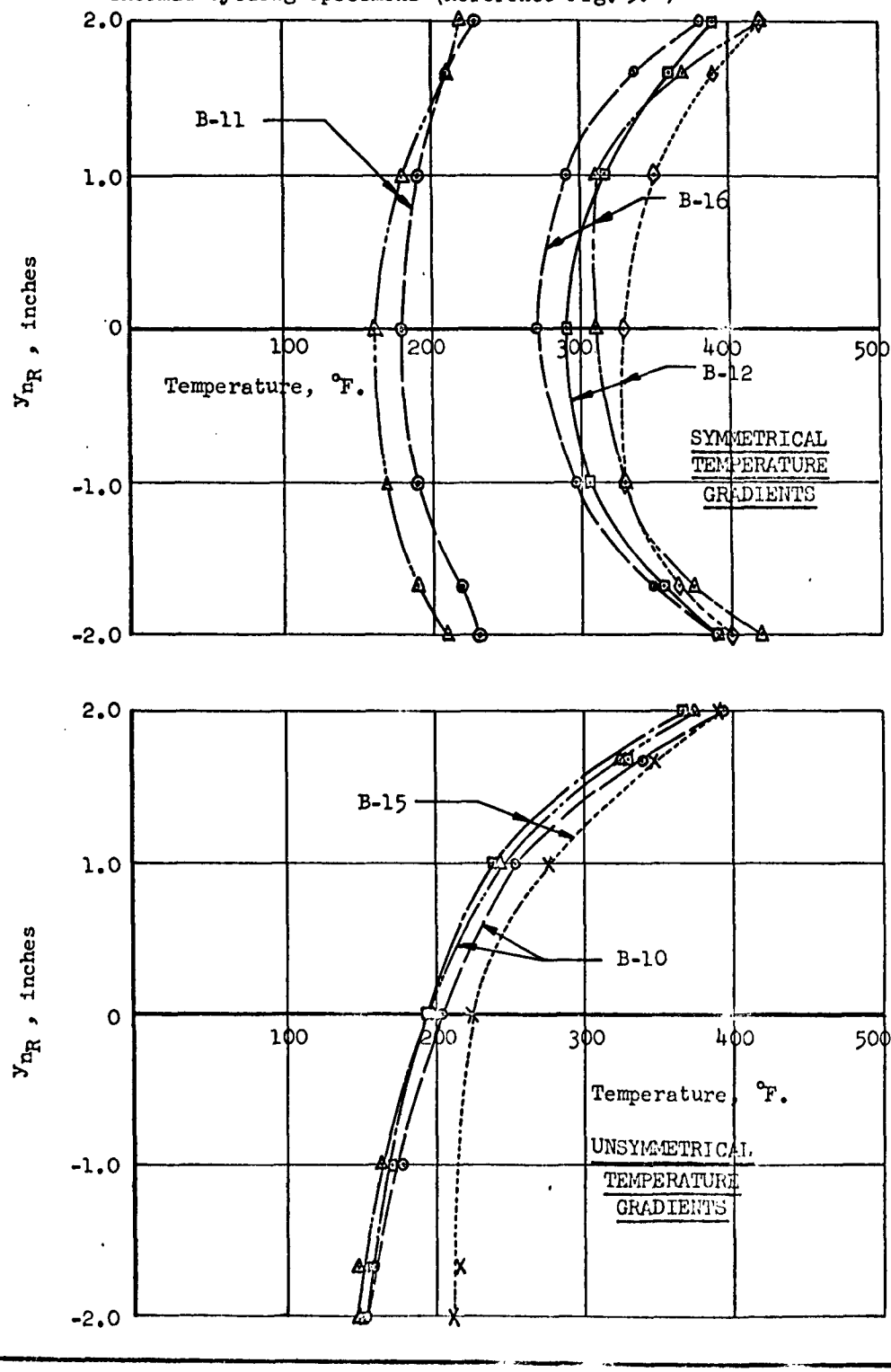

H-18-G-1

Figure 6.16
Cross-Section Temperature Distribution (Steady State)
Thermal Cycling Specimens (Reference Fig. 5.8)

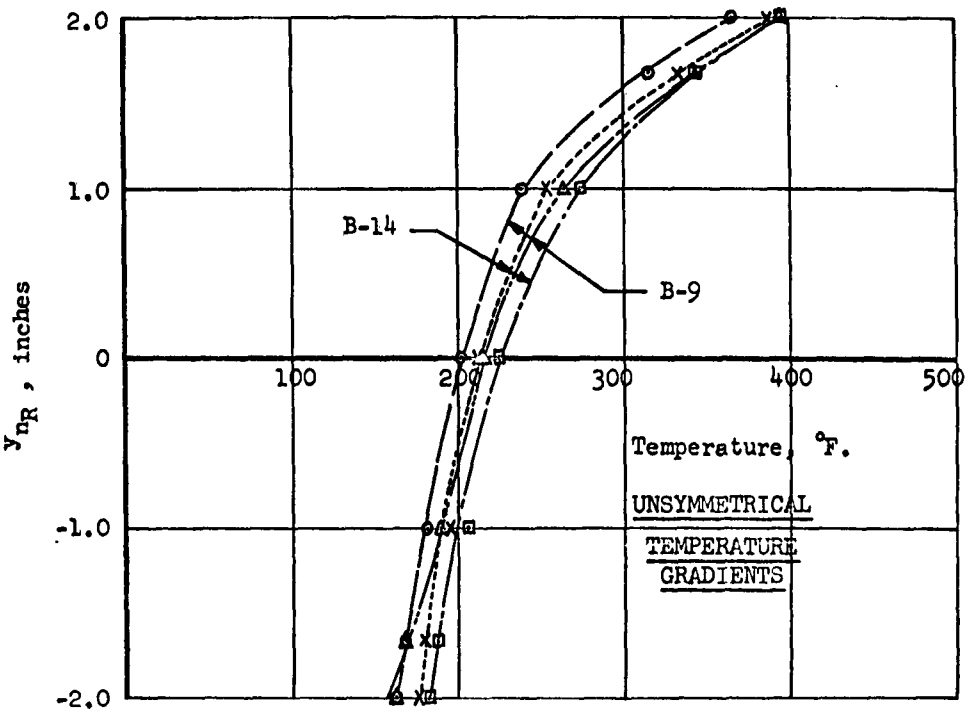

7.0 MATERIAL PROPERTIES

No methods or procedures for defining the ultimate strength or a given amount of permanent set for a particular structure can be any better than the basic material properties used as imput data. Since a comparison of analytical and experimental load-deformation curves was of particular importance in this study, considerable attention was given to the definition of the basic properties used to establish the proper Ramberg-Osgood stress-strain curve for each element in the cross-section. The use of 7075-T6 aluminum alloy at temperatures above the aging temperature, and complex temperature exposure histories due to strain gage curing and varying times at the higher test temperatures considerably complicate the problem of defining the structural element material properties. Prior to the consideration of any elevated temperature properties it was necessary to define the basic room temperature properties reasonably accurately. Ordinarily this would not be necessary in the design problem since the use of either 90 percent probability or minimum guaranteed values from Ref. (d) ensures some conservatism in the design. However, for this study any comparison of analytical and experimental data could not be made if a common material properties basis were not used. The definition of the yield stress is particularly important since this value is most critical in the Ramberg-Osgood equation. The exact value of the ultimate stress is somewhat less important, particularly for structures which tend to fail by local instability. The evaluation of elevated temperature properties must include the effects of previous temperature exposure, especially when the previous temperatures may have exceeded the aging temperature.

The following sections describe the procedures used to define the material properties for all test specimens. The temperature exposure histories and the structural temperature distributions are shown in the figures in Sec. 6.0. Summary tables of applicable element material properties are given for each of the elevated temperature test specimens.

Appendix A includes all curves for the tensile and compression coupons.

7.1 TENSION AND COMPRESSION COUPON DATA

In order to establish compatibility between the test specimens and the theoretical analysis, a separate coupon test program was initiated to determine the basic material properties of the specific aluminum alloy sheets used for specimen fabrication and to determine room and elevated temperature properties after exposure to an elevated temperature environment. Essentially the limited coupon program served three specific functions:

(a) The basic room temperature material properties were defined for 0.125 inch and 0.187 inch 7075-T6 bare sheet and 0.125 inch clad sheet.

(b) The recovery of material properties for the three thickness-material combinations was defined for a specific elevated temperature exposure history (theoretically, 2 hours at 350° and 1/2 hour at 450°F.).

(c) Compression coupons were taken from two tensile coupons and one box crippling specimen to verify the assumption that compression yield recovery was similar to tension yield recovery and to investigate the variation of properties with a variation in elevated temperature soaking time between the box specimens and test coupons.

The tensile coupon material properties data summary table is shown in Figure 7.1 where the yield stress is the conventional value defined by the 0.002 in./in. offset. The tensile coupon Ramberg-Osgood summary table is shown in Figure 7.2 where the three parameters for defining the analytical representation of the stress-strain curve are shown for each coupon. Figure 7.3 shows the material properties data and the Ramberg-Osgood data for the compression coupons. The individual tensile and compression coupon stress-strain curves as measured during the tests are shown in Figures A.1.1 through A.1.10 in Appendix A. Using these curves, the modulus of elasticity, the yield stress for $E_{sec} = 0.7E$, and the stress-strain curve shape factor were defined. The shape factor m was determined using two points on the stress-strain curve as described in Reference (f). Note that the maximum value shown for m (tension) or m (compression) is 40. This is the maximum value that can be handled by the Ramberg-Osgood stress-strain subroutine of the IBM 709 digital computer program used in this study. The errors introduced by this simplification are very small since the stress-strain curve with m = 40 has a very sharp knee in the yield region and considerably higher values of m produce only slight changes in the shape of the curve. The actual calculated values of m are shown for purposes of comparison. The difference in the shape factor m for tension and compression was considered by comparing the typical tension and compression stress-strain curves of Figure 3.2.7.1.6(a) of Reference (d).

The individual data points for the tensile and compression coupons are plotted in Figures 7.4 and 7.5 for the 0.002 in./in. offset yield stress and tensile ultimate, respectively. This coupon data is used in conjunction with the curves of Figures 7.11 and 7.13 to define test specimen element material properties.

Although the anticipated temperature-time history for the material recovery tensile coupons was 2 hours at 350°F. and 1/2 hour at 450°F., the actual temperature-time history as measured in the furnace was as shown in Figure 6.6. This temperature exposure history was used to calculate the Larson-Miller Parameters for the tensile coupons as shown in Section 7.2.2.

Details of the tensile and compression coupons and the methods of testing are described in Section 5.4.

FIGURE 7.1

TENSILE COUPON MATERIAL PROPERTIES DATA

Tensile Coupon No.	Material	Nominal Thickness, t, inches	Area, $Inches^2$	Temperature History	Test Temp. °F.	Modulus of Elasticity, E, psi	F_{ty}, (0.002 in./in. offset, psi	F_{tu}, psi
2-3	↓	0.187	0.09232	R.T.	R.T.	10.07×10^6	70750	79500
2-10	7075-T6	0.187	0.09166	R.T.	R.T.	9.77×10^6	72220	81100
1-10	Aluminum	0.187	0.09460	↓	R.T.	9.9×10^6	42150	57800
1-12	Alloy	0.187	0.09526	2 hrs. at	200	10.0×10^6	41750	47100
1-14	(Bare)	0.187	0.09507	350°F.; $\frac{1}{2}$ hr.	300	8.53×10^6	38700	38900
2-6	↓	0.187	0.09249	at 450°F.	350	7.38×10^6	33050	33600
2-13	↓	0.187	0.09351	↓	400	7.65×10^6	29670	29800
6-1	↓	0.125	0.06207	R.T.	R.T.	9.97×10^6	77000	82500
6-12	7075-T6	0.125	0.06060	R.T.	R.T.	10.07×10^6	77750	83300
5-5	Aluminum	0.125	0.06060	↓	R.T.	10.0×10^6	41500	56250
5-9	Alloy	0.125	0.06077	2 hrs. at	200	10.12×10^6	40250	47250
5-15	(Bare)	0.125	0.06124	350°F.; $\frac{1}{2}$ hr.	300	8.9×10^6	35200	35400
7-4	↓	0.125	0.06069	at 450°F.	350	7.6×10^6	32550	32700
7-10	↓	0.125	0.06104	↓	400	6.97×10^6	29530	29900
4-1	↓	0.125	0.06190	R.T.	R.T.	9.52×10^6	65150	73000
4-8	7075-T6	0.125	0.06167	R.T.	R.T.	9.83×10^6	65150	71750
4-7	Aluminum	0.125	0.06217	↓	R.T.	9.64×10^6	36750	51700
4-2	Alloy	0.125	0.06187	2 hrs. at	200	9.62×10^6	37100	43000
4-3	(Clad)	0.125	0.06214	350°F.; $\frac{1}{2}$ hr.	300	8.77×10^6	33050	33050
4-4	↓	0.125	0.06189	at 450°F.	350	8.3×10^6	29250	29250
4-5	↓	0.125	0.06165	↓	400	7.83×10^6	26500	26500
5-3	↓	0.125	0.06037	$\frac{1}{2}$ hr.at 450°F.	R.T.	10.04×10^6	50900	64300
6-7	7075-T6	0.125	0.06080	2 hrs.at 450°F.	R.T.	10.48×10^6	31930	51250
5-13	(Bare)	0.125	0.05996	6 hrs.at 450°F.	R.T.	10.0×10^6	29630	47300

FORM H 19-G-1

FIGURE 7.2

TENSILE COUPON RAMBERG-OSGOOD DATA

*Maximum value used for digital computer calculations

Tensile Coupon No.	Material	Nominal Thickness, t, inches	Modulus of Elasticity, E, psi	$(F_{ty})_{0.7E}$, psi	RAMBERG-OSGOOD SHAPE FACTORS		
					m (calculated)	m (tension)	m (compression)
2-3	7075-T6 Aluminum Alloy (Bare)	0.187	10.07×10^6	72100	28	28	13
2-10		0.187	9.77×10^6	73250	29	29	13
1-10		0.187	9.9×10^6	42250	68.7	40*	31
1-12		0.187	10.0×10^6	41500	46.6	40*	21
1-14		0.187	8.53×10^6	38650	76.8	40*	35
2-6		0.187	7.38×10^6	33050	28.5	28	13
2-13		0.187	7.65×10^6	29600	36.5	37	16
6-1		0.125	2.97×10^6	77500	172.5	40*	40*
6-12		0.125	10.07×10^6	78000	99	40*	40*
5-5		0.125	10.0×10^6	41600	32.7	32	15
5-9		0.125	10.12×10^6	40100	42.4	40*	19
5-15		0.125	8.9×10^6	35000	44.9	40*	20
7-4		0.125	7.6×10^6	32550	26.8	27	12
7-10		0.125	6.97×10^6	29500	26.7	27	12
4-1		0.125	9.52×10^6	66350	49.6	40*	22
4-8	7075-T6 Aluminum Alloy (Clad)	0.125	9.83×10^6	66200	56.5	40*	25
4-7		0.125	9.64×10^6	36500	33.9	34	15
4-2		0.125	9.62×10^6	36850	25.7	26	12
4-3		0.125	8.77×10^6	33000	84.2	40*	38
4-4		0.125	8.3×10^6	29250	27.9	28	13
4-5		0.125	7.83×10^6	26500	138.9	40*	40*
5-3		0.125	10.04×10^6	51000	36.8	37	17
6-7	7075-T6 (Bare)	0.125	10.48×10^6	34600	51.7	40*	18
5-18		0.125	10.0×10^6	29250	33	33	15

FORM H (5-6-)

FIGURE 7.3
COMPRESSION COUPON MATERIAL PROPERTIES AND
RAMBERG-OSGOOD DATA

MATERIAL PROPERTIES DATA

Compression Coupon No.	Material	Nominal Thickness, t, inches	Area, inches^2	Temperature History	Test Temp., °F.	Modulus of Elasticity, E, psi	F_{cy} (0.002 in./in. offset), psi
1-10-1	7075-T6 Bare	0.187	.0703	2 hrs.@ 350°F.; ½ hr. @ 450°F.	R.T.	10.3 x 10^6	43400
1-10-2		0.187	.0710		R.T.	10.0 x 10^6	44500
1-10-3		0.187	.0710		R.T.	10.0 x 10^6	43650
5-5-1		0.125	.0649		R.T.	9.8 x 10^6	40000
5-5-2		0.125	.0642		R.T.	10.2 x 10^6	41550
5-5-3		0.125	.0655		R.T.	9.8 x 10^6	40250
A-4-1		0.187	.0710	Refer to Fig. 6.6	R.T.	10.36 x 10^6	60300
A-4-2		0.187	.0714		R.T.	10.5 x 10^6	59500
A-4-3		0.125	.0469		R.T.	10.06 x 10^6	55850
A-4-4		0.125	.0470		R.T.	9.86 x 10^6	52350

RAMBERG-OSGOOD DATA

Compression Coupon No.	Material	Nominal Thickness, t, inches	Modulus of Elasticity, E, psi	$(F_{cy})_{0.7E}$, psi	Ramberg-Osgood Exponent, m
1-10-1	7075-T6 Bare	0.187	10.1 x 10^6	43766	32
1-10-2					
1-10-3					
5-5-1		0.125	9.93 x 10^6	40200	13
5-5-2					
5-5-3					
A-4-1		0.187	10.43 x 10^6	60300	22
A-4-2					
A-4-3		0.125	9.96 x 10^6	51500	12
A-4-4					

H-18-G-1

7.2 COMPLEX TEMPERATURE EXPOSURE

The static tests and data evaluation of aluminum alloy structures may be affected considerably by previous temperature exposure histories whether the tests are performed at elevated temperature or are simulated at room temperature. In either case it is necessary to know the net material properties if permanent set, yield, and ultimate test data are to be interpreted correctly. These temperature exposure histories may be produced by several factors depending upon whether the test is performed at elevated temperature or is simulated at room temperature. First, if the elevated temperature test is to be performed, the use of elevated temperature strain gages requires curing at high temperatures for specific times. These temperatures, may, in some cases, be beyond the aging temperature of the material and produce permanent losses of material properties which must be accounted for. Second, the flight mission temperature-time histories must be allowed for either by simulation or by actually heating and cooling the structure for various periods of time. Finally, the actual test temperature-time history and structural temperature distribution add to the complexity of the temperature exposure history. The problems are much more pronounced with aluminum alloy and are highly dependent on the actual temperatures involved in each of the aforementioned factors.

The simulated elevated temperature test at room temperature precludes the use of high temperature curing for elevated temperature strain gages and eliminates this factor from consideration. However, the flight mission temperature-time history and the critical design condition structural temperature distribution must be included in the calculated elevated temperature load-deformation curve for each cross-section. The effects of these various temperature exposure histories are additive and some realistic accumulation procedure must be used to obtain a final net allowable stress for each element in the cross-section.

Since the material properties data in Ref. (d) is incomplete from a recovery standpoint the procedures of Ref. (e) were investigated and appear to work quite well.

7.2.1 ACCUMULATION PROCEDURE FOR COMPLEX TEMPERATURE HISTORIES

The use of a time-temperature exposure parameter such as the Larson-Miller Parameter where

$$L.M. = T(C + \log t)$$

to define the strength of aluminum alloys at any temperature after exposure to a given time-temperature environment has been successfully demonstrated by Reference (e). The specific thermal exposure curves for 7075-T6 aluminum alloy (Figures 1 and 6 of Reference (e) are replotted in Figures 7.4 and 7.5 of this report showing the correlation between North American Aviation, Inc. tensile and compressive coupon data and the curves from Reference (e) where the specific Larson-Miller Parameter is

$$L.M. = T(16.5 + \log t)$$

Refer to Reference (e) for the determination of the material constant for 7075-T6 aluminum alloy, C = 16.5. Considering the normal scatter of elevated temperature coupon data when complex temperature histories are involved, the correlation was considered sufficiently accurate to allow the use of Figures 7.4 and 7.5 for defining the element material properties of the bending, crippling, and long column specimens of this program.

Since the test specimens had a wide variety of temperature exposure histories which included various combinations of strain gage curing and test temperature histories, an accumulation procedure is required to accurately define the final value of the Larson-Miller Parameter for each structural element in the test specimen cross-section. Reference (e) essentially indicates two distinctly different processes which may be used to determine design strength after exposure to a complex thermal environment. The conversion process of Section 3.3 of Reference (e) and the use of a reference temperature, $T_{ref.}$, as outlined in Section 4.1 of Reference (e) may be sufficiently accurate for many cases, but may have some limitations, depending upon the particular time temperature history. Previous studies by North American Aviation, Inc. (Columbus Division) have indicated that the net recovery of material properties is not only a function of time and temperature accumulation, but is very probably a function of the order in which the time-temperature increments are applied. The summation of equivalent times at some reference temperature does not allow for the order of the time-temperature increments. The studies performed by the Columbus Division of North American Aviation, Inc. have shown that by reversing the order of two specific time-temperature increments, it is possible to obtain two distinctly different values of the material property recovery factor. Reference (e) has made a valuable contribution to the solution of the material property recovery problem in the use of the Larson-Miller Parameter. However, it is believed that insufficient evidence is available to establish the use of equivalent time at some reference temperature for complex exposure histories. Therefore, the procedures of Reference (e) were slightly modified to account for the order of time-temperature increments in defining the material properties for analysis of the test specimens.

The accumulation procedure used is essentially that described in Section 3.3 of Reference (e) where the first increment time and temperature are converted to an equivalent time at the temperature of the second increment. The time at the second increment temperature is added to the equivalent time from the first increment to obtain a net equivalent time at the second increment temperature. This net equivalent time is converted to a new equivalent time at the temperature of the third time-temperature increment and the actual time at the third increment temperature is added to obtain the total equivalent time at the third increment temperature. This procedure is continued for as many finite time-temperature increments as necessary to define the time-temperature exposure of any structural element. The significance of this extension of the procedures of Section 3.3 of Reference (e) lies in the fact that the time-temperature increments are considered in the order in which they actually occur. The conversion to an equivalent time in each case is performed as described in Reference (e), using Figure 7.4 or 7.5 (Figure 1 or 6 of Reference (e)). The net result of this accumulation procedure is an equivalent time at the final (or test) temperature whereby the net Larson-Miller Parameter is readily calculated using this time and temperature.

The calculations to determine the Larson-Miller Parameters for the structural elements of the test specimens and the tensile coupons are shown in Section 7.2.2.

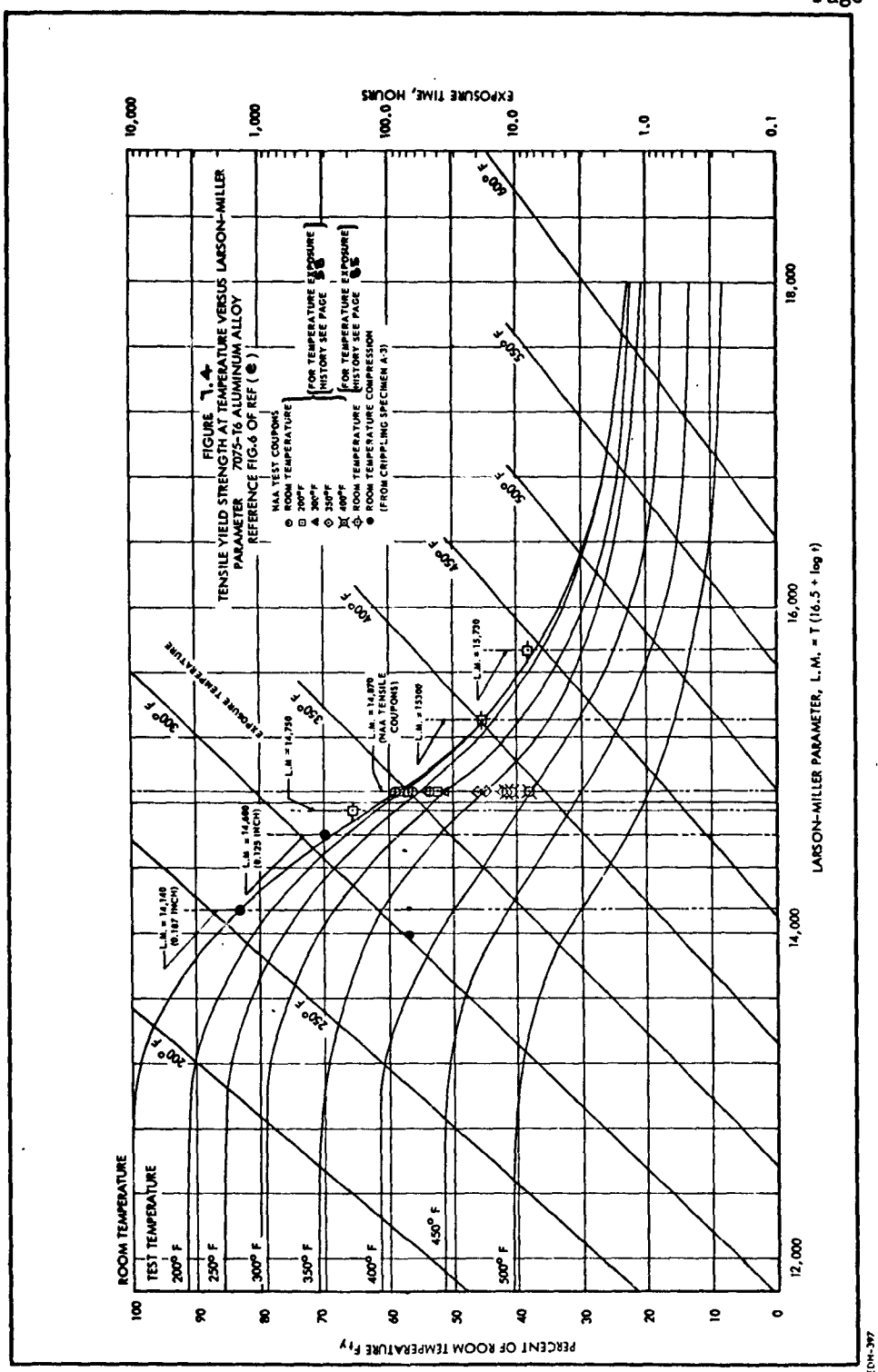
FIGURE 7.4
TENSILE YIELD STRENGTH AT TEMPERATURE VERSUS LARSON-MILLER PARAMETER
7075-16 ALUMINUM ALLOY
REFERENCE FIG.6 OF REF ( )
NAA TEST COUPONS
ROOM TEMPERATURE
200°F
300°F
350°F
400°F
(FOR TEMPERATURE EXPOSURE HISTORY SEE PAGE)
ROOM TEMPERATURE
ROOM TEMPERATURE COMPRESSION
(FROM CRIPPLING SPECIMEN A-3)
(FOR TEMPERATURE EXPOSURE HISTORY SEE PAGE)
EXPOSURE TEMPERATURE
EXPOSURE TIME, HOURS
10,000
1,000
100.0
10.0
1.0
0.1
600° F
550° F
500° F
450° F
400° F
350° F
300° F
L.M. = 15,730
L.M. = 14,870
(NAA TENSILE COUPONS)
L.M. = 15300
L.M. = 14,750
L.M. = 14,440
(0.125 INCH)
L.M. = 14,240
(0.187 INCH)
250° F
200° F
ROOM TEMPERATURE
TEST TEMPERATURE
200° F
250° F
300° F
350° F
400° F
450° F
500° F
100
90
80
70
60
50
40
30
20
10
0
PERCENT OF ROOM TEMPERATURE Fty
18,000
16,000
14,000
12,000
LARSON-MILLER PARAMETER, L.M. = T (16.5 + log t)
EDH-397

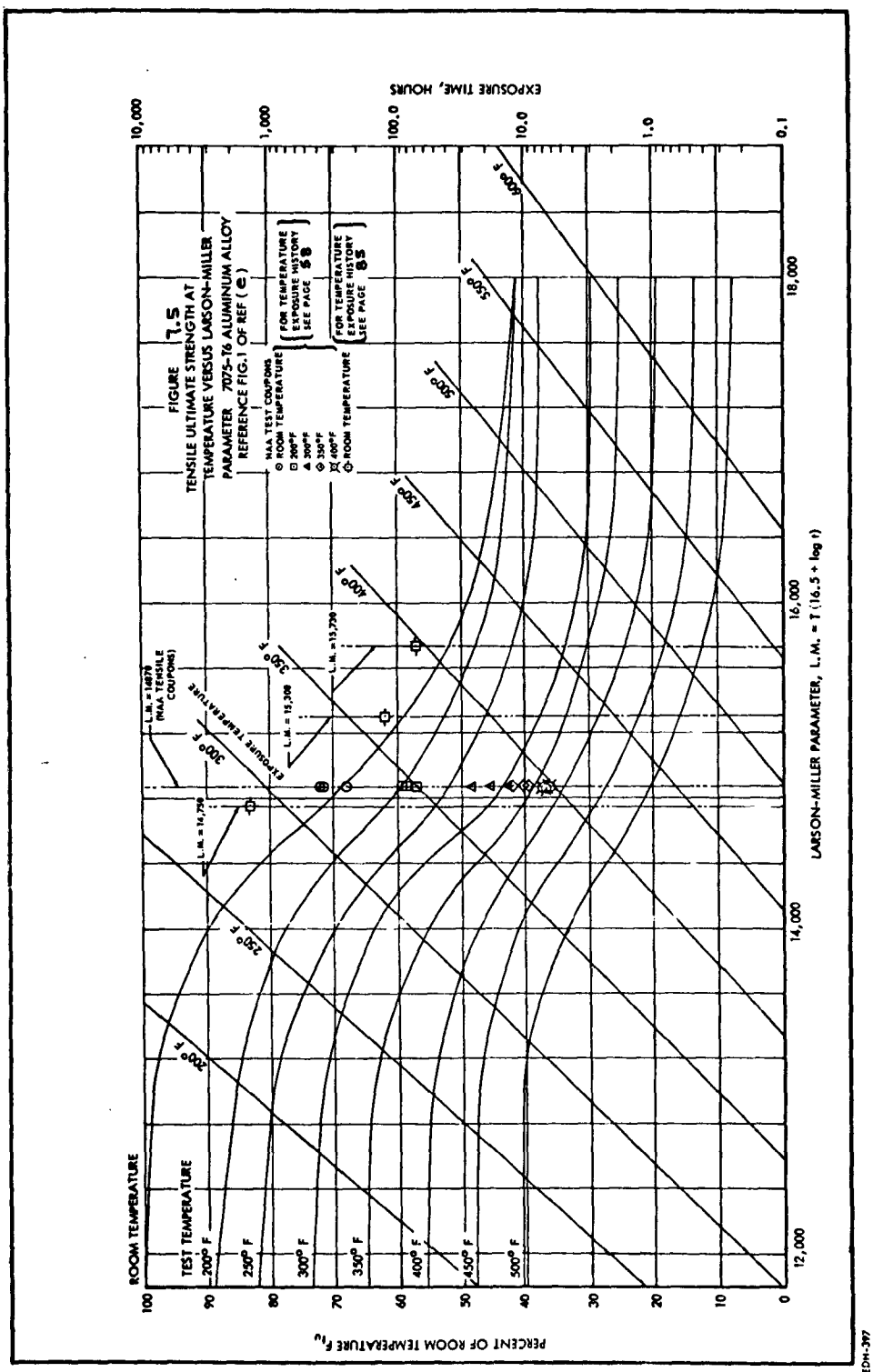
FIGURE 7.5
TENSILE ULTIMATE STRENGTH AT TEMPERATURE VERSUS LARSON-MILLER PARAMETER 7075-T6 ALUMINUM ALLOY
REFERENCE FIG. 1 OF REF (e)
NAA TEST COUPONS
ROOM TEMPERATURE
200°F
300°F
350°F
400°F
ROOM TEMPERATURE
FOR TEMPERATURE EXPOSURE HISTORY SEE PAGE 84
FOR TEMPERATURE EXPOSURE HISTORY SEE PAGE 85
EXPOSURE TIME, HOURS
10,000
1,000
100.0
10.0
1.0
0.1
ROOM TEMPERATURE
TEST TEMPERATURE
200° F
250° F
300° F
350° F
400° F
450° F
500° F
PERCENT OF ROOM TEMPERATURE F_{tu}
100
90
80
70
60
50
40
30
20
10
0
12,000
14,000
16,000
18,000
LARSON-MILLER PARAMETER, L.M. = T (16.5 + log t)
L.M. = 14879 (NAA TENSILE COUPONS)
L.M. = 14,750
L.M. = 15,300
L.M. = 15,750
EXPOSURE TEMPERATURE
EDH-397

7.2.2 DETERMINATION OF LARSON-MILLER PARAMETERS

For bending specimens B-3 through B-8 the strain gage curing temperature exposure history shown in Fig. 6.6 is divided into the following temperature-time increments.

22 min. @ 325°F. = 0.367 hr. @ 325°F.
108 min. @ 370°F. = 1.8 hrs. @ 370°F.
6.5 min. @ 400°F. = 0.109 hr. @ 400°F.
13.5 min. @ 450°F. = 0.225 hr. @ 450°F.
18 min. @ 475°F. = 0.3 hr. @ 475°F.

Using the above data the accumulation of time at temperature is defined by the methods of Ref. (e) and Sec. 7.2.1 to determine the equivalent time at the final temperature of 475°F.

0.367 hr. @ 325°F. =

.047 hr. @ 370°F.
1.800 hr. @ 370°F.
1.847 hr. @ 370°F. =

.062 hr. @ 400°F.
.109 hr. @ 400°F.
.171 hr. @ 400°F. =

.023 hr. @ 450°F.
.225 hr. @ 450°F.
.248 hr. @ 450°F. =

.040 hr. @ 475°F.
.300 hr. @ 475°F.

Equivalent time at final temperature = .340 hr. @ 475°F.

The Larson-Miller Parameter for 0.340 hr. @ 475°F. is obtained from Fig. 7.4 or 7.5, or calculated by L.M. = T(16.5 + log t) = 935 (16.5 + log 0.340) = 15000. This value of the Larson-Miller Parameter is used for all structural elements in bending specimens B-3 through B-8 which are unaffected by subsequent elevated temperature exposure during the test. Specimens B-4, B-5, and B-8 are entirely unaffected by the test temperature exposure since the maximum temperature at the middle of the cover plates is 250°F.

For those test specimens exposed to 450°F. during the performance of the test the additional temperature-time accumulation for the 450°F. elements and the associated Larson-Miller Parameters are calculated as follows.

Specimen No. B-3

The total temperature-time exposure history beginning with the net accrued strain gage curing exposure history is: 0.340 hr. @ 475°F.; 0.072 hr. @ 350°F.; 0.232 hr. @ 450°F.

where the last two increments are from Fig. 6.7. The second temperature-time interval of 0.072 hr. @ 350°F. is negligible and is not included in the accumulation calculations.

From Sec. 7.2.1,

0.340 hr. @ 475°F. = 0.950 hr. @ 450°F.
0.232 hr. @ 450°F.
Equivalent time at final temperature= 1.182 hr. @ 450°F.

The Larson-Miller Parameter for the 450°F. elements of B-3 is found from Fig. 7.4 or 7.5, or calculated to be
L.M. = 910 (16.5 + log 1.182) = 15100

The Larson-Miller Parameter for all other elements in the cross-section must then be between the values of 15000 and 15100.

Specimen No. B-6

The total temperature-time exposure history beginning with the net accrued strain gage curing exposure history is: 0.340 hr. @ 475°F.; 0.037 hr. @ 350°F.; 0.273 hr. @ 450°F. where the last two increments are from Fig. 6.7. The second temperature-time interval of 0.037 hr. @ 350°F. is not included in the accumulation calculations. From Sec. 7.2.1,

0.340 hr. @ 475°F. = 0.950 hr. @ 450°F.
0.273 hr. @ 450°F.
Equivalent time at final temperature = 1.223 hr. @ 450°F.

The Larson-Miller Parameter for the 450°F. elements of B-6 is found from Fig. 7.4 or 7.5, or calculated to be
L.M. = 910(16.5 + log 1.223) = 15120

The Larson-Miller Parameters for all other elements in the cross-section lie between the values of 15000 and 15120.

Specimen No. B-7

The total temperature-time exposure history beginning with the net accrued strain gage curing exposure history is: 0.340 hr. @ 475°F.; 0.047 hr. @ 350°F.; 0.208 hr. @ 450°F. where the last two increments are from Fig. 6.7 and the second increment of 0.047 hr. @ 350°F. is neglected in the accumulation calculations. From Sec. 7.2.1,

0.340 hr. @ 475°F. = 0.950 hr. @ 450°F.
0.208 hr. @ 450°F.
Equivalent time at final temperature = 1.158 hr. @ 450°F.

The Larson-Miller Parameter for the 450°F. elements of B-7 is found from Fig. 7.4 or 7.5, or calculated to be
L.M. = 910(16.5 + log 1.158) = 15070

The Larson-Miller Parameters for all other elements in the cross-section lie between 15000 and 15070.

Using these Larson-Miller Parameters and the test temperature distributions in Sec. 6.0 the material properties are obtained from the curves in Sec. 7.2.3 and summarized for all elements in each test specimen in Sec. 7.3.

For crippling specimens A-3 through A-6 the strain gage curing temperature exposure history of Fig. 6.6 is divided into the following temperature time increments.

15 min. @ 300°F. = 0.25 hr. @ 300°F.
113 min. @ 350°F. = 1.883 hrs. @ 350°F.
7 min. @ 375°F. = 0.117 hr. @ 375°F.
20 min. @ 425°F. = 0.333 hr. @ 425°F.
16 min. @ 450°F. = 0.267 hr. @ 450°F.

The equivalent time at the final temperature of 450°F. is defined by the methods of Ref. (e) and Sec. 7.2.1 as for the bending specimens.

0.25 hr. @ 300°F. =

.025 hr. @ 350°F.
1.883 hr. @ 350°F.
1.908 hr. @ 350°F. =

0.55 hr. @ 375°F.
0.117 hr. @ 375°F.
0.667 hr. @ 375°F. =

0.08 hr. @ 425°F.
0.333 hr. @ 425°F.
0.413 hr. @ 425°F. =

0.140 hr. @ 450°F.
0.267 hr. @ 450°F.

Equivalent time at final temperature = 0.407 hr. @ 450°F.

The Larson-Miller Parameter for 0.407 hr. @ 450°F. is calculated by L.M. = 910(16.5 + log 0.407) = 14660. However, compression coupons taken directly from A-4 (Fig. A.10) compared with the curves of Fig. 7.4 indicate that a value of L.M. = 14600 is more realistic for the 0.125 inch cover plates. The temperature exposure history of Fig. 6.6 was obtained by thermocouples on the 0.125 inch cover plates indicating, at least, favorable agreement between coupon data and the use of the Larson-Miller Parameter. Coupons taken from the 0.187 inch channel webs indicated a much higher yield stress than expected for the temperature exposure history of Fig. 6.6. Investigation

indicated the probable cause to be a lag in the temperature-time diagram and less time at the maximum temperature for the thicker material. The coupon data from Fig. A.1.10 is plotted in Fig.7.4 and indicates that a value of L.M. = 14140 is more realistic for the 0.187 inch channel elements. For reasons of material property compatibility between test specimens, and analysis and coupon data availability, the material properties for analysis were based on L.M. = 14600 for the 0.125 inch cover plates and L.M. = 14140 for the 0.187 inch channel elements. These values of the Larson-Miller Parameter were used for all structural elements in crippling specimens A-3 through A-6 which were unaffected by subsequent elevated temperature exposure during testing. Specimens A-4 and A-5 were entirely unaffected by test temperature exposure since the maximum test temperature was 250°F. Resultant material properties for A-4 and A-5 are summarized in Tables 1 and 2 of Fig. 7.15.

For specimen A-3 the intersection of L.M. = 14600 with the exposure temperature line of 450°F. indicates an equivalent time of 0.35 hr. at 450°F. for the strain gage curing alone. Beginning with this equivalent time at temperature and adding the test temperature exposure history of Fig. 6.8, the total temperature exposure history is expressed by the following increments for elements 1 and 11 of specimen A-3. The temperature-time increments for the equivalent strain gage curing and the test temperature exposure history of Fig. 6.8 are:

0.35 hr. @ 450°F.; 0.083 hr. @ 425°F.; 0.35 hr. @ 425°F. = 0.35 hr. @ 450°F. and 0.433 hr. @ 425°F.

0.35 hr. @ 450°F. = 1.000 hr. @ 425°F.
0.433 hr. @ 425°F.
Equivalent time at final temperature = 1.433 hr. @ 425°F.

The Larson-Miller Parameter for elements 1 and 11 for 1.433 hr. @ 425°F. is
L.M. = 885(16.5 + log 1.433) = 14750

The Larson-Miller Parameters for all other elements are determined in an identical manner, the material properties obtained from Figures 7.12 and 7.13 and the results summarized in Table 3 of Fig. 7.15.

For specimen A-6 the equivalent time at temperature for strain gage curing of the 0.125 inch cover plate is identical to that for specimen A-3 (0.35 hr. @ 450°F.). Beginning with this value and adding the test temperature exposure history of Fig.6.9 for element 1 the total temperature exposure history for element 1 is:

0.35 hr. @ 450°F.; 0.10 hr. @ 425°F.; 0.40 hr. @ 425°F. = 0.35 hr. @ 450°F. and 0.500 hr. @ 425°F.

0.35 hr. @ 450°F. = 1.000 hr. @ 425°F.
0.500 hr. @ 425°F.
Equivalent time at final temperature = 1.500 hr. @ 425°F.

The Larson-Miller Parameter for element 1 is
L.M. = 885(16.5 + log 1.500) = 14760

The Larson-Miller Parameters for all other elements are determined in an identical manner, depending upon the test temperatures and the material properties obtained from Figures 7.12 and 7.13. The results are summarized in Table 4 of Figure 7.15.

Long column specimens C-3 and C-4 utilized no elevated temperature strain gages and did not have a strain gage curing temperature history. In addition, the test temperature exposure history for these two specimens was a maximum of 1/2 hour at 250°F. Therefore, the conventional short time (1/2 hour) material properties can be used. For consistency, the material property factors were taken from Figures 7.12 and 7.13 for L.M. = 11800. The material properties for these two specimens are summarized in Tables 1 and 2 of Figure 7.16.

Long column specimen C-5 had no strain gage curing temperature history and the test temperature history was as shown in Figure 6.10 for the critical 7075-T6 (clad) cover plate elements. For elements 1 and 9 of specimen C-5, the total temperature exposure history can be expressed as a single increment of 9 minutes at 450°F. = 0.15 hour at 450°F. The Larson-Miller Parameter is

L.M. = 910(16.5 + log 0.15) = 14260

The coolest element in the cross-section is element 5 at 380°F. and the Larson-Miller Parameter is

L.M. = 840(16.5 + log 0.15) = 13150

All other elements in the cross-section have values between L.M. = 14260 and L.M. = 13150, which may vary according to the test temperature. The material properties are obtained from the curves of Section 7.2.3 and the results summarized in Table 3 of Figure 7.16 in Section 7.3.

Long column specimen C-6 had no strain gage curing temperature history, and the test temperature history was as shown in Figure 6.10. For element 1, a single increment of 12 minutes at 450°F. is used to represent the total temperature-time history. The Larson-Miller Parameter for element 1 is

L.M. = 910(16.5 + log 0.2) = 14375

The coolest element above the aging temperature of 250°F. is element 4 with T = 318°F. The Larson-Miller Parameter is

L.M. = 778(16.5 + log 0.2) = 12300

Elements 2 and 3 will have values between L.M. = 14375 and L.M. = 12300, while elements 5 through 9 have L.M. = 11800 (conventional short time properties). The material properties are obtained from the curves of Section 7.2.3 and the results summarized in Table 4 of Figure 7.16 in Section 7.3.

For those tensile coupons with a theoretical temperature exposure history of 2 hours at 350°F. and 1/2 hour at 450°F., the actual history is shown in Figure 6.6 and is represented by the following two increments.

134 minutes @ 350°F. = 2.23 hours @ 350°F.
40 minutes @ 450°F. = 0.67 hours @ 450°F.

Applying the accumulation procedures of Reference (e) and Section 7.2.1,

2.23 hours @ 350°F. = 0.033 hr. @ 450°F.
0.670 hr. @ 450°F.
Equivalent time at final temperature = 0.703 hr. @ 450°F.

The Larson-Miller Parameter for use with Figure 7.4 is

L.M. = 910(16.5 + log 0.703) = 14870

For tensile coupons 5-3, 6-7, and 5-18, with 1/2 hour at 450°F., 2 hours at 450°F., and 6 hours at 450°F., respectively, the Larson-Miller Parameters are as follow:

Coupon 5-3

L.M. = 910(16.5 + log 0.5) = 14750

Coupon 6-7

L.M. = 910(16.5 + log 2.0) = 15300

Coupon 5-18

L.M. = 910(16.5 + log 6.0) = 15730

The compression coupons from the tensile coupons have the same Larson-Miller Parameter as the tensile coupon. The compression coupons from crippling Specimen A-4 are described on Pages 82 and 83.

The Larson-Miller Parameters for all 450°F. thermal cycling specimens are shown in Figures 7.6 through 7.11. These values were calculated as for the bending specimens using the temperature exposure histories of Figure 6.11. Values are shown for each cycle in the temperature-load sequence since the material properties were continually varying. The effect of these varying properties must be allowed for in order to evaluate whether true thermal cycling is occurring or if any strain accumulation is predominantly due to lower stress-strain curves at each cycle. For the Larson-Miller Parameters shown the material properties are obtained from the curves of Section 7.2.3 and summarized in Tables 1 through 7 of Figure 7.17.

FIGURE 7.6

SUMMARY — LARSON-MILLER PARAMETERS FOR COVER PLATE ELEMENTS 1 AND 11 OF THERMAL CYCLING SPECIMEN NO. B-16, 450°F. SYMMETRICAL TEMPERATURE DISTRIBUTION

Temperature Cycle	LARSON-MILLER PARAMETER		
	M_{ap} =116300 (Test)	M_{ap} =124 000 (Test)	M_{ap} = 135000 (Test)
1	14120	15000	15220
2	14400	15040	15230
3	14600	15080	15260
4	14670	15130	15270
5	14740	—	15280
6	14830	—	—

FIGURE 7.7

SUMMARY — LARSON-MILLER PARAMETERS FOR COVER PLATE ELEMENTS 1 AND 11 OF THERMAL CYCLING SPECIMEN NO. B-12, 450°F. SYMMETRICAL TEMPERATURE DISTRIBUTION
M_{ap} = 168,500 (Test)

Temperature Cycle	LARSON-MILLER PARAMETER
1	15030
2	15050
3	15070
4	15090
5	15100
6	15120

FIGURE 7.8
SUMMARY — LARSON-MILLER PARAMETERS FOR STRUCTURAL ELEMENTS OF THERMAL CYCLING SPECIMEN NO. B-10, 450°F. UNSYMMETRICAL TEMPERATURE DISTRIBUTION (MAXIMUM TEMPERATURE ON TENSION SIDE)

ELEMENT NO.	LARSON-MILLER PARAMETER						
	1st Cycle	2nd Cycle	3rd Cycle	4th Cycle	5th Cycle	6th Cycle	7th Cycle
1	15070	15080	15100	15100	15120	15130	15170
2	13840	13870	13880	13900	13910	13920	13950
3	13400	13420	13440	13450	13470	13475	13500
4	12910	12920	12930	12950	12970	12975	13000
5	11800*	←				→	11800*
6	↓						↓
7							
8							
9							
10							
11	11800	←				→	11800

FIGURE 7.9
SUMMARY — LARSON-MILLER PARAMETERS FOR STRUCTURAL ELEMENTS OF THERMAL CYCLING SPECIMEN NO. B-15, 450°F. UNSYMMETRICAL TEMPERATURE DISTRIBUTION (MAXIMUM TEMPERATURE ON TENSION SIDE)

ELEMENT NO.	LARSON-MILLER PARAMETER						
	1st Cycle	2nd Cycle	3rd Cycle	4th Cycle	5th Cycle	6th Cycle	7th Cycle
1	15070	15080	15100	15100	15120	15130	15170
2	13810	13830	13850	13860	13880	13900	13920
3	13430	13450	13475	13480	13500	13500	13530
4	12980	13000	13030	13030	13050	13060	13080
5	11800*	←				→	11800*
6	↓						↓
7							
8							
9							
10							
11	11800*	←				→	11800

* Minimum value shown in Figures 7.4 and 7.5.

FIGURE 7.10
SUMMARY - LARSON-MILLER PARAMETERS FOR STRUCTURAL ELEMENTS OF THERMAL CYCLING SPECIMEN NO. B-9, 450°F. UNSYMMETRICAL TEMPERATURE DISTRIBUTION (MAXIMUM TEMPERATURE ON COMPRESSION SIDE)

ELEMENT NO.	LARSON-MILLER PARAMETER						
	1st Cycle	2nd Cycle	3rd Cycle	4th Cycle	5th Cycle	6th Cycle	7th Cycle
1	15070	15080	15100	15110	15120	15130	15175
2	13740	13750	13770	13780	13800	13810	13830
3	13320	13330	13350	13370	13380	13400	13420
4	12860	12870	12890	12900	12920	12930	12950
5	11800*						11800*
6							
7							
8							
9							
10							
11	11800*						11800*

* Minimum value shown in Figures 7.4 and 7.5.

FIGURE 7.11

SUMMARY - LARSON-MILLER PARAMETERS FOR STRUCTURAL ELEMENTS OF THERMAL CYCLING SPECIMEN NO. B-14, 450°F. UNSYMMETRICAL TEMPERATURE DISTRIBUTION (MAXIMUM TEMPERATURE ON COMPRESSION SIDE)

ELEMENT NO.	LARSON-MILLER PARAMETER						
	1st Cycle	2nd Cycle	3rd Cycle	4th Cycle	5th Cycle	6th Cycle	7th Cycle
1	15070	15080	15100	15110	15120	15140	15170
2	13900	13920	13930	13950	13965	13975	14000
3	13500	13500	13520	13530	13550	13560	13580
4	13030	13040	13050	13060	13080	13090	13110
5	11800*				11800*	11810	11830
6							11800*
7							
8							
9							
10							
11	11800*						11800*

* Minimum value shown in Figures 7.4 and 7.5.

7.2.3 MATERIAL PROPERTY CURVES

For the analysis portion of this study, the strain design procedures of Section 3.0 require certain material property values to define the structural element stress-strain curves in terms of the Ramberg-Osgood equation. These values are the yield stress at $E_{sec} = 0.7E$ defined by $(F_y)_{0.7E}$, the modulus of elasticity defined by E, the ultimate stress cut-off defined by F_{tu} and the shape factor m. Figure 7.12 shows $\%(F_{ty})_{0.7E}$ versus temperature and $\%F_{tu}$ versus temperature for various values of the Larson-Miller Parameter as calculated in Section 7.2.2. These curves are a cross-plot of the data in Figures 7.4 and 7.5. The compression yield stress is assumed equal to the tension yield stress and the recovery of compression properties is assumed identical to the recovery of tensile properties.

Figure 7.13 shows modulus of elasticity versus temperature for 7075-T6 aluminum alloy (bare and clad sheet) as determined by the tensile coupon data of Section 7.1. For purposes of comparison, the curves from Reference (d) are also plotted in Figure 7.13. Note that generally good agreement was obtained between the clad coupon data and Reference (d). The bare coupon data indicates somewhat lower values of E at $T \geq 300^{\circ}F$. than Reference (d). For purposes of analysis, the tensile coupon curves were used to define E to represent the straight line portion of the stress-strain curve. The recovery of the modulus of elasticity is unaffected by previous temperature exposure histories, and the exposure history given in Figure 7.13 is listed as a reference only.

No curves are shown for shape factor versus temperature, since Reference (d) and the tensile coupon data indicate considerable variation and randomness. The non-dimensional stress-strain curve represented by the Ramberg-Osgood equation is actually quite insensitive to the higher values of m ($m > 20$) such as those shown by the tensile coupon data. Therefore, the values of m for any particular structural element were estimated from the table in Figure 7.2 for the thickness, material, and test temperature of the element. This is sufficiently accurate for analysis since only small deviations occur in the critical yield portion of the curve, and particularly since many of the structural elements in the test specimens used a compression yield stress cut-off rather than an ultimate cut-off.

7.2.3 MATERIAL PROPERTY CURVES

For the analysis portion of this study, the strain design procedures of Section 3.0 require certain material property values to define the structural element stress-strain curves in terms of the Ramberg-Osgood equation. These values are the yield stress at $E_{sec} = 0.7E$ defined by $(F_y)_{0.7E}$, the modulus of elasticity defined by E, the ultimate stress cut-off defined by F_{tu} and the shape factor m. Figure 7.12 shows $\%(F_{ty})_{0.7E}$ versus temperature and $\%F_{tu}$ versus temperature for various values of the Larson-Miller Parameter as calculated in Section 7.2.2. These curves are a cross-plot of the data in Figures 7.4 and 7.5. The compression yield stress is assumed equal to the tension yield stress and the recovery of compression properties is assumed identical to the recovery of tensile properties.

Figure 7.13 shows modulus of elasticity versus temperature for 7075-T6 aluminum alloy (bare and clad sheet) as determined by the tensile coupon data of Section 7.1. For purposes of comparison, the curves from Reference (d) are also plotted in Figure 7.13. Note that generally good agreement was obtained between the clad coupon data and Reference (d). The bare coupon data indicates somewhat lower values of E at $T \geq 300^{\circ}F$. than Reference (d). For purposes of analysis, the tensile coupon curves were used to define E to represent the straight line portion of the stress-strain curve. The recovery of the modulus of elasticity is unaffected by previous temperature exposure histories, and the exposure history given in Figure 7.13 is listed as a reference only.

No curves are shown for shape factor versus temperature, since Reference (d) and the tensile coupon data indicate considerable variation and randomness. The non-dimensional stress-strain curve represented by the Ramberg-Osgood equation is actually quite insensitive to the higher values of m ($m > 20$) such as those shown by the tensile coupon data. Therefore, the values of m for any particular structural element were estimated from the table in Figure 7.2 for the thickness, material, and test temperature of the element. This is sufficiently accurate for analysis since only small deviations occur in the critical yield portion of the curve, and particularly since many of the structural elements in the test specimens used a compression yield stress cut-off rather than an ultimate cut-off.

FIGURE 7.12

MATERIAL PROPERTIES VARIATION WITH TEMPERATURE FOR SPECIFIC LARSON-MILLER VALUES (7075-T6 ALUMINUM ALLOY)

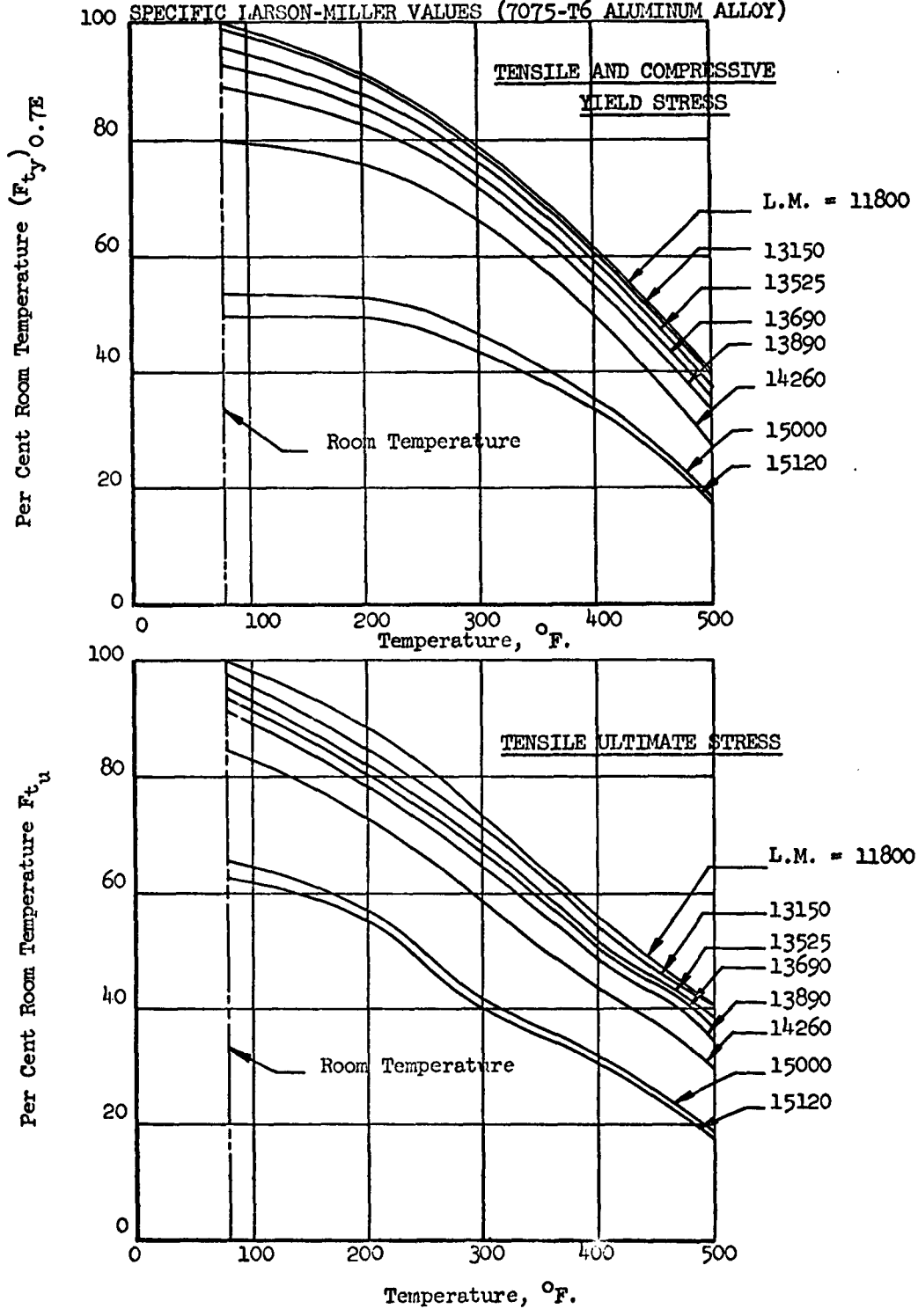

H-18-C-1

FIGURE 7.13

MATERIAL PROPERTIES VARIATION WITH TEMPERATURE
7075-T6 ALUMINUM ALLOY (BARE AND CLAD)

No Recovery Problem Produced by Previous Elevated Temperature Exposure. All Tensile Coupons had Previous Temperature Exposure History of 2 hours at 350°F. and 1/2 hr. at 450°F.

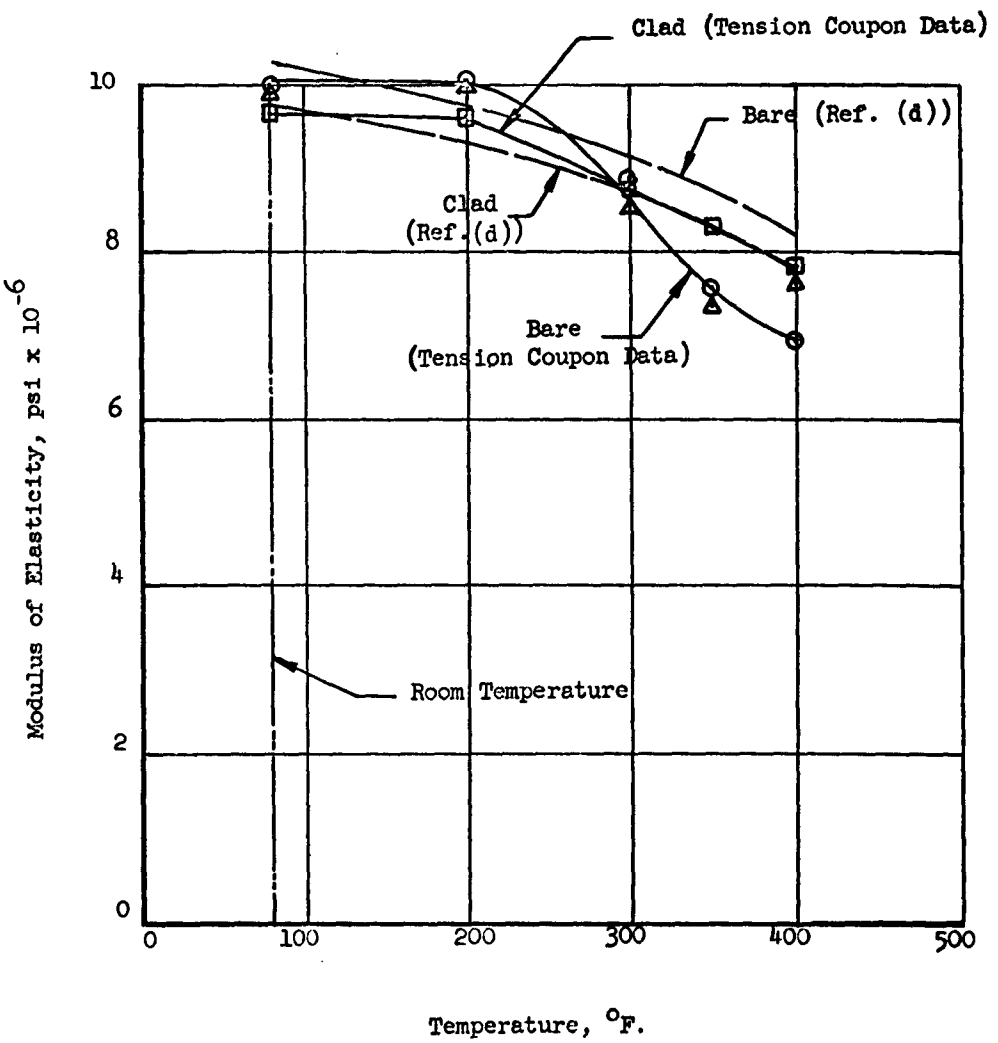

7.3 TABULATED TEST SPECIMEN ELEMENT DATA

The material properties summary tables for each test specimen are shown in the following figures. The bending, short column (crippling), long column, and thermal cycling specimens are shown in that order. These tables essentially summarize the material property data required to analytically represent the element stress-strain curves by the Ramberg-Osgood equation (3.3.6). The tables indicate considerable variation in material properties depending upon the test temperature and the temperature-time exposure histories.

This data was used as the input data for the IBM 709 digital computer program to define the analytical load-deformation curves of Section 8.0. The data for all room temperature specimens is not tabulated in this section, since the basic room temperature properties from tensile coupon data were used for all room temperature structural elements. No significant temperature-time exposure history was required for curing the high elongation strain gage bonding, therefore, no permanent loss of room temperature material properties was incurred.

FIGURE 7.14
BENDING SPECIMEN MATERIAL PROPERTIES SUMMARY
TABLE 1 - SPECIMEN NO. B-4 (250°F., SYMMETRICAL GRADIENT)

ELEMENT NO.	TEST TEMP., °F.	TEMP. HISTORY	t, INCHES	$(Fy)_{0.7E}$, psi (Room Temp)	L.M. PARAMETER	% $(Ft_y)_{R.T.}$	Fy, psi	Ft_u, psi (Room Temp)	% $(Ft_u)_{R.T.}$	Ft_u, psi	E psi x 10^{-6}	RAMBERG-OSGOOD EXPONENT, m
1	250	STRAIN GAGE CURING (FIG. 6.6)	0.125	77750	15000	.510	39650	82900	.500	41450	9.6	19*
2	220		0.125	77750		.522	40600	82900	.545	45200	9.9	19*
3	207		0.187	72675		.527	38250	80300	.560	45000	10.0	21*
4	195					.530	38500		.575	46200	10.02	21*
5	175					.531	38550		.595	47700	10.04	24*
6	175					.531	38550		.594	47700	10.04	24*
7	178					.531	38550		.590	47400	10.04	40
8	203					.528	38350		.565	45400	10.0	40
9	213		0.187	72675		.526	38200	80300	.553	44450	9.95	40
10	223		0.125	77750		.522	40600	82900	.540	44750	9.9	40
11	250		0.125	77750	15000	.510	39650	82900	.500	41450	9.6	40

* Compression m estimated from Figure 7.2.

FIGURE 7.14

TABLE 2 - SPECIMEN NO. B-5 (250°F. ON TENSION SIDE, UNSYMMETRICAL GRADIENT)

ELEMENT NO.	TEST TEMP., °F.	TEMP. HISTORY	t, INCHES	$(F_y)_{0.7E}$ psi (Room Temp.)	L.M. PARAMETER	% $(F_{t_y})_{R.T.}$	F_y, psi	F_{t_u}, psi (Room Temp.)	% $(F_{t_u})_{R.T.}$	F_{t_u}, psi	E psi x 10^{-6}	RAMBERG-OSGOOD EXPONENT, m
1	250	STRAIN GAGE CURING (FIG. 6.6)	0.125	77750	15000	.510	39650	82900	.500	41450	9.6	40
2	207		0.125	77750		.527	41000	82900	.560	46450	10.0	40
3	190		0.187	72675		.530	38500	80300	.580	46600	10.03	40
4	175					.531	38550		.596	47900	10.05	40
5	133					.532	38600		.627	50350		40
6	115					.534	38800		.637	51200		30*
7	107					.534	38800		.640	51450		30*
8	100					.534	38800		.645	51800		30*
9	100		0.187	72675		.534	38800	80300	.645	51800		30*
10	100		0.125	77750		.534	41500	82900	.645	53500		15*
11	100		0.125	77750	15000	.534	41500	82900	.645	53500	10.05	15*

* Compression m estimated from Figure 7.2.

FIGURE 7.14

TABLE 3 - SPECIMEN NO. B-8 (250°F. ON COMPRESSION SIDE, UNSYMMETRICAL GRADIENT)

ELEMENT NO.	TEST TEMP., °F.	TEMP. HISTORY	t, INCHES	$(Fy)_{0.7E}$, psi (Room Temp.)	L.M. PARAMETER	$\%\ (Ft_y)_{R.T.}$	Fy, psi	Ft_u, psi (Room Temp.)	$\%\ (Ft_u)_{R.T.}$	Ft_u, psi	E psi x 10^{-6}	RAMBERG-OSGOOD EXPONENT, m
1	250	STRAIN GAGE CURING (FIG. 6.6)	0.125	77750	15000	.510	39650	82900	.500	41450	9.6	19*
2	220		0.125	77750		.522	40600	82900	.545	45200	9.9	19*
3	212		0.187	72675		.525	38150	80300	.555	44600	10.0	21*
4	202					.528	38350		.567	45550	10.0	21*
5	163					.532	38400		.602	48350	10.05	24*
6	150					.532	38400		.615	49400		24*
7	145					.532	38400		.620	49800		40
8	142					.532	38400		.620	49800		40
9	140		0.187	72675		.532	38400	80300	.622	50000		40
10	140		0.125	77750		.532	41300	82900	.622	51550		40
11	140		0.125	77750	15000	.532	41300	82900	.622	51550	10.05	40

* Compression m estimated from Figure 7.2.

FIGURE 7.14

TABLE 4 - SPECIMEN NO. B-3 (450° SYMMETRICAL GRADIENT)

ELEMENT NO.	TEST TEMP., °F.	TEMP. HISTORY	t, INCHES	$(Fy)_{0.7E}$, psi (Room Temp)	L.M. PARAMETER	% (Ft_y) R.T.	F_y psi	Ft_u, psi (Room Temp.)	% (Ft_u) R.T.	Ft_u, psi	E psi x 10^{-6}	RAMBERG-OSGOOD EXPONENT, m
1	450	STRAIN GAGE CURING (FIG. 6.6) TEST TEMP. HISTORY (FIG. 6.7)	0.125	77750	15100	.265	20600	82900	.248	20550	6.8	12*
2	370		0.125	77750	15060	.380	29550	82900	.342	28350	7.3	12*
3	345		0.187	72675	15050	.408	29650	80300	.363	29200	7.7	13*
4	327				15030	.430	31250		.383	30800	8.0	24*
5	290				15025	.468	34000		.428	34400	8.9	34*
6	280				15020	.478	34750		.441	35400	9.1	32*
7	280				15020	.478	34750		.441	35400	9.1	40
8	322				15030	.437	31750		.390	31350	8.1	34
9	350		0.187	72675	15050	.405	29450	80300	.360	28950	7.6	28
10	380		0.125	77750	15060	.368	28650	82900	.332	27550	7.2	27
11	450		0.125	77750	15100	.265	20600	82900	.248	20550	6.8	27

* Compression m estimated from Figure 7.2.

FIGURE 7.14

TABLE 5 - SPECIMEN NO. B-7 (450° ON TENSION SIDE, UNSYMMETRICAL GRADIENT)

ELEMENT NO.	TEST TEMP., °F.	TEMP. HISTORY	t, INCHES	$(F_y)_{0.7E}$, psi (Room Temp.)	L.M. PARAMETER	% $(Ft_y)_{R.T.}$	F_y, psi	Ft_u, psi (Room Temp.)	% $(Ft_u)_{R.T.}$	Ft_u, psi	E psi x 10^{-6}	RAMBERG-OSGOOD EXPONENT, m
1	450	STRAIN GAGE CURING (FIG. 6.6) / TEST TEMP. HISTORY (FIG. 6.7)	0.125	77750	15070	.272	21150	82900	.250	20700	6.8	27
2	333		0.125	77750	15050	.420	32650	82900	.374	31000	7.9	33
3	293		0.187	72675	15025	.467	33900	80300	.420	33750	8.82	40
4	262				15000	.500	36300		.475	38200	9.4	40
5	185					.530	38500		.585	47000	10.02	40
6	155					.531	38600		.610	49000	10.05	23*
7	138					.533	38800		.623	50100		28*
8	128					.533	38800		.630	50600		29*
9	127		0.187	72675		.533	38800	80300	.630	50600		29*
10	125		0.125	77750		.534	41500	82900	.631	52300		16*
11	125		0.125	77750	15000	.534	41500	82900	.631	52300	10.05	16*

* Compression m estimated from Figure 7.2.

FIGURE 7.14

TABLE 6 - SPECIMEN NO. B-6 (450° ON COMPRESSION SIDE, UNSYMMETRICAL GRADIENT)

ELEMENT NO.	TEST TEMP., °F.	TEMP. HISTORY	t, INCHES	$(F_y)_{0.7E}$, psi (Room Temp)	L.M. PARAMETER	% (F_{t_y}) R.T.	F_y, psi	F_{t_u}, psi, (Room Temp)	% (F_{t_u}) R.T.	F_{t_u}, psi	E psi x 10^{-6}	RAMBERG-OSGOOD EXPONENT, m
1	450	STRAIN GAGE CURING (FIG. 6.6) / TEST TEMP. HISTORY (FIG. 6.7)	0.125	77750	15120	.262	20400	82900	.243	20150	6.8	12*
2	370		0.125	77750	15090	.373	29000	82900	.338	28000	7.3	12*
3	350		0.187	72675	15060	.400	29050	80300	.358	28800	7.6	13*
4	330				15030	.427	31000		.380	30550	7.95	13*
5	255				15000	.504	36600		.488	39250	9.5	28*
6	230					.520	37800		.530	42600	9.8	28*
7	217					.524	38100		.550	44200	9.9	40
8	203					.528	38400		.567	45600	10.0	40
9	200		0.187	72675		.530	38500	80300	.570	45800	10.0	40
10	197		0.125	77750		.530	41200	82900	.573	47500	10.0	40
11	197		0.125	77750	15000	.530	41200	82900	.573	47500	10.0	40

* Compression m estimated from Figure 7.2.

FIGURE 7.15
SHORT COLUMN (CRIPPLING) SPECIMEN MATERIAL PROPERTIES SUMMARY
TABLE 1 - SPECIMEN NO. A-4 (250°F., SYMMETRICAL GRADIENT)

ELEMENT NO.	TEST TEMP., °F.	TEMP. HISTORY	t, INCHES	$(F_y)_{0.7E}$, psi (Room Temp.)	L.M. PARAMETER	$(Ft_y)_{R.T.}$	F_y, psi	E, psi	RAMBERG-OSGOOD EXPONENT, m
1	250	STRAIN GAGE CURING (FIG. 6.6)	0.125	77750	14600	.633	49200	9.6×10^6	20
2	240		0.125	77750	14600	.642	49900	$9.7 \times$	20
3	225		0.187	72675	14140	.766	55650	$9.87 \times$	21
4	213					.773	56150	$9.95 \times$	21
5	183					.790	57350	$10.02 \times$	21
6	175					.794	57650	$10.05 \times$	21
7	183					.790	57350	$10.02 \times$	21
8	213					.773	56150	$9.95 \times$	21
9	227		0.187	72675	14140	.763	55400	$9.87 \times$	21
10	240		0.125	77750	14600	.642	49900	$9.7 \times$	20
11	250		0.125	77750	14600	.633	49200	9.6×10^6	20

FIGURE 7.15
SHORT COLUMN (CRIPPLING) SPECIMEN MATERIAL PROPERTIES
TABLE 2 - SPECIMEN NO. A-5 (250°F., UNSYMMETRICAL GRADIENT)

1	250	STRAIN GAGE CURING (FIG. 6.6)	0.125	77750	14600	.633	49200	9.6×10^6	20
2	222		0.125	77750	14600	.653	50770	$9.88 \times$	19
3	207		0.187	72675	14140	.777	56400	$9.99 \times$	21
4	193					.785	57000	$10.02 \times$	21
5	155					.803	58300	$10.05 \times$	21
6	133					.812	59000	$10.05 \times$	31
7	125					.816	59300	$10.05 \times$	31
8	118					.818	59400	$10.05 \times$	31
9	113		0.187	72675	14140	.820	59550	$10.05 \times$	31
10	108		0.125	77750	14600	.692	53750	$10.05 \times$	31
11	108		0.125	77750	14600	.692	53750	10.05×10^6	31

FIGURE 7.15
SHORT COLUMN (CRIPPLING) SPECIMEN MATERIAL PROPERTIES
TABLE 3 - SPECIMEN NO. A-3 (425°F., SYMMETRICAL GRADIENT)

ELEMENT NO.	TEST TEMP., °F.	TEMP. HISTORY	t, INCHES	$(F_y)_{0.7E}$, psi Room (Temp.)	L.M. PARAMETER	% (Ft_y) R.T.	F_y, psi	E, psi	RAMBERG-OSGOOD EXPONENT, m
1	425	STRAIN GAGE CURING TEST TEMP. HISTORY (FIGS. 6.6 AND 6.8)	0.125	77750	14750	0.36	28000	6.95×10^6	12
2	353		0.125	77750	14600	0.513	39900	7.5	12
3	323		0.187	72675	14160	0.646	47000	8.1	35
4	297		↑	↑	14150	0.688	50000	8.75	35
5	233		↓	↓	14140	0.759	55200	9.78	21
6	220				14140	0.769	55900	9.9	21
7	236				14140	0.757	55000	9.78	21
8	302				14150	0.68	49400	8.75	35
9	326		0.187	72675	14160	0.641	46600	8.1	35
10	352		0.125	77750	14600	0.517	39900	7.5	12
11	425		0.125	77750	14750	0.36	28000	6.95×10^6	12

TABLE 4 - SPECIMEN NO. A-6 (425°F., UNSYMMETRICAL GRADIENT)

1	425	STRAIN GAGE CURING TEST TEMP. HISTORY (FIGS. 6.6 AND 6.9)	0.125	77750	14760	0.36	28000	6.95×10^6	12
2	343		0.125	77750	14600	0.529	41200	7.7	12
3	318		0.187	72675	14160	0.652	47300	8.2	35
4	295		↑	↑	14150	0.69	50100	8.78	35
5	222		↓	↓	14140	0.768	55800	9.9	21
6	188				↑	0.788	57300	10.02	21
7	165				↓	0.800	58100	10.05	21
8	135					0.812	59000	10.05	31
9	127		0.187	72675	14140	0.815	59200	10.05	31
10	118		0.125	77750	14600	0.692	53750	10.05	31
11	118		0.125	77750	14600	0.692	53750	10.05×10^6	31

FORM H-1-8-1

FIGURE 7.16
LONG COLUMN SPECIMEN MATERIAL PROPERTIES SUMMARY
TABLE 1 - SPECIMEN NO. C-3 (250°F., SYMMETRICAL GRADIENT)

ELEMENT NO.	TEST TEMP., °F.	TEMP. HISTORY	t, INCHES	$(F_y)_{0.7E}$, psi (Room Temp.)	L.M. PARAMETER	$(F_{t_y})_{R.T.}^{\%}$	Fy, psi	F_{t_u}, psi (Room Temp.)	$(F_{t_u})_{R.T.}^{\%}$	F_{t_u}, psi	E psi x 10^{-6}	RAMBERG-OSGOOD EXPONENT, m
1*	250	NO PREVIOUS HISTORY	0.125	66275	11800**	.858	56900	72375	.825	59700	9.2	25≠
2*	240			66275		.870	57700	72375	.837	60600	9.3	25≠
3	237			77750		.873	67800	82900	.840	69700	9.74	20≠
4	233					.878	68300		.847	70250	9.76	20≠
5	227					.884	68700		.855	70900	9.84	20
6	235					.875	68000		.844	70000	9.76	20
7	238			77750		.872	67800	82900	.840	69700	9.74	20
8*	240			66275		.870	57700	72375	.837	60600	9.3	25
9*	250		0.125	66275	11800**	.858	56900	72375	.825	59700	9.2	25

FIGURE 7.16
LONG COLUMN SPECIMEN MATERIAL PROPERTIES SUMMARY
TABLE 2 - SPECIMEN NO. C-4 (250°F. UNSYMMETRICAL GRADIENT)

ELEMENT NO.	TEST TEMP., °F.	TEMP. HISTORY	t, INCHES	$(F_y)_{0.7E}$, psi (Room Temp.)	L.M. PARAMETER	$(F_{t_y})_{R.T.}^{\%}$	Fy, psi	F_{t_u}, psi (Room Temp.)	$(F_{t_u})_{R.T.}^{\%}$	F_{t_u}, psi	E psi x 10^{-6}	RAMBERG-OSGOOD EXPONENT m
1*	250	NO PREVIOUS HISTORY	0.125	66275	11800**	.858	56900	72375	.825	59700	9.2	25
2*	242			66275		.868	57600	72375	.837	60600	9.28	25
3	227			77750		.885	68750	82900	.856	71000	9.85	20
4	221					.892	69300		.863	71600	9.9	20
5	205					.908	70600		.882	73100	10.0	20
6	193					.918	71300		.898	74500	10.02	20≠
7	190			77750		.922	71700	82900	.900	74700	10.03	20≠
8*	187			66275		.926	61400	72375	.904	65400	9.62	20≠
9*	187		0.125	66275	11800**	.926	61400	72375	.904	65400	9.62	20≠

* Elements 1, 2, 8, and 9 are 7075-T6 Clad; Remaining elements are 7075-T6 Bare; ≠ Compression
** Lowest value shown on curves in Figures 7.4 and 7.5.

FIGURE 7.16
LONG COLUMN SPECIMEN MATERIAL PROPERTIES SUMMARY
TABLE 3 - SPECIMEN NO. C-5 (450°F., SYMMETRICAL GRADIENT)

ELEMENT NO.	TEST TEMP., °F.	TEMP. HISTORY	t, INCHES	$(F_y)_{0.7E}$, psi (Room Temp.)	L.M. PARAMETER	% $(Ft_y)_{R.T.}$	F_y, psi	Ft_u, psi (Room Temp.)	% $(Ft_u)_{R.T.}$	Ft_u, psi	E psi x 10^{-6}	RAMBERG-OSGOOD EXPONENT m
1*	450	TEST TEMP. HISTORY REF. FIG. 6.10	0.125	66275	14260	.394	26150	72375	.374	27050	7.18	35
2*	428			66275	13920	.491	32550	72375	.423	30600	7.48	35
3	416			77750	13730	.540	42000	82900	.480	39800	6.9	27
4	405				13550	.583	45300		.511	42400	6.98	27
5	380				13150	.644	50100		.579	48000	7.17	27
6	402				13500	.583	45300		.517	42800	6.98	12≠
7	411			77750	13650	.540	42000	82900	.488	40500	6.95	12≠
8*	425			66275	13860	.491	32550	72375	.450	30600	7.48	35≠
9*	450		0.125	66275	14260	.394	26150	72375	.374	27050	7.18	35≠

FIGURE 7.16
LONG COLUMN SPECIMEN MATERIAL PROPERTIES SUMMARY
TABLE 4 - SPECIMEN NO. C-6 (450°F., UNSYMMETRICAL GRADIENT)

ELEMENT NO.	TEST TEMP., °F.	TEMP. HISTORY	t, INCHES	$(F_y)_{0.7E}$, psi (Room Temp.)	L.M. PARAMETER	% $(Ft_y)_{R.T.}$	F_y, psi	Ft_u, psi (Room Temp.)	% $(Ft_u)_{R.T.}$	Ft_u, psi	E psi x 10^{-6}	RAMBERG-OSGOOD EXPONENT m
1*	450	TEST TEMP. HISTORY REF. FIG. 6.10	0.125	66275	14375	.377	25000	72375	.354	25600	7.18	35
2*	378			66275	13240	.650	43100	72375	.570	41250	8.03	31
3	344			77750	12700	.713	55400	82900	.652	54000	7.7	27
4	318				12300	.757	58800		.698	57800	8.2	35
5	253				11800**	.853	66300		.817	67750	9.53	35
6	234					.877	68200		.847	70250	9.78	19≠
7	231			77750		.880	68400	82900	.850	70500	9.8	19≠
8*	229			66275		.883	58600	72375	.853	61750	9.38	12≠
9*	229		0.125	66275	11800**	.883	58600	72375	.853	61750	9.38	12≠

* Elements 1, 2, 8, and 9 are 7075-T6 Clad; Remaining elements are 7075-T6 Bare; ≠ Compression

** Lowest value shown on curves in Figures 7.4 and 7.5.

FIGURE 7.17
THERMAL CYCLING SPECIMEN MATERIAL PROPERTIES SUMMARY
TABLE 1 - SPECIMEN NO. B-11 (250°F., SYMMETRICAL GRADIENT)

ELEMENT NO.	TEST TEMP., °F.	TEMP. HISTORY	t, INCHES	$(F_y)_{0.7E}$, psi (Room Temp.)	L.M. PARAMETER	$\%(F_{t_y})_{R.T.}$	F_y psi	F_{t_u}, psi Room Temp.	$\%(F_{t_u})_{R.T.}$	F_{t_u}, psi	E, psi 10^{-6}	RAMBERG-OSGOOD EXPONENT, m
1	250	TEST TEMPERATURE HISTORY ONLY APPROXIMATELY 34 MINUTES AT 250°F.	0.125	77750	11800*	.858	66750	82900	.824	68300	9.6	19**
2	222		0.125	77750		.890	69200	82900	.862	71500	9.9	19**
3	216		0.187	72675		.900	65350	80300	.870	69900	9.95	20**
4	207					.907	65900		.880	70700	10.0	21**
5	180					.930	67500		.912	73300	10.03	24**
6	172					.938	68100		.922	74100	10.03	24**
7	175					.937	68000		.918	73800	10.03	40
8	200					.913	66300		.890	71500	10.02	40
9	211		0.187	72675		.903	65600	80300	.877	70500	9.98	40
10	218		0.125	77750		.897	69750	82900	.867	71900	9.92	40
11	250		0.125	77750	11800*	.858	66750	82900	.824	68300	9.6	40

* Minimum value shown in Figures 7.4 and 7.5.
** Compression m estimated from Figure 7.2.

FIGURE 7.17
THERMAL CYCLING SPECIMEN MATERIAL PROPERTIES SUMMARY
TABLE 2 — SPECIMEN NO. B-16 (450°F., SYMMETRICAL GRADIENT)

ELEMENT NO.	TEST TEMP., °F.	TEMP. HISTORY	YIELD STRESS $(F_y)_{0.7E}$, psi							
			1st CYCLE	2nd CYCLE	3rd CYCLE	4th CYCLE	5th CYCLE	6th CYCLE	E, psi x 10^{-6}	m
1	450	TEST TEMP. HISTORY REF. FIG. 6.11	32300	28900	26420	25650	24900	23700	6.8	12
2	395		47400	46800	45250	44600	43700	43000	7.03	12
3	373		48100	47700	47500	47100	46750	46500	7.23	12
4	345		51800	51600	51400	51300	51300	51500	7.67	12
5	297		57750	57650	57400	57400	57400	57400	8.73	20
6	290		58400	58400	58400	58400	58400	58400	8.9	20
7	305		56800	56800	56800	56800	56800	56800	8.52	35
8	352		51100	50800	50800	50750	50600	50250	7.55	27
9	375		47800	47350	46850	46650	46500	46250	7.22	27
10	400		46650	45750	43550	42900	42100	41000	7.0	27
11	450		32300	28900	26420	25650	24900	23700	6.8	27
1	450	TEST TEMP. HISTORY REF. FIG. 6.11	21400	21250	20800	20200			6.8	12
2	395		40000	39550	39000	38500			7.03	12
3	373		44600	44250	43900	43600			7.23	12
4	345		51100	51000	50800	50600			7.67	12
5	297		57400	57300	57250	57200			8.73	20
6	290		58250	58200	58100	58100			8.9	20
7	305		56500	56400	56400	56300			8.52	35
8	352		49600	49500	49500	49400			7.55	27
9	375		43800	43500	43250	43000			7.22	27
10	400		38050	37600	37100	36700			7.0	27
11	450		21400	21250	20800	20200			6.8	27
1	450	TEST TEMP. HISTORY REF. FIG. 6.11	19450	19150	18900	18750	18670		6.8	12
2	395		37700	37400	37100	36800	36600		7.03	12
3	373		42500	42350	42250	42100	41900		7.23	12
4	345		50700	50600	50400	50300	50250		7.67	12
5	297		57500	57300	57300	57200	57200		8.73	20
6	290		58100	58100	58100	58100	58100		8.9	20
7	305		56500	56500	56500	56500	56500		8.52	35
8	352		49200	48900	48750	48500	48300		7.55	27
9	375		42250	42100	42000	41800	41700		7.22	27
10	400		35700	35400	35100	34950	34700		7.0	27
11	450		19450	19150	18900	18750	18670		6.8	27

Refer to Figure 8.33 for the three load levels applicable to the above three tables of material properties.

FIGURE 7.17

THERMAL CYCLING SPECIMEN MATERIAL PROPERTIES SUMMARY
TABLE 3 - SPECIMEN NO. B-12 (450°F., SYMMETRICAL GRADIENT)

ELEMENT NO.	TEST TEMP., °F.	TEMP. HISTORY	Yield Stress, $(F_y)_{0.7E}$, psi						E $psi \times 10^{-6}$	m
			1ST CYCLE	2ND CYCLE	3RD CYCLE	4TH CYCLE	5TH CYCLE	6TH CYCLE		
1	450	TEST TEMP. HISTORY REFER TO FIG. 6.11	21381	20992	20837	20603	20370	20215	6.8	12
2	405		36154	36154	35920	35765	35762	34987	7.0	12
3	387		39971	39971	39608	39608	38244	39244	7.15	12
4	373		43968	43968	43605	43460	43387	43242	7.25	12
5	325		54142	54142	54142	54142	54142	54142	8.05	20
6	310		57050	57050	57050	57050	57050	57050	8.4	20
7	314		56977	56977	56977	56977	56977	56977	8.3	35
8	350		49564	49419	42274	49200	49128	49055	7.6	27
9	370		45058	45058	44913	44695	44477	44331	7.3	27
10	385		44317	44317	43695	43695	43151	42762	7.1	27
11	450		21381	20992	20837	20603	20370	20215	6.8	27

FORM H-18-G-1

FIGURE 7.17
THERMAL CYCLING SPECIMEN MATERIAL PROPERTIES SUMMARY, TABLE 4 - SPECIMEN NO. B-10 (450°F., UNSYMMETRICAL GRADIENT, MAXIMUM TEMPERATURE ON TENSION SIDE)

Element No.	Test Temp., °F.	Temp. History	Yield Stress $(F_y)_{0.7E}$, psi							E, -6 psix10	m
			1st Cycle	2nd Cycle	3rd Cycle	4th Cycle	5th Cycle	6th Cycle	7th Cycle		
1	450	Test Temp. History Refer to Fig. 6.11	21000	20800	20700	20600	20400	20100	19830	6.8	27
2	377		46300	46100	45850	45650	45350	45200	45100	7.2	27
3	350		49500	49400	49300	49250	49200	49100	49000	7.6	28
4	320		54650	54600	—	—	—	54600	54500	8.15	35
5	237		63300	—	—	—	—	—	63300	9.78	40
6	200		66200	—	—	—	—	—	66200	10.02	21
7	175		68000	—	—	—	—	—	68000	10.03	24
8	158		68900	—	—	—	—	—	68900	10.05	26
9	155		69000	—	—	—	—	—	69000	10.05	26
10	150		74200	—	—	—	—	—	74200	10.05	17
11	150		74200	—	—	—	—	—	74200	10.05	17

FIGURE 7.17
THERMAL CYCLING SPECIMEN MATERIAL PROPERTIES SUMMARY, TABLE 5 - SPECIMEN NO. B-15 (450°F., UNSYMMETRICAL GRADIENT, MAXIMUM TEMPERATURE ON TENSION SIDE)

Element No.	Test Temp., °F.	Temp. History	Yield Stress $(F_y)_{0.7E}$, psi							E, psix10^{-6}	m
			1st Cycle	2nd Cycle	3rd Cycle	4th Cycle	5th Cycle	6th Cycle	7th Cycle		
1	450	Test Temp. History Refer to Fig. 6.11	21000	20800	20700	20600	20400	20100	19830	6.8	27
2	375		46650	46500	46350	46200	46000	45840	45750	7.22	27
3	352		49600	49500	49500	49450	49400	49300	49250	7.55	28
4	325		54000	53900	53900	53900	53800	53800	53750	8.05	34
5	245		62700						62700	9.65	40
6	215		65400						65400	9.95	24
7	200		66250						66250	10.02	21
8	190		67000						67000	10.03	22
9	187		67200						67200	10.03	23
10	185		72000						72000	10.03	18
11	185		72000						72000	10.03	18

FIGURE 7.17

THERMAL CYCLING SPECIMEN MATERIAL PROPERTIES SUMMARY, TABLE 6 - SPECIMEN NO. B-9 (450°F., UNSYMMETRICAL GRADIENT, MAXIMUM TEMPERATURE ON COMPRESSION SIDE)

Element No.	Test Temp., °F.	Temp. History	Yield Stress $(F_y)_{0.7E}$, psi							E, psix10^{-6}	m
			1st Cycle	2nd Cycle	3rd Cycle	4th Cycle	5th Cycle	6th Cycle	7th Cycle		
1	450	Test Temp. History Refer to Fig. 6.11	21000	20750	20500	20400	20350	20200	19750	6.8	12
2	370		48200	48100	48000	47900	47700	47600	47400	7.3	12
3	345		50600	50550	50500	50400	50300	50300	50250	7.7	13
4	317		55200	—	—	—	—	—	55200	8.22	28
5	240		63200	—	—	—	—	—	63200	9.7	27
6	210		65750	—	—	—	—	—	65750	9.98	23
7	190		67000	—	—	—	—	—	67000	10.03	35
8	173		68000	—	—	—	—	—	68000	10.05	35
9	168		68300	—	—	—	—	—	68300	10.05	35
10	165		73300	—	—	—	—	—	73300	10.05	35
11	165		73300	—	—	—	—	—	73300	10.05	35

FIGURE 7.17
THERMAL CYCLING SPECIMEN MATERIAL PROPERTIES SUMMARY, TABLE 7 - SPECIMEN NO. B-14 (450°F., UNSYMMETRICAL GRADIENT, MAXIMUM TEMPERATURE ON COMPRESSION SIDE)

Element No.	Test Temp., °F.	Temp. History	Yield Stress $(F_y)_{0.7E}$, psi							E, psix10^{-6}	m
			1st Cycle	2nd Cycle	3rd Cycle	4th Cycle	5th Cycle	6th Cycle	7th Cycle		
1	450	Test Temp. History Refer to Fig. 6.11	21000	20750	20450	20450	20350	20150	19800	6.8	12
2	380		45600	45400	45250	45000	44800	44600	44300	7.2	12
3	355		48300	48200	48200	48200	48100	48000	47900	7.5	13
4	327		53750	53750	53650	53650	53650	53600	53500	8.0	24
5	250		62250						62250	9.6	28
6	222		64650						64650	9.9	24
7	205		66100						66100	10.0	35
8	187		67200						67200	10.03	35
9	182		67500						67500	10.04	35
10	180		72500						72500	10.04	35
11	180		72500						72500	10.04	35

8.0 TEST-ANALYSIS COMPARISON

This section contains the evaluation of all strain data, unknown end restraint conditions and the comparison of analytical and experimental load-deformation curves. Sec. 8.1 describes the analysis of the strain data used to define, as nearly as possible, the critical buckling strains since edge restraint conditions are somewhat questionable and an over-conservative assumption would only unduly complicate the comparison between the test and calculated load-deformation curves. This investigation was carried out using strain data from room temperature bending and short column (crippling) specimens only. Section 8.2 is included to consider end restraint conditions as a separate item due to variations in the end moment restraints encountered during the tests of the long column and short column (crippling) specimens.

The performance of short column tests in a test machine may lead to unknown end moment conditions if unsymmetrical temperature gradients are present. Section 8.2.1 shows another possible use of calculated load-deformation data when used in conjunction with static test strain data. The original calculations for crippling specimen A-6 were performed assuming the cross-section to be restrained-in-bending at or near the ultimate load. However, this is not the correct moment restraint condition and the actual bending moment at any axial load level is unknown. Section 8.2.1 describes the complete analytical-experimental evaluation of the problem and attempts to define the bending moment variation with axial load from zero to failure.

As is usually the case with long column test specimens, the ideal pin-ended condition is very difficult to achieve in a test machine and some variation is to be expected. The analyses performed in Section 8.2.2 consider each of the long column specimens in terms of the test buckling load and indicate the probable end fixity value, c, for each of the specimens tested. These values of c were used in the analysis to obtain a comparative load-deformation curve for Section 8.3.3. The variation in end fixity between test specimens did not allow a comparison of test and analysis applied load ratios in Section 9.0 as for the bending and short column specimens. However, additional calculations were performed for each column specimen based

on a common value of end fixity of c = 1.25 and the table of long column applied load ratios in Section 9.0 is calculated on this basis. This allows some evaluation to be made considering only the variables associated with the temperature.

Section 8.3, in conjunction with Section 9.0, summarizes the results for the primary objective of this study. For proper simulation of the elevated temperature static test the complete load-deformation curve is important as well as the ultimate failing load. This is particularly true for the load-deformation curve with all load and temperature removed since this curve defines the permanent set characteristics of the structure and hence the allowable yield load. The experimental and analytical curves shown are based on the strain data of Appendix A and the procedures of Section 3.0, respectively. Most of the load-deformation curves shown are plotted for the temperature-load sequence +T, +P since this is compatible with the test conditions. Some calculated curves are shown in Section 8.3.1 to illustrate the use of the curves for the +T, +P, -P, -T sequence to define an applied load ratio at the 0.002 in./in. offset yield or any other permanent set criteria. In addition, these comparative curves tend to establish the validity of the analytical procedures of Section 3.0.

Detailed explanations of the bending, short column (crippling), long column, and thermal cycling specimens are given in Sections 8.3.1, 8.3.2, 8.3.3, and 8.3.4, respectively.

8.1 BUCKLING

Since edge restraint conditions on the compression cover have a considerable effect on the local buckling strain, the buckling coefficients were defined for the various test specimens using strain gage data from the room temperature bending and crippling specimens. The data is shown in Fig. 8.1 for the bending specimens and in Fig. 8.2 for the crippling specimens. The critical buckling strain is shown and has been defined as the average strain at the last recorded increment prior to a marked deviation from the initial elastic slope. This point denotes the strain at which the effective area of the compression cover begins to reduce. The value of e_{cr} obtained in this manner is used in Eq. (3.5.4) to define the effective area coefficient C_n for the compression covers. For digital computer calculations, the buckling coefficients are defined in the following sections for use in Eq. (3.5.1). This data was used in the analytical determination of the load-deformation curves for compatibility between test and analysis and to eliminate, insofar as possible, an unnecessary variable from the comparison of load-deformation curves. Although the buckling strains and the associated buckling coefficients were determined by using data from room temperature specimens, the same buckling coefficients were used for calculating the load-deformation curves of the elevated temperature specimens assuming that the compression cover edge restraint conditions did not vary appreciably from those at room temperature.

8.1.1 BENDING SPECIMEN BUCKLING COEFFICIENT

From specimen No. B-1 data in Fig. 8.1 , the critical buckling strain is $e_{cr} = -0.00283$ in./in. With b = 5 in. and t = 0.125 in. the buckling coefficient is

$$K = -e_{cr}\left(\frac{b}{t}\right)^2 = 0.00283\left(\frac{5}{0.125}\right)^2 = 4.525$$

From specimen No. B-17 data in Fig. 8.1 , the critical buckling strain is $e_{cr} = -0.00258$ in./in. With b = 5 in. and t = 0.125 in. the buckling coefficient is

$$K = -e_{cr}\left(\frac{b}{t}\right)^2 = 0.00258\left(\frac{5}{0.125}\right)^2 = 4.125$$

The average buckling coefficient for the two room temperature specimen compression covers is K = 4.325. This value was

used to define the critical buckling strain and effective area coefficient for the compression covers of all bending specimens. The calculated load-deformation curves of Section 8.2 reflect a degree of buckling at each load level which is consistent with K = 4.325. From Figure 14.25 of Ref. (i) this value indicates edge conditions between simply supported and clamped for a panel aspect ratio $a/b = 3$ (5 inches by 15 inches).

8.1.2 CRIPPLING SPECIMEN BUCKLING COEFFICIENT

For the room temperature specimens subjected to compression loads, strain data from both 0.125 inch covers was used to evaluate the buckling coefficient. For specimen No. A-1 in Figure 8.2, two values of the critical buckling strain are shown as defined by each pair of strain gages. From the curve, the critical buckling strains are $e_{cr} = -0.00254$ in./in. and $e_{cr} = -0.00356$ in./in. for which the buckling coefficients are K = 4.07 and K = 5.70, respectively. The average buckling coefficient for the two covers of specimen No. A-1 is K = 4.885. The strain data for specimen No. A-2 in Figure 8.2 is shown for a single pair of strain gages only (2 and 7). These two gages form the total width of the band with gages 5 and 8 between 2 and 7. In addition, gages 5 and 8 become non-linear at the same strain as 2 and 7 , therefore defining a single value of the critical buckling strain for both cover plates of specimen A-2. From the curve in Figure 8.2 $e_{cr} = -0.00307$ in./in. and the associated buckling coefficient is K = 4.915. The average buckling coefficient for both specimens is K = 4.90 which is quite close to the average value of K = 4.985 between simply supported (K = 3.62) and clamped (K = 6.35). For analytical definition of the load-deformation curves in Section 8.2, the buckling coefficient for the 0.125 in. covers was taken as K = 4.985.

8.1.3 LONG COLUMN BUCKLING COEFFICIENT

Since no local buckling of the 0.125 in. cover plates occurs prior to reaching the column buckling or Euler load, the local buckling problem is present only in the post-buckling stage when relatively high induced bending moments are present and the axial load on the column is somewhat less than the critical buckling load. With bending of primary importance when local buckling does occur, the local buckling coefficient of the 0.125 in. cover plates was taken as K = 4.325. This presumes that the edge restraint conditions for the beam-column (post-buckling) are identical to those of the bending specimens and is probably fairly realistic since local buckling in both types of specimens is produced by the same mode of loading; i.e., bending moment rather than a direct axial load.

8.1.4 THERMAL CYCLING SPECIMEN BUCKLING COEFFICIENT

The thermal cycling specimen test methods, test jigs, support points and restraints were identical to those used for the static bending specimens and, in the absence of measured strain data to evaluate the critical buckling strain, the buckling coefficients were assumed to be identical to those for the bending specimens. Sec. 8.1.1 shows an average K for calculation purposes of 4.325. This value was used to define the critical buckling strain and effective area coefficient for the compression covers of all thermal cycling specimens.

FIGURE 8.1

EXPERIMENTAL DETERMINATION OF

BUCKLING COEFFICIENT

(Bending Specimens)

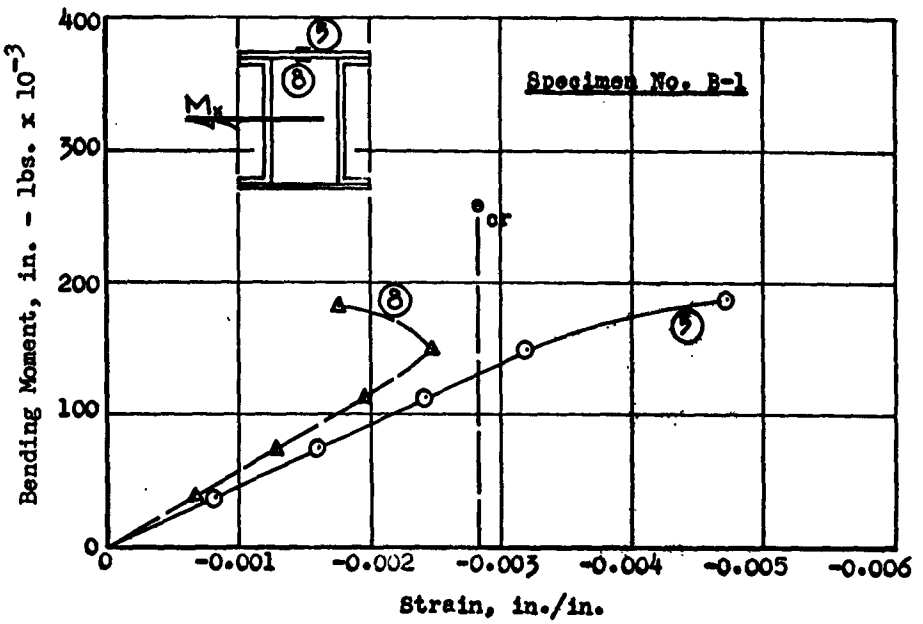

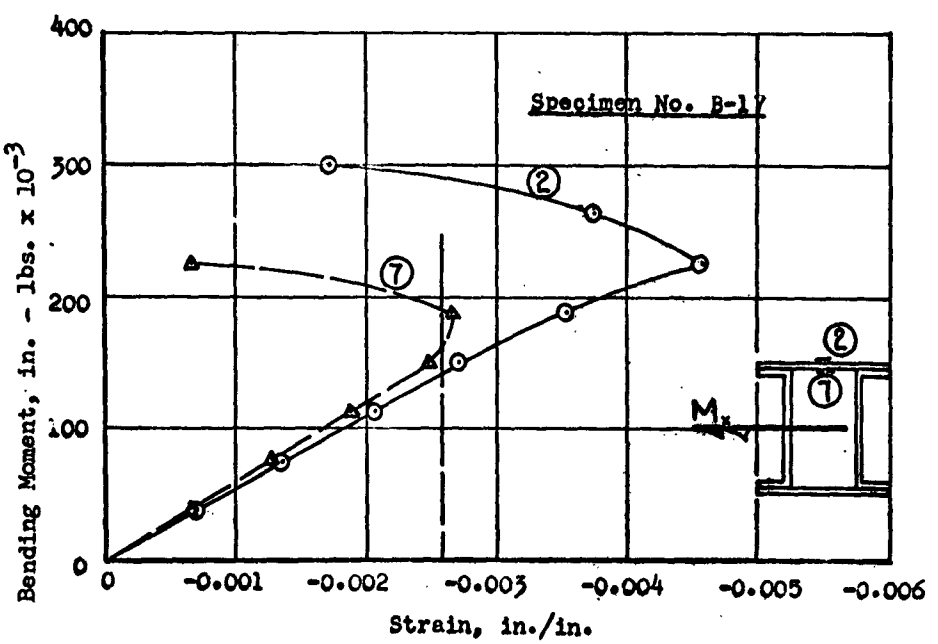

FIGURE 8.2

EXPERIMENTAL DETERMINATION OF BUCKLING COEFFICIENT

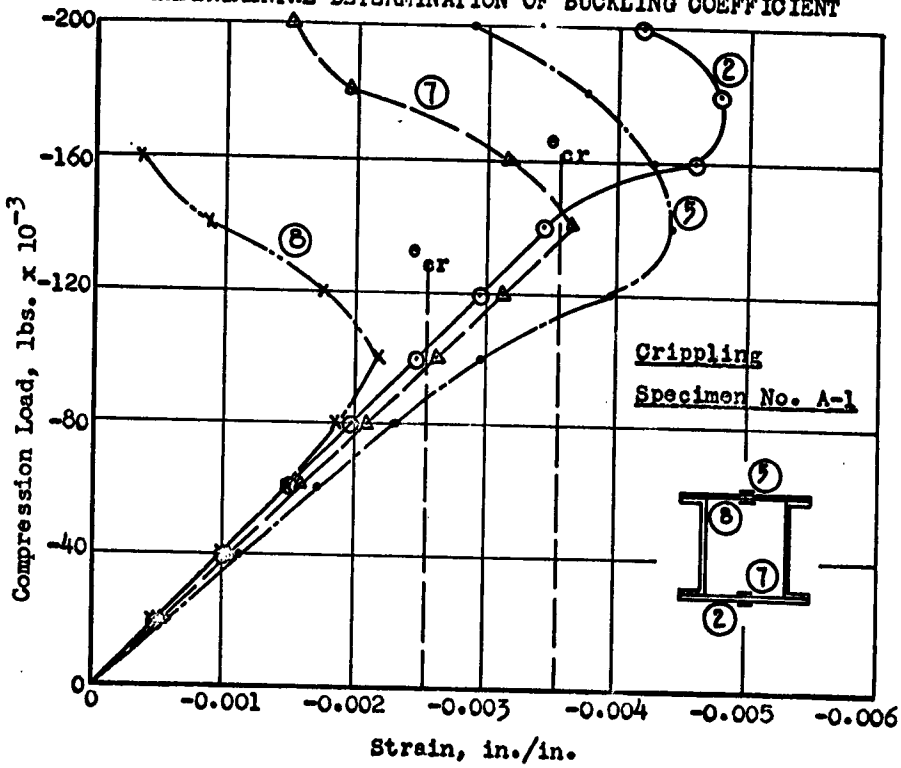

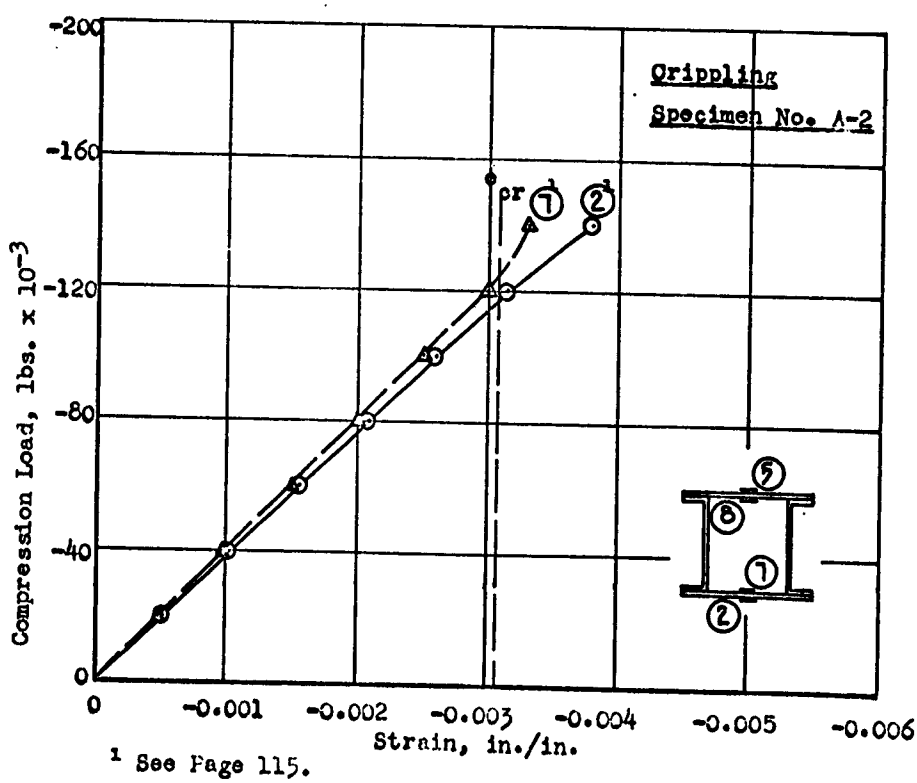

[1] See Page 115.

8.2 END RESTRAINT CONDITIONS

8.2.1 CRIPPLING SPECIMENS

For consistent test conditions on all crippling specimens, both room temperature and elevated temperature, no adapters or end fittings were used on the elevated temperature specimens with unsymmetrical temperature gradients present. The testing procedures for crippling specimens A-1 through A-6 are described in Section 5.0 . For specimens A-1 and A-2 at room temperature and specimens A-3 and A-4 with symmetrical temperature gradients, the flat and parallel end conditions necessary for testing in the Baldwin-Southwark testing machine were essentially maintained. However, specimens A-5 and A-6 with unsymmetrical temperature gradients were initially bowed by the temperature which rotated the plane of the cross-section and did not provide the flat and parallel surfaces necessary for a uniform applied strain distribution. Consequently, in both cases the expanded hot cover plate was loaded in compression before other elements in the cross-section. This indicates the presence of bending moments on the cross-section during the load application step. If this bending moment were supplied by a couple load, then this applied bending moment would have a maximum value of M_T when the couple had rotated the cross-section to its original unheated position. If the temperature gradient is very steep, then the rotational moment strain denoted by K_T may be produced by two moments; i.e., one an elastic applied bending moment where $M_{ap} \leq M_T$, and an inelastic moment, M_p, where $M_{ap} + M_p = M_T$. This latter case can arise if the rotational restraint strains are sufficiently large to produce buckling and/or inelastic stress-strain relationships. The above conditions are met only under true restrained-in-bending conditions where the rotational restraint is provided by a pure moment.

In the test machine, however, the bending moment on the cross-section is produced by an eccentric load which produces a variable moment throughout the load range from zero to failure. The bending moment introduced in this manner can reach a value considerably higher than the elastic thermal moment at some time during the load application. The value of this bending moment and the variation of the moment depend upon a number of factors. Among these are the cross-section

geometry of the test specimen, the temperature distribution through the cross-section, material properties variation through the cross-section, buckling, and inelastic stress-strain relationships. These factors establish the degree of eccentricity during load application by affecting the point of load application and shift of the elastic neutral axis.

For purposes of calculating the load-deformation characteristics of specimens A-5 and A-6 for a temperature-load sequence of +T, +P, it was questionable whether the true restrained-in-bending case could be assumed at the +T step. This presumes that at any applied load level the total rotational strain is equal to the thermal moment rotational strain defined by K_T whether elastic or inelastic. This assumption was made in the calculations for specimen A-5 which had a temperature differential of approximately 100°F. between the two cover plates. Evaluation of the test data and comparison of calculated and experimental load-deformation curves for specimen A-5 (Fig. 8.20, page 152) showed the assumption to be reasonable in this particular case, even if not entirely correct throughout the load range. However, applying the same assumption to specimen A-6 which had a temperature differential of approximately 225°F. between the two cover plates over-predicted the peak, or failing, load by a considerable margin. A comparison of calculated and experimental strain data indicated the presence of considerably higher bending moments than would be present in the true restrained-in-bending case.

To investigate this problem further, the test strain data obtained from extensometers was used in conjunction with the digital computer methods of Section 3.0 to determine the bending moment variation during load application. The end restraint conditions were changed from restrained-in-bending to unrestrained at the temperature application step (+T) of the temperature-load sequence in the calculations. At the load application step (+P) of the temperature-load sequence the calculations were performed using a series of applied axial loads and bending moments to obtain element strain data and interaction load-deformation curves for various combinations of axial load and bending moment. To ensure compatibility throughout, considering the sensitivity of strain measurements at the higher loads, the measured strain data was compared with the calculated interaction strain data by two different criteria.

Assuming the extensometer data from Figure A.3.14 to be compatible as to strain differential between the extreme fiber elements (0.125 inch cover plates, elements 1 and 11, page 36) the cross-section slope, or rotational restraint, is shown in Figure 8.3 and is defined by

$$de/dh = \frac{e_5 - e_2}{y_1 - y_{11}}$$

where e_5 and e_2 are the strains from Appendix A for extensometer no's. 5 and 2, respectively. Extensometer No. 4 was not used in the evaluation due to erratic behavior in the low load regions and incompatibility with the remaining three extensometers. As shown in Appendix A , the data from extensometer 3 was very nearly identical to that of extensometer 2 so that the data from either could have been used. From the calculated interaction data, a family of load-rotational restraint curves is plotted in Figure 8.3 with bending moment as parameter. The intersections of these curves with the experimental curve define the bending moments present on the cross-section at each applied load to failure. Note that each calculated curve intersects the experimental curve at two points indicating that as the applied axial load is increased, the bending moment reaches a peak value and then begins to diminish as the axial load approaches ultimate. For the calculated curves in Figure 8.3 the rotational restraint is defined by

$$de/_{dh} = \frac{K_{apx} + \sum_j K_{px_j}}{c}$$

which includes both elastic and inelastic effects. The bending moment versus axial load curve (1) shown in Figure 8.5 is a plot of the intersections of the calculated and experimental curves and indicates a bending moment at the test failing load of approximately -32000 in. - lbs. It should also be noted that the peak bending moment is considerably above the elastic thermal moment of -69500 in. - lbs. whereas the bending moment at failure was considerably below the elastic thermal moment. In certain types of compression specimens, the bending moment may diminish to zero at the failing load; i.e., no column action or local buckling, and very ductile materials.

The bending moment variation during load application was also determined by comparing the strain data from extensometer 5 to the critical element strains from the calculated data where the calculated strains are defined by

$$e_1 = e_{ap} + \sum_j e_{p_j} + \left[K_{ap_x} + \left(\sum_j K_{px_j} \right) \right] \frac{y_1}{c}$$

with element 1 being the critical compression element. The experimental critical element strain data from extensometer 5 data (Appendix A) is shown in Figure 8.4 where the calculated interaction data with bending moment as parameter is also plotted in the form of a load-strain curve. Actually this data is identical to that shown in Figure 8.3 except for the change in the scale on the abscissa. The two procedures shown differ only in the specific use made of the experimental strain data. From the curves of Figure 8.5, the peak bending moments occur at very nearly the same axial load and differ in magnitude by only about 8%.

The difficulties encountered during this test and the subsequent evaluation of the problems emphasizes a primary problem of testing crippling specimens in a test machine or similar test fixture. In the elevated temperature case with an unsymmetrical temperature gradient through the cross-section, the test results could be considerably in error (approximately 30% in this case) toward the conservative side if the proper end restraint conditions are not duplicated. The eccentric load condition produced during the testing of specimen A-6 was not representative of an aircraft structure end restraint condition since the continuous type aircraft structure introduces a moment restraint which is adequately represented by the less critical restrained-in-bending case. Due to the difficulty of duplicating end restraint conditions in performing certain types of elevated temperature tests, it may well be that the room temperature tests and the comparative load-deformation approach may actually be more reliable in many cases than the elevated temperature test itself. In any case, the importance and the critical nature of the end restraint conditions cannot be over-emphasized particularly for very short columns where non-uniform temperature distributions are present and local instability (crippling) failures are involved.

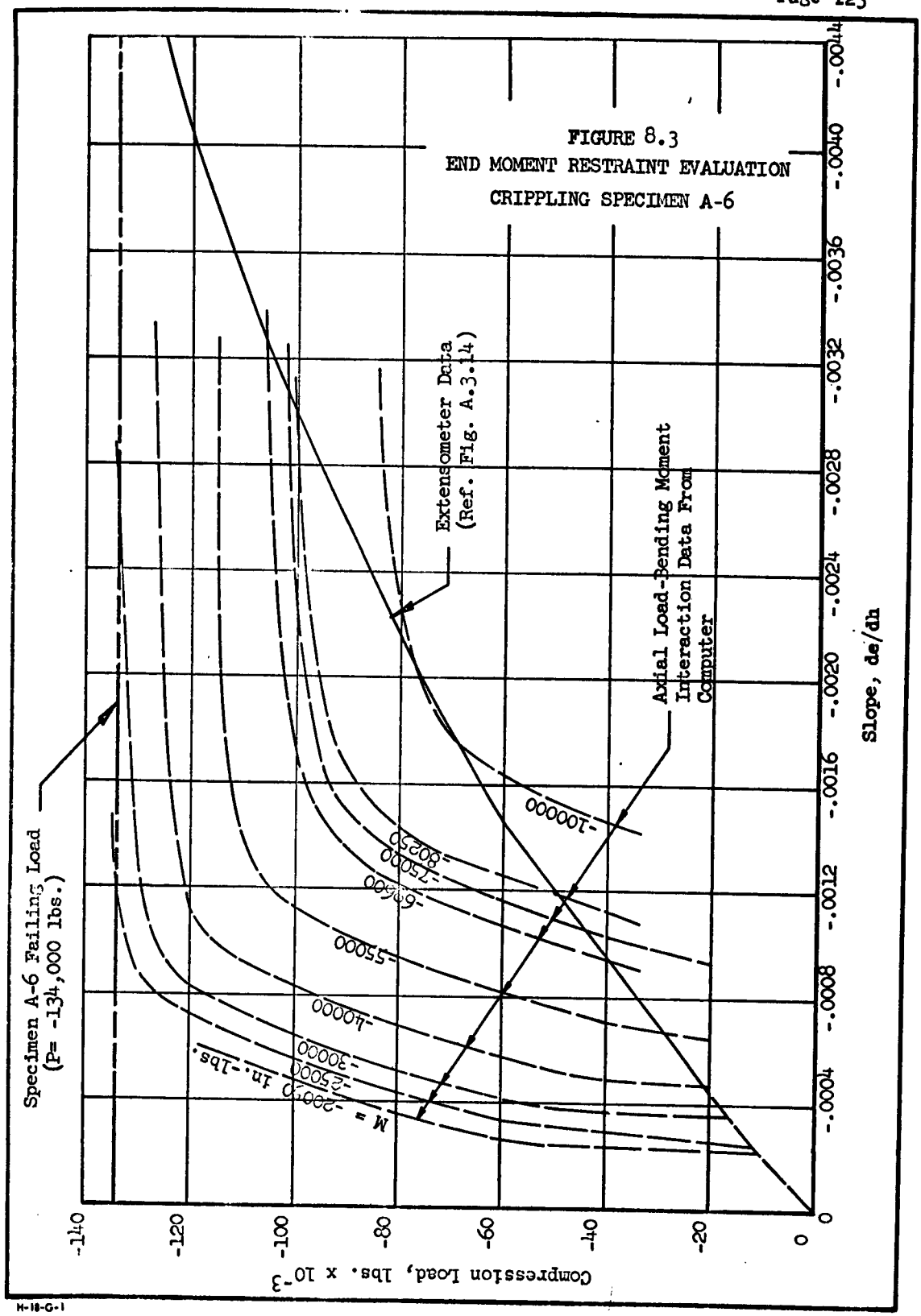

FIGURE 8.3
END MOMENT RESTRAINT EVALUATION
CRIPPLING SPECIMEN A-6

H-18-G-1

FIGURE 8.4

END MOMENT RESTRAINT EVALUATION

CRIPPLING SPECIMEN A-6

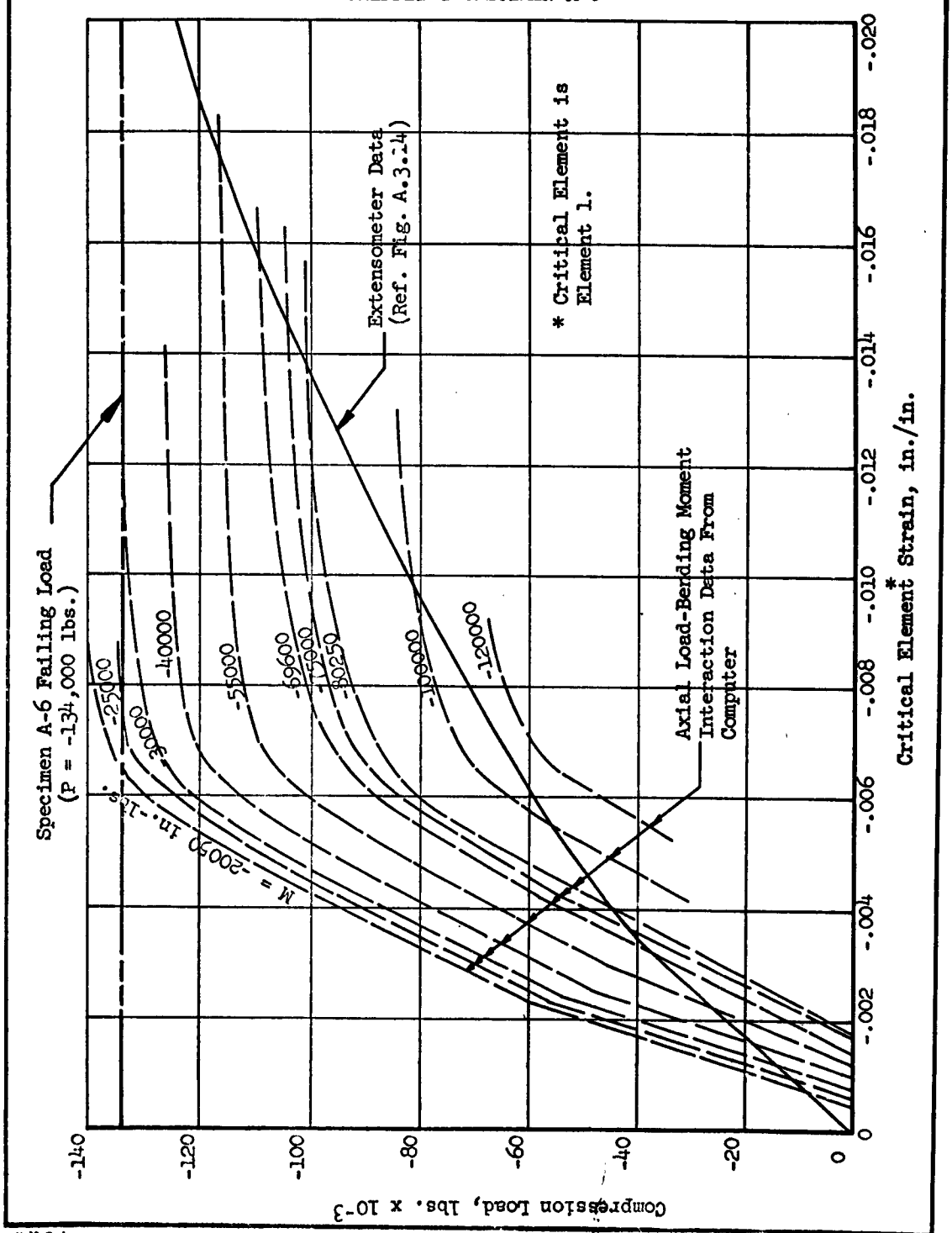

H-18-G-1

Figure 8.5

Bending Moment Variation With Applied Axial Load

Crippling Specimen A-6

Plotted from Figures 8.3 and 8.4 using intersections of strain gage data curve and calculated interaction data.

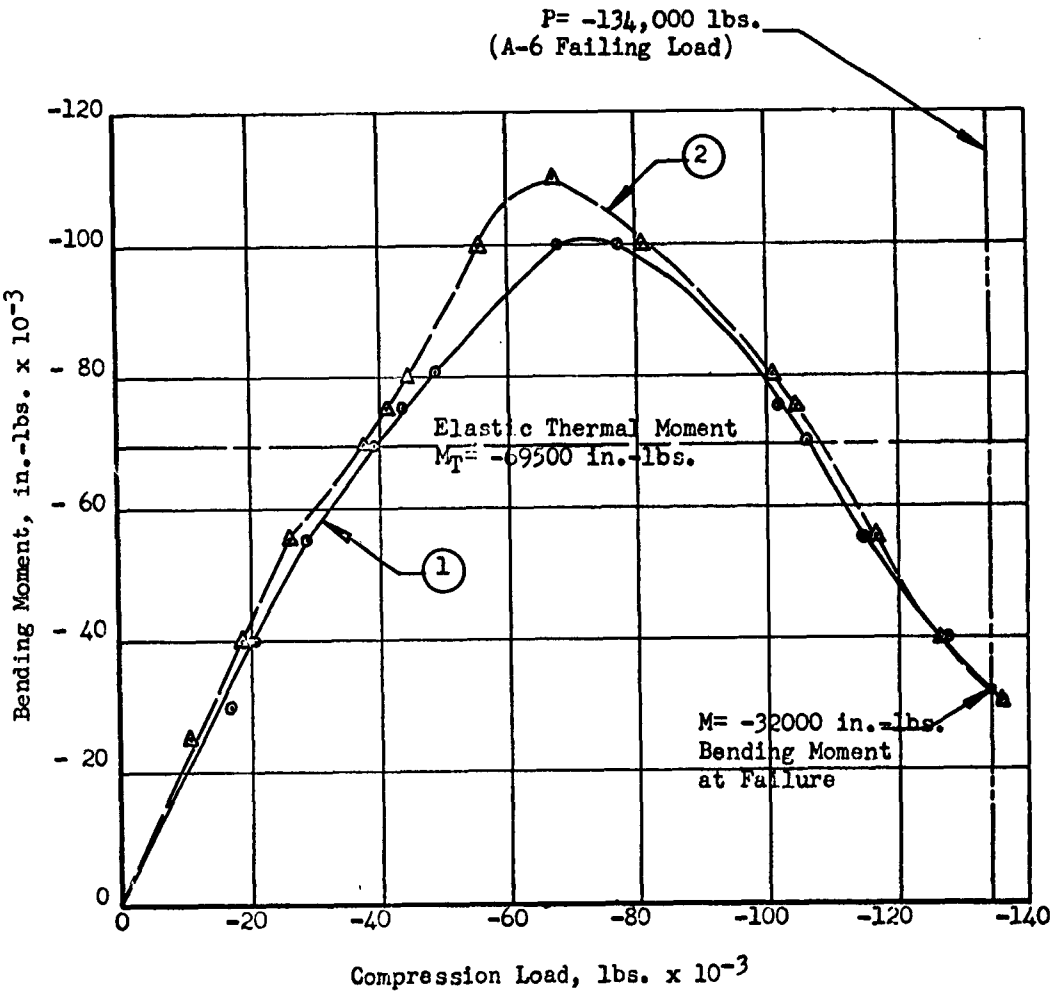

(1) Plotted from slope data of Figure 8.3

(2) Plotted from critical element strain data (Extensometer 5 of Figure A.3.14)

H-18-G-1

8.2.2 LONG COLUMN SPECIMENS

Although spherical ball and socket type fittings were used on all test specimens to obtain end fixity conditions as close as practicable to pin-ended (c = 1.0) the buckling loads of the two room temperature specimens indicated either greater bending stiffness than originally calculated or end fixity greater than c = 1.0. The critical long column (Euler) buckling loads from the room temperature tests were

P_{cr} = -26,700 lbs. (Specimen No. C-1)
P_{cr} = -24,600 lbs. (Specimen No. C-2)

as compared with a preliminary calculated value of

P_{cr} = -21,250 lbs. (based on E = 10.3×10^6, element areas based on nominal thickness, and c = 1.0)

From preliminary digital computer calculations

$$\sum A_n E_n = 18.857 \times 10^6 \text{ and } EI_x = 11.175 \times 10^6$$

Since specimen C-1 indicated a buckling load somewhat higher than the calculated value, specimen C-2 was supported as a simple beam and 50 lb. increments of load were applied at the center with deflection readings taken at each load increment to determine the actual bending stiffness (EI_x). This data is plotted in Figure 8.6 and shows the curve as corrected for support deflection. From Figure 8.6 the maximum deflection at the center is δ = 0.229 inch for a load of 500 lbs. From the deflection equation for a simple beam

$$EI_x = \frac{PL^3}{48\delta} = \frac{500\ (61.875)^3}{48(0.229)} = 10.79 \times 10^6$$

which is approximately 3.5% below the calculated value of 11.175×10^6. From the column test of specimen C-2 and the above value of EI_x for specimen C-2, the Euler equation $P_{cr} = \pi^2\ EI/L^2$ is solved for the effective length.

$$L' = \sqrt{\frac{\pi^2\ EI}{P_{cr}}} = \sqrt{\frac{(3.14)^2(10.79 \times 10^6)}{24600}} = 65.75 \text{ inches}$$

If the end fixity conditions are assumed identical for specimens C-1 and C-2, the buckling load of specimen C-1 is substituted in the Euler equation to solve for the bending stiffness of C-1.

$$EI_x = \frac{P_{cr}L^2}{\pi^2} = \frac{26700(65.75)^2}{(3.14)^2} = 11.71 \times 10^6$$

which is approximately 4.5% above the calculated value of 11.175×10^6. Essentially, the variations may be attributed to some variation in depth between the two specimens in addition to tensile coupons showing slightly lower E values than 10.3×10^6.

Since the strain gages and extensometers on specimen C-1 showed good agreement and the extensometers on C-1 agreed well with those on specimen C-2, this data was used to determine the value of $\sum A_nE_n$ experimentally. Using the average elastic slope of strain gages and extensometers from specimen C-1,

$$\sum A_nE_n = \frac{P}{e} = \frac{-20,000}{-0.00111} = 18.02 \times 10^6$$

where e = -0.00111 in./in. is from Figure 8.24 . Using the average elastic slope of the extensometers from specimen C-2,

$$\sum A_nE_n = \frac{P}{e} = \frac{-20,000}{-0.0011075} = 18.05 \times 10^6$$

where e = -0.0011075 is from Figure 8.24 . These values are approximately 4.5% below the original calculated value of 18.857×10^6 which was based on an elastic E of 10.3×10^6. Subsequent tensile coupon data showed E = 9.675×10^6 psi for the 0.125 inch 7075-T6 aluminum alloy (clad) cover plates and 10.02×10^6 psi for the 0.125 inch 7075-T6 aluminum alloy (bare) channels.

With the experimental values of EI_x and $\sum A_nE_n$ from specimen C-2, the radius of gyration is

$$\rho = \sqrt{EI/EA} = \sqrt{10.79/18.05} = 0.773 \text{ inch}$$

which is almost exactly that used in the original calculations

(0.770 inch) which establishes the higher buckling loads to be primarily a function of effective length (end fixity). Using the effective length of $L' = 65.75$ inches determined for specimen C-2, the critical column buckling strain is

$$e_{cr} = \frac{\pi^2 \rho^2}{L'^2} = \frac{3.14^2 (0.773)^2}{(65.75)^2} = 0.001363 \text{ in./in.}$$

Using the tensile coupon values of E, the final corrected values of EI_x and $\sum A_n E_n$ are $EI_x = 10.54 \times 10^6$ which is 2.3% below the experimental value of 10.79×10^6 from specimen C-2, and $\sum A_n E_n = 17.907 \times 10^6$ which is 0.8% below the experimental value of 18.05×10^6 from specimen C-2.

Assuming $(EI_x)_{C-1} = (EI_x)_{C-2}$ since $\sum A_n E_n$ values and measured depths of the two cross-sections are very nearly identical, it is presumed that some difference in end fixity exists between the two room temperature specimens. The effective length of specimen C-2 has been previously calculated as $L' = 65.75$ inches. The effective length of specimen C-1 is

$$L' = \sqrt{\frac{\pi^2 EI_x}{P_{cr}}} = \sqrt{\frac{(3.14)^2 (10.79 \times 10^6)}{26700}} = 63.2 \text{ inches.}$$

Column end fixity for the two specimens is defined by

$$L' = \frac{L}{\sqrt{c}} \text{ where}$$

$$c = \left(\frac{L}{L'}\right)^2 = \left(\frac{72}{63.2}\right)^2 = 1.3 \text{ (Specimen C-1)}$$

$$c = \left(\frac{L}{L'}\right)^2 = \left(\frac{72}{65.75}\right)^2 = 1.2 \text{ (Specimen C-2)}$$

The average end fixity is $c = 1.25$ and this value is used in the room temperature analytical procedures for compatability in defining the room temperature reference curves. With

$$L' = \frac{L}{\sqrt{c}} = \frac{72}{\sqrt{1.25}} = 64.3 \text{ inches}$$

the critical buckling strain is

$$e_{cr} = \frac{\pi^2 \rho^2}{(L')^2} = \frac{(3.14)^2\ (0.767)^2}{(64.3)^2} = 0.001402 \text{ in./in.}$$

where this value is used in the analytical procedures.

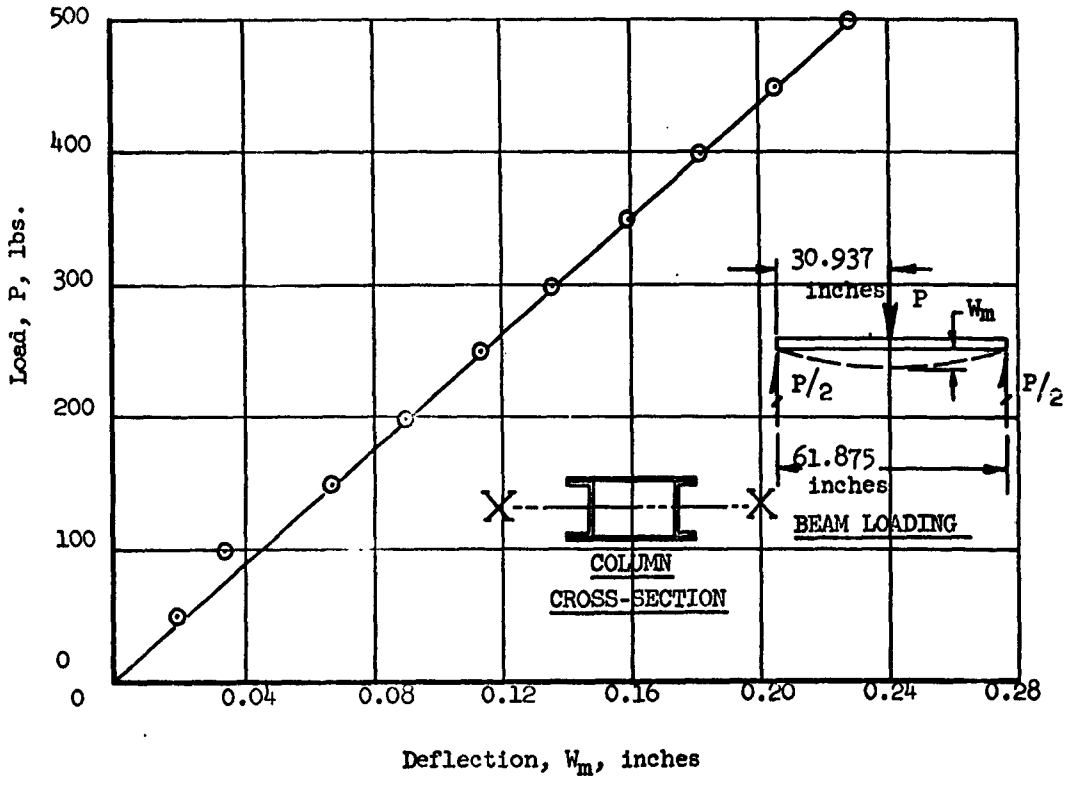

FIGURE 8.6
COLUMN SPECIMEN - SIMPLE BEAM DEFLECTION DATA

The elevated temperature long columns showed considerable variation in end fixity according to the critical buckling loads attained during the tests. Specimen C-3 with a 250°F. symmetrical temperature gradient indicated the highest value of end fixity with c = 1.643 and a critical buckling strain of e_{cr} = -0.001838 in./in. Specimen C-5 with a 450°F. symmetrical temperature gradient compared favorably with the room temperature specimens with c = 1.307 and e_{cr} = -0.001463 in./in. as opposed to c = 1.25 and e_{cr} = -0.001402 in./in. as an average for the two room temperature specimens. This data tends to indicate that the buckling strain, e_{cr}, of long, stable columns is relatively unaffected by symmetrical temperature gradients if the combined thermal and applied strains are not sufficient to produce local buckling prior to the Euler buckling of the column. The significant effects of these symmetrical temperature gradients would be restricted to the post-buckling portion of the column load-deformation curve where inelastic effects are more pronounced.

The test buckling loads of specimens C-4 and C-6 with unsymmetrical temperature gradients indicated that the initial temperature bowing and the associated induced bending moments may have been large enough to overcome any small end restraint moments. The peak test loads for C-4 and C-6 were both somewhat below that predicted by the simple Euler equation

$$e_{cr} = -\frac{\pi^2 \rho^2}{L^2}$$

as would be expected due to the initial eccentricity produced by the temperature bowing. For these two specimens the end fixity was considered to be c = 1.0 (pin end) and the associated critical buckling strain is e_{cr} = -0.001135 in./in.

The following table summarizes the results of the end fixity evaluation for both room temperature and elevated temperature long column specimens.

FIGURE 8.7

SUMMARY TABLE, LONG COLUMN END FIXITY

Column Specimen No.	Test Temp. Condition	Peak Test Load, lbs.	Test Specimen End Fixity, c	Calculated Critical* Buckling Strain, e_{cr}, in./in.
C-1	R.T.	26700	1.30	-.001463
C-2	R.T.	24600	1.20	-0.001363
C-3	250°F. Symmetrical	31700	1.643	-0.001838
C-4	250°F. Unsymmetrical	17800	1.00**	-0.001135
C-5	450°F. Symmetrical	19000	1.307	-0.001463
C-6	450°F. Unsymmetrical	14000	1.00**	-0.001135

* Based on test end fixity.
** Minimum value (pin end).

8.3 LOAD-DEFORMATION CURVE COMPARISON

This section describes the load-deformation curves as calculated by the methods of Sec. 3.0 and obtained experimentally during the test phase of the program. Comparisons and deviations are discussed in addition to presenting both the calculated and experimental curves. The experimental curves were obtained from the strain data of Appendix A where the specific use of the strain data is explained in Sections 8.3.1, 8.3.2, 8.3.3, and 8.3.4. For test load-deformation data three different strain measurement systems were used depending upon the type of specimen. See Sec. 5.0 for details of the strain measuring systems. For the bending and short column (crippling) specimens the extensometer and/or strain gage data for the critical element was used to define the experimental curve. For the long columns the overall foreshortening was used which was measured between the loading heads of the test machine. Similar data was also taken for the short column specimens and is shown in addition to the extensometer data for the short column specimens.

8.3.1 SYMMETRICAL BENDING MOMENT-DEFORMATION CURVES

The curves in this section represent the analytical-experimental comparison necessary to establish the validity of the procedures for defining applied load ratios for purposes of simulation. Room temperature reference curves, both analytical and experimental, are shown in Fig. 8.8. These curves are used as the reference basis for comparison with the curves at elevated temperature. Two room temperature specimens were tested to ensure compatibility and the curves were plotted for the critical compression element using strain gage and extensometer data. These specimens (B-1 and B-17) were also used to investigate the local buckling problem as described in Sec. 8.1.1. The value of the buckling coefficient, K, derived from that investigation was used for all room temperature and elevated temperature compression cover plates in the theoretical analysis. For calculation purposes, the room temperature material properties were taken directly from the table in Fig. 7.2 which summarizes the results of the tension coupon tests. Both the experimental and analytical curves shown in Fig. 8.8 represent the deformation of the cross-section with the load applied. These curves, then, do not necessarily reflect the permanent set of the structure since non-linear elastic effects (elastic buckling) affect the shape of the curve. Generally, the agreement is considered favorable between test and analysis. The use of MIL-HDBK-5, Ref. (d), material properties would show about 4 or 5 percent conservative comparison between the analytical and experimental curve.

Although the curves in this section could be plotted with F_{ap_m} as ordinate, the bending moment on the cross-section is used since the external applied loads and/or moments are of particular interest for purposes of static test. The bending moment in terms of the elastic rotational strain is

$$M_{ap} = \frac{K_{ap_x} (EI_x)}{c}$$

from Eq. (3.1.5) for symmetrical bending. The critical element strain for element m is defined by Eq. (4.0.2) as $e_m = F_{ap_m/E_m} + e_{p_{s_m}}$ where the terms for the symmetrical bending case are

$$F_{ap_m/E_m} = K_{ap_x}\left(\frac{y_m}{c}\right)$$

and,

$$e_{p_{sm}} = \sum_j e_{p_j} + \left(\sum_j K_{p_{xj}}\right)\frac{y_m}{c}$$

Fig. 8.9 shows the effects of a 250°F. symmetrical temperature gradient (cover plates hot, center of spar webs cool). These curves represent the temperature-load sequence +T, +P and do not reflect the permanent set of the structure, but only the deformation with temperature and load applied. It should be noted for this curve and all bending specimen curves at elevated temperature that the large reduction from room temperature values is not due primarily to the effects of the test temperature and temperature distribution. The strain gage curing temperature exposure history of approximately 2 hours at 350°F. and 1/2 hour at 450°F. produced severe permanent losses of material properties in the 7075-T6 material. The actual temperature exposure history is shown in Fig. 6.6. This effect is primarily responsible for the large reduction in strength from that at room temperature and is shown by both the analytical and experimental curves of Fig. 8.9. To illustrate the probable magnitude of the effect on the elevated temperature curve the calculations were also performed assuming that no prior temperature exposure was present. The results are shown as the Calculated Reference Curve in Fig. 8.9. This emphasizes the importance of the material properties problem, particularly in aluminum alloy. Fig. 8.9 is also used to illustrate the effect of using MIL-HDBK-5, Ref. (d), material properties as opposed to using the higher yield stress values obtained from tensile coupon data. This curve allows for the previous temperature exposure history, but used F_y = 67000 psi, Ref. (d), instead of F_y = 77750 psi and F_y = 72675 psi for the basic room temperature yield stress. The comparison between test and analysis is considered favorable, especially considering the variations present when large reductions of material properties are involved.

Figs. 8.10 and 8.11 show the test-analysis comparison curves for 250°F. unsymmetrical temperature gradients (tension or compression cover plate hot, opposite cover plate cool). These curves are also plotted for the temperature-load sequence +T, +P and do not reflect permanent set of the structure. The strain gage curing temperature exposure history was included and good agreement was obtained between test and analysis for the failing loads. This indicates compatibility between test and analysis material properties (F_y). However, the marked deviation in the shape of the two curves indicates some variation in modulus of elasticity and earlier buckling than predicted using K = 4.325. No buckling strain data was available; therefore, the calculated curves are shown for K = 4.325 for purposes of comparison.

The comparison curves for the 450°F. symmetrical temperature gradient (cover plates hot, center of spar webs cool) are shown in Fig. 8.12. These curves reflect not only the previous temperature exposure history for strain gage curing but additional time at the test temperatures as well. It should be pointed out that the cumulative effects on various elements through the cross-section vary considerably due to the non-uniform temperature distribution. For example, cover plate elements are affected severely by the 450°F. test temperature history while the center elements of the spar webs are relatively unaffected since the temperature was considerably less (approx. 275°F.). Excellent agreement is shown throughout the entire load range for these curves which reflect deformation with temperature and load applied.

Figs. 8.13 and 8.14 show the comparison curves for the 450°F. unsymmetrical temperature gradients (tension or compression cover plate hot, opposite cover plate cool). These curves reflect the effects of the total temperature exposure history from both strain gage curing and test as in the 450°F. symmetrical gradient case. The temperature-load sequence is +T, +P and does not reflect the permanent set of the structure. Generally, the test-analysis agreement is good throughout the load range except for the ultimate on specimen B-6. Considering the large reduction of material properties this might be accounted for by some variation in the yield stress of critical compression elements. In any case, it should be noted that the calculated curve is on the conservative side and the deviation is still within the limits of predictability of present methods at room temperature.

Fig. 8.15 is a summary of all experimental deformation curves and shows the effect of the large reduction in strength due to the previous temperature exposure history for strain gage curing. In general, the material properties reductions for aluminum alloys may be considerably more significant than the effects of thermal stresses on ultimate strength.

Fig. 8.16 is a summary of all calculated deformation curves for a direct comparison. The reference curve for specimen B-4 is included to further illustrate the effects of permanent losses of material properties on the load-deformation curves and the ultimate strength.

For permanent set characteristics and the yield load comparison a summary of calculated permanent set curves is shown in Fig. 8.17. Insufficient test data was taken to adequately evaluate the permanent set problem. However, considering the analytical strain procedures used to define the load-deformation characteristics, it may be assumed that the test-analysis comparison of permanent set curves (+T, +P, -P, -T) would produce similar accuracy to that shown for the load-deformation curves.

FIGURE 8.8

SYMMETRICAL BENDING MOMENT - DEFORMATION CURVE
CALCULATED - TEST COMPARISON
ROOM TEMPERATURE

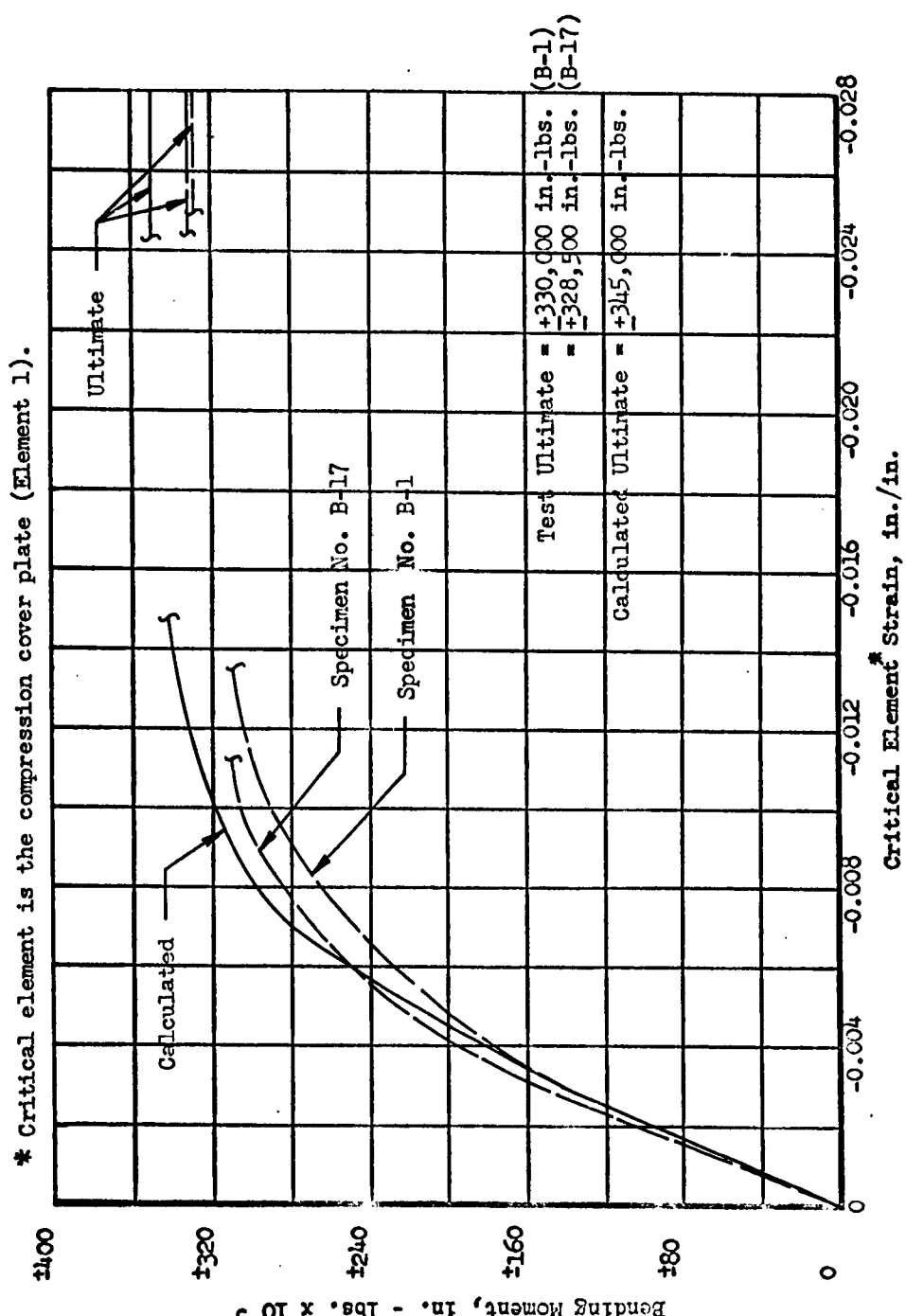

FIGURE 8.9

SYMMETRICAL BENDING MOMENT - DEFORMATION CURVE
CALCULATED - TEST COMPARISON
SYMMETRICAL TEMPERATURE GRADIENT
MAXIMUM TEMPERATURE OF 250°F. ON
BOTH COVER PLATES

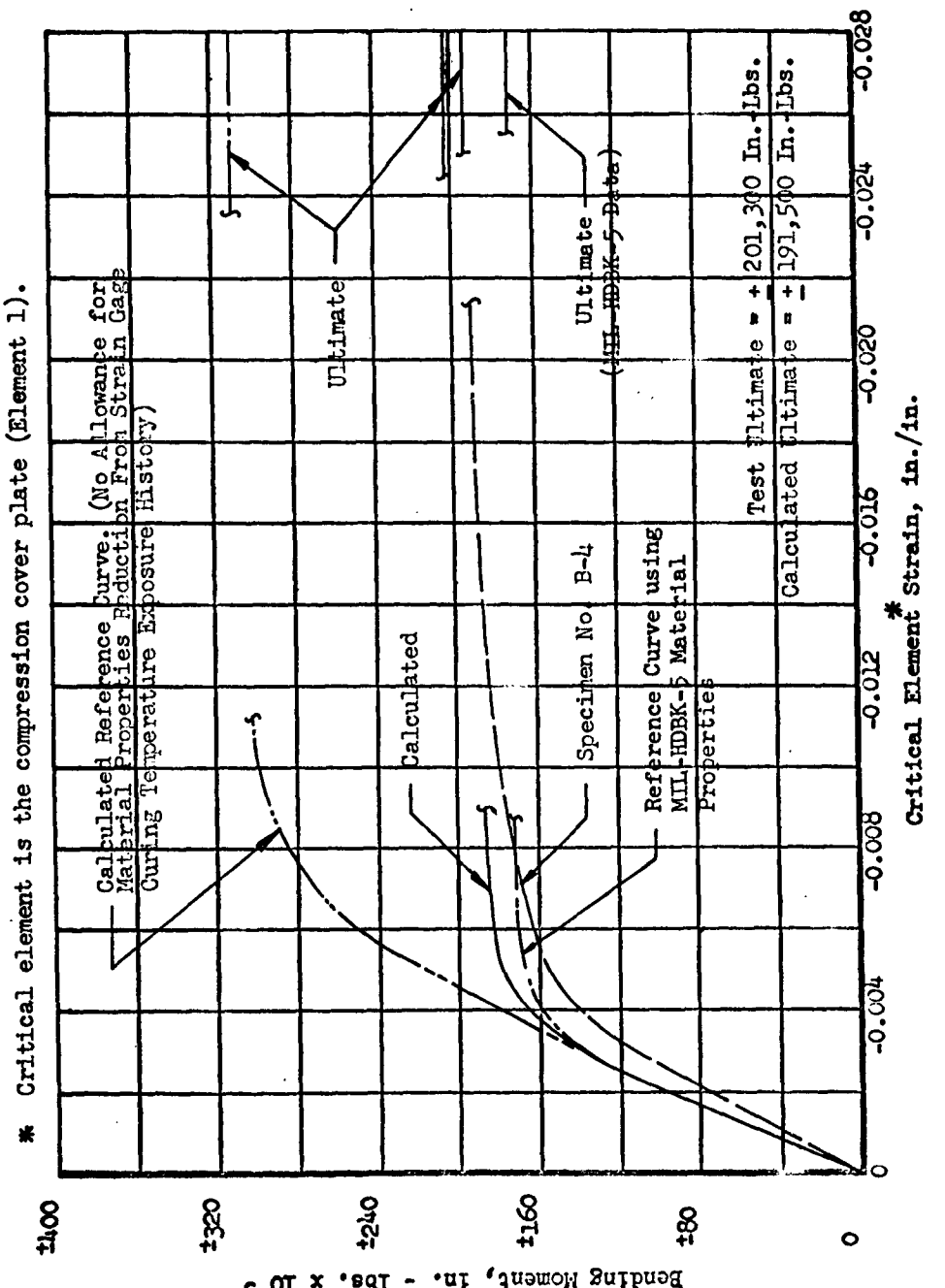

FIGURE 8.10 .

SYMMETRICAL BENDING MOMENT - DEFORMATION CURVE
CALCULATED - TEST COMPARISON
UNSYMMETRICAL TEMPERATURE GRADIENT
MAXIMUM TEMPERATURE OF 250°F. ON
TENSION COVER PLATE

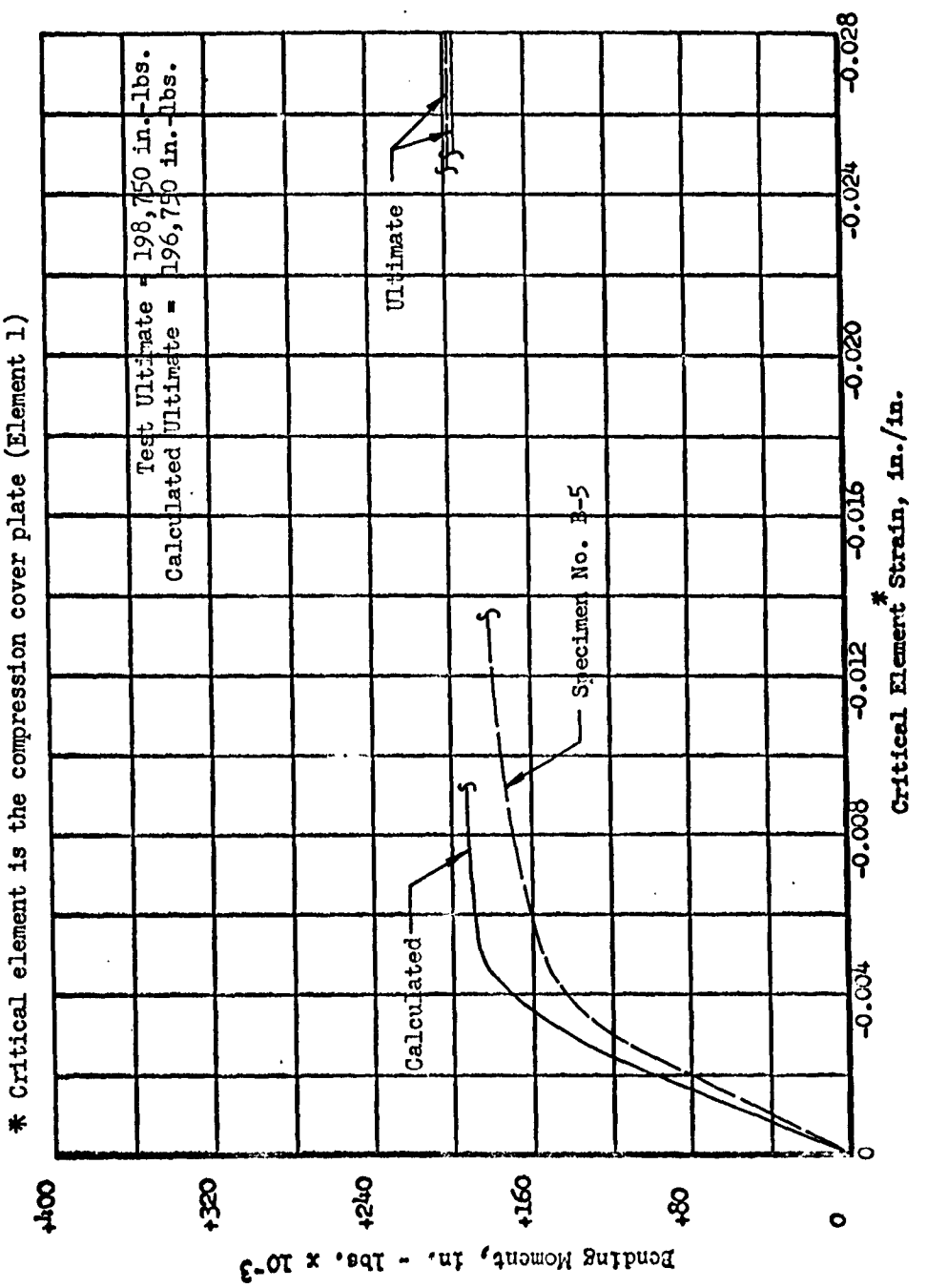

FIGURE 8.11

SYMMETRICAL BENDING MOMENT - DEFORMATION CURVE
CALCULATED - TEST COMPARISON
UNSYMMETRICAL TEMPERATURE GRADIENT
MAXIMUM TEMPERATURE OF 250°F. ON
COMPRESSION COVER PLATE

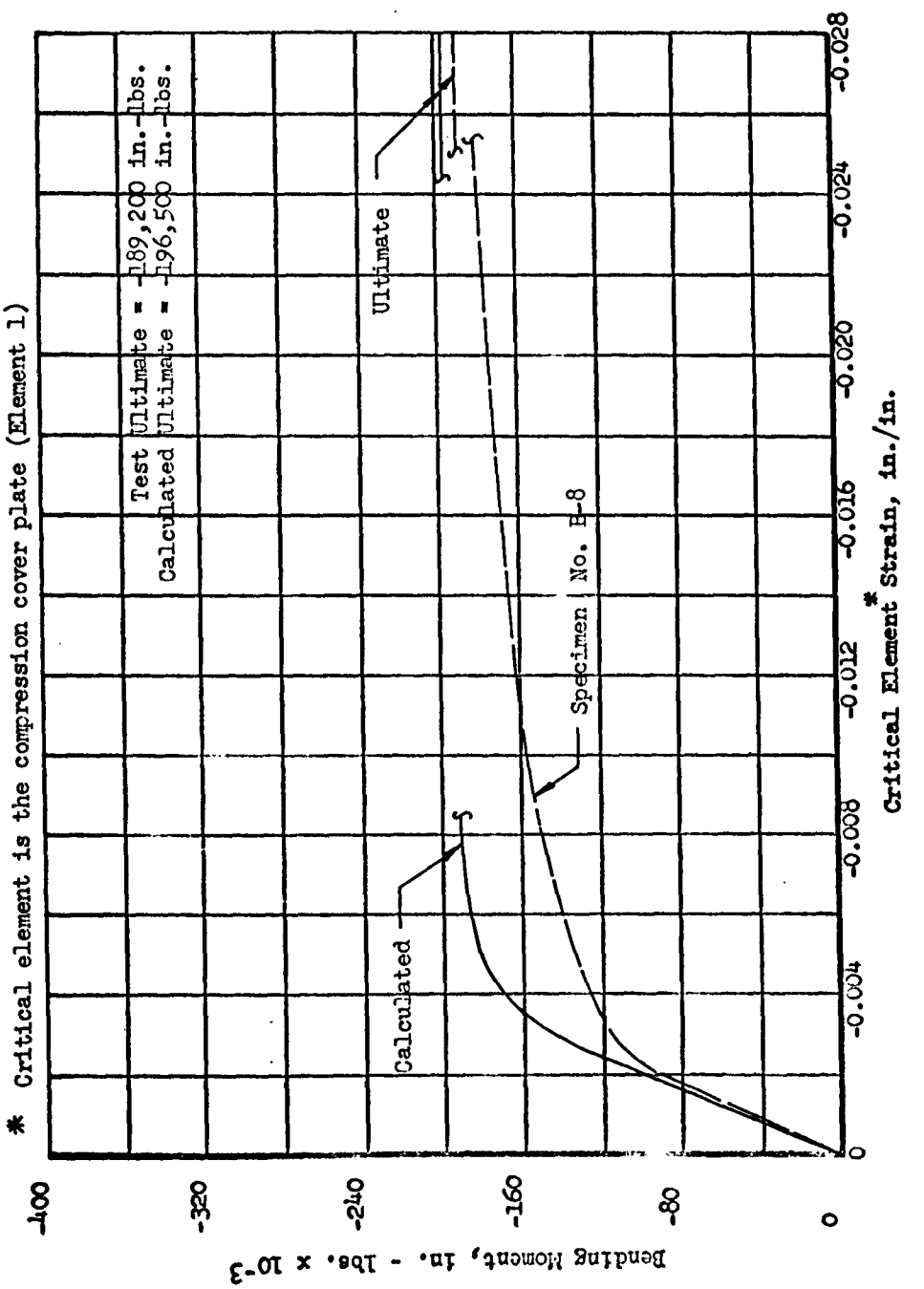

FIGURE 8.12

SYMMETRICAL BENDING MOMENT - DEFORMATION CURVE

CALCULATED - TEST COMPARISON
SYMMETRICAL TEMPERATURE GRADIENT
MAXIMUM TEMPERATURE OF 450°F. ON
BOTH COVER PLATES

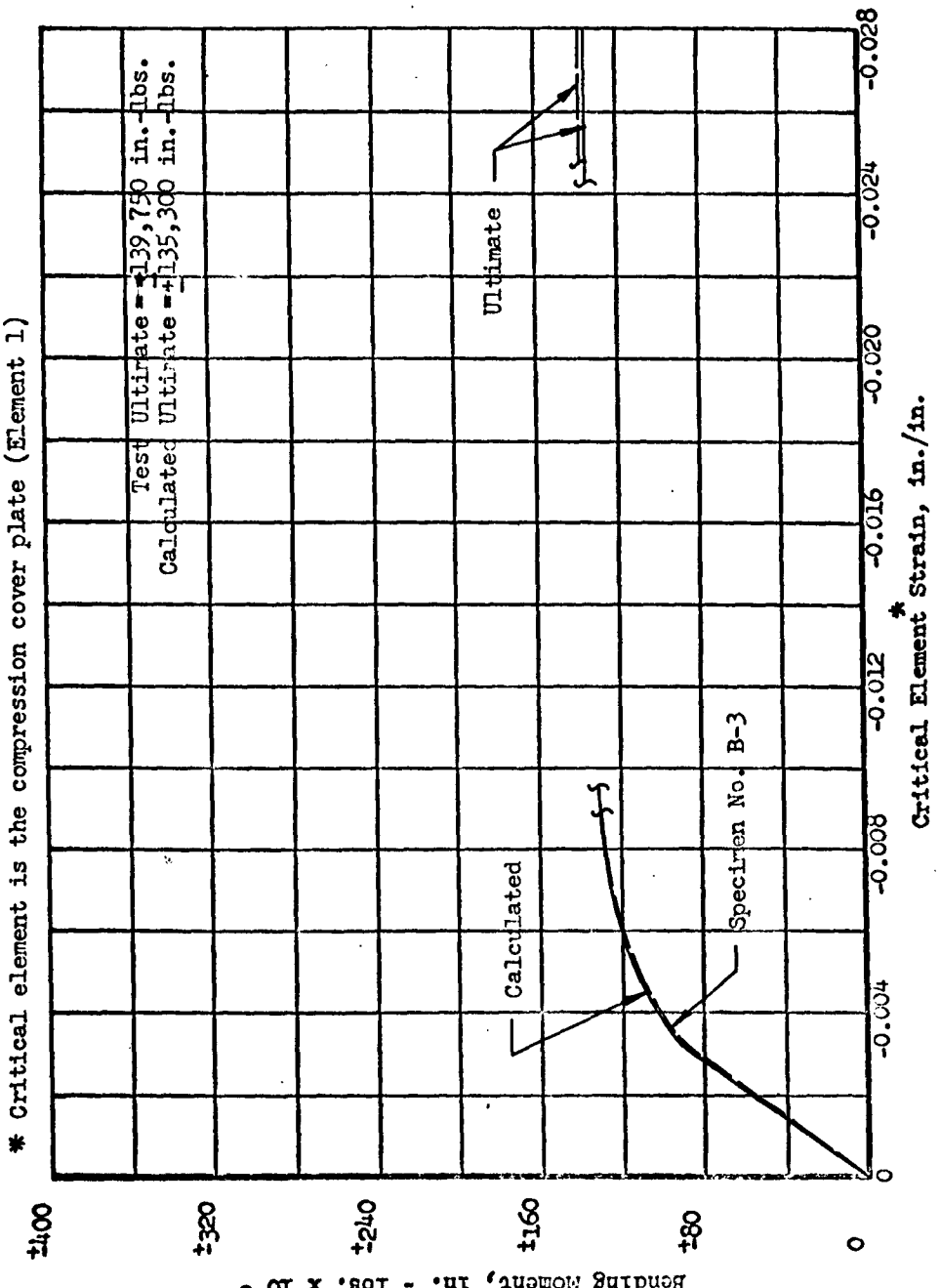

FIGURE 8.13

SYMMETRICAL BENDING MOMENT - DEFORMATION CURVE

CALCULATED - TEST COMPARISON
UNSYMMETRICAL TEMPERATURE GRADIENT
MAXIMUM TEMPERATURE OF 450°F. ON
TENSION COVER PLATE

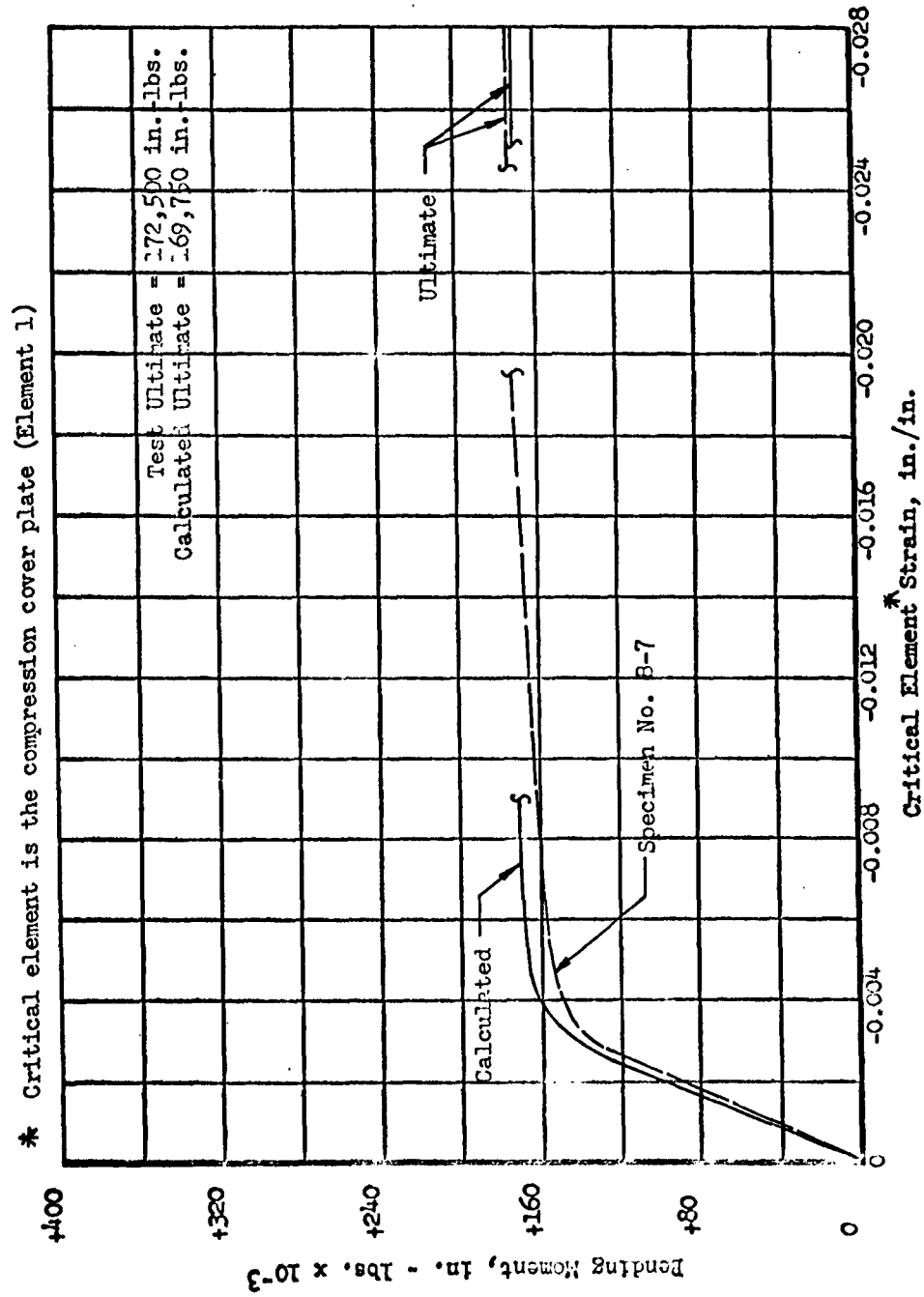

FIGURE 8.14

SYMMETRICAL BENDING MOMENT - DEFORMATION CURVE

CALCULATED - TEST COMPARISON

UNSYMMETRICAL TEMPERATURE GRADIENT
MAXIMUM TEMPERATURE OF 450°F. ON
COMPRESSION COVER PLATE

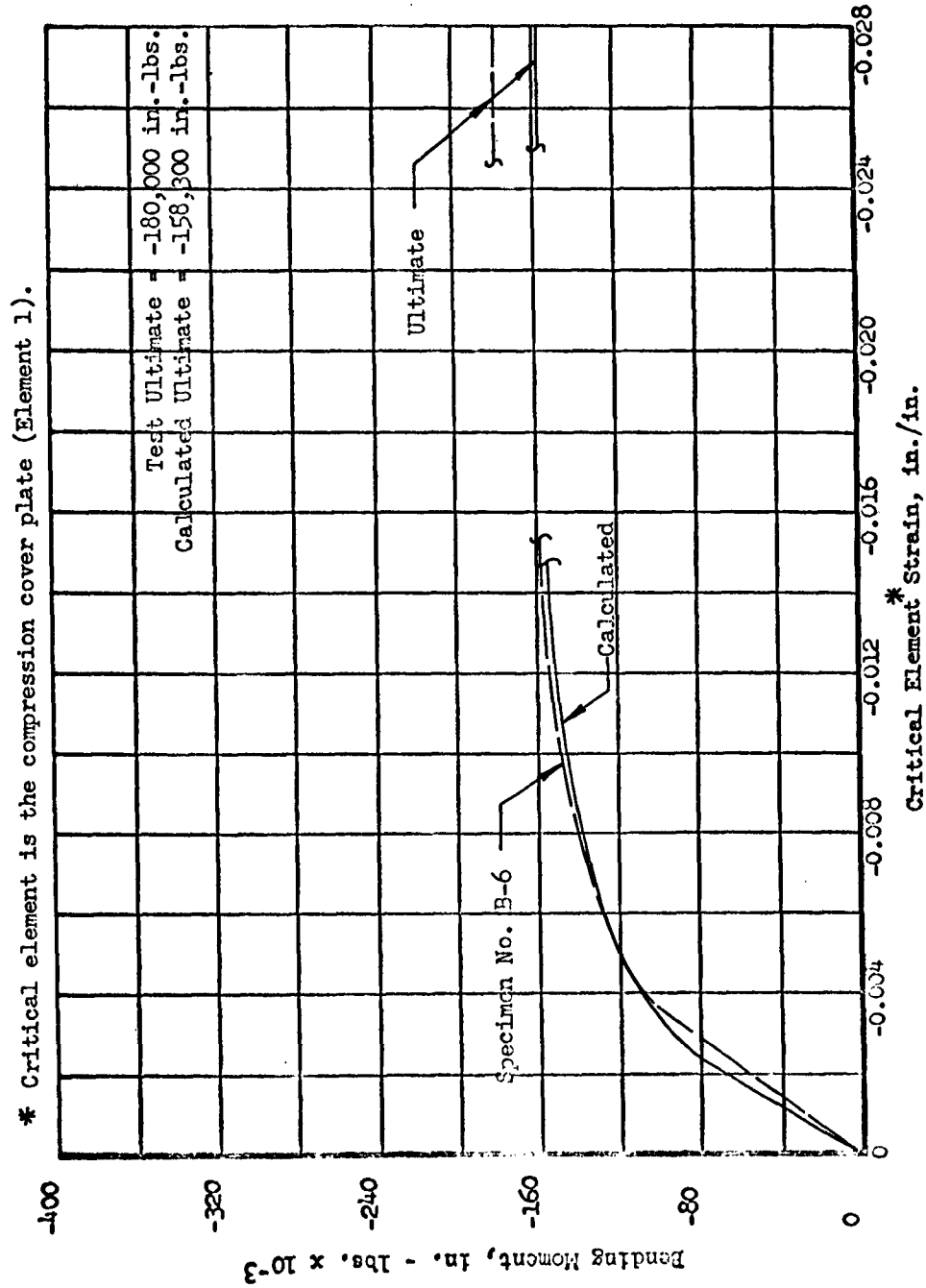

FIGURE 8.15

SYMMETRICAL BENDING MOMENT - DEFORMATION CURVE
SUMMARY
TEST MOMENT - DEFORMATION CURVES

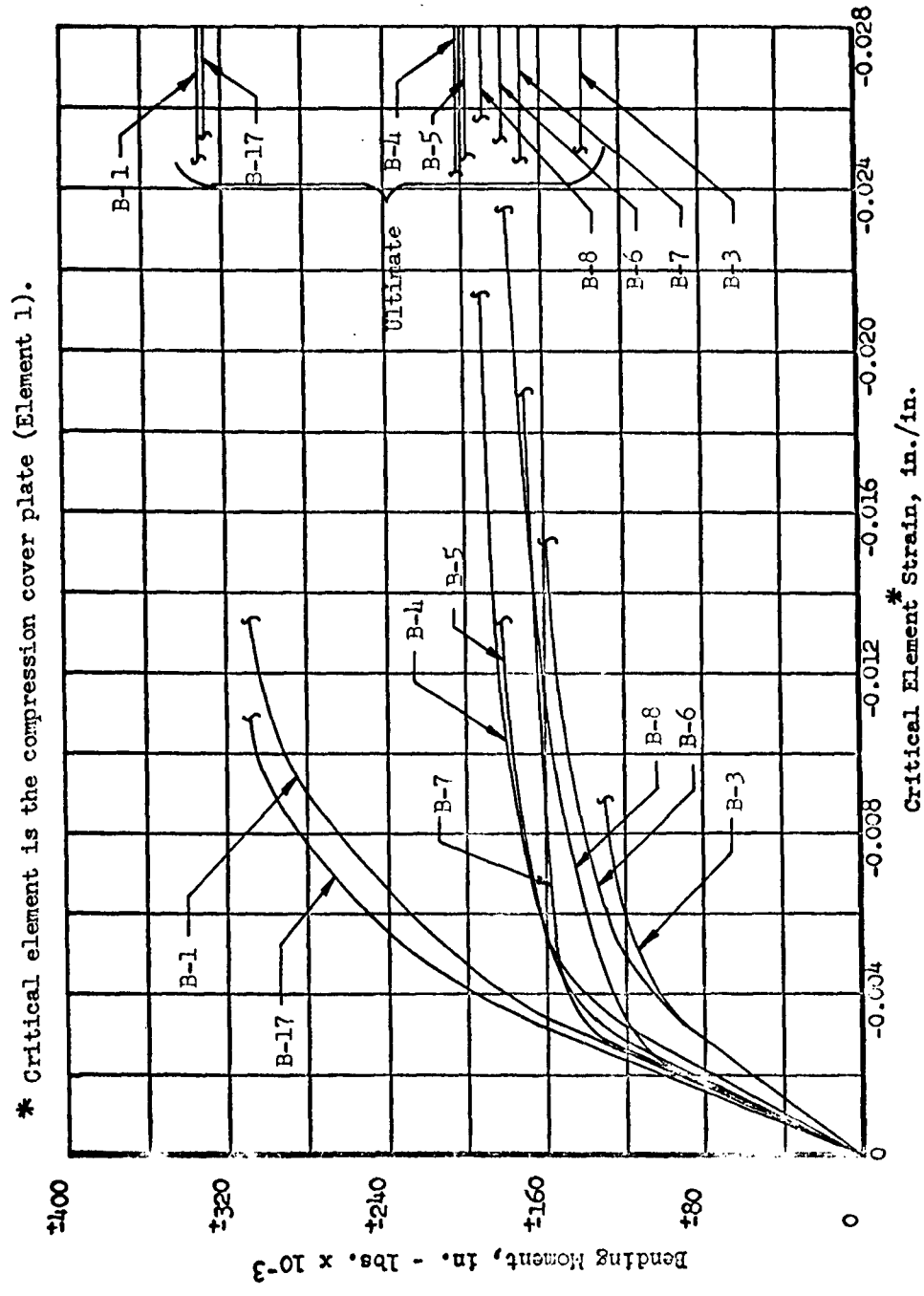

FIGURE 8.16

SYMMETRICAL BENDING MOMENT - DEFORMATION CURVE

SUMMARY

CALCULATED MOMENT - DEFORMATION CURVES

(Temperature and Load Applied; Temperature - Load Sequence (+T, +P)

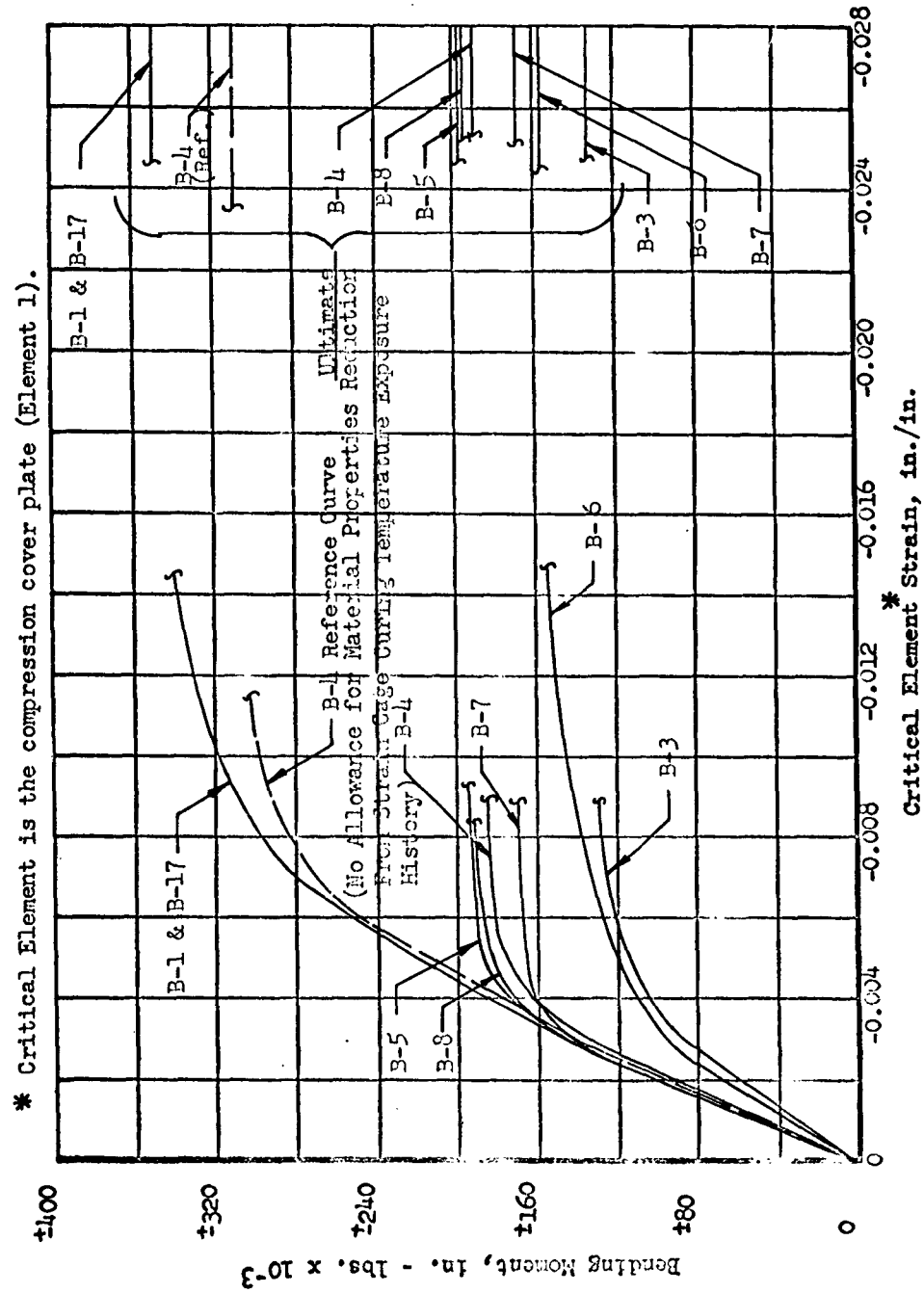

FORM H-10-G-1

FIGURE 8.17

SYMMETRICAL BENDING MOMENT - DEFORMATION CURVE

SUMMARY
CALCULATED PERMANENT SET CURVES

TEMPERATURE AND LOAD APPLIED; THEN REMOVED
TEMPERATURE - LOAD SEQUENCE (+T, +P, -P, -T)

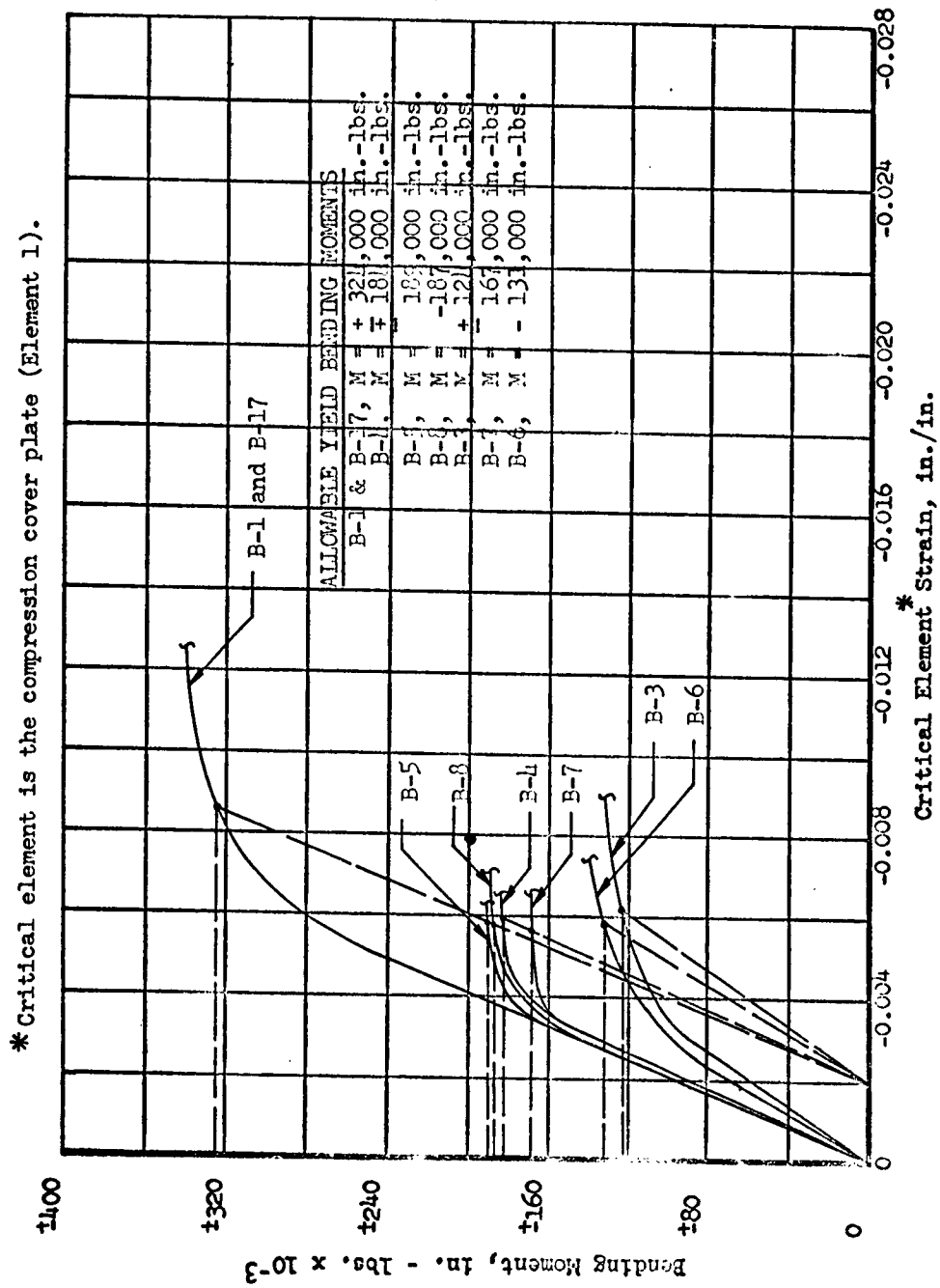

8.3.2 SHORT COLUMN LOAD-DEFORMATION CURVES

This section presents the results of the determination of load-deformation characteristics for the short column (crippling) specimens. Specimen A-6 is not included in this section due to the unique moment restraint condition encountered during the test. A rational load-deformation comparison between test and analysis could not be made considering the variation in bending moment as the axial load was increased from zero to failure. However, an analysis of the bending moment variation is shown separately in Sec. 8.2.1.

The curves in this section use the axial (compression) load as ordinate and the critical element strain for element m as abscissa. The axial load is defined in terms of the elastic applied strain as $P = e_{ap}\Sigma E_n A_n$, and the critical element strain is

$$e_m = {}^{F_{ap_m}}/_{E_m} + e_{psm}$$

where, in the case of a compression load acting alone, the elastic and inelastic terms are

$${}^{F_{ap_m}}/_{E_m} = e_{ap} \quad \text{and} \quad e_{psm} = \sum_j e_{p_j}$$

Fig. 8.18 shows the load-deformation curves of the two room temperature reference specimens compared with the calculated curve. From Sec. 8.1.2 the local buckling coefficient for the 0.125 inch cover plate is defined in Sec. 8.1.2 as K = 4.90. Since this value was quite close to the average of that for simply supported (K = 3.62) and clamped edges (K = 6.35) the buckling coefficient used for the analysis was K = 4.985. With no previous temperature exposure history the material properties are the basic room temperature properties obtained directly from the table in Fig. 7.2. As in the bending case, two room temperature specimens were tested to verify the test reference curve to be used for comparison. The two specimens correlated extremely well up to the peak (crippling) load. Although this peak load is the most important for design purposes, the X - Y plotter data shown includes the post-buckling (post-failure) portion of the load-deformation curve for academic reasons. For purposes of future analysis it is important to define

the shape of the unloading portion of the curve. The calculated curve shown compares quite well with the test data up to the crippling load at which time a strain cut-off is reached. With all elements in compression the Ramberg-Osgood stress cut-off was taken as the yield stress for every element in the cross-section. This is consistent with the yield stress cut-off used on the compression elements of the bending specimens described in the previous section. Note the slight change of slope for both the analytical and experimental curves at about P = -125,000 lbs. which indicates the load at which initial buckling of the cover plates occurred. These curves do not reflect the permanent set (or yield) of the structure as the deformation was obtained with the load acting. It should be noted that for crippling specimens only small permanent set may be present at loads just below the failing load. It is interesting to note that the peak loads in all cases were attained at or near yield strain for the critical compression element.

Fig. 8.19 shows the comparison between the analytical and experimental load-deformation curves for a 250°F. symmetrical temperature gradient (cover plates hot, channel webs cool). Elevated temperature strain gage curing produced a prior temperature exposure history as shown in Fig. 6.6 and a material properties evaluation as described in Sec. 7.0. Extensometer and strain gage data is plotted in addition to the curve from the X - Y plotter. The deviation in these two curves is probably due to the large difference in gage length (approximately one inch for the extensometer and 16 inches for the X - Y plotter). Favorable agreement between the analytical and experimental data was obtained, particularly at the peak, or crippling, load.

The data and curves of Fig. 8.20 are discussed to some degree in Sec. 8.2.1 considering the presence of induced bending moments produced by the initial bowing from the unsymmetrical temperature distribution. The general conclusions from Sec. 8.2.1 and the data comparison of Fig. 8.20 were that the magnitude of the bending moments was such that the axial load-deformation curve was relatively unaffected. Favorable agreement between test and analysis was obtained considering the material properties variation produced by the strain gage curing temperature exposure history.

Fig. 8.21 shows the results for a 425°F. symmetrical temperature gradient (cover plates hot, channel webs cool). In addition to the strain gage curing temperature exposure history, the test temperature exposure history is included in these curves for all elements with a test temperature exceeding 250°F. (aging temperature). Favorable agreement is shown between calculated and experimental curves with the calculations being slightly conservative.

Fig. 8.22 is a summary of all experimental load-deformation curves for a direct comparison of the effects of temperature distribution and temperature exposure on the peak, or crippling, loads. Specimen A-6 is included here for reference purposes only. The temperature distribution on this specimen was a 425°F. unsymmetrical temperature gradient (one cover plate hot, opposite cover plate cool). The effects of the bending moment are clearly shown by the reduction in peak load from that shown for A-3. If no bending moment were present, the peak value for A-6 should be greater than that for A-3 for axial load alone.

The summary of calculated load-deformation curves is shown in Fig. 8.23 for direct comparison of crippling loads. Specimen A-6 is not shown due to the presence of variable bending moments as described in Sec. 8.2.1.

In all cases, except A-6, the test failures were crippling failures of both cover plates. All failures were symmetrical. The calculations showed the compression cover plates to be the critical element for all specimens, which is compatible with the test results. The test failure of A-6 was similar to the other specimens, but was considerably unsymmetrical. This was due primarily to the presence of a bending moment which produced higher compression loads on one cover plate. The calculations for the analysis of Sec. 8.2.1 indicated this cover plate to be the critical element. No experimental or calculated permanent set data is shown since the effects are quite small prior to the crippling failure.

FIGURE 8.18

SHORT COLUMN LOAD - DEFORMATION CURVE
CALCULATED - TEST COMPARISON
ROOM TEMPERATURE
SPECIMEN NO'S. A-1 AND A-2

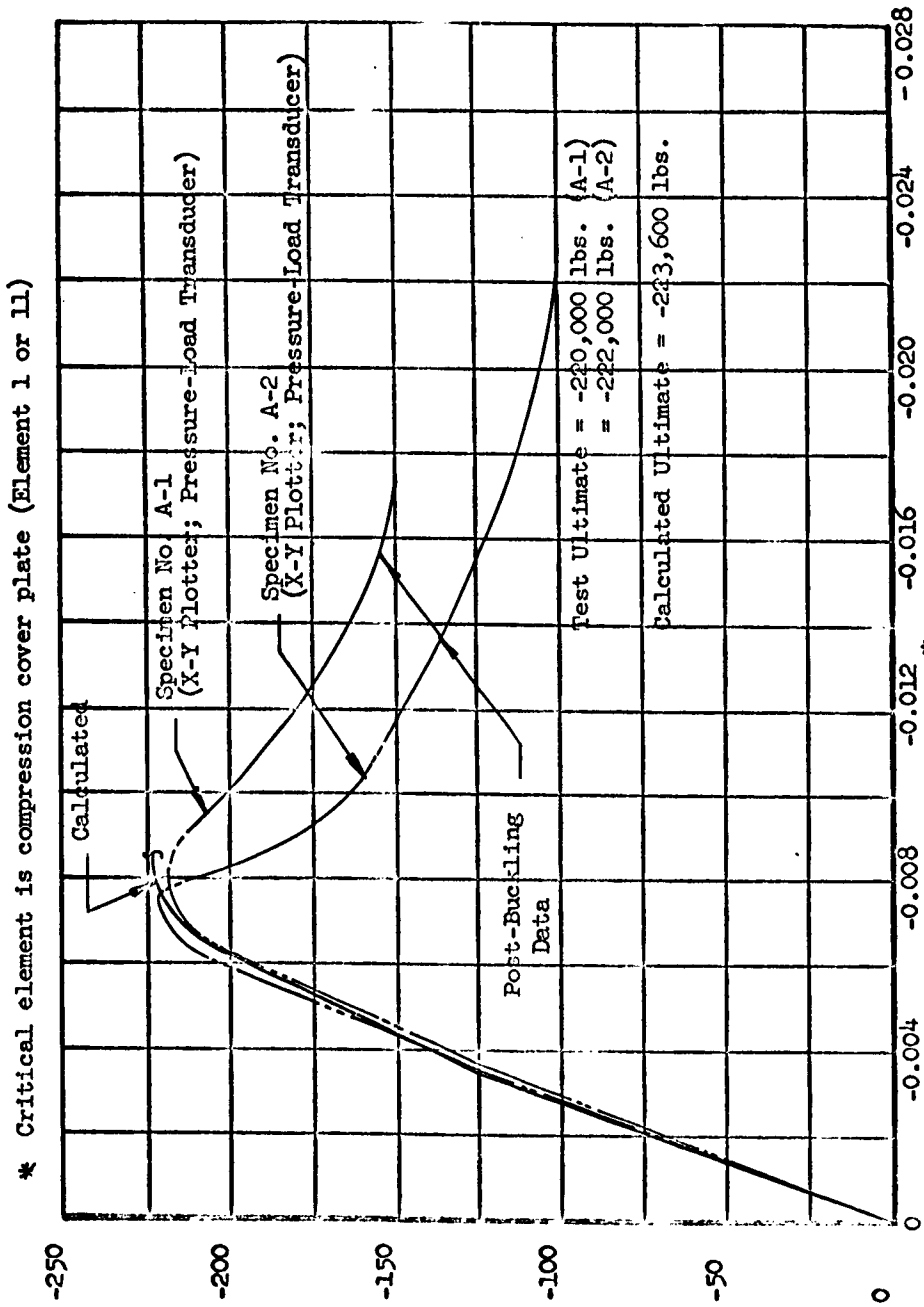

FIGURE 8.19

SHORT COLUMN LOAD - DEFORMATION CURVE
SYMMETRICAL TEMPERATURE GRADIENT
MAXIMUM TEMPERATURE OF 250°F. ON BOTH COMPRESSION COVER PLATES

SPECIMEN NO. A-4

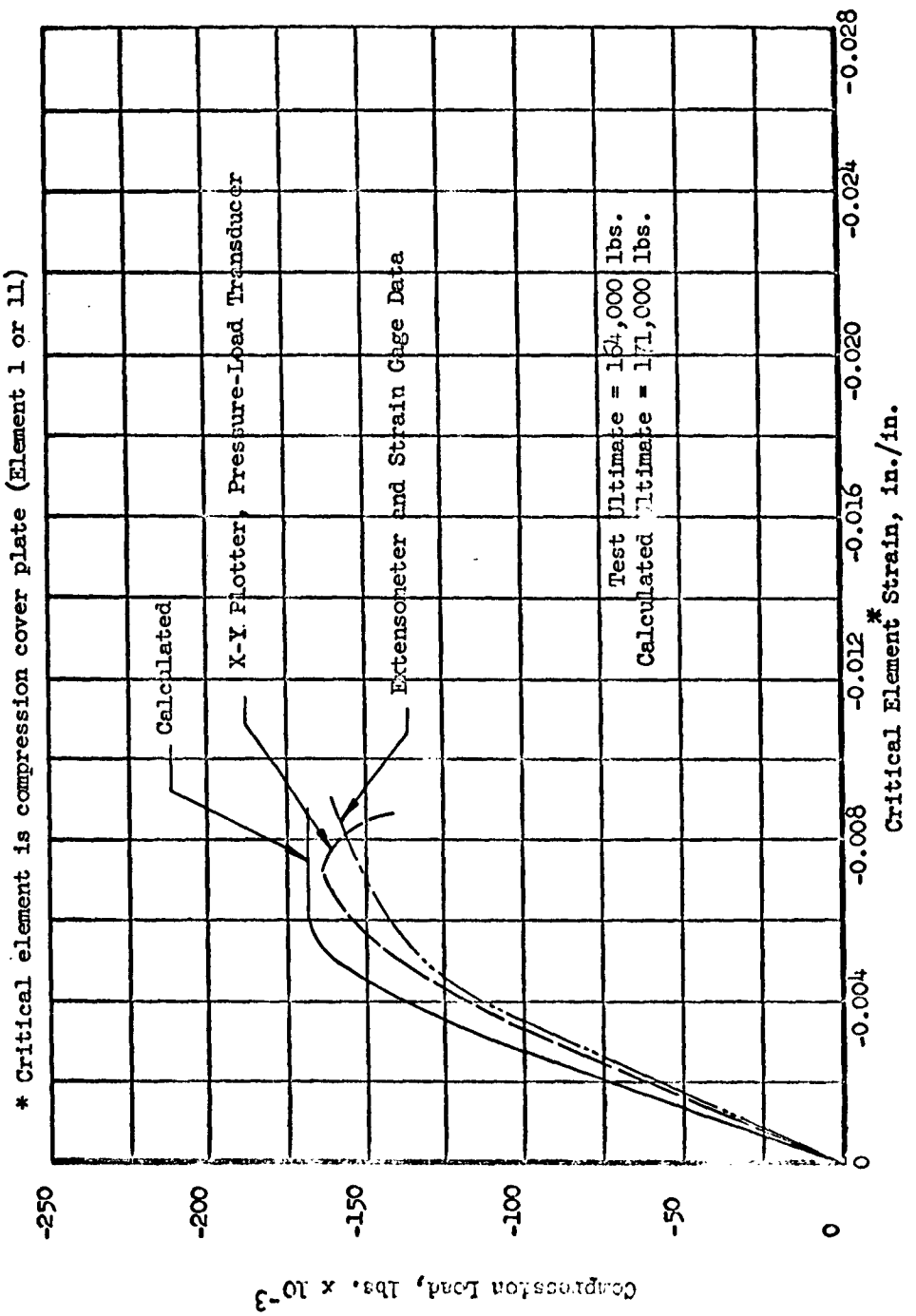

FIGURE 8.20

SHORT COLUMN LOAD - DEFORMATION CURVE

CALCULATED - TEST COMPARISON
UNSYMMETRICAL TEMPERATURE GRADIENT
MAXIMUM TEMPERATURE OF 250°F. ON
COMPRESSION COVER PLATE ELEMENT 1

SPECIMEN NO. A-5

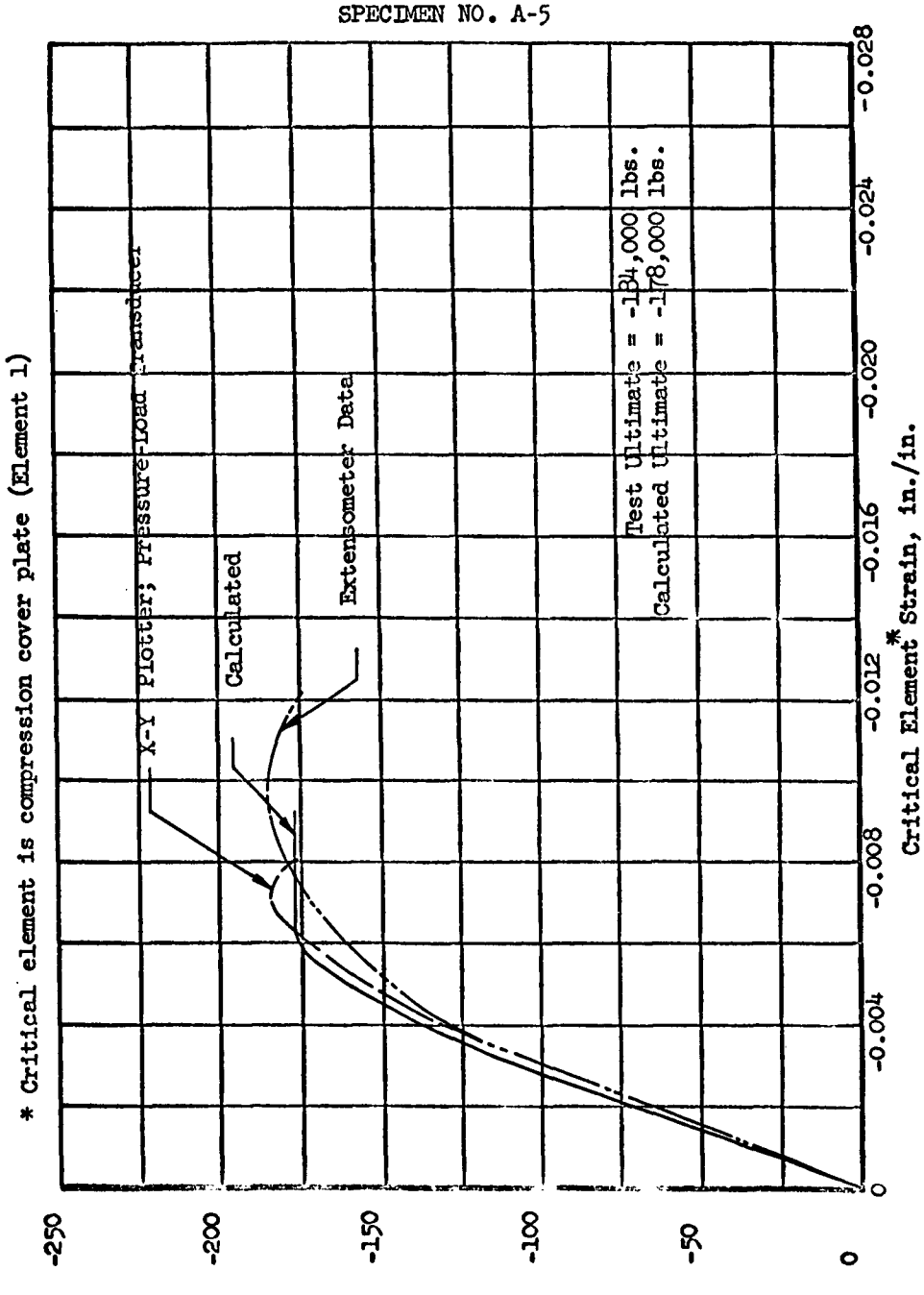

FIGURE 8.21

SHORT COLUMN LOAD - DEFORMATION CURVE
CALCULATED - TEST COMPARISON
SYMMETRICAL TEMPERATURE GRADIENT
MAXIMUM TEMPERATURE OF 425°F. ON
BOTH COVER PLATES

SPECIMEN NO. A-3

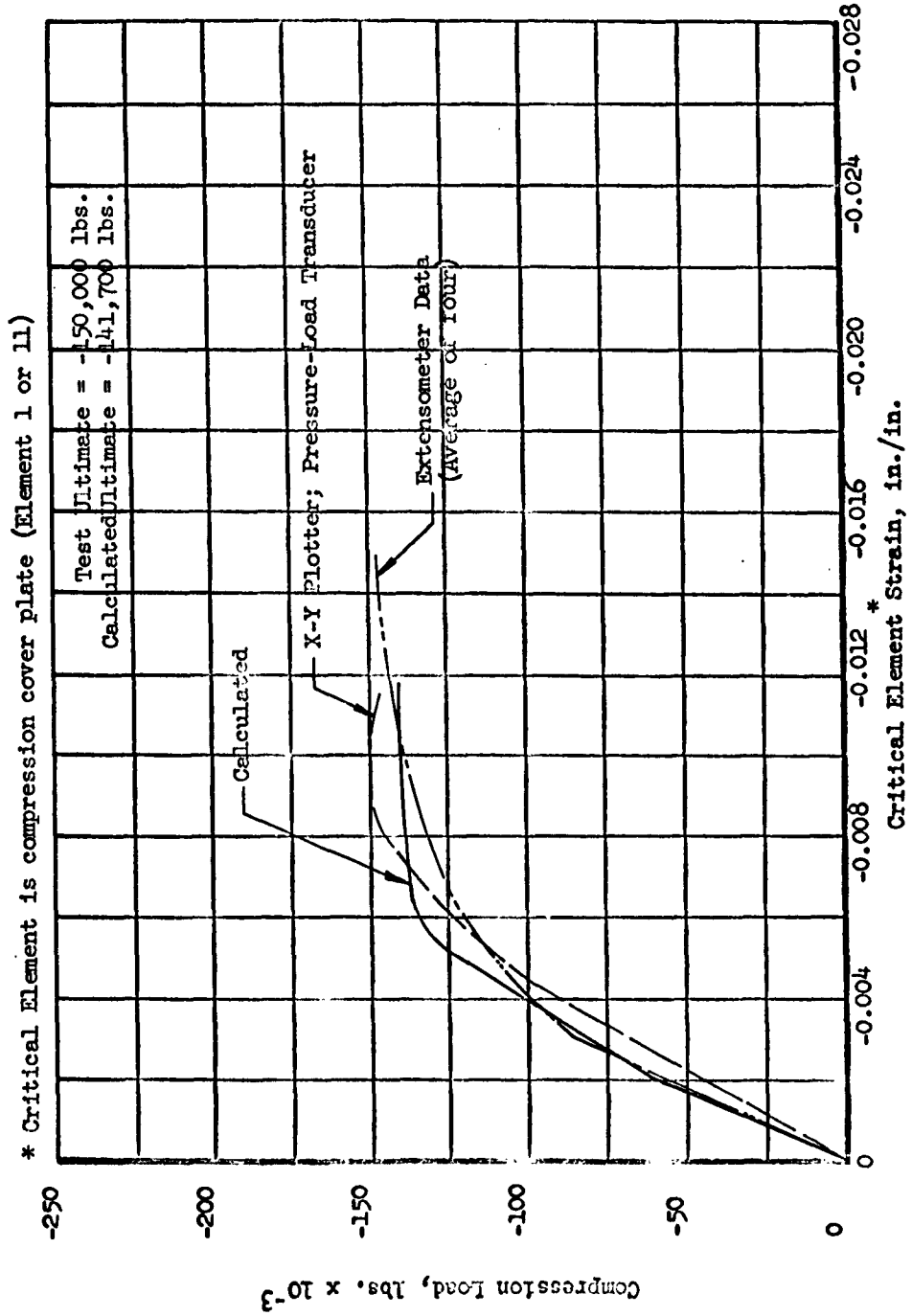

FORM H-1B C-1

FIGURE 8.22

SHORT COLUMN LOAD - DEFORMATION CURVE

SUMMARY

X-Y PLOTTER: PRESSURE-LOAD TRANSDUCER DATA

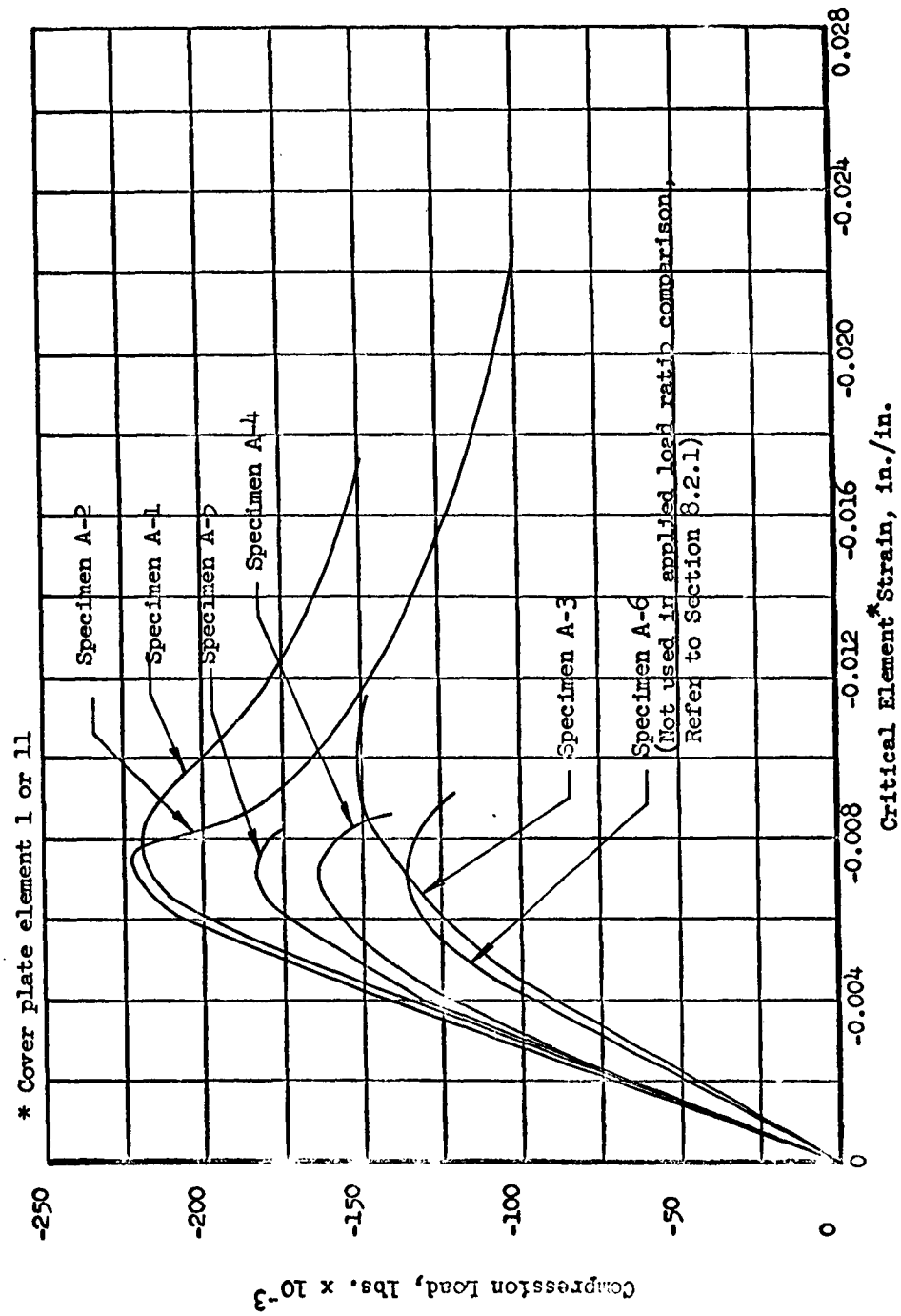

FORM H-18.C-1

FIGURE 8.23

SHORT COLUMN LOAD - DEFORMATION CURVE
SUMMARY
CALCULATED LOAD-DEFORMATION CURVES

(Specimen A-6 not shown. Refer to Section 8.2.1)

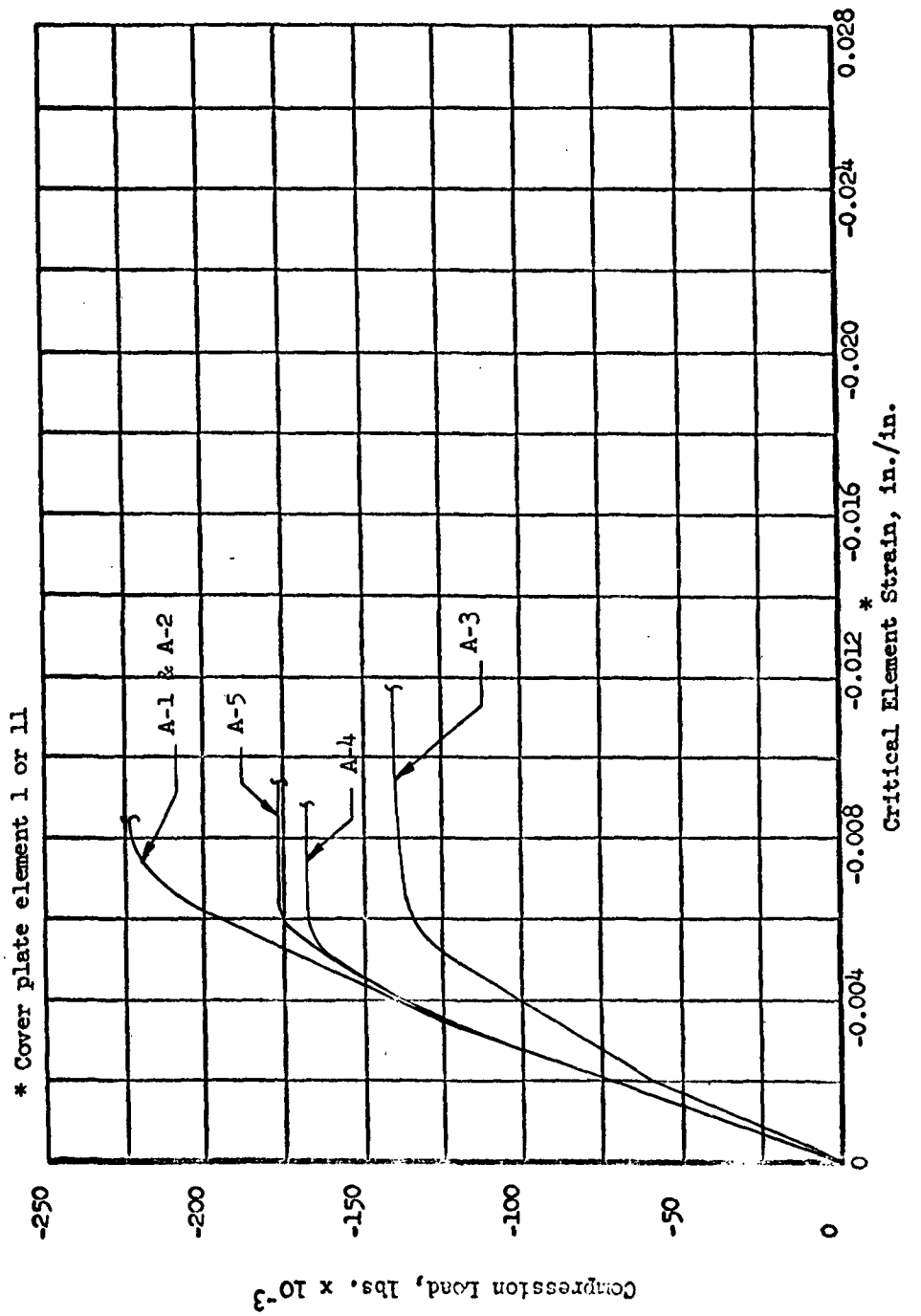

FORM 11-10-6 1

8.3.3 LONG COLUMN LOAD - DEFORMATION CURVES

This section presents the results of the determination of load-deformation characteristics for the long column specimens. The comparison between calculated and experimental results is made on a somewhat different basis than for the other types of specimens due to the wide variation in end restraint conditions between specimens. The end restraint conditions are evaluated in Section 8.2.2 and summarized in Figure 8.7. Generally, the peak, or buckling, loads are compared, but some data is shown for post-buckling sections of the load-deformation curve. To compare the calculated and experimental curves the test end restraint conditions were used in the calculations for each individual specimen except in the room temperature case where an average between the two test specimens was used.

The curves in this section use the axial (compression) load as ordinate and an overall foreshortening strain as abscissa. The axial load is defined in terms of the elastic applied strain as $P = e_{ap} \sum E_n A_n$, and the foreshortening strain is

$$e_f = (e_{ap} + e_p) + \frac{\Delta L}{L}$$

where $\frac{\Delta L}{L}$ represents the foreshortening produced by the lateral deflection. This data is plotted for the applied load (+P) and the temperature (+T) both being present on the column. No permanent set data is shown since the peak loads occur in the elastic stress region for these long columns. The permanent set data in the post-buckling region would become important, however, for a long column acting as a structural member in a complex structure.

Figure 8.24 shows the corrected x-y plotter data for the two room temperature columns compared with a calculated curve for an end restraint coefficient of c = 1.25. This is the average of c = 1.2 for C-2 and c = 1.3 for C-1. The original x-y plotter data for the test specimens was corrected for the deflection of the spherical ball and socket joint used at the loading heads of the test machine since the overall foreshortening deflection measurements were taken between the heads of the machine. Since the peak load at room temperature is predictable by the Euler formula anyway, it is expected that the calculated and experimental curves should be nearly identical up to the peak load. The interesting portion of these curves is in the post-buckling area and the strain at which the final failure occurs. Test failures were identical and occurred at very nearly the same strain. A calculated portion of the post-buckling curve showed reasonable agreement with the test data considering that the post-buckling calculations are somewhat approximate. The peak values are taken as the reference values for the determination of applied load ratios in Section 9.0.

The calculated-test comparison shown in Figure 8.25 for e_{cr} = -0.001838 in./in. (c = 1.643) tends to show that the critical buckling load is affected primarily by material properties and relatively unaffected by the thermal stresses produced by the symmetrical temperature gradient. The lower curve for e_{cr} = -0.001402 in./in. (c = 1.25) is calculated for comparison with the room temperature curve of Figure 8.24 and the applied load ratios of Section 9.0. The test curve of Figure 8.25 is based on extensometer data since the x-y plotter data was not complete due to the unexpected high load (-31,700 lbs.).

Specimen C-4 shown in Figure 8.26 indicates that the effect of an unsymmetrical temperature gradient on these specimens tends to produce end restraint conditions very close to a pin end. This is indicated by the comparison of calculated and experimental data where the buckling strain for purposes of calculation was taken as e_{cr} = -0.001135 in./in. (c = 1.0). x-y plotter data was used to plot the experimental curve. No correction was made for ball and socket deflection which accounts for some of the deviation in test and calculated slopes. The higher calculated curve for e_{cr} = -0.001402 in./in. is shown for reference purposes since this curve is used in defining the applied load ratios of Section 9.0.

Figure 8.27 shows the effect of a symmetrical temperature gradient and maximum cover plate temperature of 450°F. As in the 250°F symmetrical gradient case, the indications are that the peak load is primarily affected by material properties and is relatively unaffected by the thermal stresses. Assuming this is correct, the end restraint coefficient is c = 1.307 which is fairly realistic when compared with the room temperature test specimens. For c = 1.307 the critical buckling strain is e_{cr} = -0.001463 in./in. and the calculated curve is shown for this value. An additional calculated curve is shown for e_{cr} = -0.001402 in./in. (c = 1.25) for the applied load ratios of Section 9.0.

The unsymmetrical temperature gradient (450°F maximum temperature) produced considerably more initial bowing than the 250°F unsymmetrical condition. Although the initial slope of the test curve was not corrected for ball and socket deflection, it appears that the slope deviation between test and analysis is produced by initial bowing due to temperature rather than end fitting deflection. This tends to be substantiated by comparing the slope

deviation between the 250°F and 450°F unsymmetrical gradient cases. Further substantiation is provided by comparing unsymmetrical temperature gradient test curves with those from the symmetrical temperature gradient tests. As in the 250°F unsymmetrical gradient case, the peak load attained, as shown in Figure 8.28, indicates that the initial bowing produced an end restraint condition of c = 1.0 (pin end). The test peak load compares favorably with that calculated for e_{cr} = -0.001135 in./in. (c = 1.0). The higher calculated curve shown is for reference only using e_{cr} = -0.001402 in./in. (c = 1.25) for a comparison of applied load ratios in Section 9.0 on a common end fixity basis.

Figure 8.29 is a summary of all experimental long column curves as obtained from either x-y plotter or extensometer data. End restraint conditions were as defined in Section 8.2.2 which also shows a more detailed evaluation of the test end restraint problem.

Figure 8.30 is a summary of calculated load-deformation curves for each specimen and temperature distribution based upon the end fixity conditions as defined by the test specimens. These curves were computed for direct comparison with the curves obtained from test data.

With generally favorable agreement obtained between test and analysis peak loads the summary of calculated load-deformation curves shown in Figure 8.31 was obtained for a constant end fixity of c = 1.25 based upon the average of the room temperature specimens. The peak loads obtained from these curves are used to define the applied load ratios of Figure 9.4 in Section 9.0.

FIGURE 8.24

LONG COLUMN LOAD - DEFORMATION CURVE
CALCULATED-TEST COMPARISON
ROOM TEMPERATURE

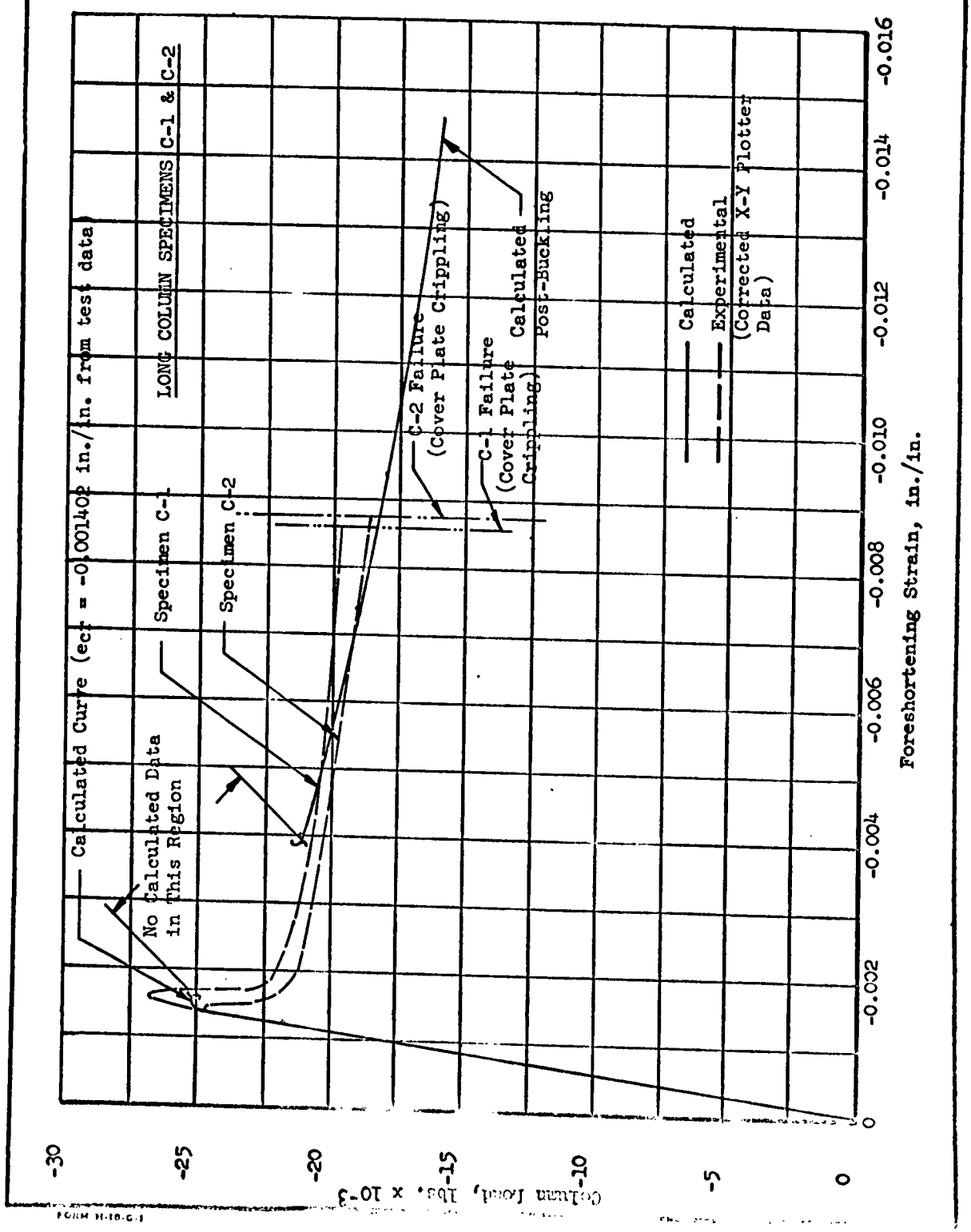

FIGURE 8.25

LONG COLUMN LOAD - DEFORMATION CURVE
CALCULATED - TEST COMPARISON
SYMMETRICAL TEMPERATURE GRADIENT

MAXIMUM TEMPERATURE OF 250°F. ON BOTH COVER PLATES

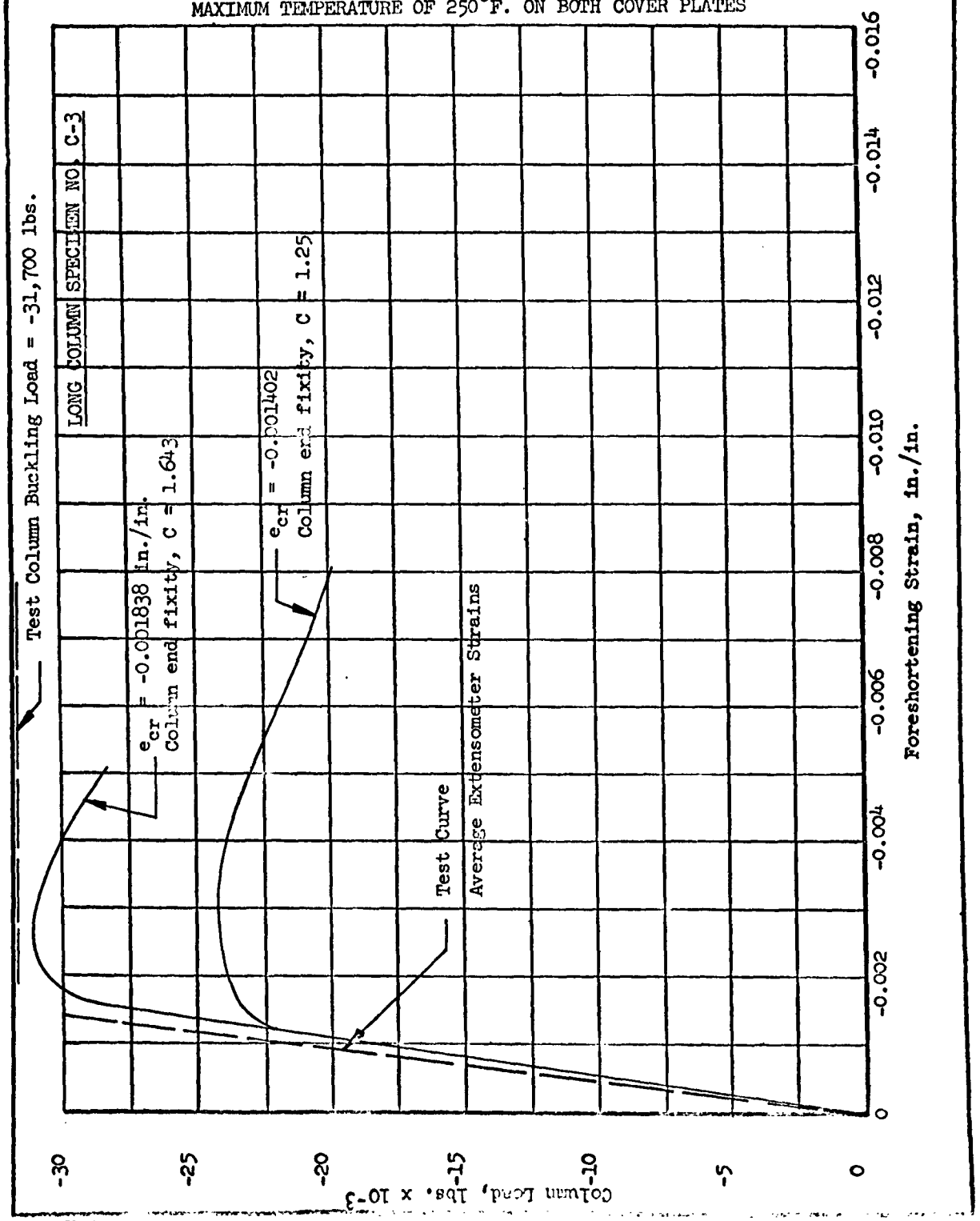

FORM H-10-C-1

FIGURE 8.26

LONG COLUMN LOAD - DEFORMATION CURVE
CALCULATED-TEST COMPARISON
UNSYMMETRICAL TEMPERATURE GRADIENT

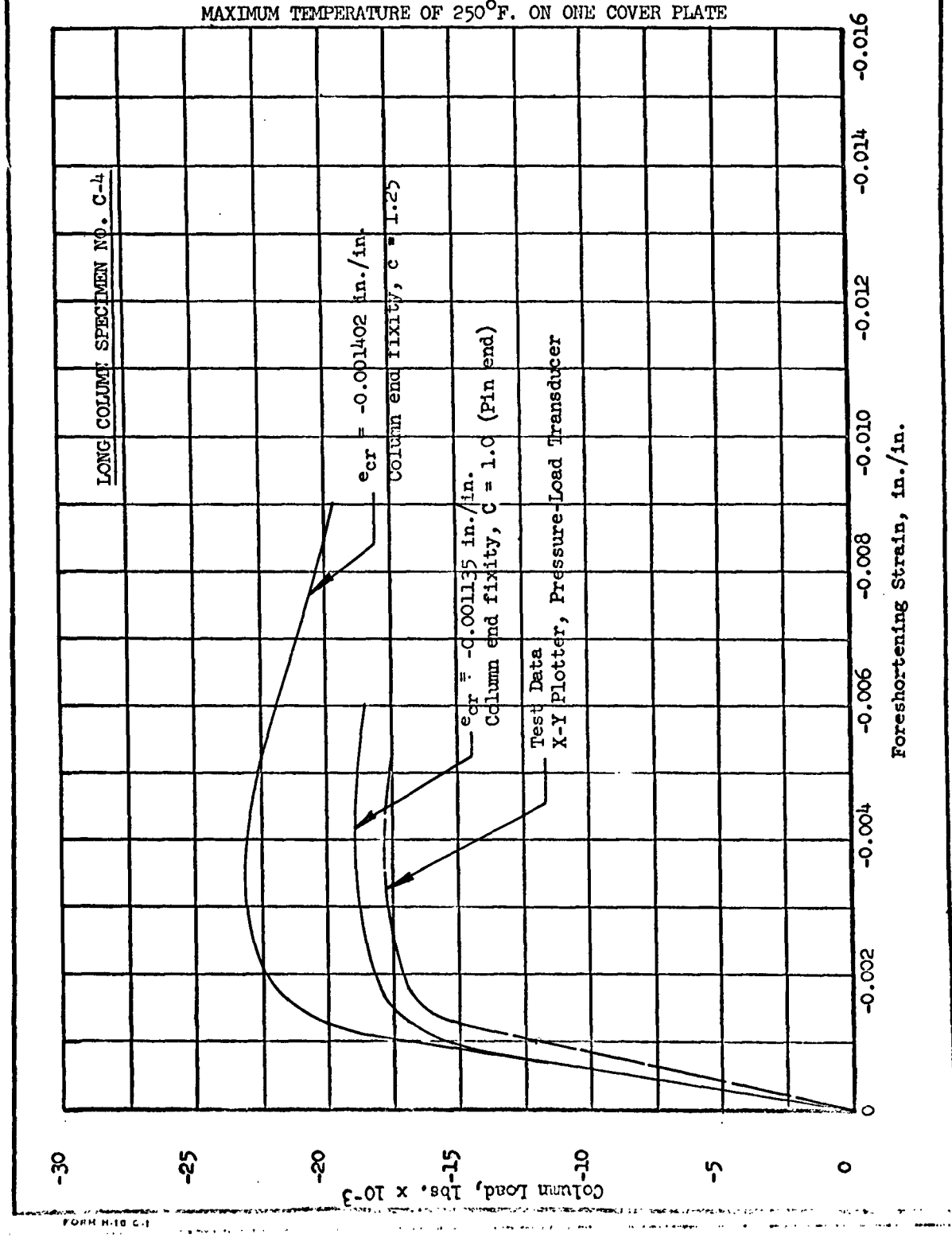

FORM H-16 C-1

FIGURE 8.27

LONG COLUMN LOAD - DEFORMATION CURVE
CALCULATED-TEST COMPARISON
SYMMETRICAL TEMPERATURE GRADIENT

MAXIMUM TEMPERATURE OF 450°F. ON BOTH COVER PLATES

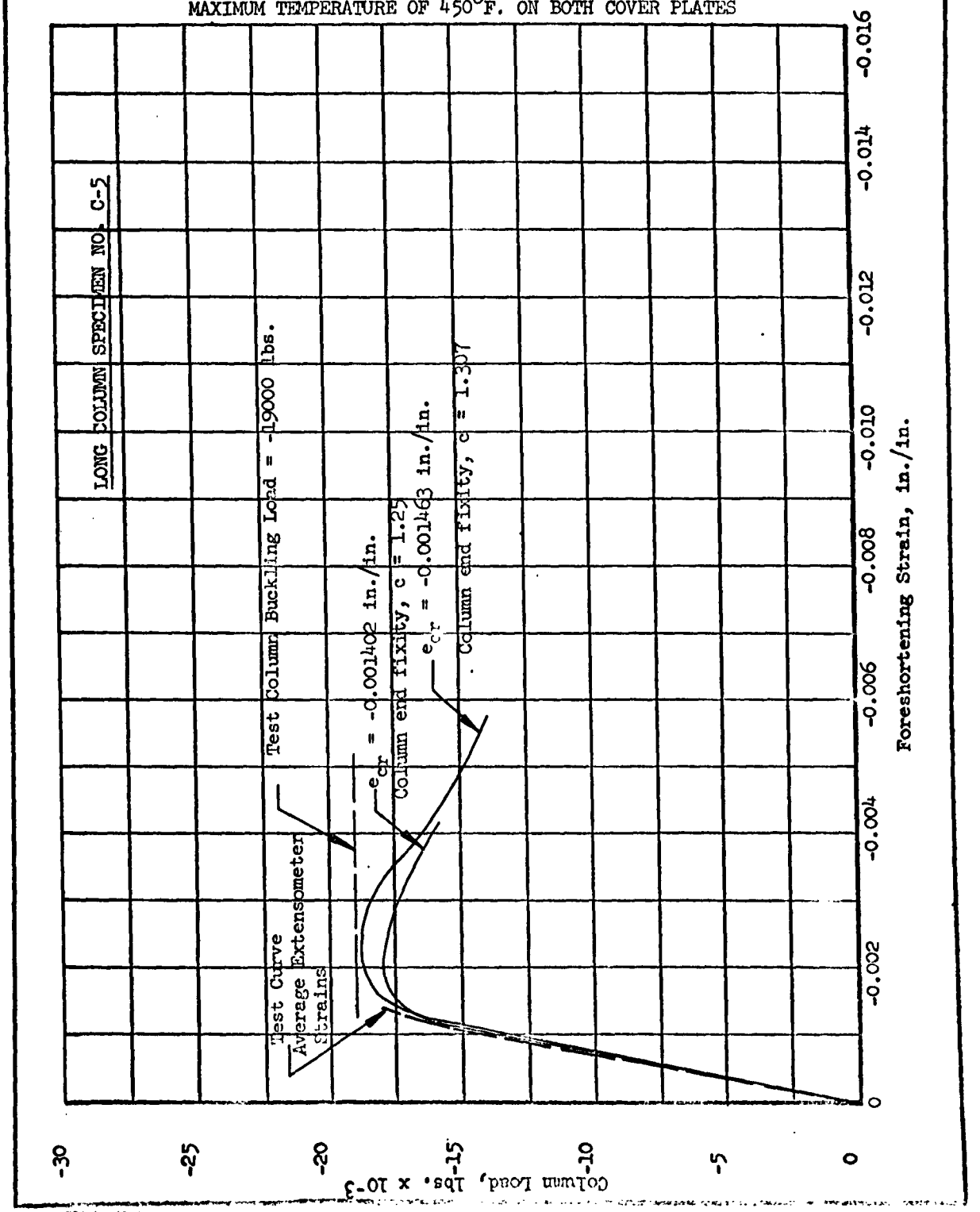

FORM H-18-G-1

FIGURE 8.28

LONG COLUMN LOAD - DEFORMATION CURVE
CALCULATED-TEST COMPARISON
UNSYMMETRICAL TEMPERATURE GRADIENT

MAXIMUM TEMPERATURE OF 450°F. ON ONE COVER PLATE

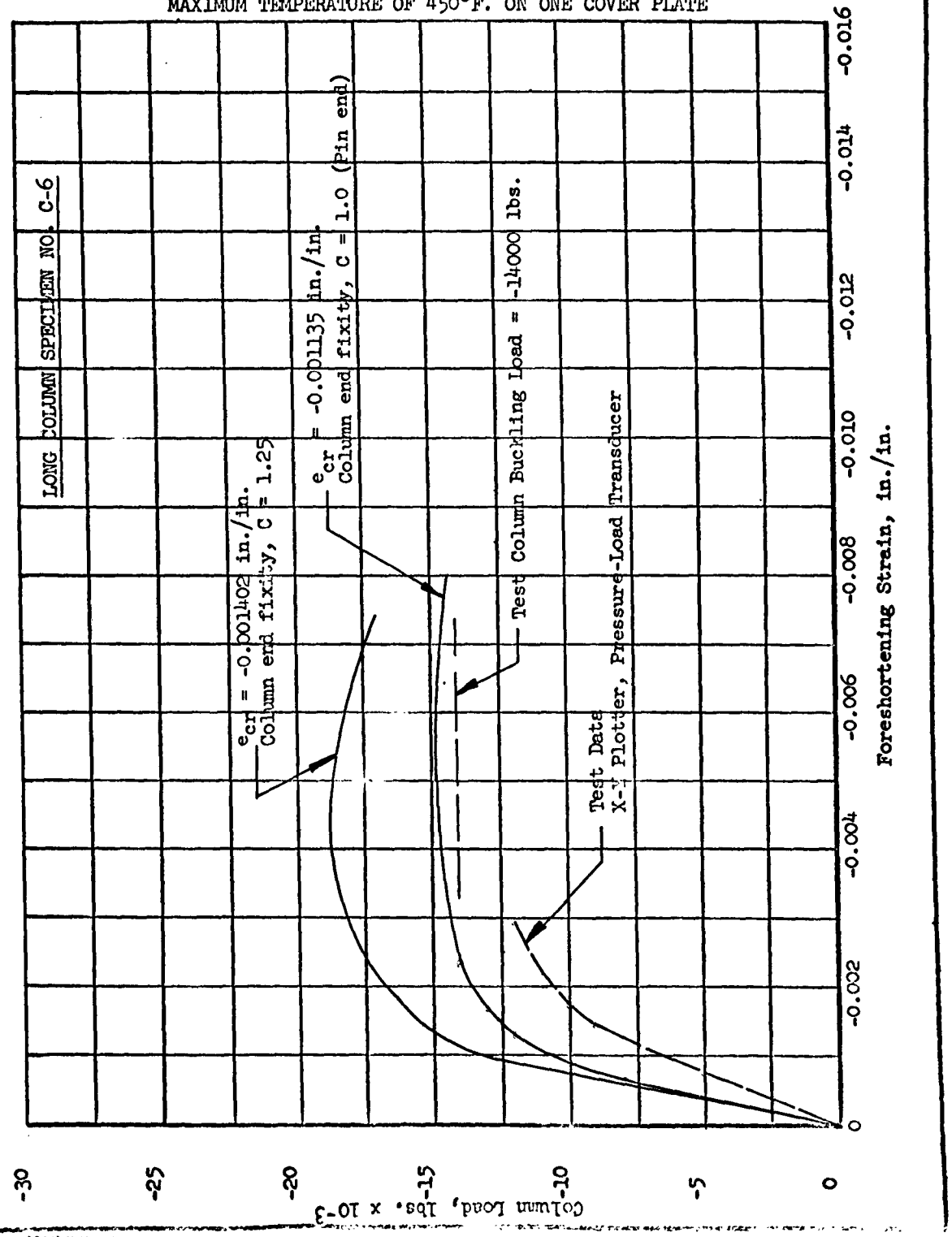

FORM H-10 C-1

FIGURE 8.29

LONG COLUMN LOAD - DEFORMATION CURVE
SUMMARY - EXPERIMENTAL LOAD-DEFORMATION CURVES
FOR END RESTRAINT CONDITIONS REFER TO SECTION 8.2.2

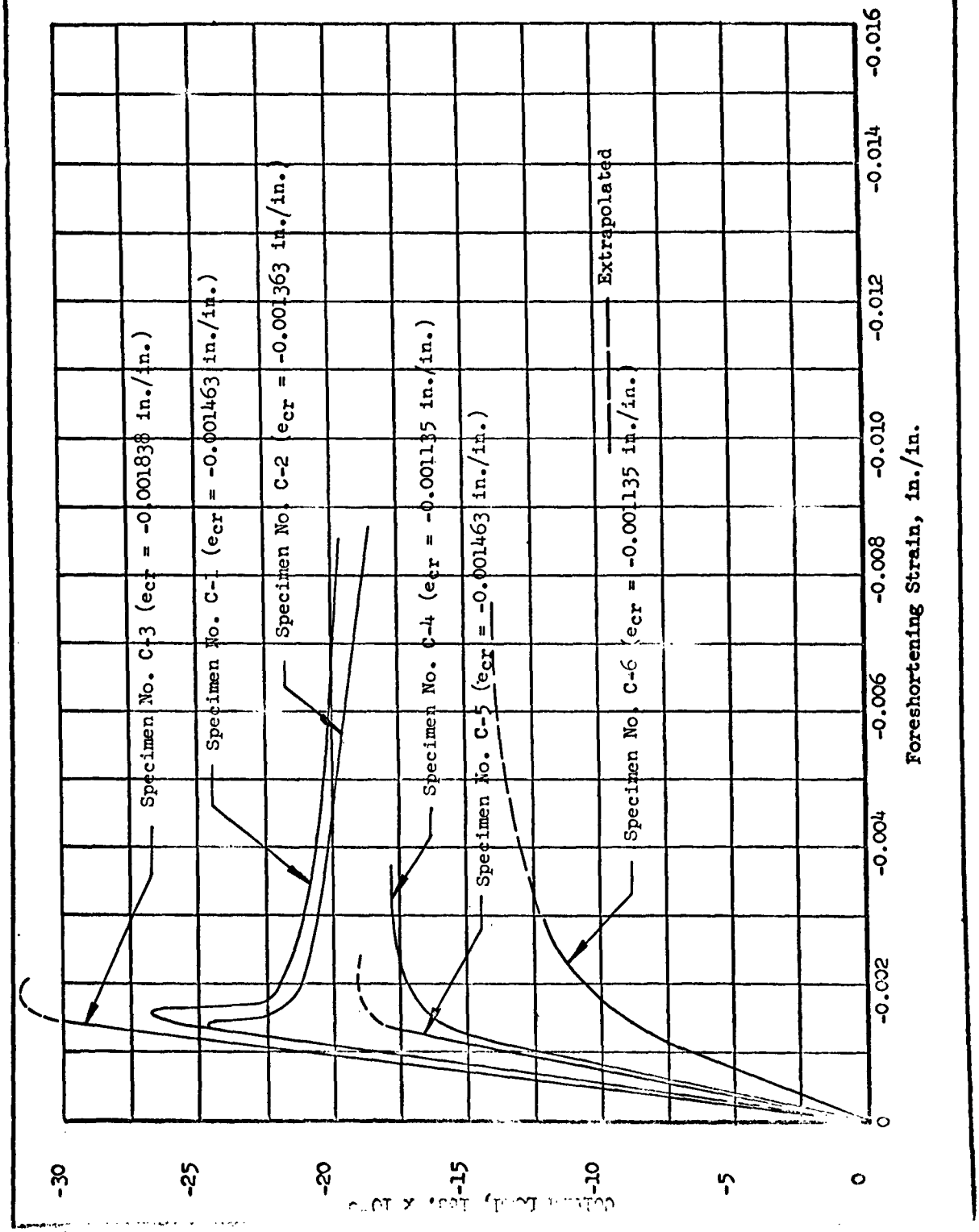

FIGURE 8.30

LONG COLUMN LOAD - DEFORMATION CURVE

SUMMARY — CALCULATED LOAD-DEFORMATION CURVES
END RESTRAINT CONDITIONS AS PER TEST (REFER TO SECTION 8.2.2)

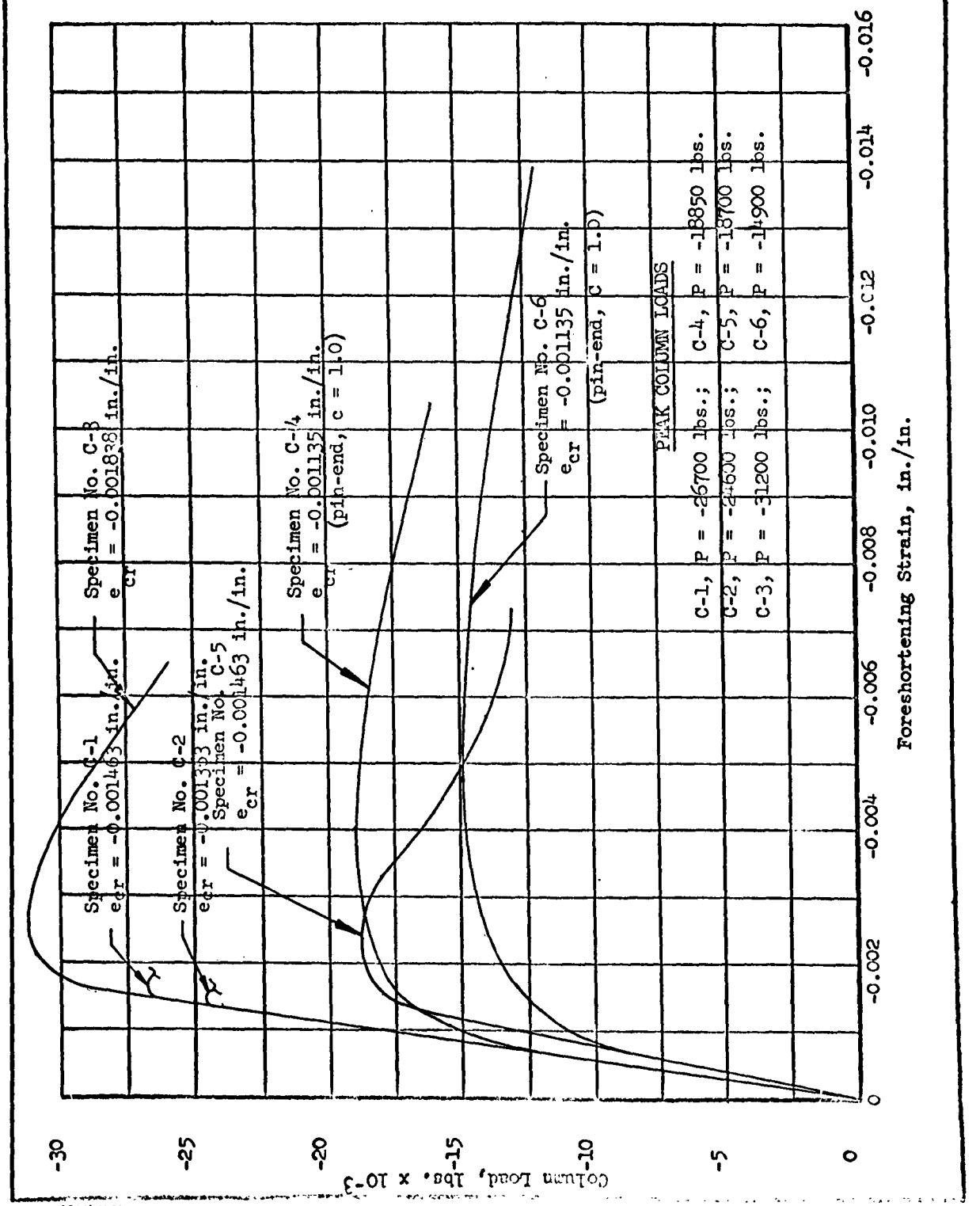

FORM H-1R C-1

FIGURE 8.31

LONG COLUMN LOAD - DEFORMATION CURVE

SUMMARY — CALCULATED LOAD-DEFORMATION CURVES
FOR ASSUMED CONSTANT END RESTRAINT (c = 1.25)

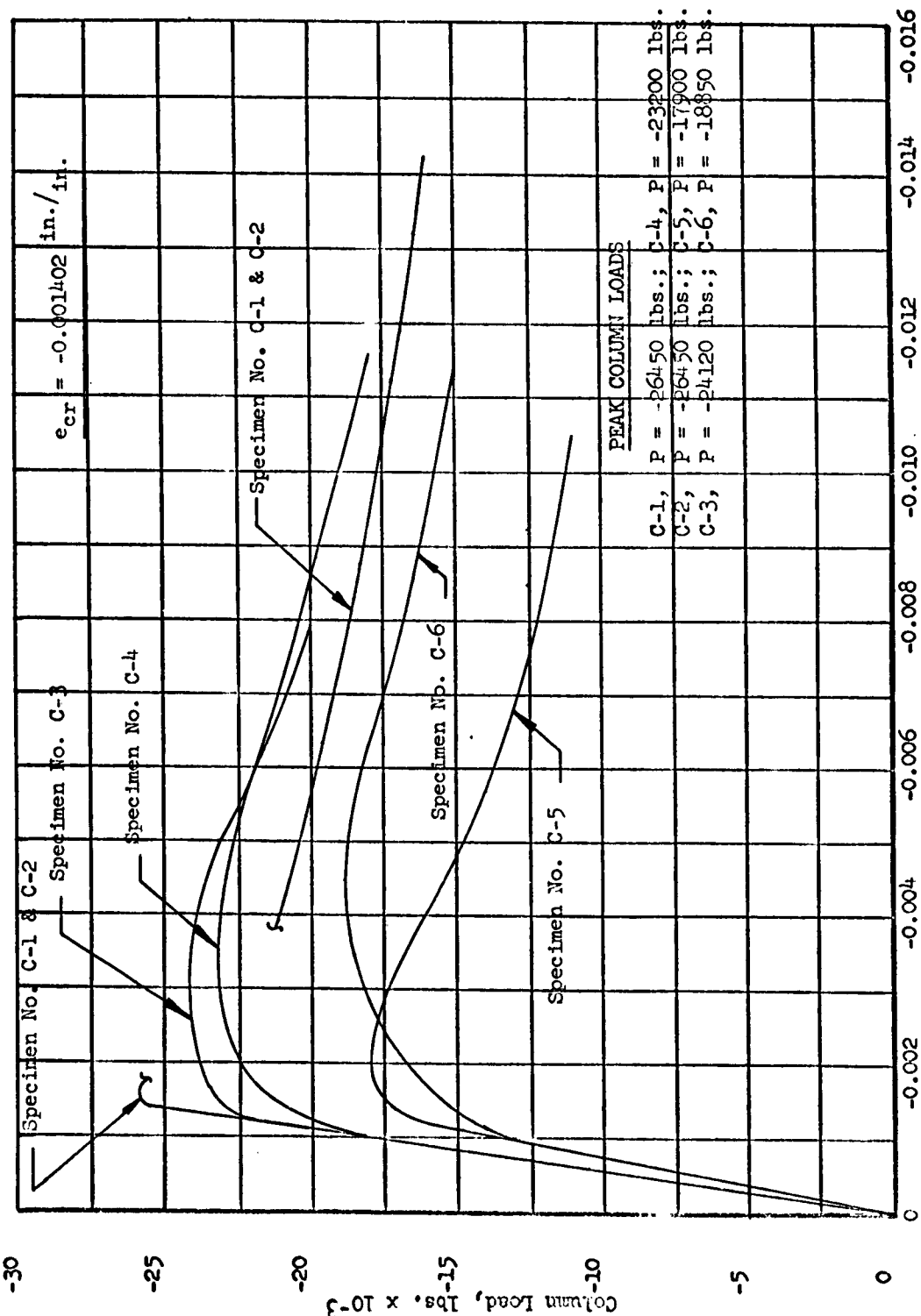

FORM H-10-G-1

8.3.4 THERMAL CYCLING LOAD-DEFORMATION CURVES

Thermal cycling tests were performed on eight specimens for a variety of temperatures, temperature distributions, applied bending moments, and bending moment direction. Essentially these tests were performed by alternately applying and removing the temperature at some fixed value of bending moment on the cross-section. All strain data was recorded from extensometers mounted at the four corners of the box beam. No elevated temperature strain gages were used which eliminated the necessity of considering a strain gage curing temperature exposure history in the evaluation of the material properties. On specimens B-13 and B-11 the test temperature exposure history did not affect the material properties. Therefore, short time elevated temperature properties were adequate to define the material properties.

Two specimens were tested at various levels of cross-section bending moment for a 250°F. symmetrical temperature distribution (cover plates hot, spar webs cool). The first specimen (B-13) was loaded at room temperature to a bending moment of 315,000 in.-lbs. Crippling failure of the compression cover plate and channel flanges occurred at the first application of temperature. The strain data recorded during the room temperature loading was nearly identical to that for the original room temperature bending specimens (B-1 and B-17) and no data at elevated temperature was recorded. Temperature cycling at four values of bending moment was performed on specimen B-11 with the results shown in Figure 8.32. Generally, this data indicates a trend toward elastic shakedown at all load levels with any significant strain accumulation occurring only at, or very close to, the ultimate load. Since the material properties are not changing from one cycle to the next and the time-temperature relationship is not sufficient to produce significant creep, the experimental data shown reflects, essentially, some strain accumulation. However, the shape of the knee of the curve and the low strain instability type failures are indicative of the presence of only small inelastic effects at load levels just below the ultimate which results in elastic shakedown, Reference (b), after only a small number of temperature cycles. This may infer that significant strain

accumulation in structures which fail by local instability is restricted to a very small range of loads close to the ultimate. The calculated curve for the temperature-load sequence shown in Figure 8.32 indicated elastic shakedown at the first temperature cycle at all load levels. This indicates the sensitivity of the shape of the curve and the necessity of defining the element yield stress quite accurately if analytical strain accumulation studies are to be performed accurately.

Two specimens (B-16 and B-12) were tested in a 450°F. symmetrical temperature environment for various bending moments on the cross-section. Temperature exposure histories and the variation of material properties during the test (Tables 2 and 3 of Figure 7.17) affect the element strains in these cases. This variation is accounted for in the determination of the analytical data points shown in Figures 8.33 and 8.34. Specimen B-16 experimental and analytical data shown in Figure 8.33 were obtained for loads well below the static ultimate load, and reflect, primarily, the effects of material properties variation with an increase in temperature cycles. The favorable comparison between analytical and experimental data points and the small strain change between cycles is indicative of small changes in material properties only. No curves are drawn since the previous strain history affects the strain at each succeeding load level. Therefore, the curves would not be representative of a true thermal cycling curve. Seven complete temperature cycles were applied to specimen B-12 at a fixed value of bending moment yielding the experimental data shown in Figure 8.34. The calculations were performed for a fixed number of temperature cycles at three different load levels with the two lower loads showing elastic shakedown at the first temperature cycle. At a load near the ultimate both the analytical and experimental data show some strain accumulation. The small changes in material properties and the short time intervals between cycles indicate that creep and material properties variation between cycles probably represent only a small part of the accumulation. This, coupled with the fact that both the tension

and compression cover plates were inelastic indicates some thermal cycling strain accumulation to be present. In addition, the experimental data indicates a trend toward elastic shakedown at the seventh cycle. The comparison of analytical and experimental data is considered favorable in light of the material properties variation and variations in the shape of the stress-strain curves. With the compression element critical and the mode of failure as local instability, the tendency to elastic shakedown is shown even at very high loads.

To investigate the effects of both positive and negative bending moments on beams with unsymmetrical temperature gradients present the final group of four specimens was tested in a controlled temperature environment and temperature exposure history. Two specimens (B-10 and B-15) were tested for the 450°F. unsymmetrical gradient condition with the applied bending moments producing tension on the 450°F. cover plate. Two specimens (B-9 and B-14) were tested for the 450°F. unsymmetrical gradient condition with the applied bending moment producing compression on the 450°F. cover plate. The intent of this portion of the study was to compare and evaluate the strain accumulation for a given temperature environment and history for critical compression elements and critical tension elements. For this comparison seven temperature cycles were applied to each of the four specimens at some specified bending moment. The calculations were performed for seven temperature cycles at several bending moment values in the range of the applied test moments. The maximum temperature (450°F.) and the time at maximum temperature during initial loading and at each temperature cycle were controlled as closely as practicable to produce uniformity of temperature environment between specimens. The temperature distribution through the cross-section could not be as easily controlled as shown by Figures 6.15 and 6.16. Therefore, the variation in element temperatures between specimens affects the material properties, and, consequently the shape of the load-deformation curve. The experimental curves for B-10 and B-15, and for B-9 and B-14 indicate the effect of material property variation between specimens to be relatively small.

The critical tension element curves for specimens B-10 and B-15 illustrate typical strain accumulation at both load levels with a tendency toward elastic shakedown after a very limited number of cycles. It is possible that elastic shakedown would not occur, however, since the accumulating temperature exposure history is producing continually decreasing material properties. In addition, creep effects could become significant as time at temperature is increased. The calculated data shows a similar trend but the correlation with test data is highly dependent upon the accuracy of the material properties, particularly the yield stress of the material. Any variation in the yield stress affects the sensitivity of the strains in and beyond the knee of the stress-strain curve. From Figures 8.35 and 8.36 it is apparent that the yield stress values for critical extreme fiber elements in the analysis were somewhat higher than the actual values for the specimens. It should be noted, however, that only a 5% variation could be serious when strain calculations in the knee of the stress-strain curve are involved.

Specimens B-9 and B-14 defined the critical compression element curves as shown in Figures 8.37 and 8.38. Both specimens showed small strain accumulation effects and rapid shakedown to the elastic case similar to previous specimens where the critical element was the compression cover plate. As in the tension case the calculated data showed results similar to the experimental data (either no strain accumulation or small accumulation and rapid elastic shakedown). The elastic shakedown occurs fairly rapidly in temperature-load environments of this type for several reasons. The inelastic effects present on the hot side, with compression loads acting, are directly related to the buckling of the cover plate. The cool side, with tension loads acting, has considerably higher material properties, thus, delaying the onset of inelastic strain. Furthermore, with buckling occurring on the hot side, the neutral axis tends to shift toward the tension side and further delays the onset of inelastic strain on the tension side. For true thermal cycling strain accumulation to

occur in bending, both sides of the beam must be inelastic. This, coupled with the fact that the compression instability failure is essentially a low strain failure, tends to explain why very little strain accumulation occurs at loads just below the failing load for specimens B-9 and B-14.

Comparing the curves of B-10 and B-15 with those for B-9 and B-14 illustrates the difference in strain accumulation when the hot side is in tension and when the hot side is in compression. The greater strain accumulation shown by B-10 and B-15 is produced by the fact that the inelastic effects tend to occur on both cover plates as opposed to B-9 and B-14 where, in general, the inelastic strains on the tension covers of B-9 and B-14 are reduced as described in the preceding paragraph. This effect is noted in both the analytical and experimental data. However, the comparison between test and analysis can only be made on a qualitative basis to define the relative effects of strain accumulation due to the sensitivity of the yield stress and shape of the stress-strain curve.

For plotting purposes the ordinate and abscissa are as defined in Section 8.3.1 for the bending specimens.

FIGURE 8.32
THERMAL CYCLING - 250°F. SYMMETRICAL TEMPERATURE GRADIENT
SPECIMEN NO. B-11

H-18-G-1

FIGURE 8.33

THERMAL CYCLING - 450° F. SYMMETRICAL TEMPERATURE GRADIENT (MAXIMUM TEMPERATURE ON BOTH COVER PLATES)

SPECIMEN NO. B-16

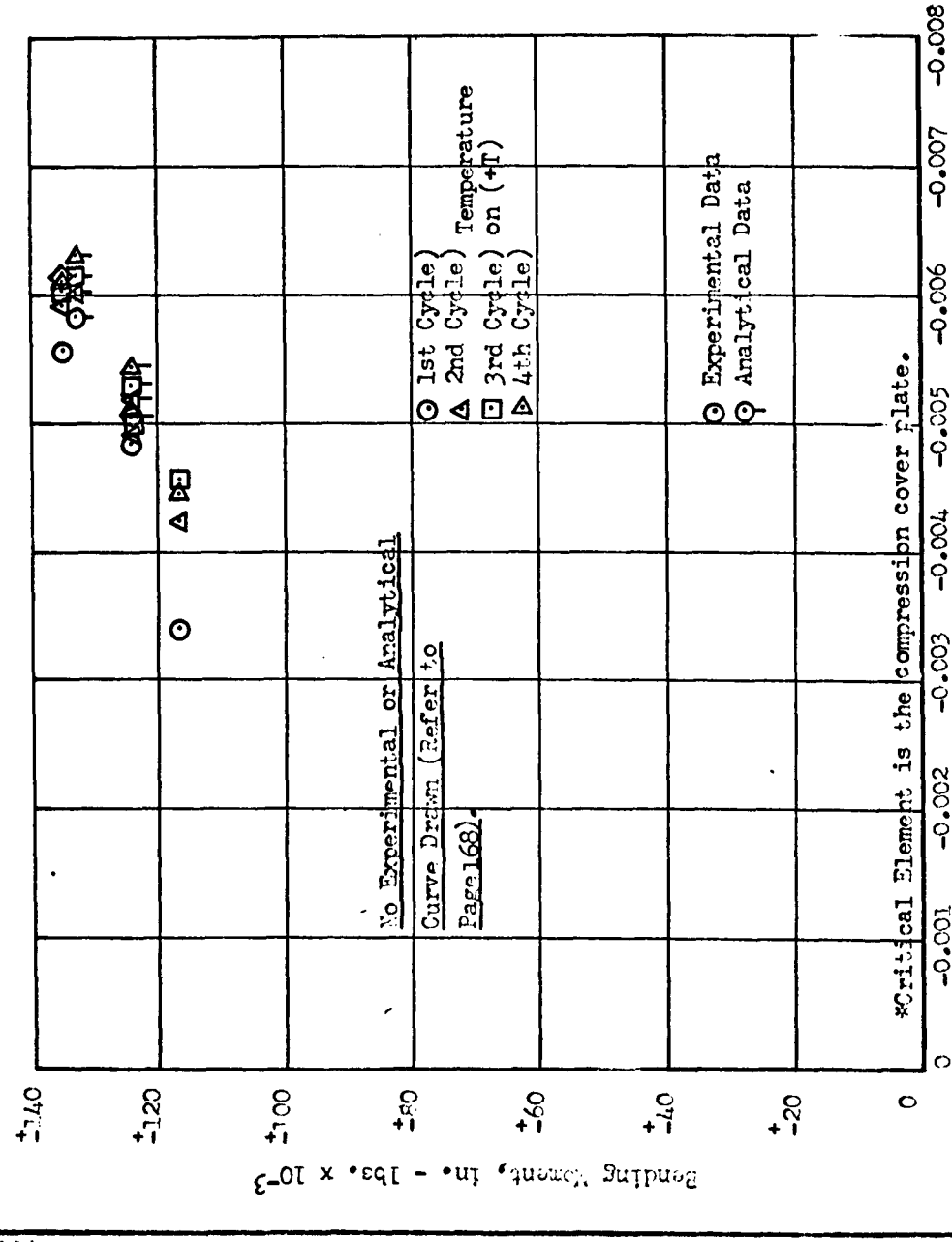

H-18-G-1

FIGURE 8.34

THERMAL CYCLING - 450° F. SYMETRICAL TEMPERATURE GRADIENT (MAXIMUM TEMPERATURE ON BOTH COVER PLATES)

SPECIMEN NO. B-12

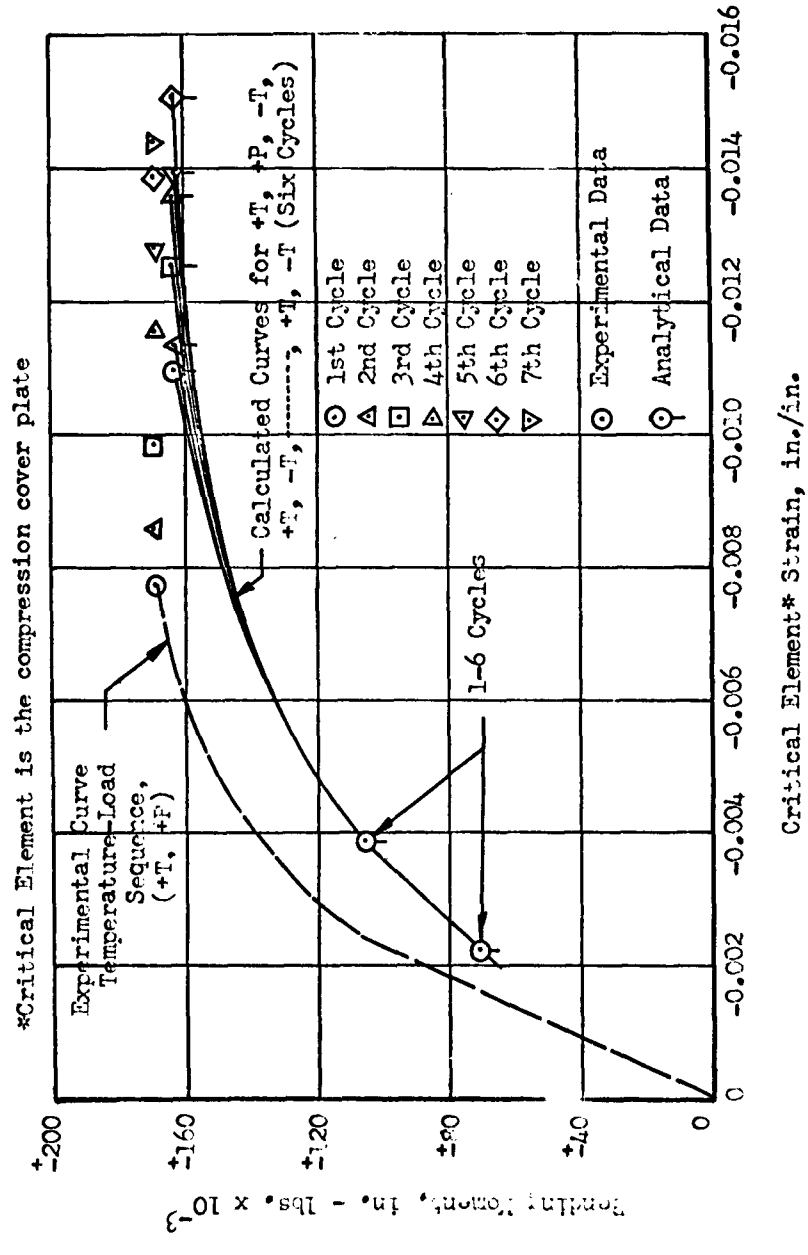

M-10-G-1

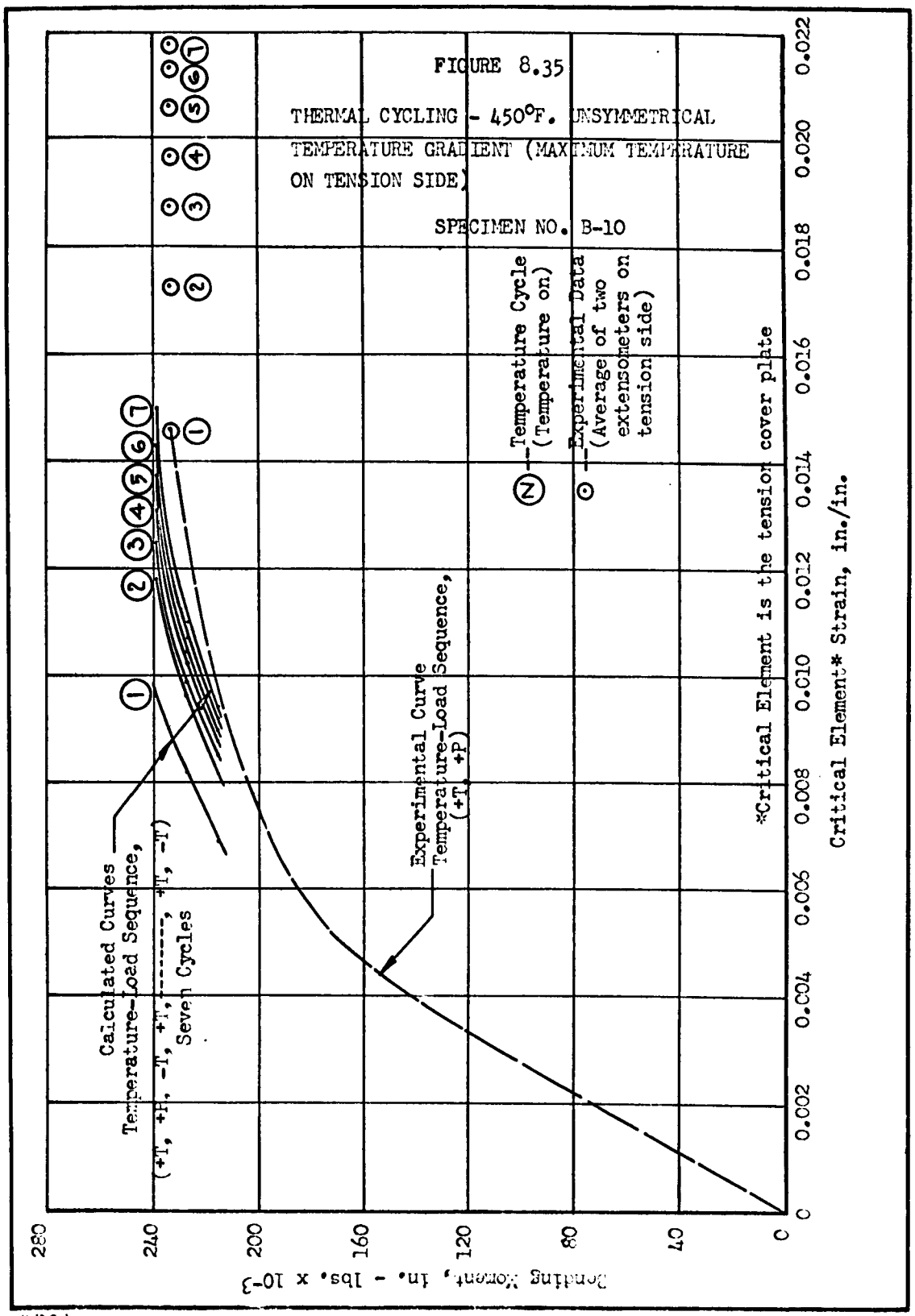
FIGURE 8.35
THERMAL CYCLING - 450°F. UNSYMMETRICAL TEMPERATURE GRADIENT (MAXIMUM TEMPERATURE ON TENSION SIDE)
SPECIMEN NO. B-10
Temperature Cycle (Temperature on)
Experimental Data (Average of two extensometers on tension side)
Calculated Curves Temperature-Load Sequence, (+T, +P, -T, +T, -T, +T, -T) Seven Cycles
Experimental Curve Temperature-Load Sequence, (+T, +P)
*Critical Element is the tension cover plate
Critical Element* Strain, in./in.
Bending Moment, in. - lbs. x 10-3
0
40
80
120
160
200
240
280
0.002
0.004
0.006
0.008
0.010
0.012
0.014
0.016
0.018
0.020
0.022

H-18-G-1

FIGURE 8.36

THERMAL CYCLING - 450° F. UNSYMMETRICAL TEMPERATURE GRADIENT (MAXIMUM TEMPERATURE ON TENSION SIDE)

SPECIMEN NO. B-15

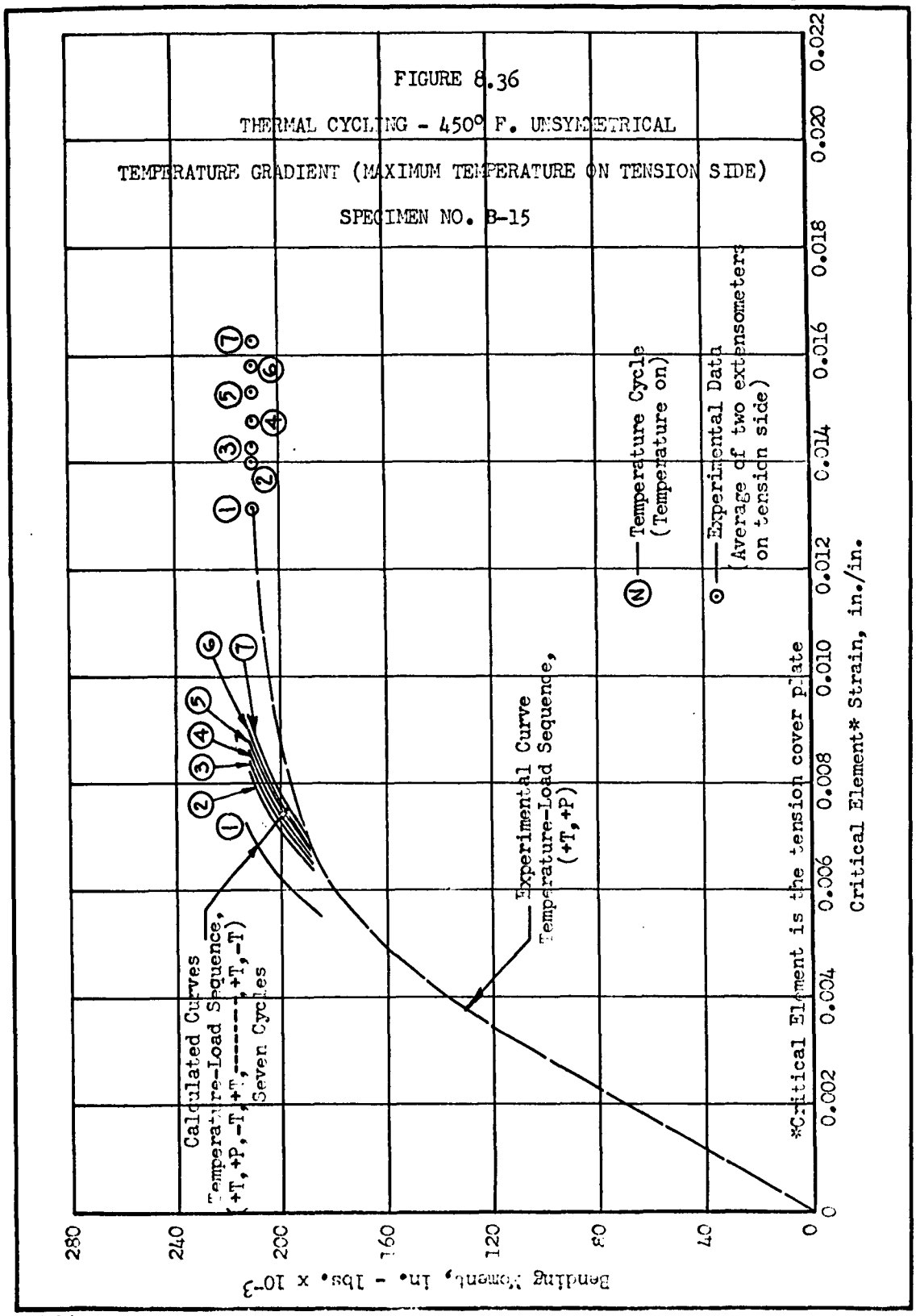

H-18-G-1

FIGURE 8.37

THERMAL CYCLING - 450° F. UNSYMMETRICAL TEMPERATURE GRADIENT (MAXIMUM TEMPERATURE ON COMPRESSION SIDE)

SPECIMEN NO. B-9

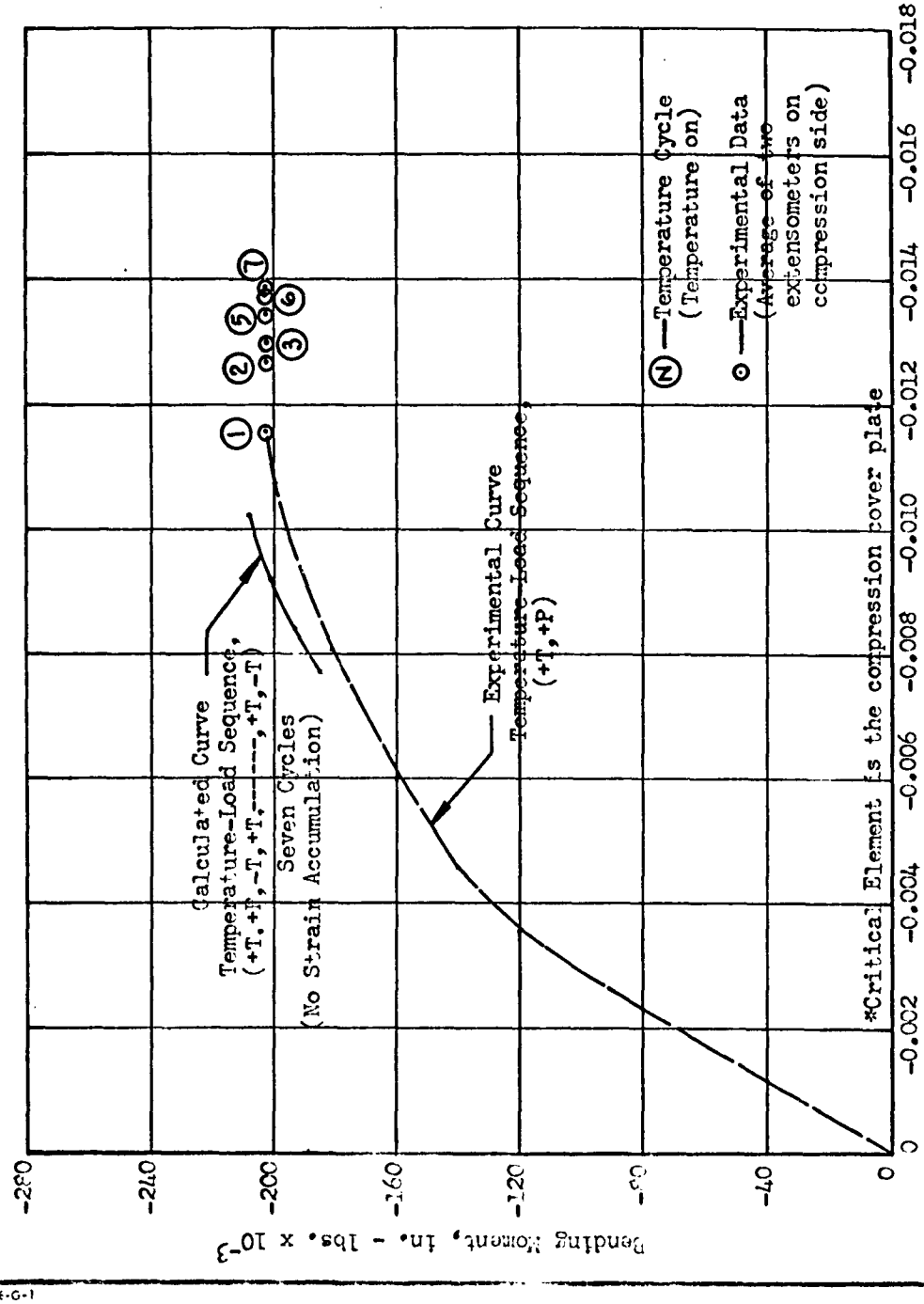

H-16-G-1

FIGURE 8.38

THERMAL CYCLING - 450° F. UNSYMMETRICAL TEMPERATURE GRADIENT (MAXIMUM TEMPERATURE ON COMPRESSION SIDE)

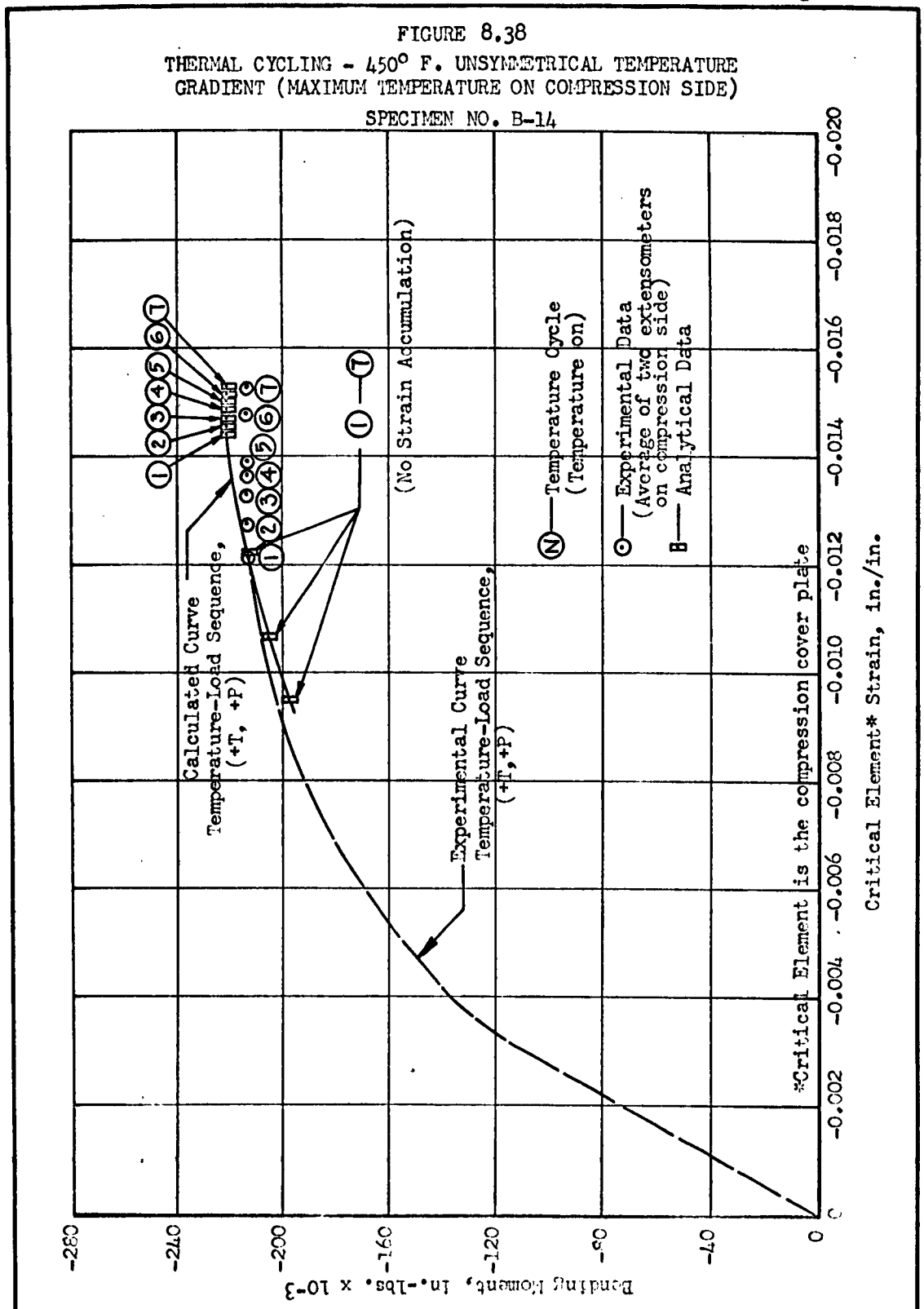

H-18-G-1

9.0 APPLIED LOAD RATIOS

The structural design (and test) condition which includes both a load and temperature environment may, under certain circumstances, be adequately simulated for test purposes by the load environment alone. Considering axial load and/or bending moment, no cross-section warping, and precluding shear or joint failures the elevated temperature static test may be simulated at room temperature if the applied load ratios consider certain specific factors. For a realistic definition of elevated temperature structural integrity the following factors must be considered:

1. Variation of material properties through the cross-section where the reduction of material properties on any structural element must, in some cases, allow for the effects of previous complex temperature exposure histories.

2. The effects of thermal stresses.

3. Inelastic stress-strain relationships.

4. Buckling.

5. Possible use of mixed materials.

The load-deformation procedures described in this report allow for these factors and provide a means whereby an applied load ratio can be defined for ultimate load, yield load defined by the 0.002 in./in. offset strain, or any other desired value of permanent set. In addition, these procedures allow for temperature-load sequencing which indicates a possibility of simulating thermal cycling with either a single temperature cycle or a single static test at room temperature.

This section describes and compares the analytical and test results in terms of applied load ratios for the bending, short column (crippling), and long columns. Calculated ultimate applied load ratios are compared directly with the test values and typical calculated yield load ratios are compared with the calculated ultimate load ratios for the bending specimens. The tables illustrate what might be expected as typical applied load ratios for 7075-T6 aluminum alloy structures when subjected to temperature environments and exposure histories similar to those of this study.

9.1 TEST SUMMARY AND ANALYSIS COMPARISON

9.1.1 BENDING SPECIMENS

The ultimate applied load ratios for all bending specimens are shown in Figure 9.1. This table shows the ultimate (failure) bending moments from both test and analysis along with the per cent deviation of the calculated value from the test value. All test failures were a general instability (crippling) failure of the compression cover including the flanges of the channel spar webs. Calculations showed the compression cover plate to be the critical element in all cases. The agreement is considered quite favorable since the deviations, in most cases, are well within the accuracy afforded by material properties variation alone, particularly when complex temperature exposure histories are involved. In addition, Figure 9.1 compares the calculated and test applied load ratios where the applied load ratio is a multiplying factor on the applied loads at elevated temperature and is defined by

$$R_{ult.} = \frac{(M_{ult.})_{R.T.}}{(M_{ult.})_{E.T.}}$$

where the values of $(M_{ult.})_{R.T.}$ were taken as 329,500 in.-lbs. and 345,000 in.-lbs. for test and analysis ratios, respectively. Generally, good agreement was obtained with the positive deviations indicating the analytical procedures to be slightly conservative. The use of MIL-HDBK-5 material properties (as required for design) would ensure conservatism in the simulated test at room temperature when used in conjunction with the load-deformation technique described in this report.

A comparison of calculated ultimate and calculated yield applied load ratios is shown in Figure 9.2 to illustrate the fact that it may be necessary to define applied load ratios for each

structural design criterion. This also serves to define which criterion is critical, such as yield or ultimate. The calculated ultimate moments and applied load ratios shown are based on the cut-off moment defined by the load-deformation curve with temperature and load acting (temperature-load sequence, +T, +P). The calculated yield moments and applied load ratios are based on the applied bending moment defined by the 0.002 in./in. offset yield strain on the critical element load-deformation (strain) curve with temperature and load applied and then removed (temperature-load sequence, +T, +P, -P, -T). The yield applied load ratios are multiplying factors on the applied load at elevated temperature and are defined by

$$R_{yield} = \frac{(M_{yield})_{R.T.}}{(M_{yield})_{E.T.}}$$

where the calculated value of $(M_{yield})_{R.T.}$ in Figure 9.2 is 324,000 in.-lbs. Insufficient test data was available for comparison of calculated and test yield values. However, satisfactory agreement between test and analysis curves with temperature and load acting (+T, +P) implies, at least, favorable agreement between calculated and test permanent set curves defined by the temperature-load sequence +T, +P, -P, -T.

FIGURE 9.1
TEST SUMMARY AND ANALYSIS COMPARISON
BENDING SPECIMENS

BENDING SPECIMEN NO.	TEST TEMPERATURE CONDITION	LOADING CONDITION	TEST ULTIMATE MOMENT IN.-LBS.	ANALYSIS ULTIMATE MOMENT IN.-LBS.	PER CENT DEVIATION	TEST APPLIED LOAD RATIO	ANALYSIS APPLIED LOAD RATIO	PER CENT DEVIATION
B-1	R.T.	(±) Bending	±330,000	±345,000	+4.3	1.000*	1.000	--
B-17	R.T.	(±) Bending	±328,500	±345,000	+4.8	1.000*	1.000	--
B-4	250°F. max. (symmetrical)	(±) Bending	±201,300	±191,500	-4.8	1.636	1.800	+9.2
B-5	250°F. max. (unsymmetrical)	(+) Bending	+198,750	+196,750	-1.0	1.657	1.753	+5.5
B-8	250°F. max. (unsymmetrical)	(-) Bending	-189,200	-196,500	+3.2	1.740	1.756	+0.8
B-3	450°F. max. (symmetrical)	(±) Bending	±139,750	±135,300	-3.2	2.355	2.550	+7.7
B-7	450°F. max. (unsymmetrical)	(+) Bending	+172,500	+169,750	-1.6	1.910	2.032	+6.1
B-6	450°F. max. (unsymmetrical)	(-) Bending	-180,000	-158,300	-12.2	1.830	2.180	+16.1

*Average value of B-1 and B-17 used as reference, M = ±329,500 in.-lbs.

FIGURE 9.2
SUMMARY - CALCULATED ULTIMATE AND YIELD APPLIED LOAD RATIOS
BENDING SPECIMENS

Bending Specimen No.	Test Temperature Condition	Loading Condition	Calculated Ultimate Moment, In.-Lbs.	Calculated Ultimate Load Ratio	Calculated Yield Moment, In.-Lbs.	Calculated Yield Load Ratio	Critical Condition
B-1	R.T.	(±)Bending	±345,000	1.000	±324,000	1.000	- -
B-17	R.T.	(±)Bending	±345,000	1.000	±324,000	1.000	- -
B-4	250°F. max.(symmetrical)	(±)Bending	±191,500	1.800	±184,000	1.762	Ultimate
B-5	250°F.max. (unsymmetrical)	(+)Bending	+196,750	1.753	+189,000	1.714	Ultimate
B-8	250°F.max. (unsymmetrical)	(-)Bending	-196,500	1.756	-187,000	1.733	Ultimate
B-3	450°F. max.(symmetrical)	(±)Bending	±135,300	2.550	±124,000	2.613	Yield
B-7	450°F.max. (unsymmetrical)	(+)Bending	+169,750	2.032	+167,000	1.940	Ultimate
B-6	450°F.max. (unsymmetrical)	(-)Bending	-158,300	2.180	-131,000	2.473	Yield

9.1.2 SHORT COLUMN SPECIMENS

The applied load ratios for the crippling loads of all short column specimens are summarized and compared in Figure 9.3. All test and calculated failures were similar with the 0.125 inch cover plates being the critical elements. The agreement between test and analysis crippling loads is quite good, especially considering the material properties variation when complex temperature exposure histories are involved. The applied load ratios are multiplying factors on the applied loads at elevated temperature and are defined by

$$R_{cc} = \frac{(P_{cc})_{R.T.}}{(P_{cc})_{E.T.}}$$

where the values of $(P_{cc})_{R.T.}$ were taken as -221,000 lbs. and -223,600 lbs. for test and analysis ratios, respectively. As in the case of the bending specimens the use of MIL-HDBK-5 material prperties would ensure conservatism for calculated applied load ratios used to perform the simulated elevated temperature static test at room temperature.

No yield values are shown since the crippling failures occur near yield strain and the permanent set effects for the specimens in this study were quite small until the peak, or crippling, load was reached. It does appear, however, that another important structural design criterion should be related to permanent buckling in addition to the 0.002 in./in. offset yield and the ultimate strength. This is particularly true when the thermal strains from non-uniform temperature distributions have a severe effect on the initial buckling of plate elements in the cross-section. For many structures which fail by local instability it may be that the permanent buckling criterion should replace the 0.002 in./in. offset yield.

Although not investigated in this study, the use of load-deformation (strain design) techniques seems to offer a means to define the point at which permanent buckling occurs. The relative shape of bending and compression load-deformation curves seems to indicate that a structural design criterion associated with permanent buckling may apply more to compression produced by bending than by a compression load alone. In any case, some consideration should be given to further studies related to the experimental and analytical determination of permanent buckling. With permanent buckling defined at both room and elevated temperature an applied load ratio could be defined as for the 0.002 in./in. offset yield and ultimate load.

FIGURE 9.3
TEST SUMMARY AND ANALYSIS COMPARISON
CRIPPLING SPECIMENS

(Specimen No. A-6 is used in the bending moment restraint analysis of Section 8.2.1)

CRIPPLING SPECIMEN NO.	TEST TEMPERATURE CONDITION	LOADING CONDITION	TEST CRIPPLING LOAD, LBS.	ANALYSIS CRIPPLING LOAD, LBS.	PER CENT DEVIATION	TEST APPLIED LOAD RATIO	ANALYSIS APPLIED LOAD RATIO	PER CENT DEVIATION
A-1	R.T.	Compression	-220,000	-223,600	+1.6	1.000**	1.000	--
A-2	R.T.	Compression	-222,000	-223,600	+0.7	1.000**	1.000	--
A-4	250°F. max. (symmetrical)	Compression	-164,000	-171,000	+4.2	1.348	1.308	-3.0
A-5	250°F. max. (unsymmetrical)	Compression* and Bending	-184,000	-178,000	-3.3	1.202	1.257	+4.3
A-3	425°F. max. (symmetrical)	Compression	-150,000	-141,700	-5.6	1.475	1.577	+6.5
A-6	425°F. max. (unsymmetrical)	Compression* and Bending	-134,000	*	--	--	--	--

* Refer to Section 8.2.1 for discussion of bending moment restraint.

** Average value of A-1 and A-2 used as reference, P = -221,000 lbs.

9.1.3 LONG COLUMN SPECIMENS

The variation in test end fixity between column specimens would not allow a compatible comparison of applied load ratios. However, to demonstrate the procedure, calculations were performed for all column specimens for a given column buckling strain (e_{cr} = -0.001402 in./in.) which corresponds to an end fixity of c = 1.25 which was the average test value for the two room temperature specimens. The calculated applied load ratios are summarized in Figure 9.4 to illustrate the effect of various temperature distributions on the applied loads for room temperature simulation. The applied load ratios in Figure 9.4 are calculated by

$$P_{cr} = \frac{(P_{max.})_{R.T.}}{(P_{max.})_{E.T.}}$$

The comparison of the calculated peak loads and the Euler buckling loads indicates the major effect on the maximum load to be produced by material properties variation and initial bowing of the column induced by unsymmetrical temperature gradients through the cross-section. Note particularly colmn specimen C-5 which seems to indicate that the peak load is still very close to P_{cr} as defined by

$$P_{cr} = e_{cr} \sum E_n A_n$$

despite the presence of comparatively large thermal stresses as long as the temperature gradient is symmetrical. This may not be true, however, if buckling is produced by the thermal stresses. No data is available to substantiate the critical buckling load versus maximum load comparison in this case.

FIGURE 9.4

SUMMARY — CALCULATED PEAK APPLIED LOAD RATIOS
LONG COLUMN SPECIMENS
Based on end fixity coefficient, c = 1.25

e_{cr} = -0.001402 in./in.

COLUMN SPECIMEN NO.	TEST TEMPERATURE CONDITION	CALCULATED PEAK LOAD, LBS.	CALCULATED PEAK LOAD RATIO	EULER* BUCKLING LOAD, LBS.
C-1	R.T.	-26450	1.00	-26450
C-2	R.T.	-26450	1.00	-26450
C-3	250°max. (symmetrical)	-24120	1.097	-24150
C-4	250°max. (unsymmetrical)	-23200	1.140	-24650
C-5	450°max. (symmetrical)	-17900	1.480	-18200
C-6	450°max. (unsymmetrical)	-18850	1.404	-22080

* $P_{cr} = e_{cr} \sum E_n A_n$ (Reference only)

9.1.4 THERMAL CYCLING SPECIMENS

Although load-deformation curves are presented in Section 8.0 for the thermal cycling specimens, no table of applied load ratios is shown. The applied load ratio procedure could be used, however, by selecting some specific design criterion, such as 0.002 in./in. offset (yield), some fixed value of total strain, or ultimate load. In general, the most important thermal cycling curve to consider for simulation at room temperature is the elastic shakedown curve. This is the lowest of the thermal cycling curves and represents a different number of temperature cycles at each load level. The elastic shakedown curve is representative of aircraft, or other vehicles, where more than one temperature cycle is expected or various types of missions are to be performed. Using this curve the applied load ratio may be based on some specific maximum total strain or maximum permanent set strain rather than failure, or the number of cycles at failure (elongation of the material) may be selected as the design criterion.

9.2 COMPARISON WITH SIMPLE APPROXIMATE RATIOS

As pointed out in Sec. 1.0 many contractors have used various forms of simplified approximate applied load ratios to simulate an elevated temperature static test at room temperature. Many of these ratios have considered only the reduction in basic material properties (F_{tu}, F_{ty}, F_{cy}, or E), and some have considered material properties reduction plus the effect of the addition of thermal stresses to the applied stresses. Usually this latter case has been defined by adding elastically the applied and thermal stresses. This section purports to show how some of these approximate ratios compare with the actual test results of the specimens tested in this program and also how they compare with the load-deformation ratios investigated in this study. Note that in certain instances a simplified ratio may compare quite favorably with the test, but the only consistently favorable agreement was obtained using load-deformation ratios. The following sections define the approximate ratios used and show specific examples. The resulting ultimate applied load ratios are tabulated for comparison with the load-deformation and test results.

9.2.1 BENDING SPECIMENS

Four approximate procedures for obtaining applied load ratios were investigated.

(a) Material properties reduction only where the yield stress (F_{ty} or F_{cy}) of the hottest element was compared with the room temperature yield stress of the element.

(b) Material properties reduction only where the bending stiffness (EI) of the cross-section at temperature is compared with the room temperature EI.

(c) A somewhat more realistic use of basic material properties alone where the yield stress (F_{ty} or F_{cy}) of each element in the cross-section is considered by comparing $\sum F_{yn} A_n y_n$ at temperature with $\sum F_{yn} A_n y_n$ at room temperature.

(d) Material properties reduction plus the elastic sum of the applied and thermal stresses compared to the yield stress of the critical extreme fiber compression element.

The methods used for cases (a) through (d) above are demonstrated in the example below using data from bending specimen B-3. For case (a) the room temperature F_y and critical elevated temperature F_y are 77750 psi and 20600 psi, respectively. The applied load ratio is $R = \frac{77750}{20600} = 3.81$. The yield stresses are from Fig. 7.14 and include all elevated temperature effects involved with the temperature-time history. This procedure does not allow for the presence of thermal stresses but is considerably over-conservative for all six specimens as shown in Fig. 9.5.

For case (b) the bending stiffness parameters (EI) at room and elevated temperature are 96.5×10^6 and 70.8×10^6, respectively. The applied load ratio is

$$R = \frac{96.5 \times 10^6}{70.8 \times 10^6} = 1.363.$$

This procedure does not account for thermal stresses and provides a very unconservative estimate of the applied load ratio as shown by the comparison in Fig. 9.5 . However, the highly unconservative margin in this case is not attributed to neglecting the thermal stresses. The failure of specimens of this type is primarily a function of the yield stress of the material which has sustained a marked decrease not only due to the test temperature, but also because of the previous elevated temperature history. The modulus of elasticity of the material does not decrease as sharply with temperature and is relatively unaffected by previous elevated temperature history. The effects of the reduction of F_y are much more influential in this case than either the thermal stresses or the reduction of E with temperature, therefore, the use of EI ratios would be a very poor choice for test simulation.

Case (c) is a more realistic approach to an approximate applied load ratio considering material properties alone. The calculations for defining the psuedo-yield moment values are shown in the following table.

ELEMENT NO.	A_n	$(y_n)_{R.T.}$	$(F_{y_n})_{R.T.}$	$(F_{y_n}A_n y_n)_{R.T.}$	$(y_n)_{E.T.}$	$(F_{y_n})_{E.T.}$	$(F_{y_n}A_n y_n)_{E.T.}$
1	0.625	1.9375	-77750	-94,200	1.9385	-20600	-29,450
2	0.125	1.9375	-77750	-18,820	1.9385	-29550	- 7,160
3	0.2806	1.782	-72675	-36,300	1.783	-29650	-14,830
4	0.386	1.5875	-72675	-44,500	1.5885	-31250	-19,150
5	0.2804	0.75	-72675	-15,280	0.751	-34000	- 7,160
6	0.2804	0	72675	0	0.001	-34750	- 10
7	0.2804	-0.75	72675	-15,280	-0.749	34750	- 7,310
8	0.386	-1.5875	72675	-44,500	-1.5865	31750	-19,450
9	0.2806	-1.782	72675	-36,300	-1.781	29450	-14,710
10	0.125	-1.9375	77750	-18,820	-1.9365	28650	- 6,940
11	0.625	-1.9375	77750	-94,200	-1.9365	20600	-24,930
Σ				-418,200			-146,600

The element yield stresses in the above table are from Fig. 7.14 and include the effects of a previous temperature history. The applied load ratio is

$$R = \frac{-418,200}{-146,600} = 2.853$$

Although this procedure does not allow for the presence of thermal stresses, the comparison table of Fig. 9.5 shows this procedure to be quite conservative in all cases. Comparison of these ratios with the test ratios also indicates that the reduction in bending strength is predominantly a function of the yield stress. However, these results should not be interpreted to establish the relative importance of material properties and thermal stresses since the material property reduction is exaggerated by extreme elevated temperature histories prior to testing. Considerable variation in the relative importance of material properties and thermal stresses in a realistic design situation can be expected when severe temperature history environments affect the recovery of basic material properties.

Case (d) reflects the reduction of material properties plus the elastic sum of the applied and thermal stresses. The allowable applied stress is considered to be the difference between the yield stress of the critical extreme fiber element and the thermal stress on that element where

$$(F_{ap})_{allowable} = F_y - F_T$$

From this allowable extreme fiber stress a psuedo-allowable elevated temperature bending moment is calculated by

$$M = \frac{(F_{ap})_{allowable}\ (EI)}{y_m\ E_m}$$

A value of M is also calculated for room temperature by the same expression for comparative purposes. For specimen B-3, $(F_{ap})_{allowable}$ = -20600 + 8130*= -12470 psi and

$$M = \frac{-12470\ (70.8 \times 10^6)}{1.9385\ (6.8 \times 10^6)} = -67000 \text{ in.-lbs.}$$

The room temperature moment calculated on the same basis is

$$M = \frac{-77750\ (96.5 \times 10^6)}{1.9375\ (10.0 \times 10^6)} = -387{,}000 \text{ in.-lbs.}$$

and the applied load ratio for the cross-section is

$$R = \frac{-387{,}000}{-67{,}000} = 5.775.$$

The results for all specimens are summarized in the table in Fig. 9.5 and compared with the actual test ratio and the load-deformation procedure investigated during this study. Note that the use of the hot element yield stress ratio produces an over-conservative estimate of the applied load ratio which is due primarily to the fact that no allowance is made for cooler elements in the cross-section which have higher yield stress values. Consequently, even greater conservatism

* From IBM calculations for Specimen B-3.

is noted in the applied plus thermal stress ratio due to the addition of the thermal stresses. This indicates, when compared with the test ratios, that the primary effect is the reduction of material properties and the thermal stresses have little effect on the failing bending moment. This is further shown by the generally good agreement between the load-deformation procedure and the test values. The load-deformation procedures place proper emphasis on the reduction of material properties and on the thermal stresses which, as may be seen in Fig. 9.5, become more important as higher temperatures and steeper temperature gradients are encountered.

FIGURE 9.5
SUMMARY - TABULATED APPLIED LOAD RATIOS TO COMPARE SIMPLE RATIOS
WITH LOAD-DEFORMATION AND STATIC TEST RESULTS
BENDING SPECIMENS

Specimen No.	Hot Element Yield Stress Ratio	EI Ratio	$\Sigma F_{yn} A_n Y_n$ Ratio	Applied + Thermal Stress Ratio	Load-Deformation Ratio	Static Test Ratio
B-4 (250° Symm.)	1.962	1.018	1.927	2.170	1.800	1.636
B-5 (250° on Tens. Side Unsymm.)	1.962	1.004	1.894	1.952	1.753	1.657
B-8 (250° on Comp. Side Unsymm.)	1.962	1.005	1.907	2.092	1.756	1.740
B-3 (450° Symm.)	3.773	1.363	2.853	5.775	2.550	2.355
B-7 (250° on Tens. Side Unsymm.)	3.673	1.124	2.185	2.088	2.032	1.910
B-6 (250° on Comp. Side Unsymm.)	3.810	1.177	2.167	5.000	2.180	1.830

9.2.2 SHORT COLUMN SPECIMENS

As in Section 9.2.1, four approximate procedures for obtaining applied load ratios were investigated.

(a) Material properties reduction using only the yield stress of the hottest element compared with the room temperature yield stress.

(b) Material properties reduction using axial stiffness as parameter where $\sum E_n A_n$ at elevated temperature is compared with that at room temperature.

(c) More realistic use of material properties where $\sum F_{y_n} A_n$ at elevated temperature is compared with that at room temperature.

(d) Material properties plus the elastic sum of the applied and thermal stresses compared to the yield stress of the critical element.

(a) through (c) have no allowance for thermal stresses while (d) considers only the elastic stresses on the critical element.

The limited data shown in Figure 9.6 shows results similar to those in Figure 9.5 for the bending specimens. Method (a) is considerably over-conservative since it does not allow for other elements in the structure which may have higher yield stresses. Method (b) is quite unconservative since the modulus of elasticity is relatively unaffected by severe temperature exposure histories as to recovery of material properties. The use of $\sum F_{y_n} A_n$ produces somewhat more realistic applied load ratios on a simplified basis, but still somewhat conservative in many cases. This indicates the major effect to be produced by the variation in yield stress with temperature through the cross-section for an ultimate load comparison.

The use of applied plus thermal stresses on the critical element is considerably over-conservative, primarily because the elastic stresses are considered on the critical element only where no allowance is made for other elements in the cross-section.

As for the bending specimens, the load-deformation ratios are generally the most realistic but still tend to produce slightly conservative results in most cases. In the design case, the use of MIL-HDBK-5 material properties would ensure conservatism in the majority of cases. Using material properties defined by tensile coupon tests the load-deformation ratios compare most favorably with the test results since the load-deformation procedures place proper emphasis on the factors affecting both room temperature and elevated temperature strength.

FIGURE 9.6
SUMMARY - TABULATED APPLIED LOAD RATIOS TO COMPARE SIMPLE RATIOS
WITH LOAD-DEFORMATION AND STATIC TEST RESULTS
SHORT COLUMN (CRIPPLING) SPECIMENS

Specimen No.	Hot Element Yield Stress Ratio	E_nA_n Ratio	$\sum F_{yn}A_n$ Ratio	Applied + Thermal Stress Ratio	Load-Deformation Ratio	Static Test Ratio
A-4 (250° Symm.)	1.580	1.014	1.397	1.658	1.308	1.348
A-5 (250° Unsymm.)	1.580	1.002	1.345	1.964	1.257	1.202
A-3 (425° Symm.)	2.775	1.216	1.762	3.49	1.577	1.475
A-6 (425° Unsymm.)	Not used in applied load ratio comparison					

10.0 FASTENER EVALUATION

Fabrication of all bending, thermal cycling, and short column specimens incorporated either NAS 464 close tolerance bolts or HS52P close tolerance Hi-Shear rivets. All long column specimens were fabricated using NAS 464 close tolerance bolts. This type of fastener was selected primarily to preclude any fastener failures which would interfere with the primary purpose of the test; i.e., to define the load-deformation curve of a given cross-section in a given temperature environment. Close tolerance fasteners were required since the combination of bolt spacing and tolerances on standard bolts and drilled holes could conceivably exceed the temperature expansion strain ($\alpha\Delta T$) of the cover plate elements and possibly reduce the thermal stresses in the cross-section. For purposes of this study it was essential that the thermal stresses be as high as practicable.

For the small amount of buckling strain data involved and only two bending and two short column specimens there was an indication that the Hi-Shear rivets may have produced slightly better edge conditions than the bolts installed with a normal installation torque of about 70 in.-lbs. However, the difference was small ($K = 4.3$ to about $K = 4.9$) and the data from both bending and compression specimens indicated that this difference was more likely due to the type of loading where the bending radius of curvature, inward skin panel buckling, and slight rolling of the channel flanges tended to reduce the edge restraint slightly for the compression covers of the bending specimens. Therefore, it may be concluded that the use of rivets or bolts for the same spacing had a negligible effect on the panel edge restraint conditions.

The comparison of calculated and test load-deformation curves and random spot-checking of some thermal strain data (no applied load) indicates the joints to be fairly tight, allowing the cross-section to deform as an integral structure. In evaluating all of the bending specimens no particular trend was noted as to deviation of calculated load-deformation curves with the test curves for any type of fastener.

No evaluation of joint conductance was made nor considered necessary to achieve the objectives of these tests.

11.0 PROCEDURE FOR STATIC TEST COMPONENTS

Basically, the load-deformation procedures described in this report are a cross-sectional analysis and would apply, typically, to a wing, stabilizer, or fuselage station. The methods are, at present, confined to the simulation of tests where bending and/or axial load are the primary modes of failure. Shear, torsion, and combined load failures are precluded, but further studies should investigate these effects, both singly and in combination. In defense of what might appear to be an over-simplification, it should be noted that a large number of static test major structural failures are either tension, or compression instability collapse where the tension and compression are produced by bending or combined bending and axial load. This loading is particularly true of missiles, and the use of room temperature simulation is particularly amenable to missiles, or missile sections, where extremely severe temperature environments may be encountered.

In order to perform the elevated temperature static test at room temperature using applied load ratios it is first necessary to obtain the load-deformation and permanent set curves for a number of cross-sections along the span of the component. These curves are obtained for both the design elevated temperature condition and for room temperature. The methods of Section 3.0 (or similar methods using strain design techniques) are employed to obtain the necessary curves for defining the applied load ratios. This does not imply, however, that large numbers of separate calculations need to be made at the structural test phase of a vehicle program. Methods such as those in Section 3.0 actually represent the design analysis tool which should be used at the design phase of the vehicle program, in which case the design elevated temperature condition curves would already be available. Since methods of this type require high speed digital computers for solution anyway, it is a relatively simple matter to change material properties to the room temperature values and recalculate the critical cross-section or cross-sections to obtain the room temperature curves.

From the design analysis the critical cross-section is selected and the applied load ratios obtained for ultimate load, yield load (permanent set), and for any other design criteria required to substantiate the structural integrity of the component. These multiplying factors are applied

to the loads and/or moments for the original design condition to obtain the loads and spanwise load distribution for the simulated test at room temperature.

It may be that several critical cross-sections need to be investigated since some variation in design condition may exist. It is also possible that a given cross-section which is critical for ultimate load may not be the critical cross-section for yield or permanent set criteria. In this case it would be necessary to base the ultimate applied load ratios on one cross-section and yield applied load ratios on another.

Since an increase in applied loads (such as air loads) is involved, the net effect is an overall increase in shear, bending moment, and torque on any given surface at room temperature. The attendant increase in shear stresses should be investigated to ensure that no premature or undue shear failures will occur at the higher loads on the room temperature structure.

This procedure may work well for establishing overall strength and rigidity for large components in extreme temperature environments but does not preclude the testing of specific splices, fittings, small components, etc. at elevated temperature. Some fastener evaluation at elevated temperature may also be required to support the simulated elevated temperature program at room temperature.

12.0 CONCLUSIONS AND RECOMMENDATIONS

Generally, it may be concluded that within the limits of this study the simulation of elevated temperature static tests at room temperature may be performed in a satisfactory manner if the room temperature and elevated temperature load-deformation curves are defined on a compatible basis. Considering the necessity of obtaining accurate strain and deflection data in a severe elevated temperature environment where the temperature distribution may be inaccurate, it may be that the room temperature test would be more reliable, produce more accurate data, and, at the same time, be considerably more economical than the elevated temperature test.

From the standpoint of design, analysis, and test the problem of material properties and material property evaluation is most important, particularly for aluminum alloy. Complex temperature exposure histories producing permanent losses of material properties must be accounted for in the design of airframes. Data from Reference (e) presents an excellent means whereby accumulated time-temperature histories can be considered. It is recommended that the basic principles and procedures of Reference (e) be expanded to consider other structurally important materials for aircraft, missiles and space vehicles. In addition, it was noted that for strain-sensitive problems such as thermal cycling and fatigue (room temperature and elevated temperature) the shape of the stress-strain curve and more precise definitions of yield stress are important. It should be noted that the 7075-T6 aluminum alloy used in this study behaved in a stable, uniform, and fairly predictable manner at temperatures of 450°F. for short times even when previous temperature exposure histories at 480°F. severely affected the basic properties.

It appears that strain design procedures used to define load-deformation characteristics could include fatigue effects if some parameter related to overall deformation (strain) could be derived or defined by fatigue studies at a more basic level; i.e., studies associated with the basic mechanism of fatigue.

Additional studies considered important in the structural evaluation and test phases are associated with shear stresses and more optimum use of matrices to more fully evaluate the problems. The shear stress distribution in beams with inelastic bending stresses present may be of particular importance in shallow, thick spar webs. Preliminary calculations have indicated a considerable rise in shear stress near the neutral axis in thick sections. In certain materials this could be quite serious and some investigation should be considered where a combined analytical and experimental program could be performed to evaluate the seriousness of the problem and provide procedures similar to those shown in this report for design and test evaluation. In addition, the inclusion of inelastic effects in more optimum matrix procedures for indeterminate structures would allow large numbers of elements to represent more realistically an entire structure. This would eliminate the assumption of plane sections used in this report and allow evaluation of more complex structures where cutouts, sweepback, varying spanwise and chordwise temperature distributions, and other factors add to the complexity of the problem. Generally, the aim is to extend the cross-section analysis procedures shown in this report to include entire structural components.

Some consideration should also be given to defining permanent buckling criteria, particularly for structures operating in severe non-uniform temperature environments where initial buckling, and, consequently, permanent buckling are directly affected by the presence of temperature-induced strains (thermal stresses).

Another factor related to the design of elevated temperature vehicles is that a more sound, rational basis must be established for material comparison and selection. Short time material properties at temperature are not necessarily, indicative of the best material in any given temperature environment and are wholly inadequate as a criterion when the mission profile and mission variations are considered. Of immediate secondary importance to the short time properties is a knowledge of the elongation of the material, not only in the longitudinal direction, but in the transverse and short transverse directions as well. Creep and material recovery properties for temperature and load exposure histories for some expected life of the vehicle must be considered. Material properties alone do not define the problem, but a strength and deformation analysis of representative sections of the vehicle could be made to more fully evaluate the materials under consideration.

Although this study was primarily concerned with static test simulation at room temperature, another possibility arises which may be equally important. Using the load-deformation procedures the static tests could be performed in some lesser temperature environment than the actual temperature environment (not necessarily at room temperature) in cases of extremely severe design temperature conditions. For some future vehicles the electrical power requirements for heating lamps may be far beyond that which is available in many existing structural test laboratories at the present time. In addition, it would be uneconomical to attempt to perform elevated temperature tests in temperature environments beyond the state-of-the-art for strain measuring devices.

Assuming that it is considered necessary to perform the elevated temperature static test in the actual design temperature environment, the temperature distributions through the cross-section must be maintained as well as the surface temperatures nearest the heat source. It is unlikely that these distributions can be easily maintained within acceptable limits considering variations in conductivity and additional heat sinks provided by loading jigs, etc. Therefore, the load-deformation techniques could be employed to determine load-deformation curves for the theoretical and test temperatures and temperature distributions to define whether the test had adequately verified the structural integrity and permanent set characteristics of the component.

APPENDIX A

TEST DATA

FIGURE A.1.1

TENSILE COUPON STRESS - STRAIN CURVE

BASIC ROOM TEMPERATURE PROPERTIES

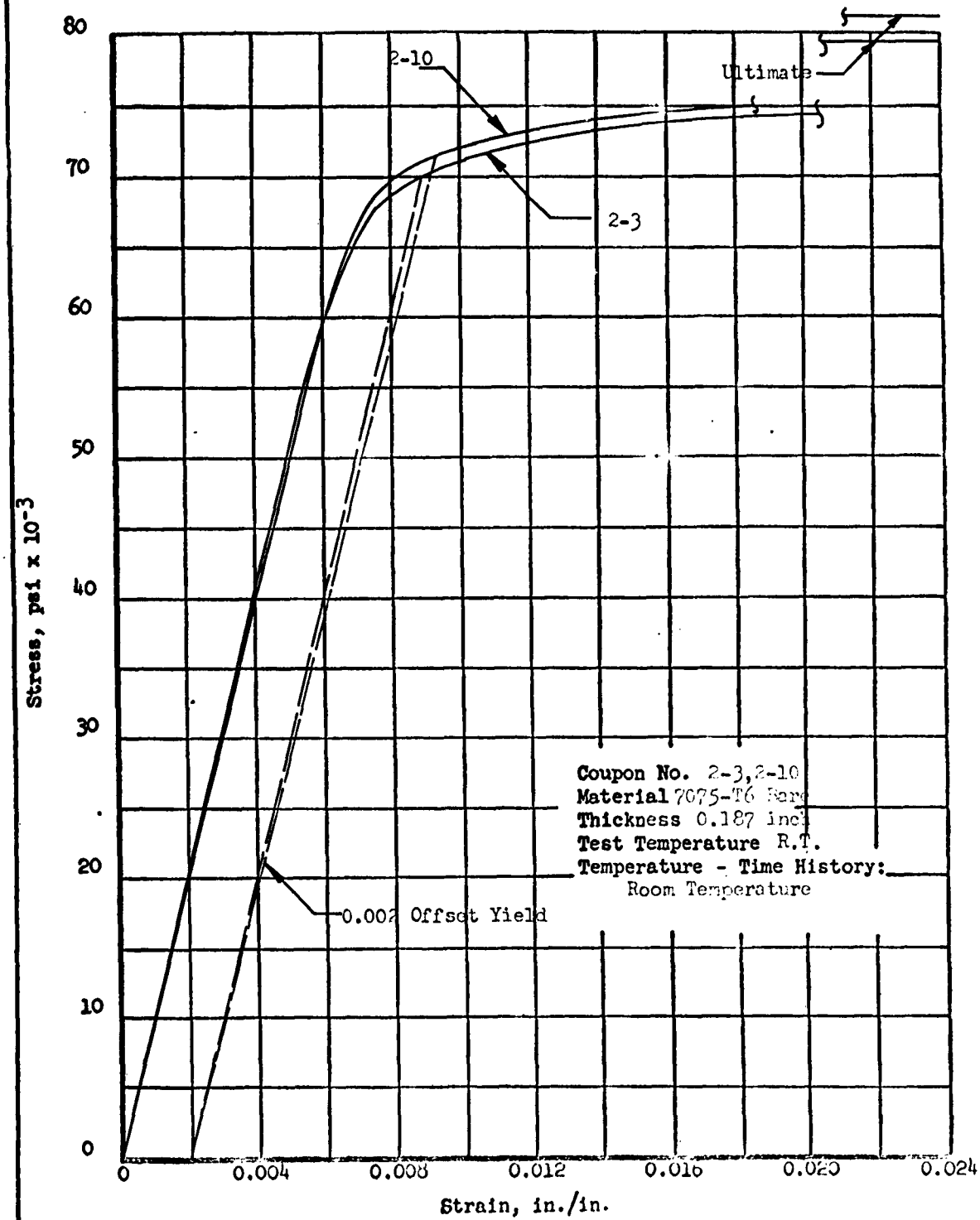

FIGURE A.1.2

TENSILE COUPON STRESS - STRAIN CURVE

BASIC ROOM TEMPERATURE MATERIAL PROPERTIES

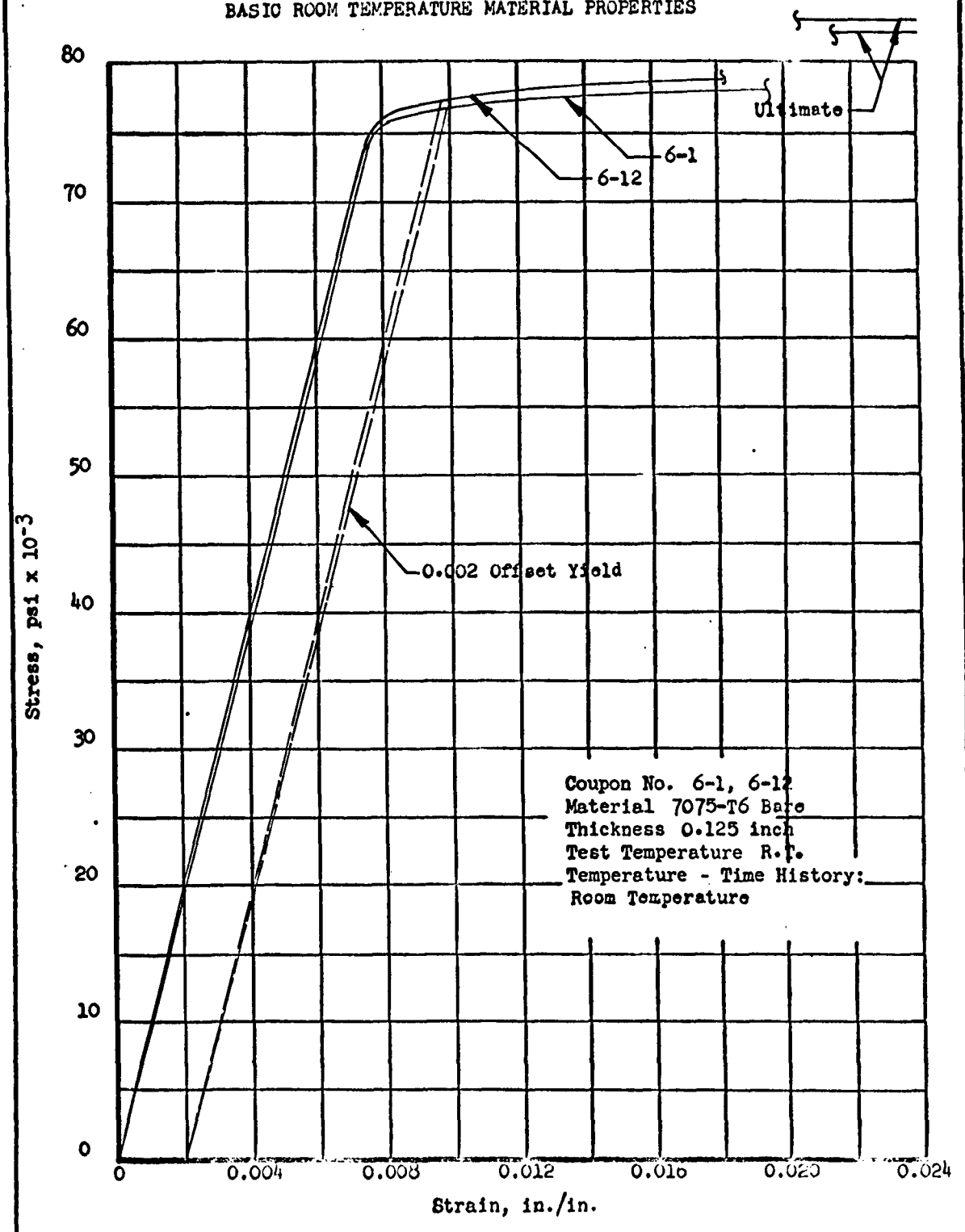

FIGURE A.1.3

TENSILE COUPON STRESS - STRAIN CURVE

BASIC ROOM TEMPERATURE PROPERTIES

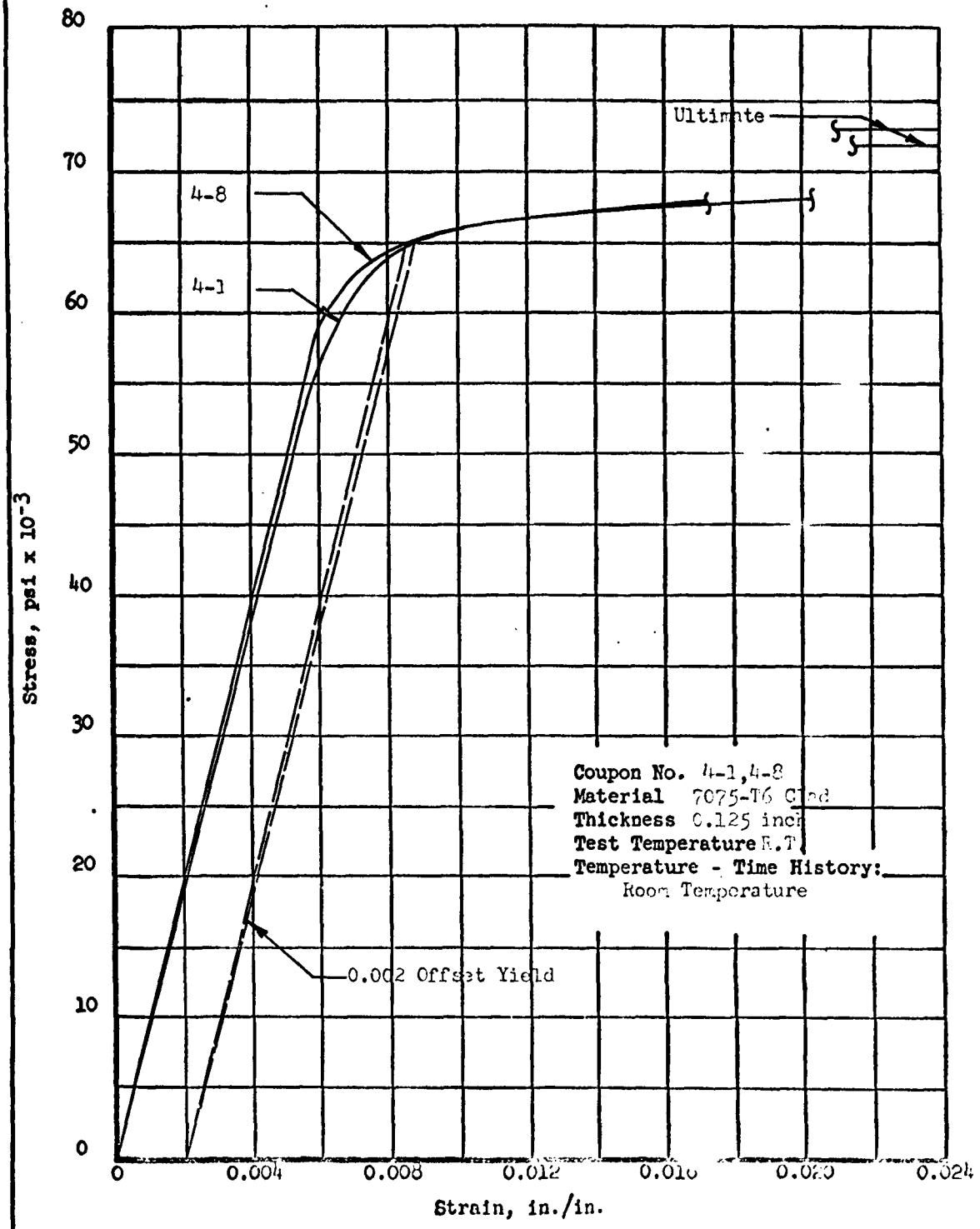

FIGURE A.1.4

TENSILE COUPON STRESS - STRAIN CURVE

RECOVERY OF ROOM AND ELEVATED TEMPERATURE MATERIAL

PROPERTIES AFTER EXPOSURE TO ELEVATED TEMPERATURE

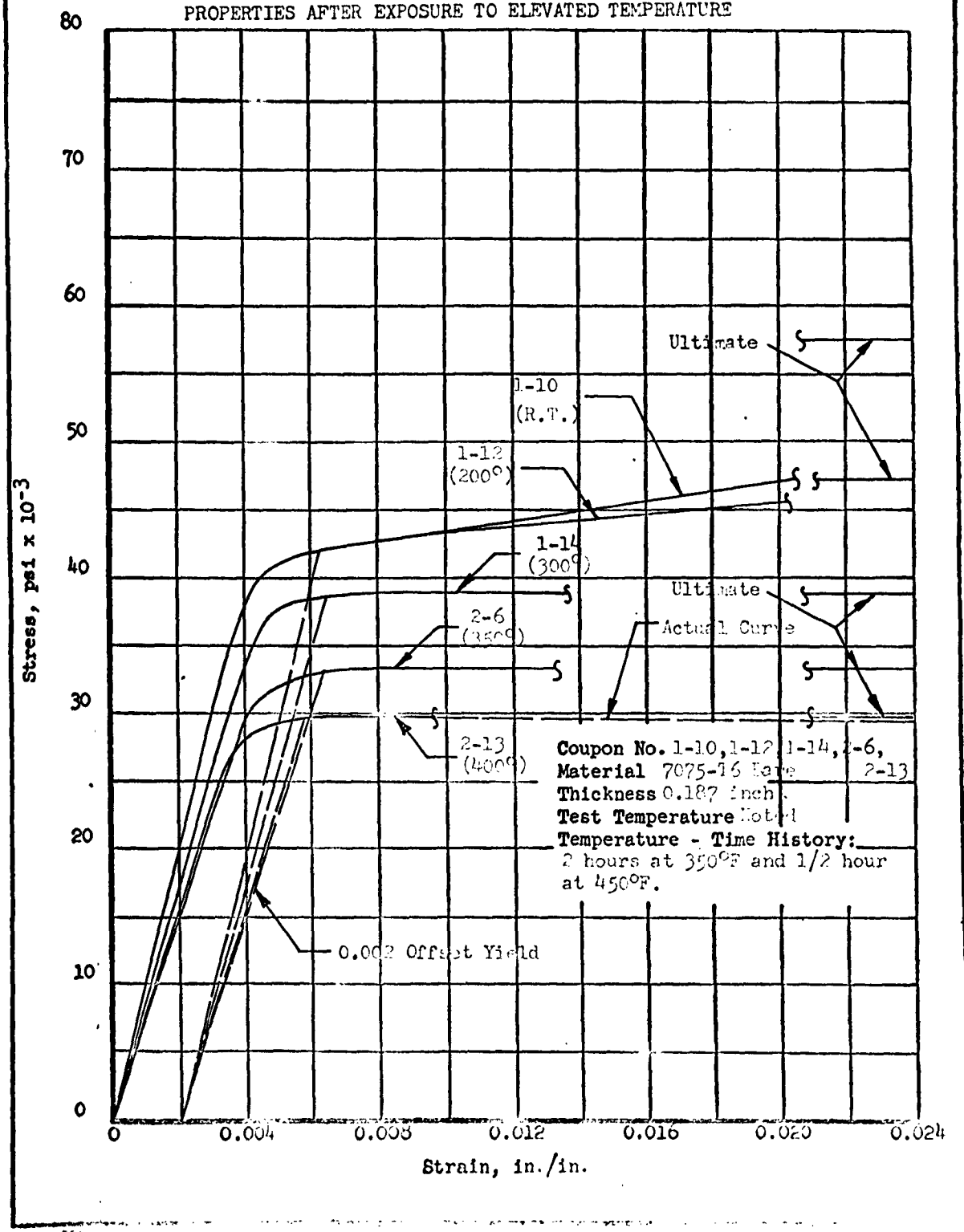

FIGURE A.1.5

TENSILE COUPON STRESS - STRAIN CURVE

RECOVERY OF ROOM AND ELEVATED TEMPERATURE MATERIAL

PROPERTIES AFTER EXPOSURE TO ELEVATED TEMPERATURE

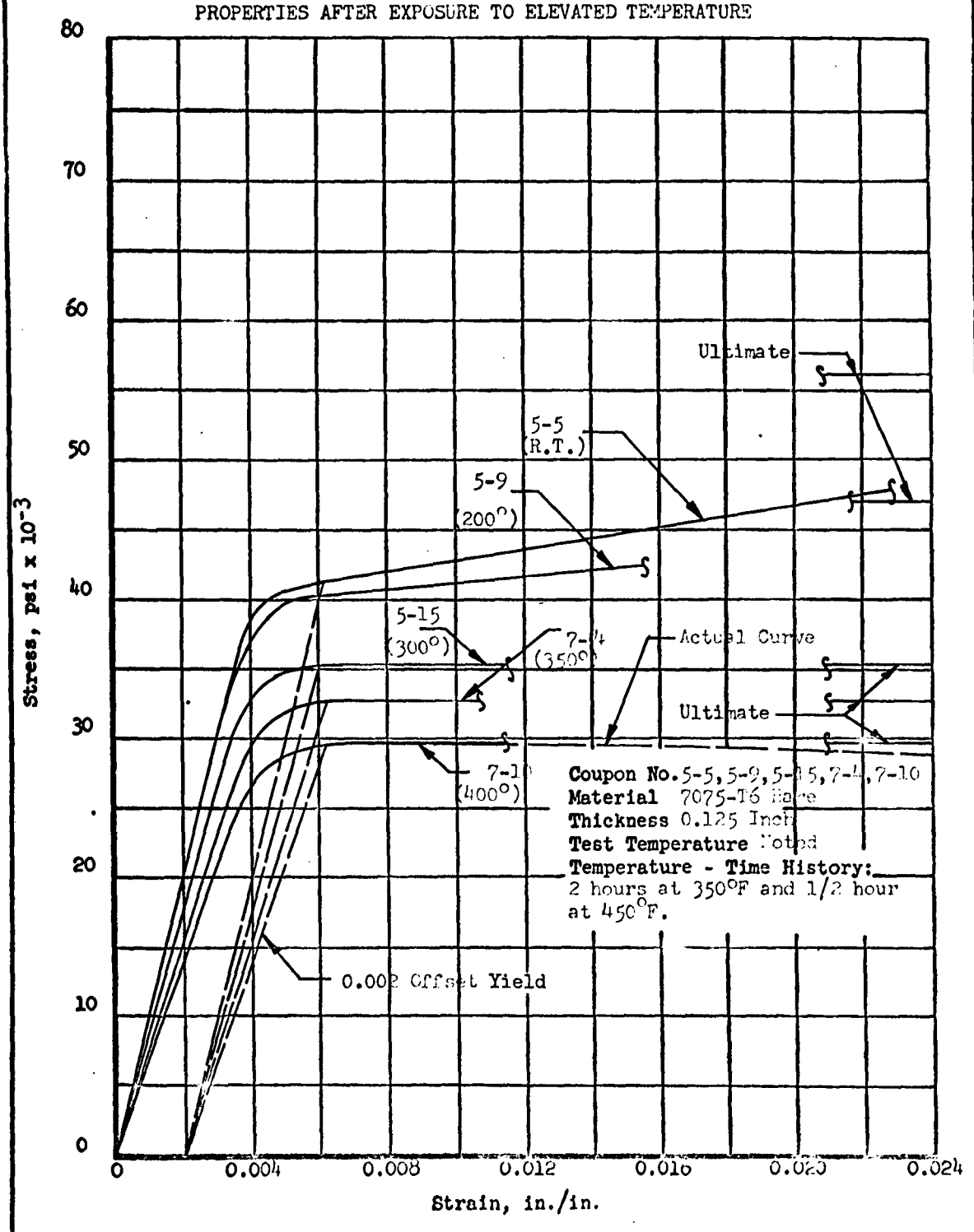

FORM H-10-C-1

FIGURE A.1.6

TENSILE COUPON STRESS - STRAIN CURVE

RECOVERY OF ROOM AND ELEVATED TEMPERATURE MATERIAL

PROPERTIES AFTER EXPOSURE TO ELEVATED TEMPERATURE

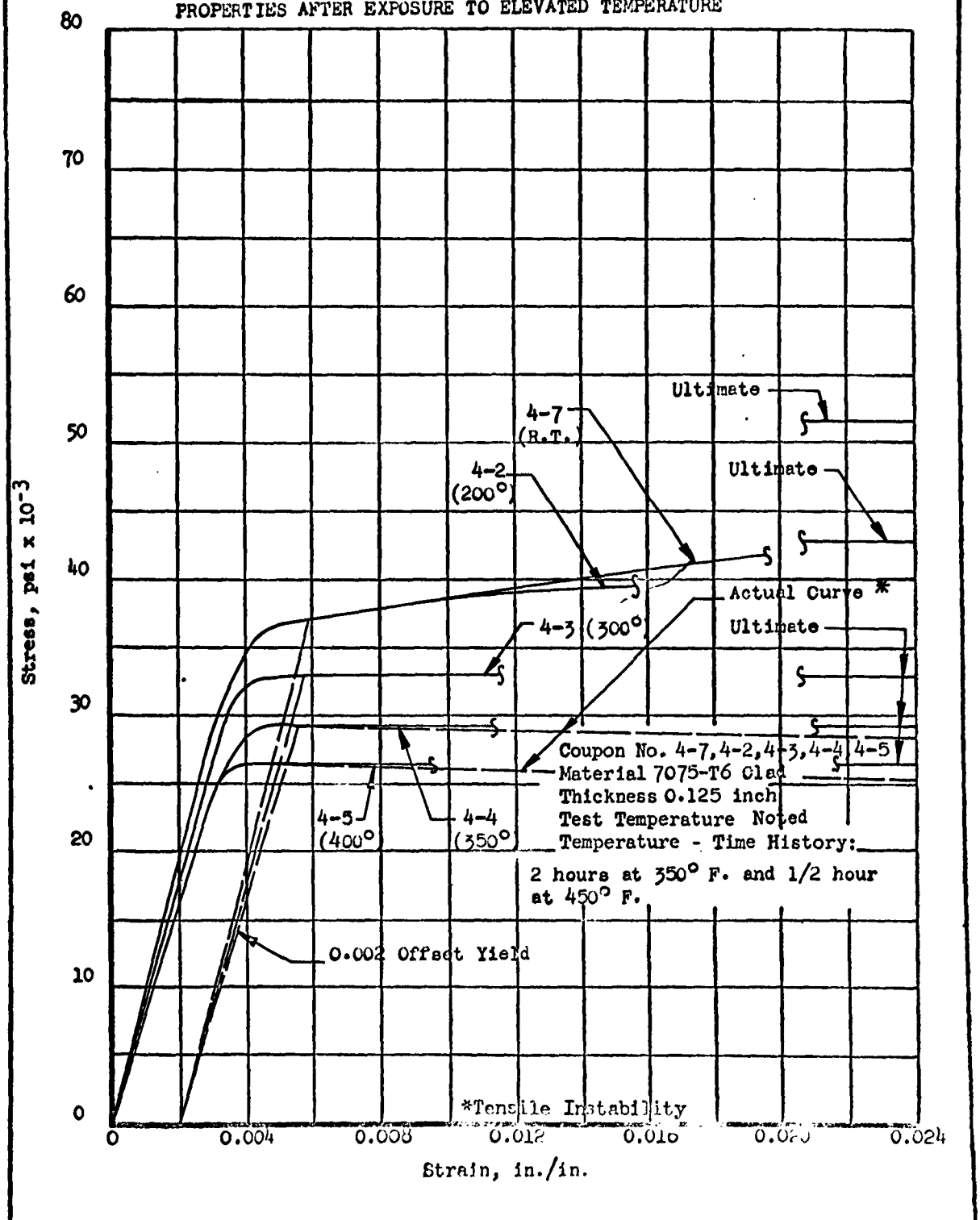

FORM H-10-G-1

FIGURE A.1.7

TENSILE COUPON STRESS - STRAIN CURVE

RECOVERY OF ROOM TEMPERATURE MATERIAL PROPERTIES

AFTER EXPOSURE TO ELEVATED TEMPERATURE

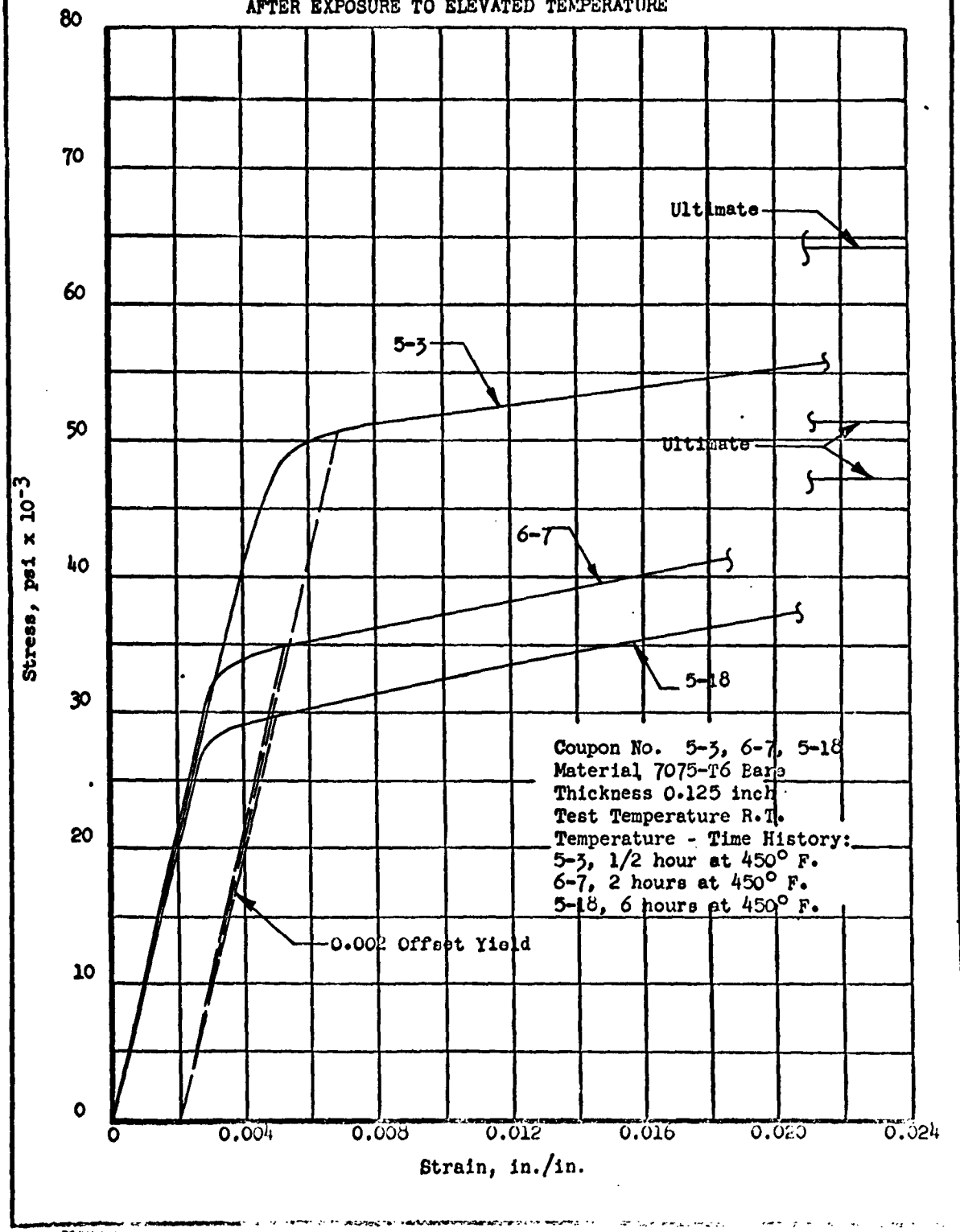

FORM H-10 C-1

FIGURE A.1.8

COMPRESSION STRESS-STRAIN CURVE
RECOVERY OF ROOM TEMPERATURE MATERIAL PROPERTIES
AFTER EXPOSURE TO ELEVATED TEMPERATURE

All coupons obtained from
tensile coupon 1-10.

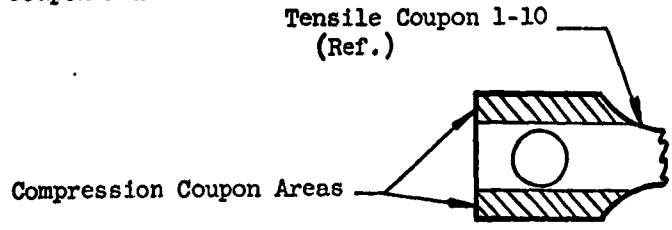

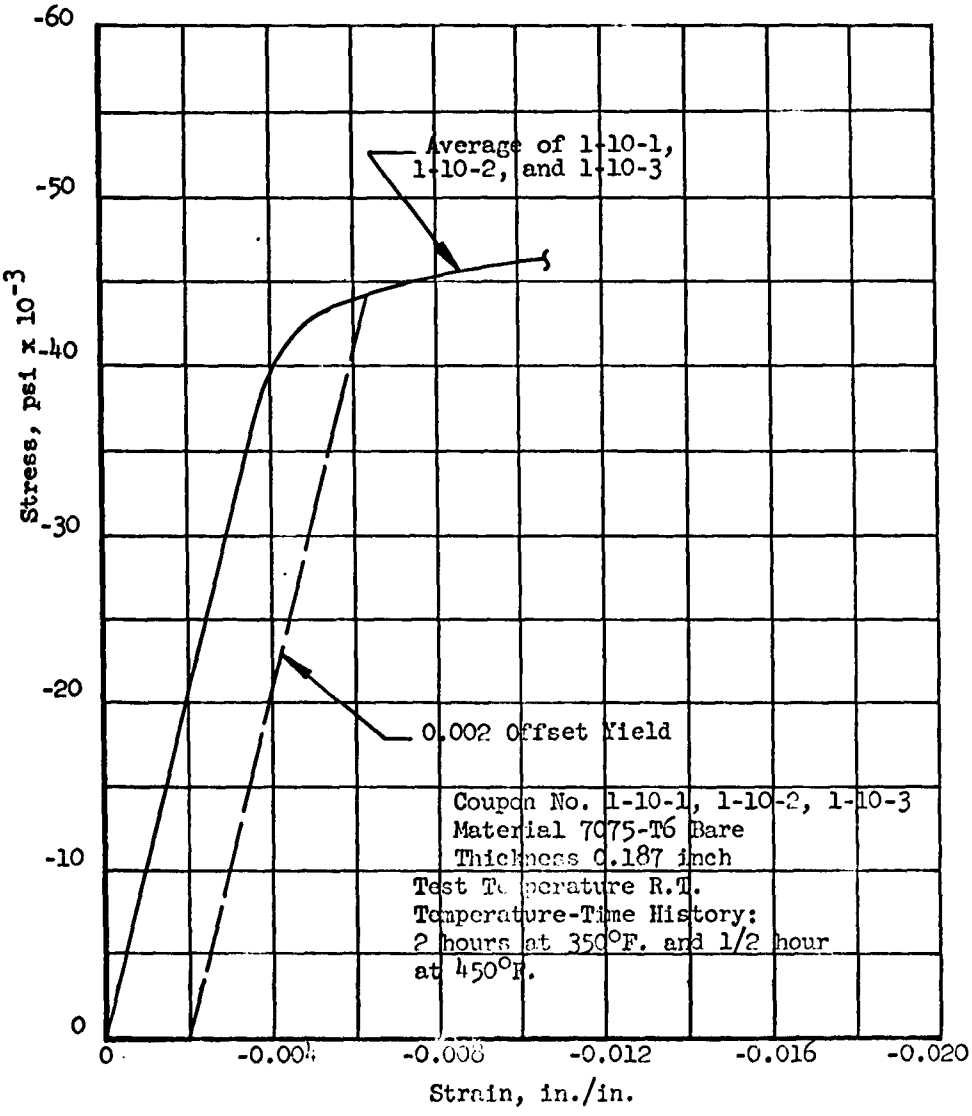

FIGURE A.1.9
COMPRESSION STRESS-STRAIN CURVE
RECOVERY OF ROOM TEMPERATURE MATERIAL PROPERTIES
AFTER EXPOSURE TO ELEVATED TEMPERATURE

All coupons obtained from tensile coupon 5-5.

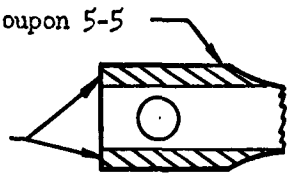

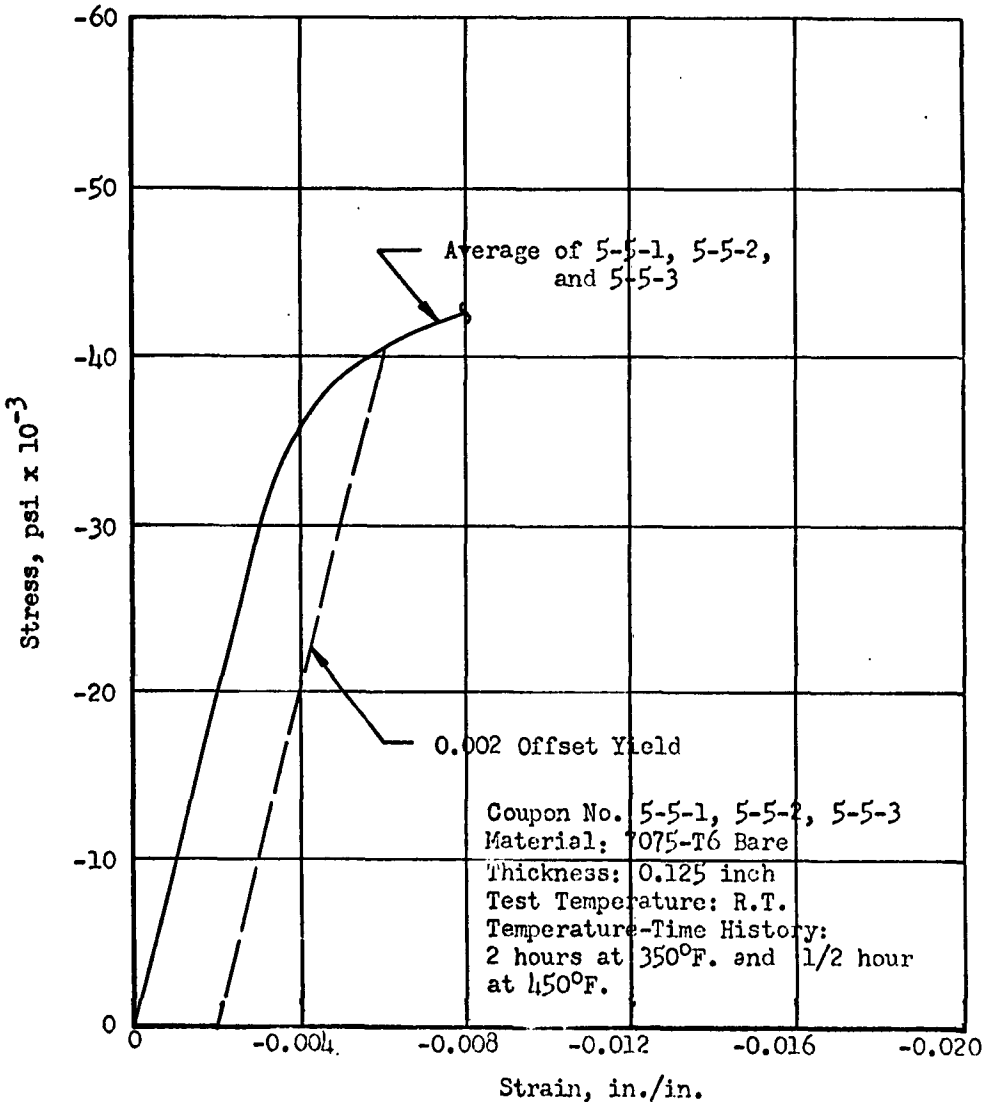

H-1c G-1

FIGURE A.1.10

COMPRESSION COUPON STRESS - STRAIN CURVE

RECOVERY OF ROOM TEMPERATURE MATERIAL

PROPERTIES AFTER EXPOSURE TO ELEVATED TEMPERATURE

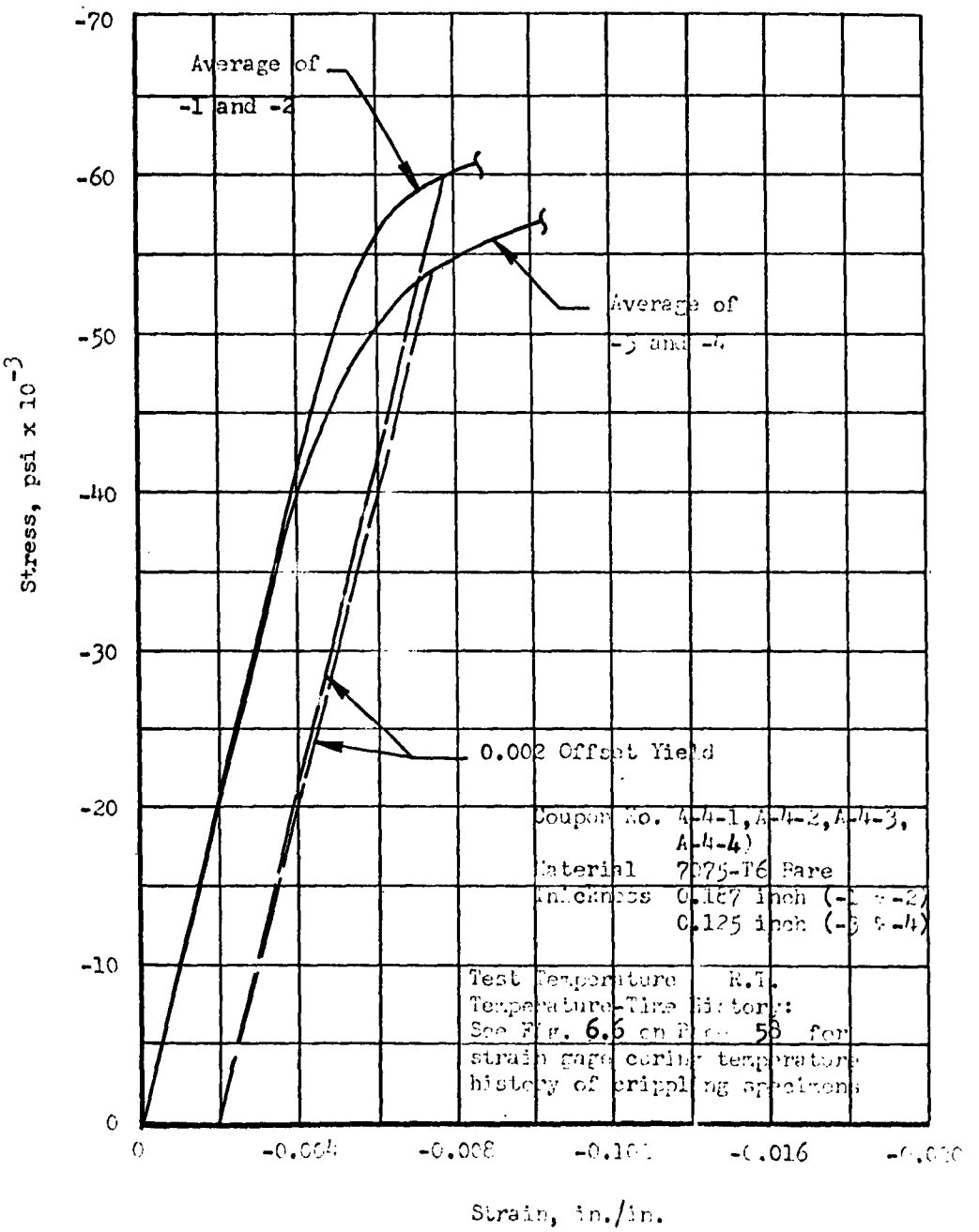

FORM H-10-G-1

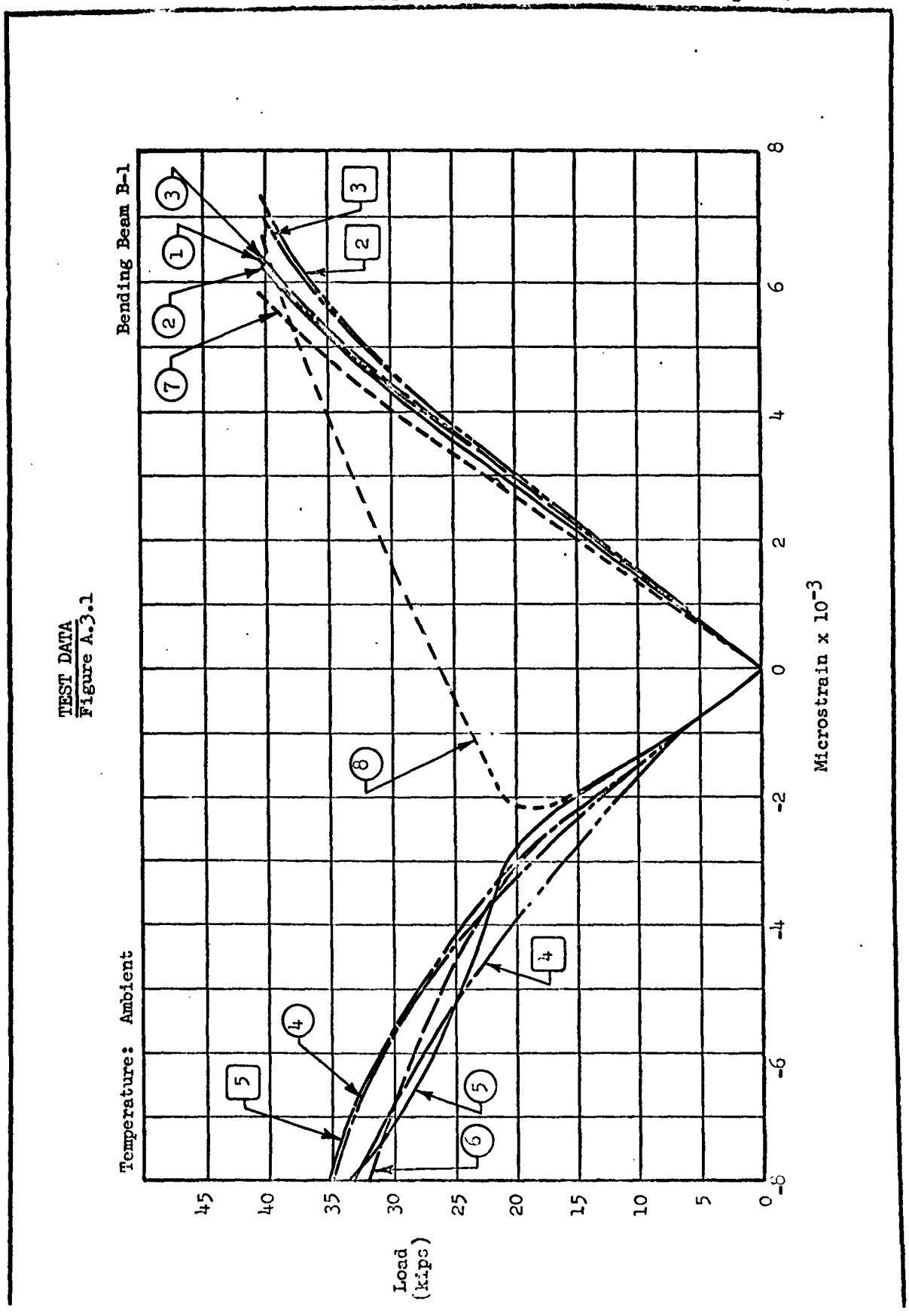
TEST DATA
Figure A.3.1
Bending Beam B-1
Temperature: Ambient
Load (kips)
Microstrain x 10^{-3}
45
40
35
30
25
20
15
10
5
0
8
6
4
2
0
-2
-4
-6
-8
1
2
3
4
5
6
7
8

TEST DATA

Figure A.3.2

Strain Gage and Extensometer Data

Bending Beam B-3

Both Covers Heated
Temperature: 450°F

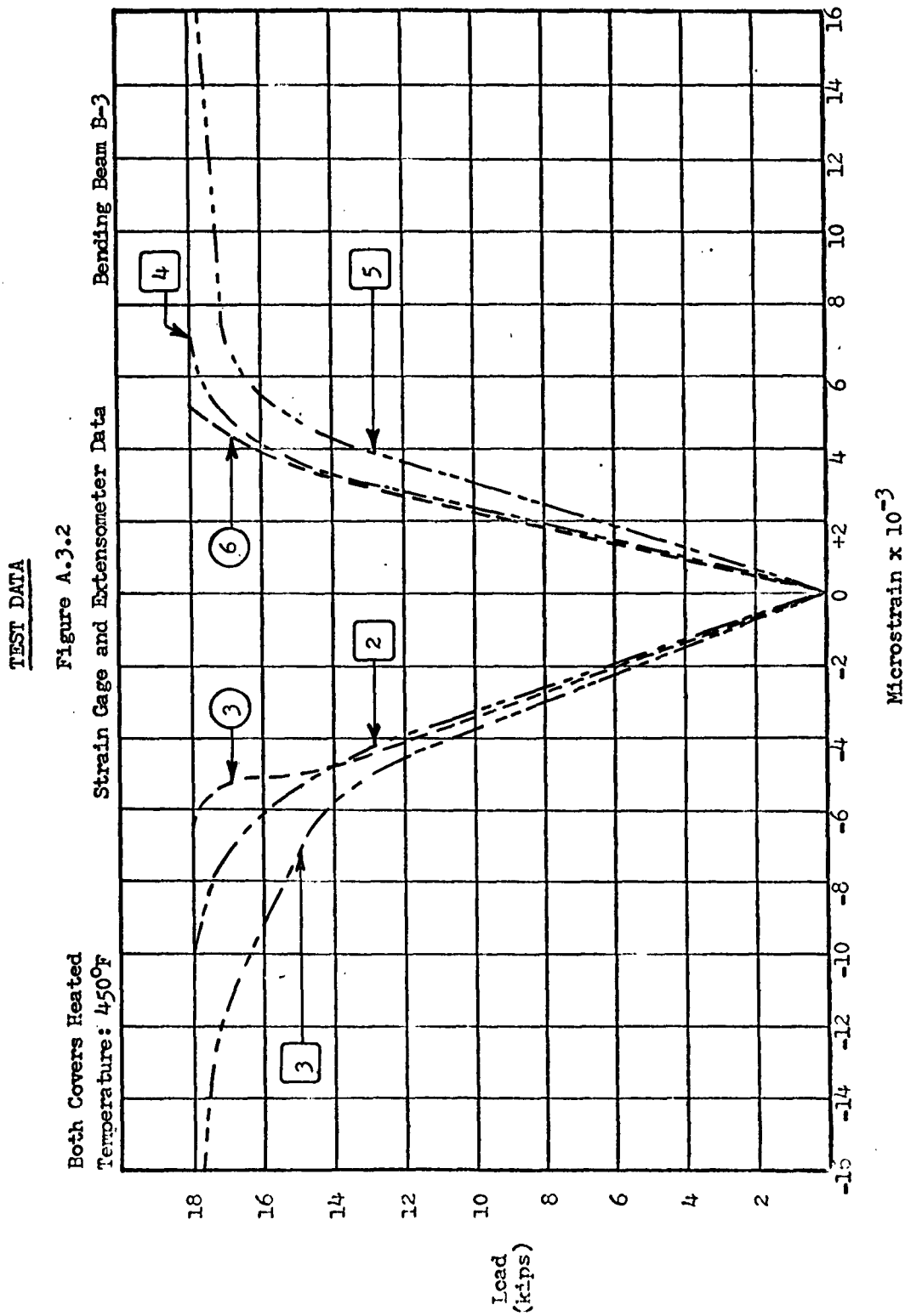

TEST DATA

Figure A.2.3

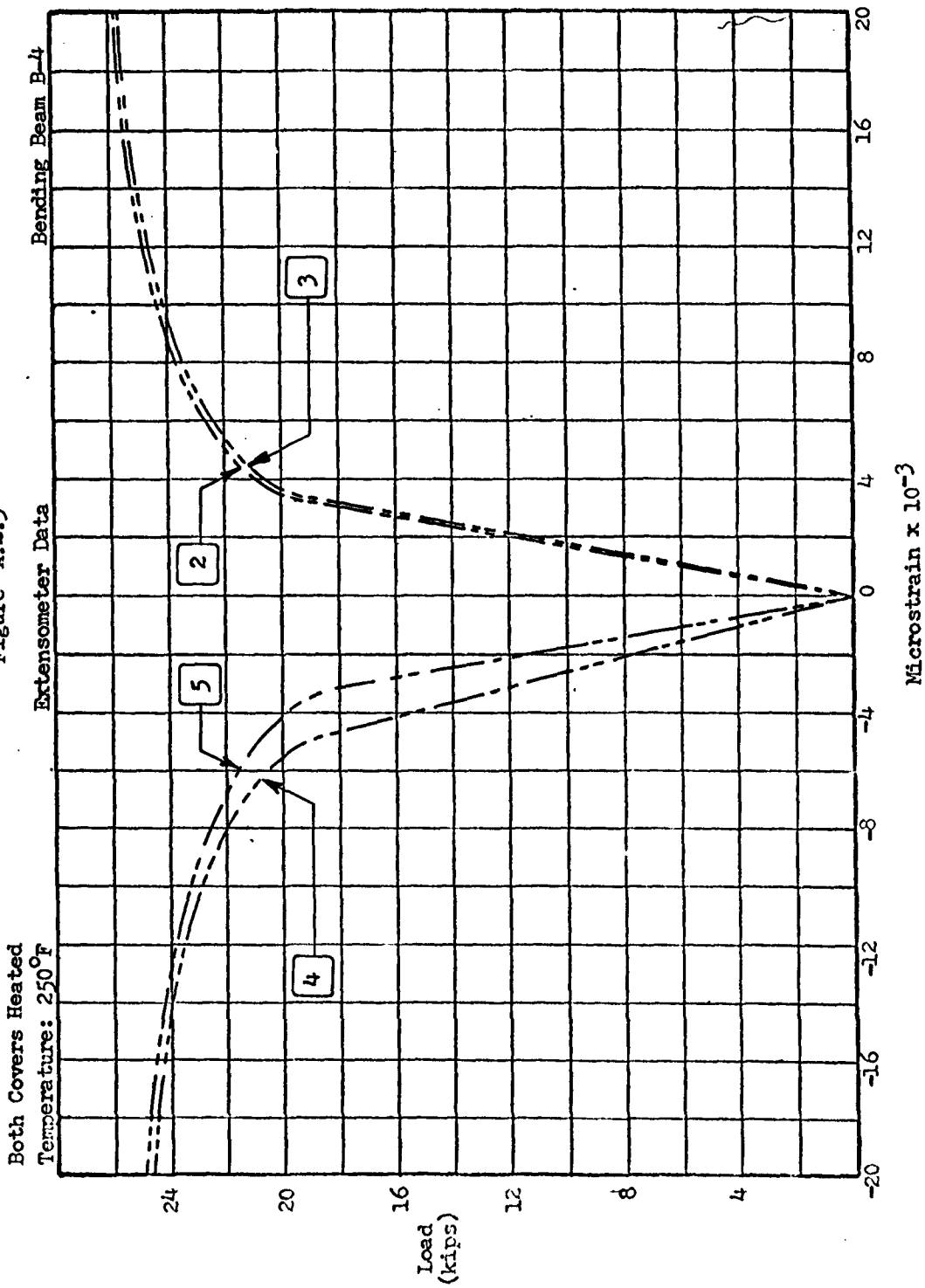

TEST DATA

Figure A.2.4

Strain Gage and Extensometer Data

Bending Beam B-5

Tension Cover Heated
Temperature: 250°F

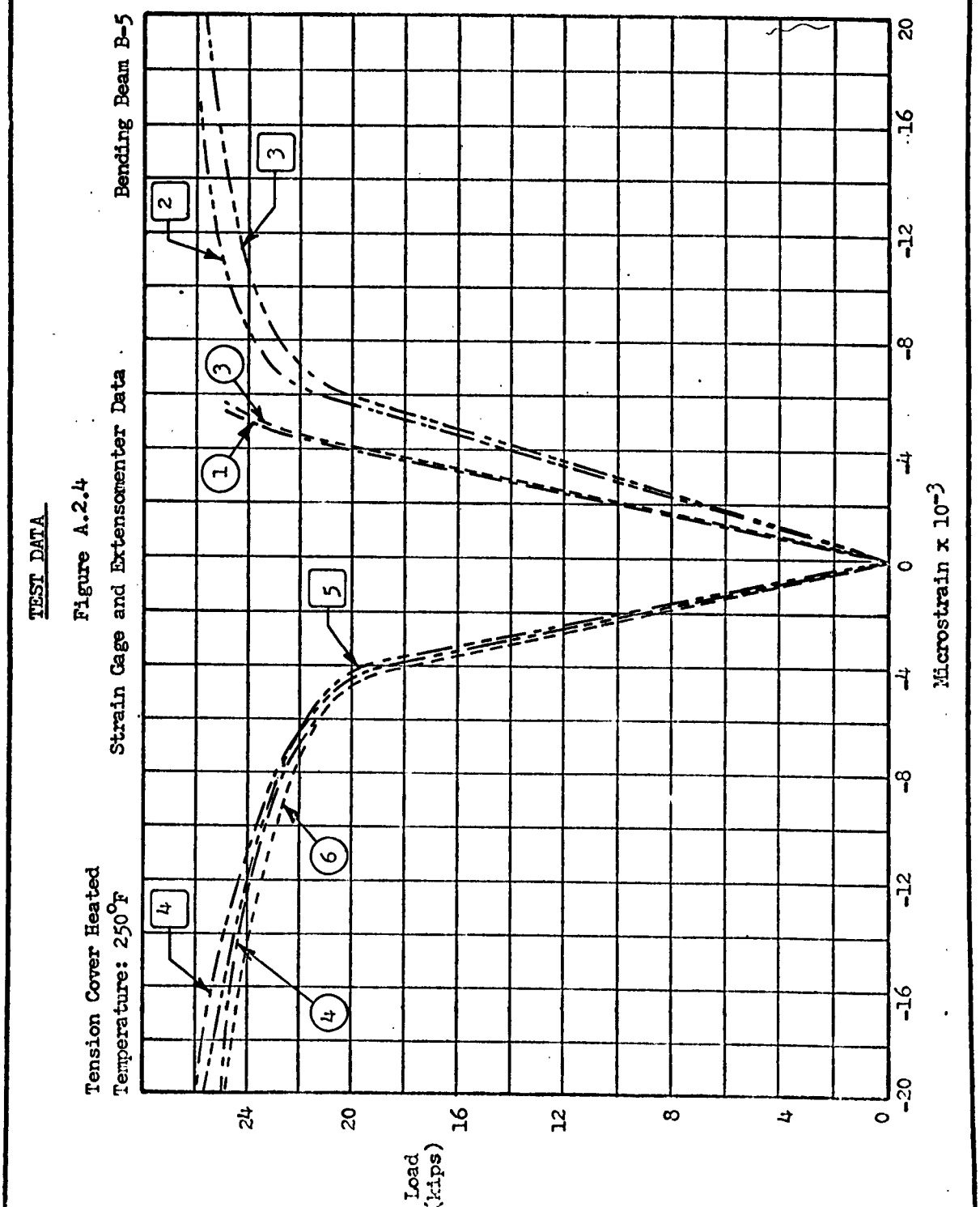

TEST DATA

Figure A.2.5

Strain Gage and Extensometer Data

Bending Beam B-6

Compr. Cover Heated

Temperature: 450°F

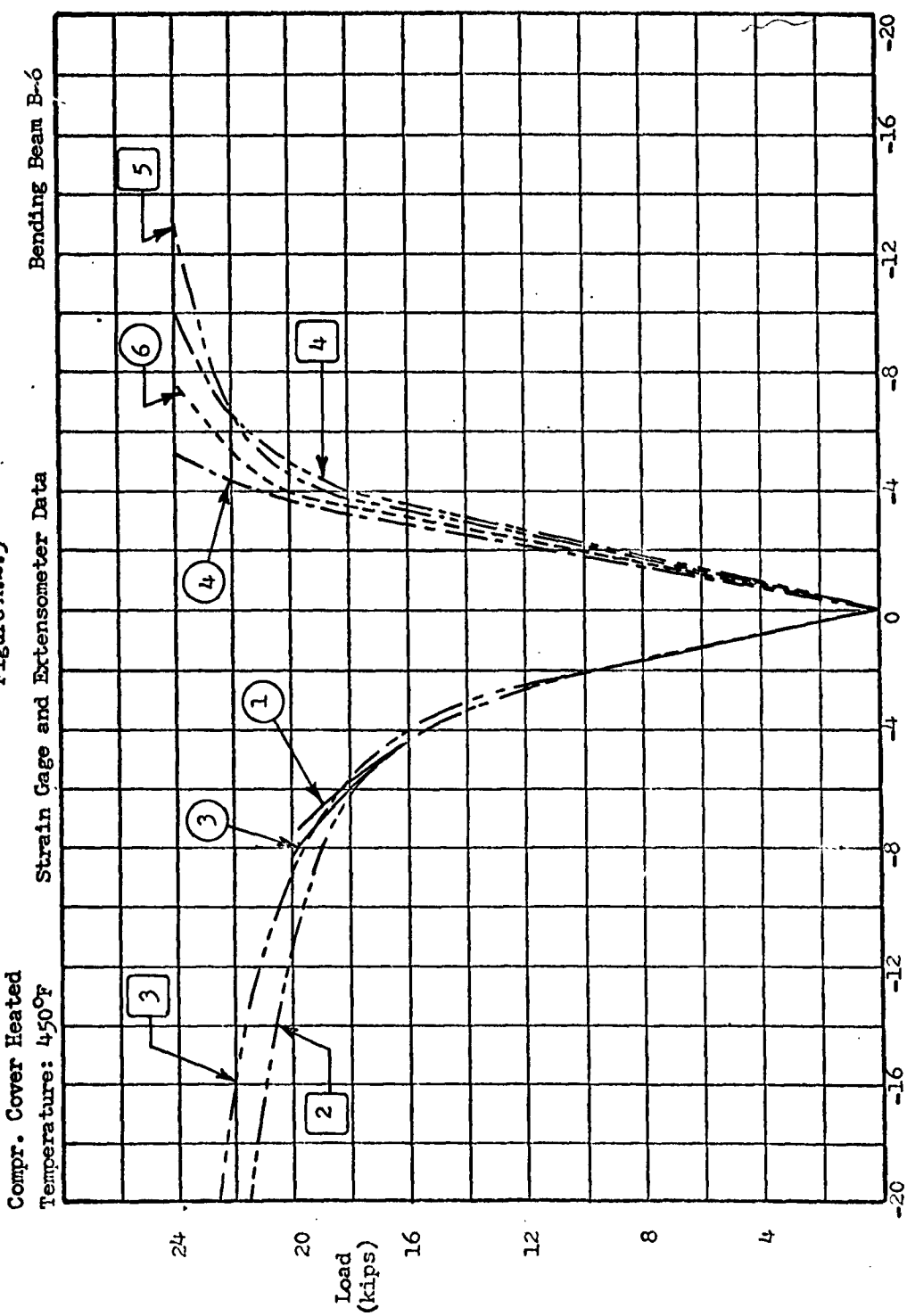

TEST DATA

Figure A.2.6

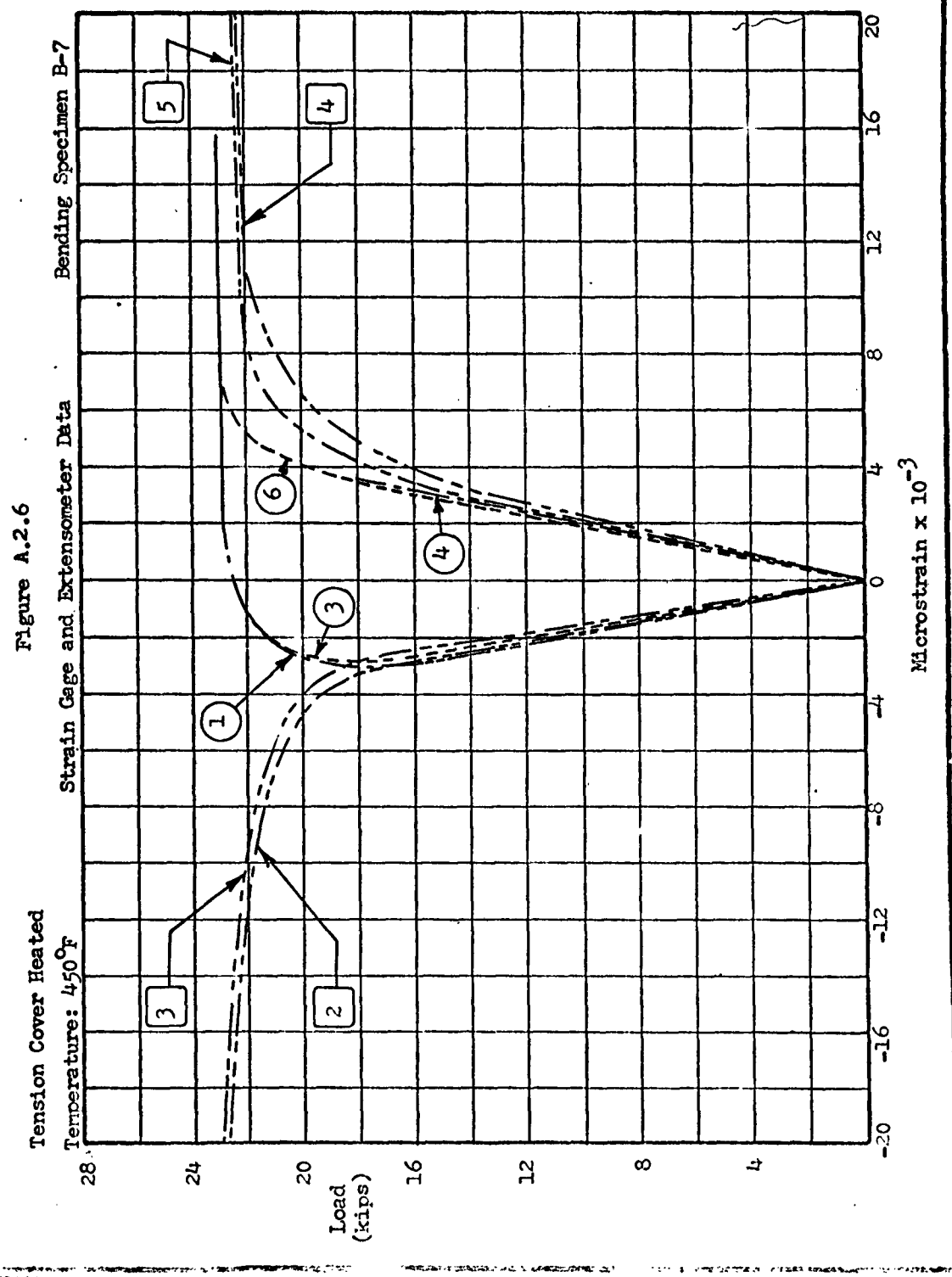

TEST DATA

Figure A.2.7

Strain Gage and Extensometer Data

Bending Beam B-8

Compr. Cover Heated
Temperature: 250°F

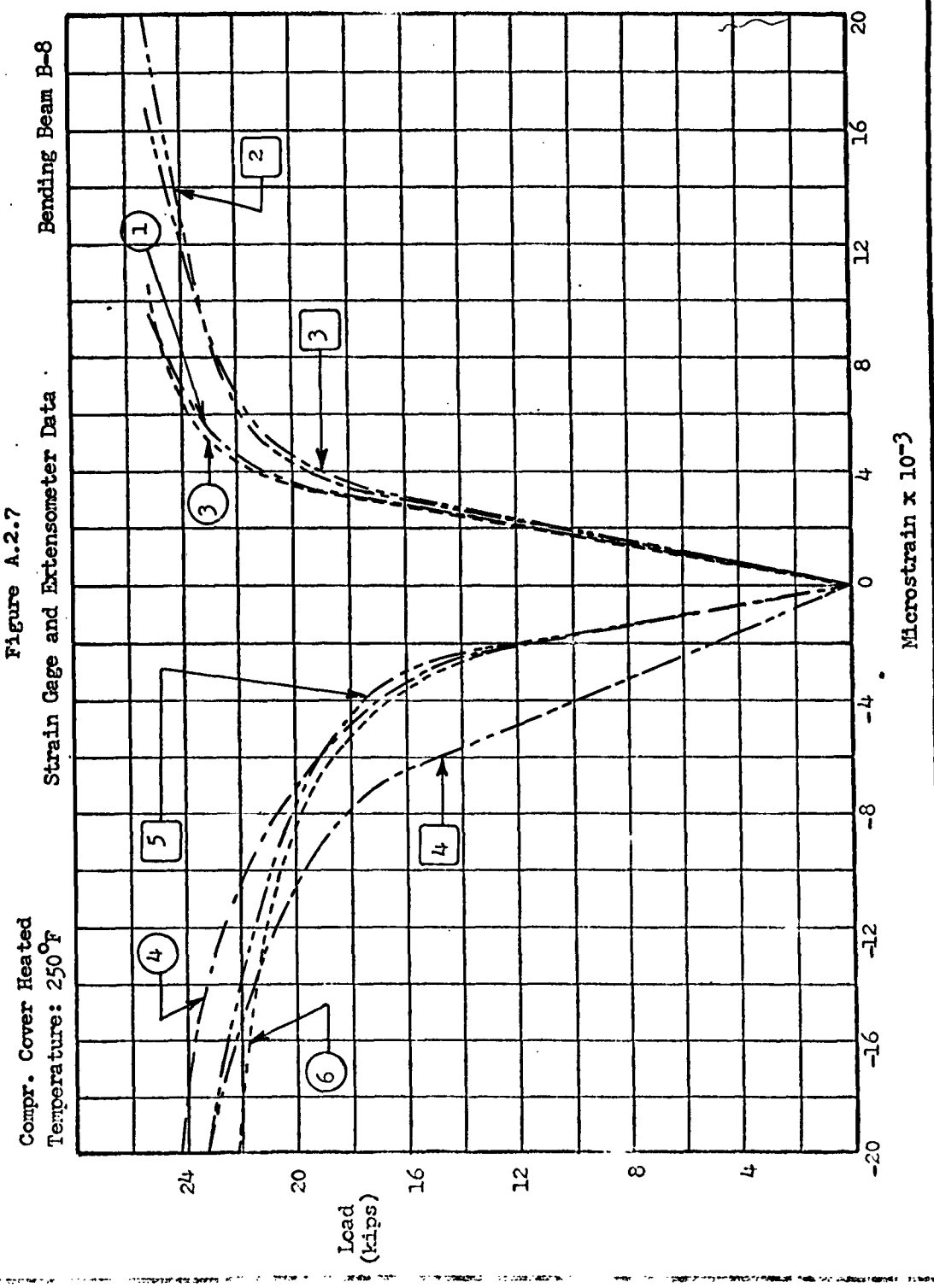

TEST DATA
Figure A.2.8

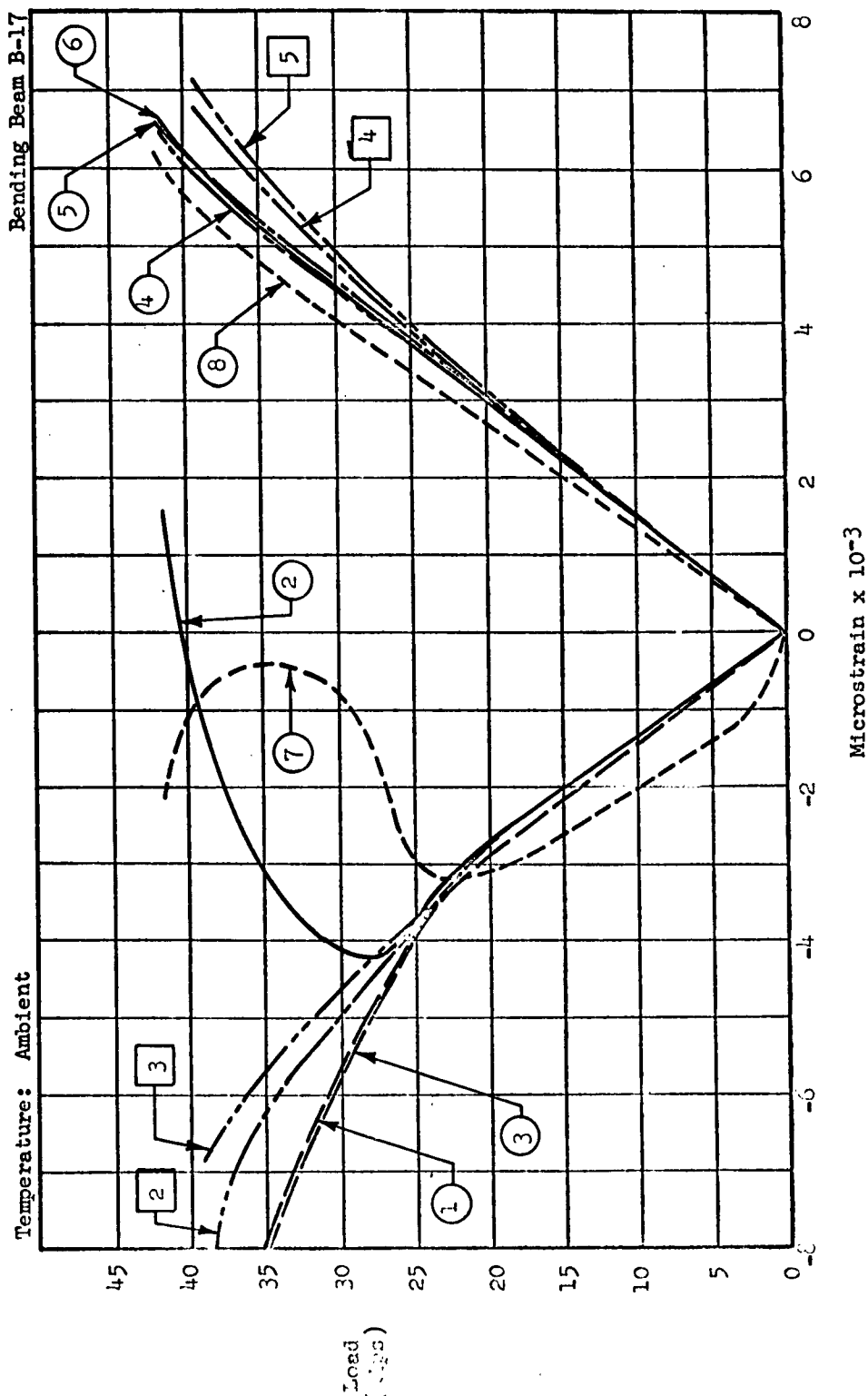

TEST DATA
Figure A.2.9

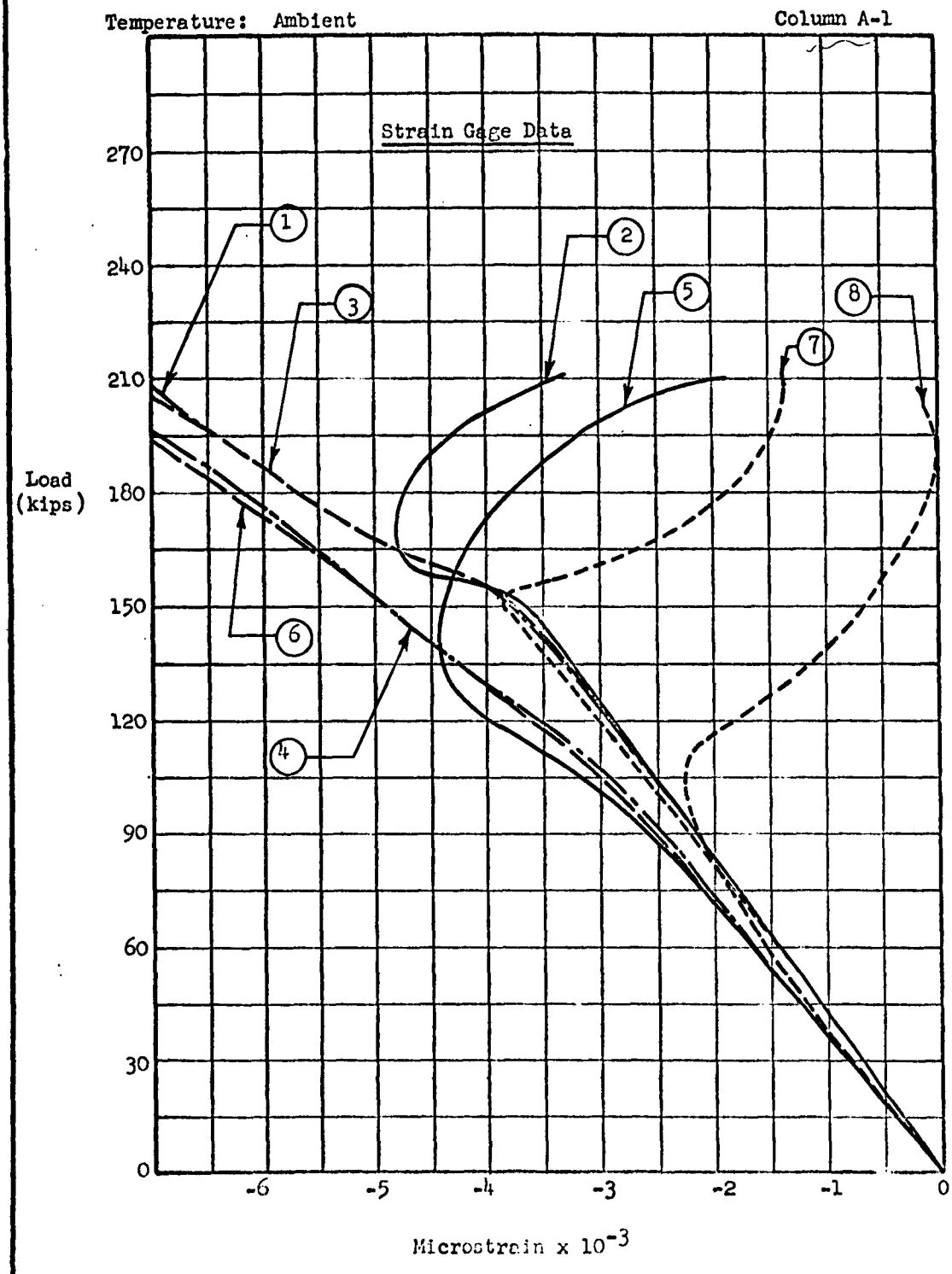

TEST DATA
Figure A.2.10

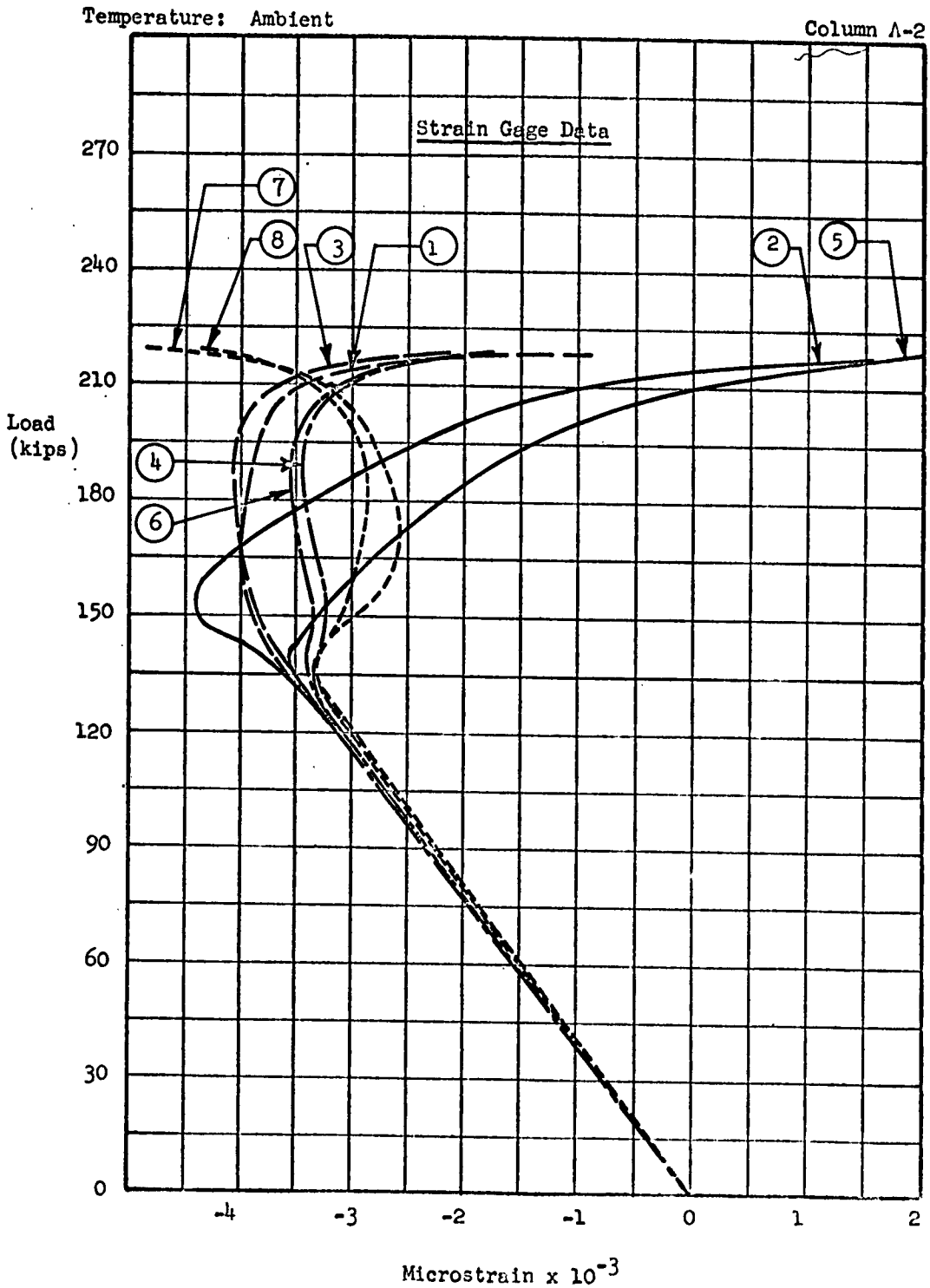

TEST DATA

Figure A.2.11

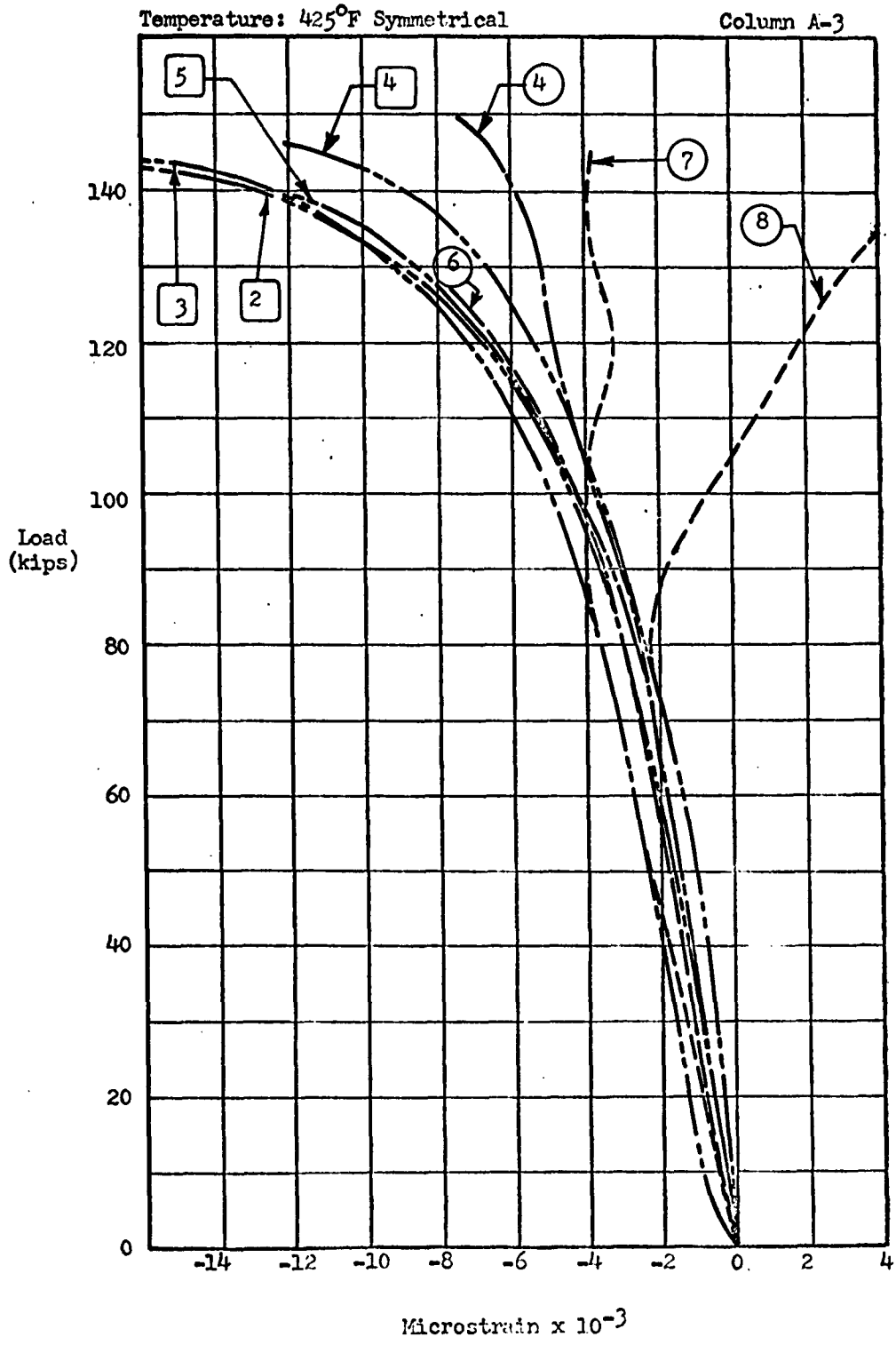

TEST DATA

Figure A.2.12

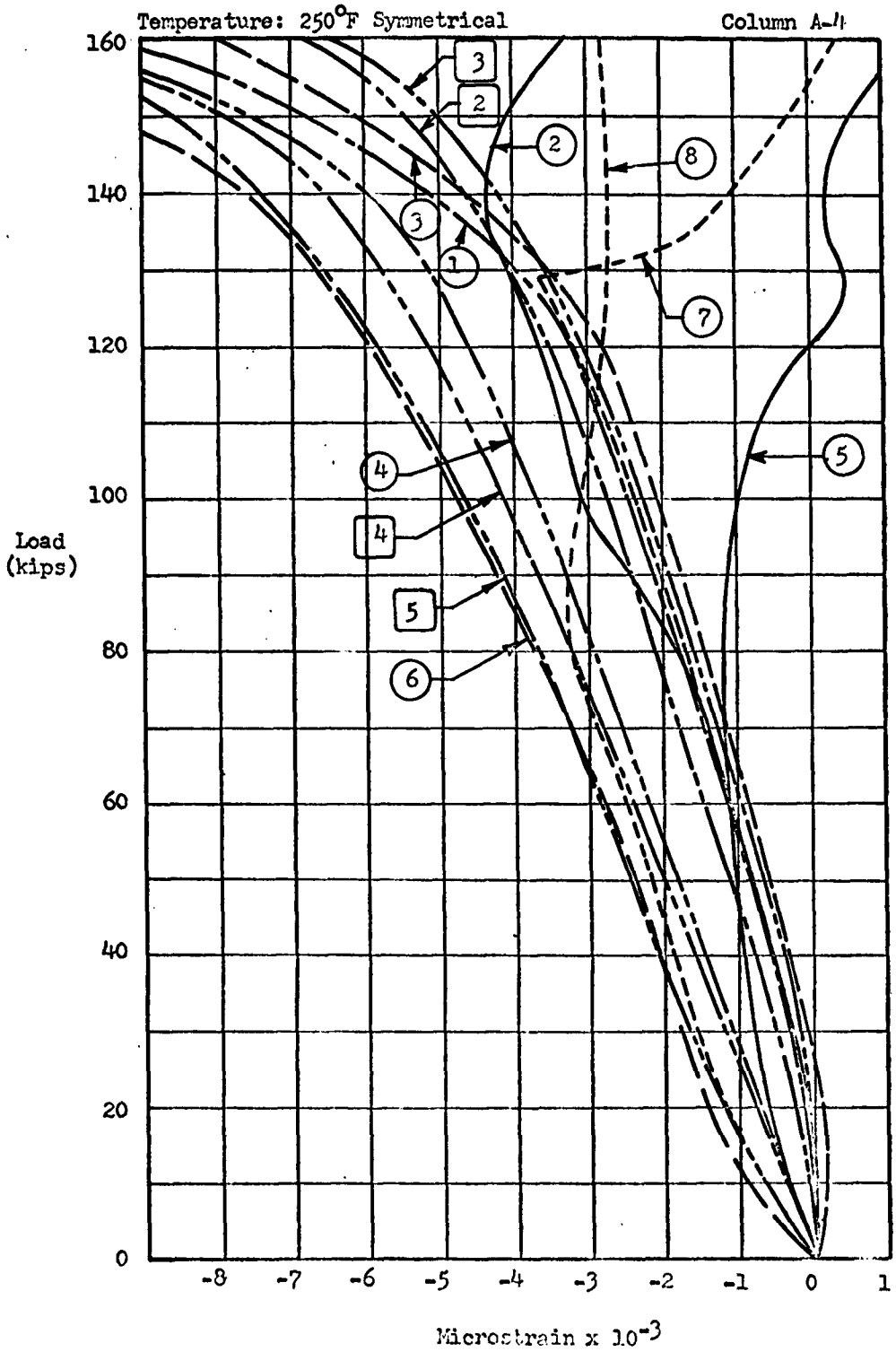

TEST DATA

Figure A.2.13

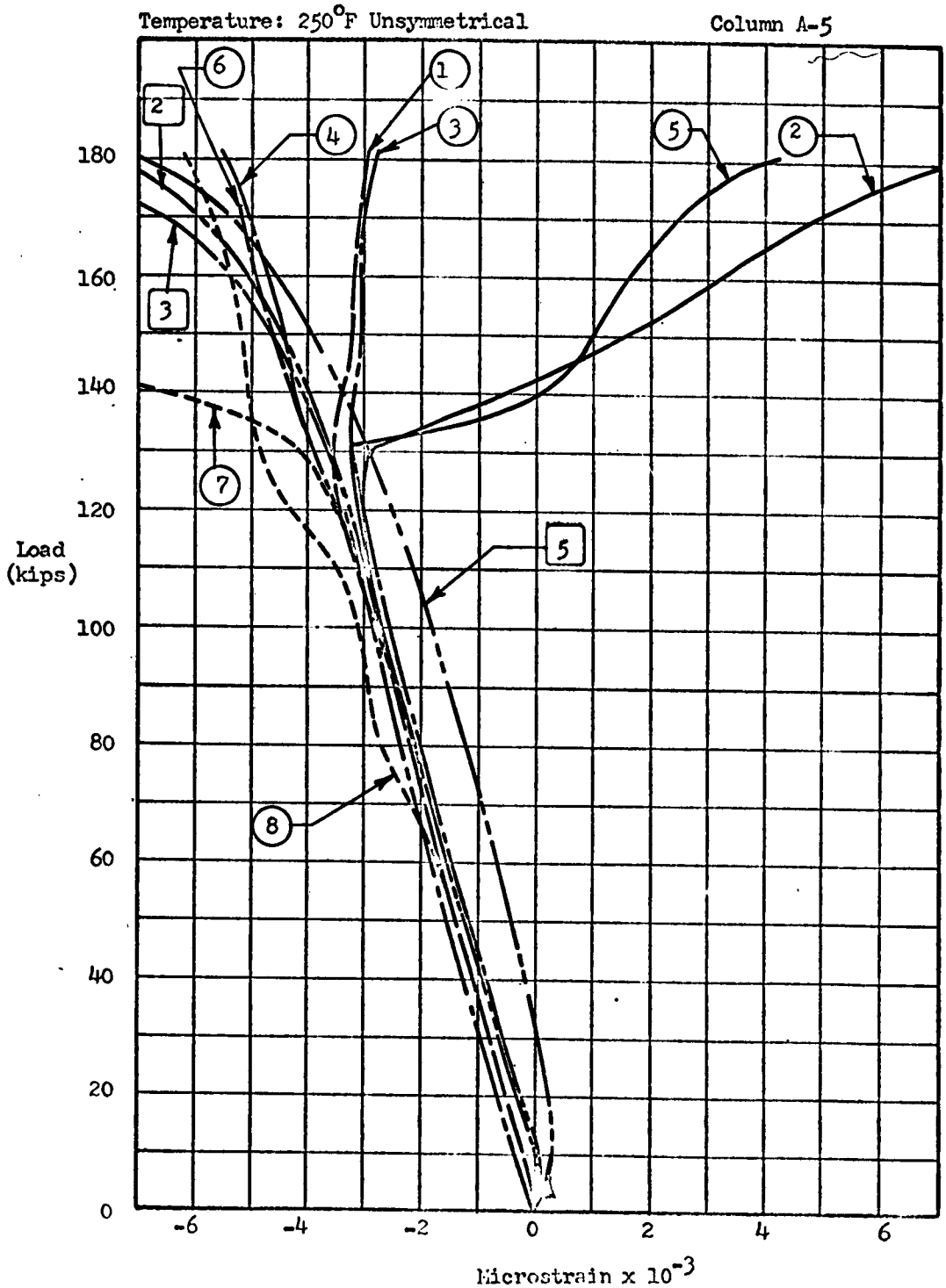

TEST DATA

Figure A.2.14

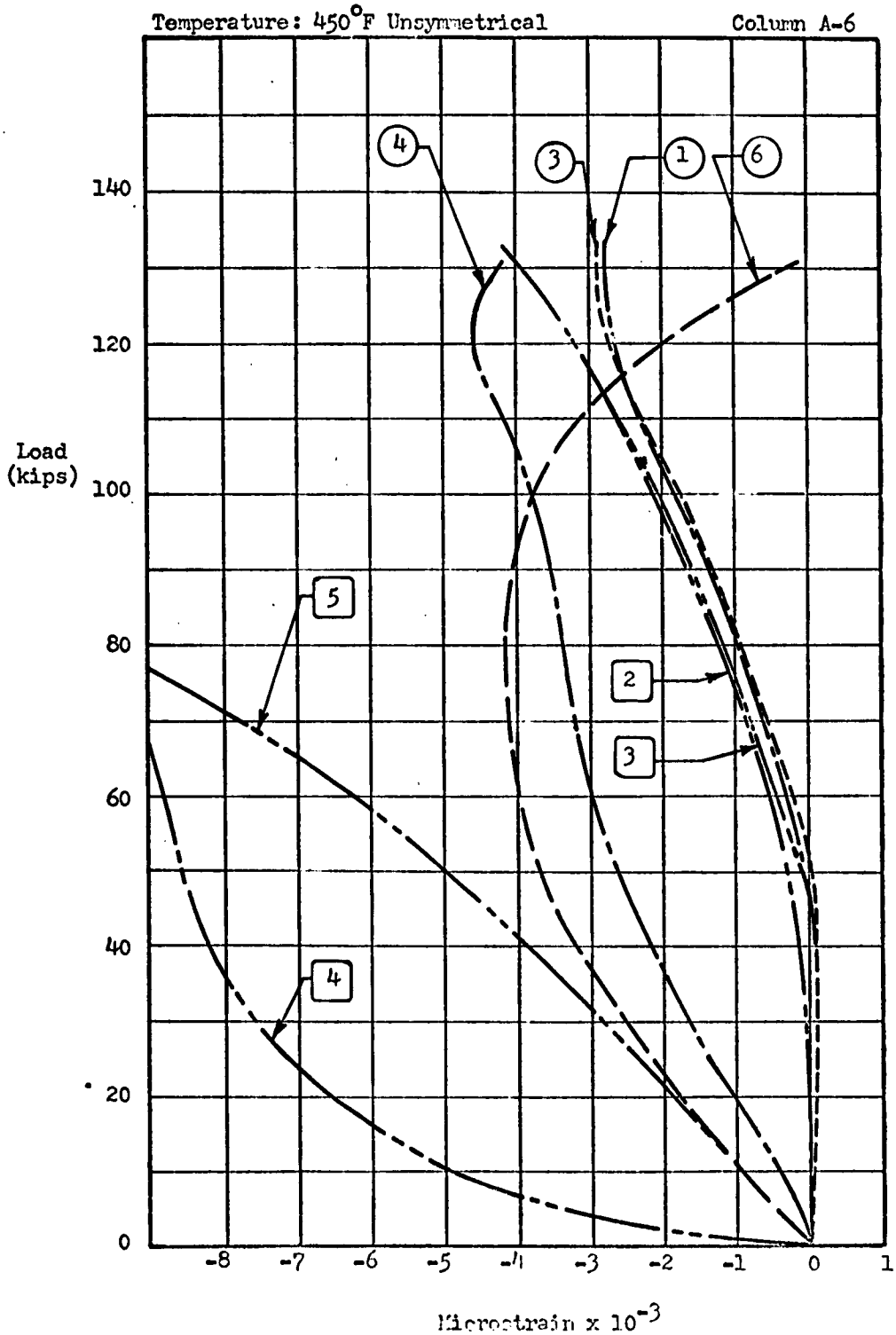

TEST DATA
Figure A.2.15

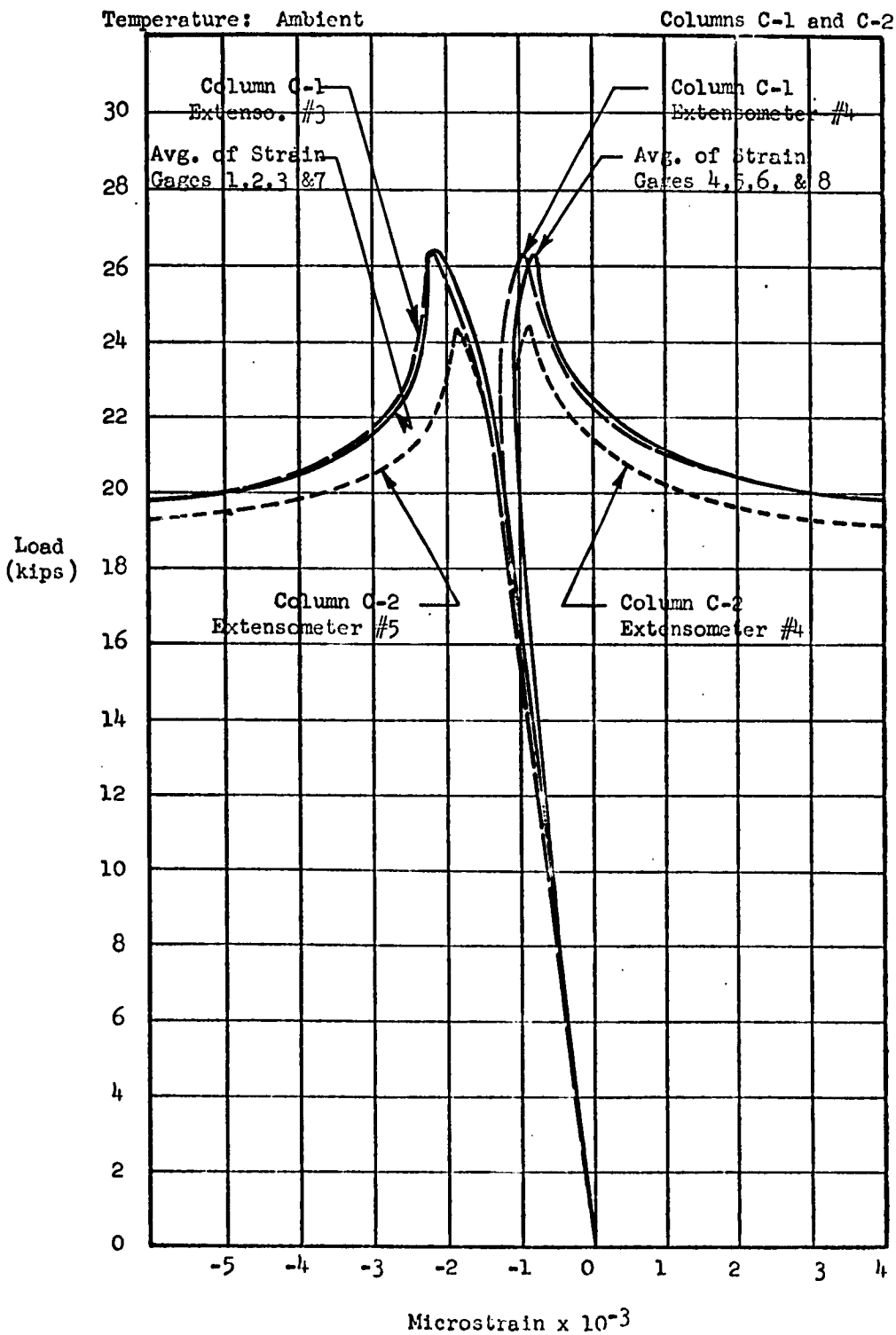

TEST DATA
Figure A.2.16

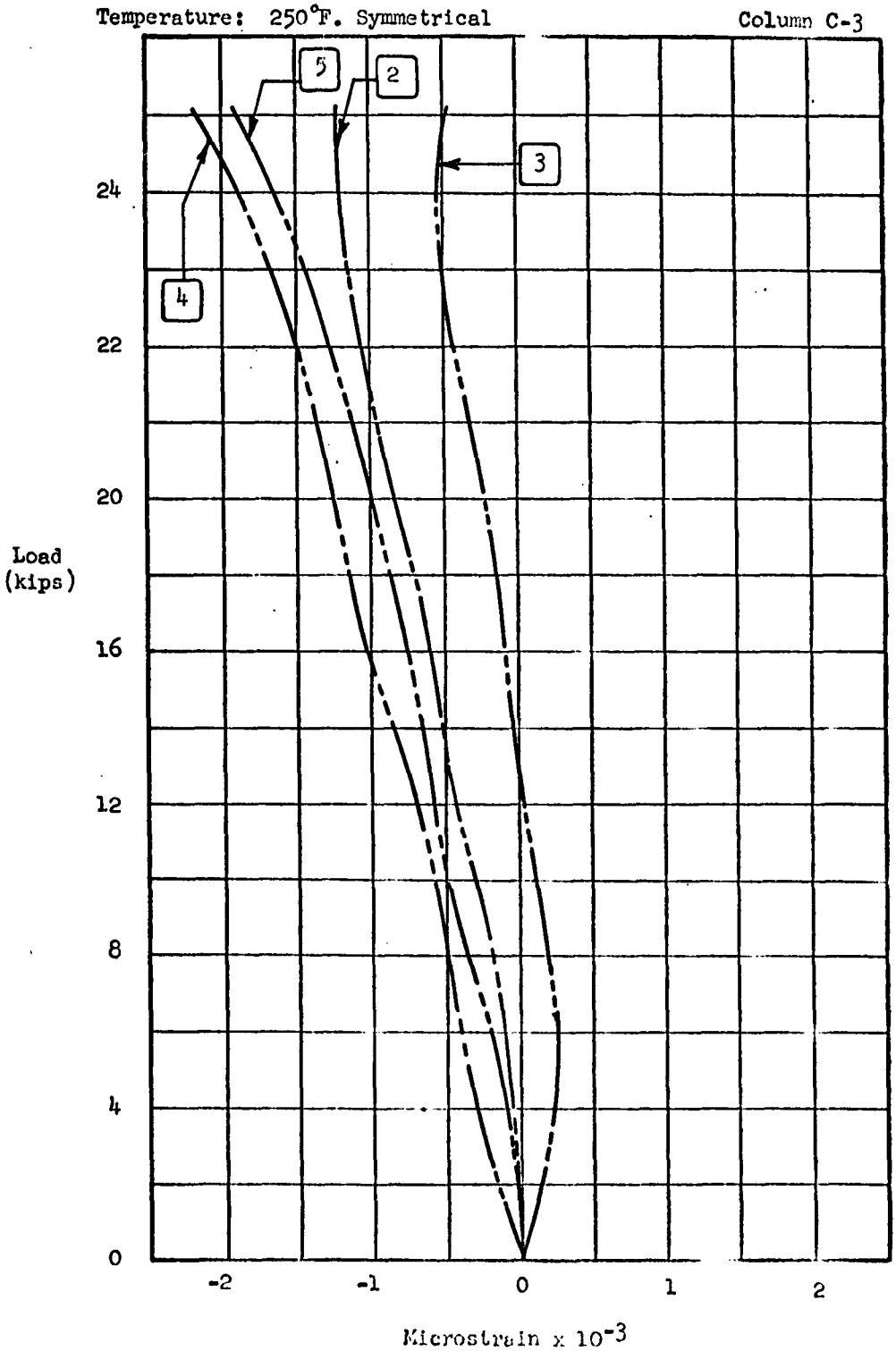

TEST DATA
Figure A.2.17

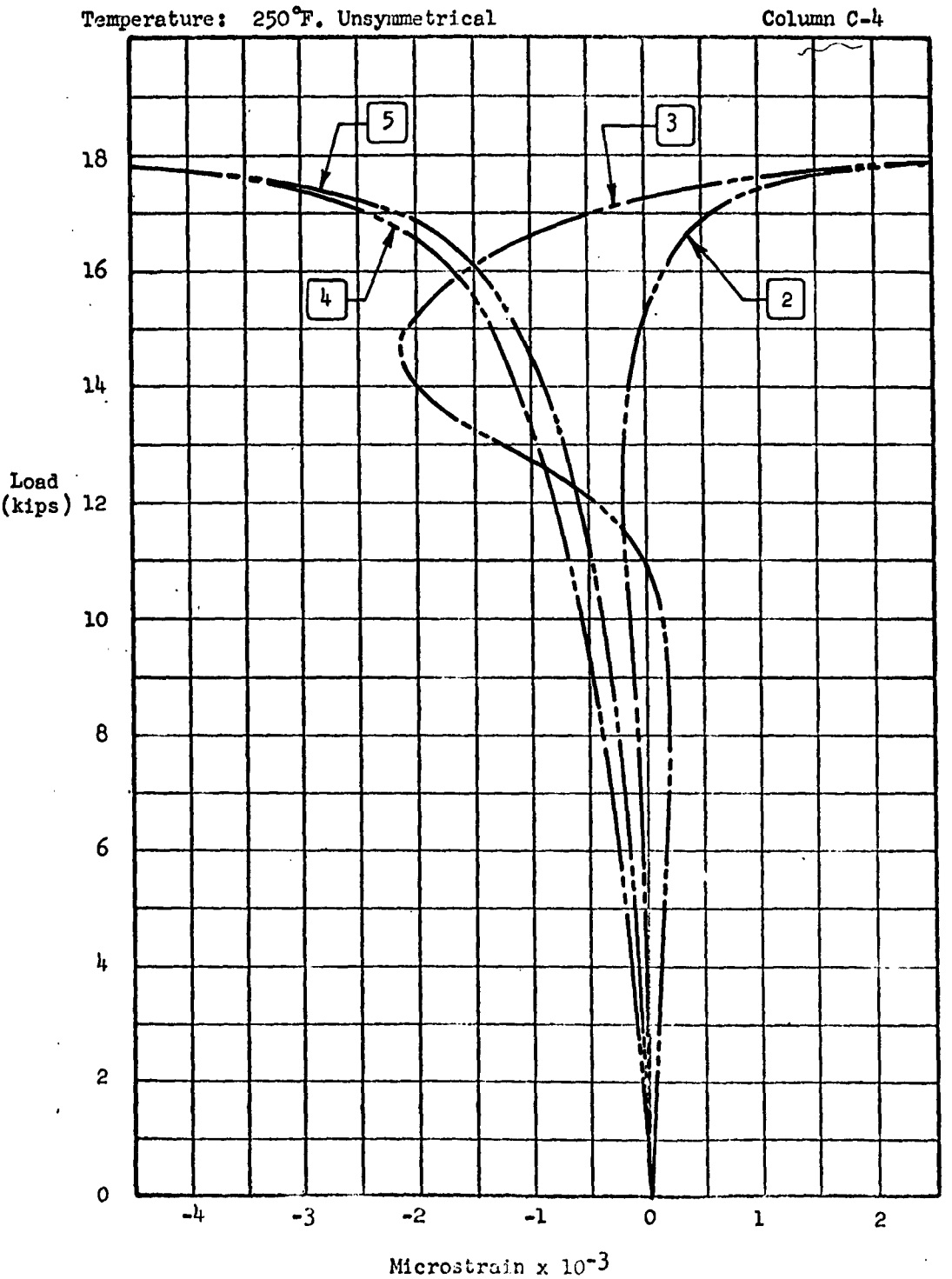

FORM H-10-G-1

TEST DATA
Figure A.2.18

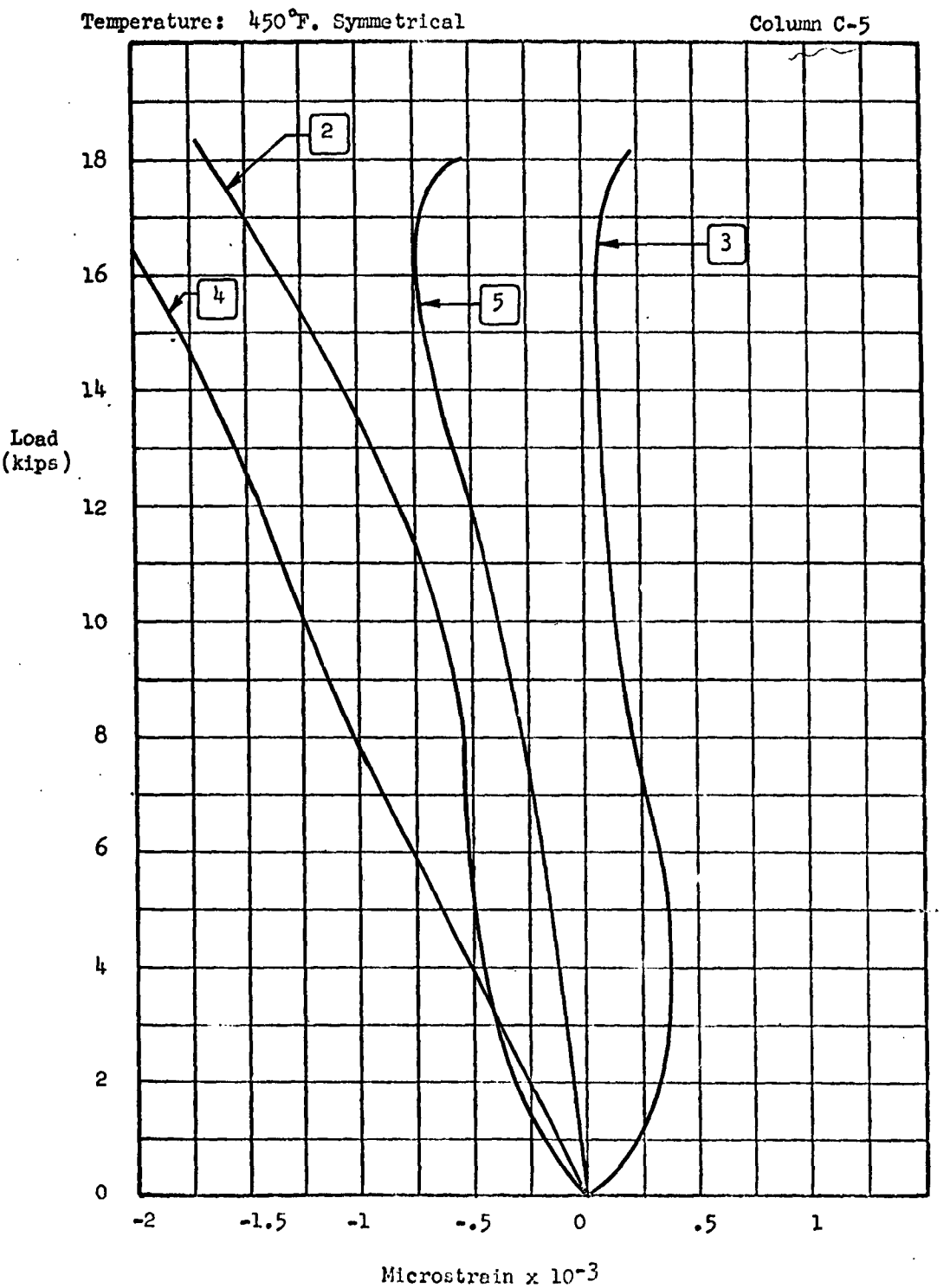

TEST DATA
Figure A.2.19

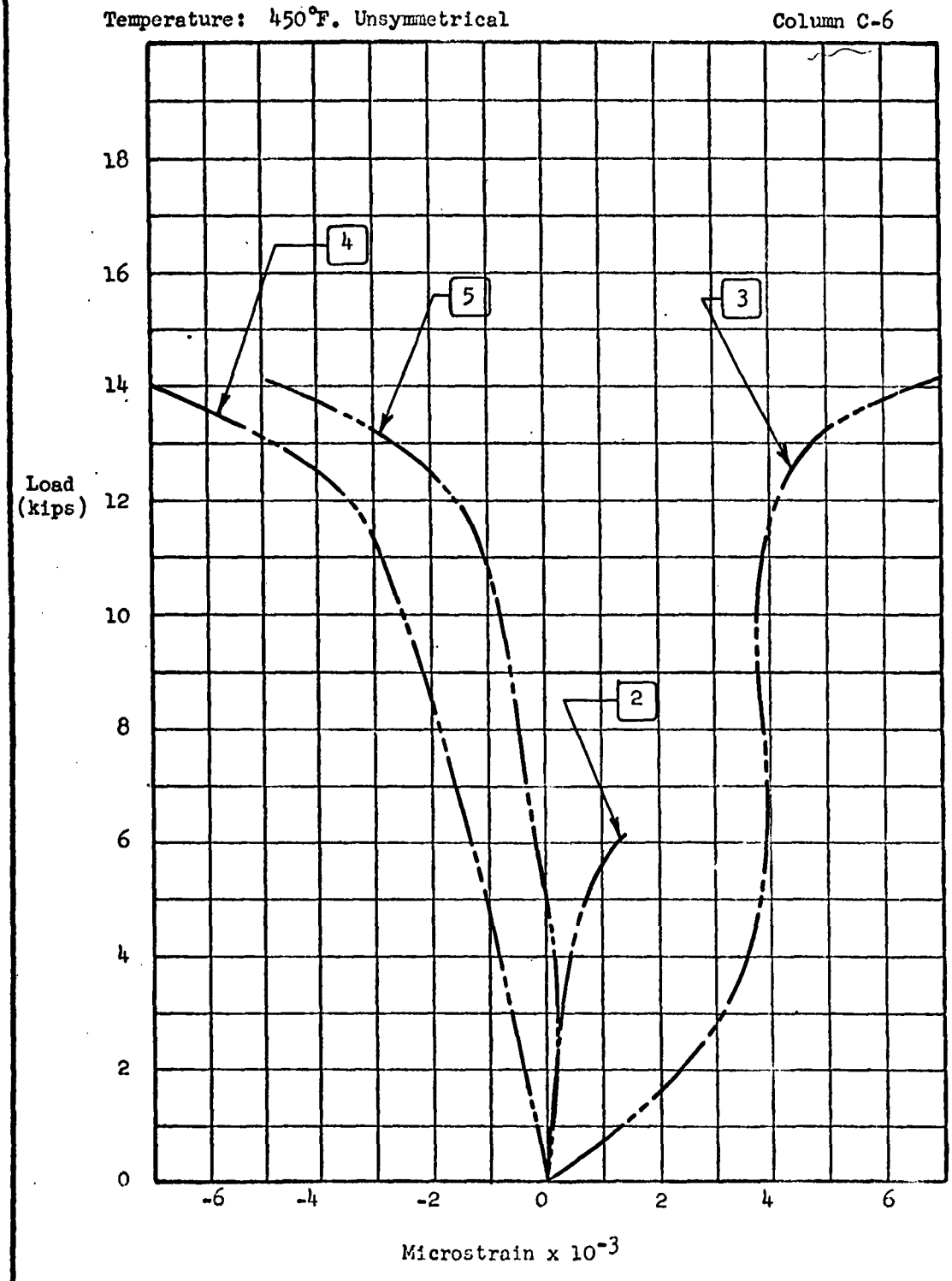

TEST DATA

SPECIMEN B-9

UNSYMMETRICAL HEATING - COMPRESSION COVER HOT

Temperature: 450°F

Heat Cycle	Load (Pounds)	Control Temp. (°F)	MICROSTRAIN				Elapsed Time (Min.)
			Extenso-meter #2	Extenso-meter #3	Extenso-meter #4	Extenso-meter #5	
	2,000	Ambient	-	-	-	-	
	2,000	450	-	-	-	-	
	5,000	450	+ 540	+ 530	- 560	- 620	
	10,000	450	+1,450	+1,510	- 1,550	- 1,570	
	15,000	450	+2,450	+2,480	- 2,760	- 2,830	
	20,000	450	+3,690	+3,480	- 4,740	- 4,440	
	21,000	450	+3,930	+3,600	- 5,470	- 5,280	
	22,000	450	+4,160	+3,790	- 6,080	- 4,290	
	23,000	450	+4,300	+4,050	- 7,000	- 6,500	
	24,000	450	+4,670	+4,240	- 8,160	- 7,150	
	25,000	450	+4,850	+4,430	- 9,000	- 7,880	
	26,000	450	+5,160	+4,630	- 9,960	- 8,380	
1	27,000	450	+5,630	+4,880	-12,380	- 9,760	
	27,000	120	+4,790	+4,170	-13,400	-13,910	70
2	27,000	450	+5,320	+4,660	-13,190	-10,850	
	27,000	120	+4,780	+4,110	-13,980	-14,210	72
3	27,000	450	+5,350	+4,660	-13,670	-11,280	
	27,000	Ambient	+4,310	+3,270	-14,200	-15,450	74
4	27,000	450	+5,320	+4,220	-14,110	-10,040	
	27,000	120	+4,710	+2,930	-14,850	-14,880	76
5	27,000	450	+5,250	+3,660	-14,120	-11,690	
	27,000	100	+4,570	+2,550	-14,910	-15,310	78
6	27,000	450	+5,280	+3,650	-14,470	-11,900	
	27,000	120	+4,710	+2,340	-15,290	-15,200	80
7	27,000	450	+5,390	+3,650	-14,780	-11,930	
	20,000	450	+4,440	+2,810	-13,880	-10,600	
	10,000	450	+2,920	+1,080	-11,420	- 8,500	
	5,000	450	+2,070	+ 180	- 9,990	- 7,250	
	2,000	450	+1,530	- 380	- 8,990	- 6,420	89

TEST DATA

SPECIMEN B-10

UNSYMMETRICAL HEATING - TENSION COVER HOT

Temperature: 450°F

Heat Cycle	Load (Pounds)	Control Temp. (°F)	MICROSTRAIN				Elapsed Time (Min.)
			Extenso-meter #2	Extenso-meter #3	Extenso-meter #4	Extenso-meter #5	
	2,000	Ambient	-	-	-	-	
	2,000	450	-	-	-	-	40
	5,000	450	+ 600	+ 560	- 450	- 940	
	10,000	450	+ 1,590	+ 1,540	-1,210	-1,170	
	15,000	450	+ 2,530	+ 2,740	-1,940	-2,000	
	20,000	450	+ 3,690	+ 4,080	-2,690	-2,750	
	25,000	450	+ 4,960	+ 6,000	-3,770	-3,890	
	26,000	450	+ 5,700	+ 7,110	-4,040	-4,140	
	26,500	450	+ 6,100	+ 7,980	-4,260	-4,420	
	27,000	450	+ 6,600	+ 8,740	-4,420	-4,560	
	28,000	450	+ 7,090	+ 9,690	-4,750	-5,020	
	29,000	450	+ 8,400	+11,320	-5,150	-5,340	
	30,000	450	+ 9,280	+13,071	-5,710	-6,170	
1	31,000	450	+11,770	+16,400	-6,580	-7,100	66
	31,000	95	+ 9,390	+15,670	-6,440	-8,170	
2	31,000	450	+14,380	+19,170	-6,720	-7,760	69
	31,000	120	+10,880	+16,660	-6,850	-8,160	
3	31,000	450	+15,840	+20,620	-7,130	-7,900	71
	31,000	120	+12,110	+18,150	-7,060	-8,440	
	31,000	Ambient	+11,670	+18,280	-6,760	-8,860	
4	31,000	450	+16,680	+21,660	-7,120	-8,170	74
	31,000	120	+13,090	+18,990	-7,190	-8,500	
5	31,000	450	+17,480	+22,720	-7,400	-8,230	77
	31,000	120	+13,920	+20,060	-7,370	-8,710	
6	31,000	450	+18,010	+23,600	-7,470	-8,440	79
	31,000	85	+14,040	+19,540	-7,260	-9,090	
7	31,000	450	+18,300	+24,170	-7,510	-8,590	
	25,000	450	+17,740	+23,280	-6,580	-7,370	
	15,000	450	+15,860	+21,220	-4,530	-5,310	
	5,000	450	+13,760	+19,090	-2,560	-1,890	
	2,000	450	+13,060	+18,280	-2,030	-2,630	86

TEST DATA

SPECIMEN B-11

SYMMETRICAL HEATING

Temperature: 250°F

Heat Cycle	Load (Pounds)	Control Temp. (°F)	MICROSTRAIN Extenso-meter #2	Extenso-meter #3	Extenso-meter #4	Extenso-meter #5	Elapsed Time (Min.)
	2,000	Ambient	-	-	-	-	
	5,000	Ambient	+ 500	+ 560	- 490	- 500	
	10,000	Ambient	+1,350	+ 1,330	- 1,240	- 1,300	
	15,000	Ambient	+2,090	+ 2,150	- 1,930	- 2,070	
	20,000	Ambient	+2,850	+ 3,040	- 2,480	- 2,890	
	25,000	Ambient	+3,630	+ 3,930	- 3,280	- 3,850	
	30,000	Ambient	+4,470	+ 4,880	- 4,190	- 5,110	
	32,000	Ambient	+4,790	+ 5,500	- 4,640	- 5,740	
	34,000	Ambient	+5,400	+ 5,890	- 5,200	- 6,510	
	36,000	Ambient	+5,530	+ 6,400	- 5,820	- 7,470	
	37,000	Ambient	+5,730	+ 6,660	- 6,170	- 8,060	
1	37,000	250	+8,500	+21,180	-10,070	-14,810	2
	37,000	120	+7,110	+ 8,560	-10,980	-16,770	
2	37,000	250	+8,610	+20,900	-10,380	-11,020	4
	37,000	120	+7,190	+ 7,120	-11,180	-16,980	
3	37,000	250	+8,710	+18,510	-10,590	-15,670	5
	37,000	120	+7,280	+ 6,770	-11,420	-17,240	
4	37,000	250	+8,750	+18,790	-10,800	-15,850	6
	37,000	120	+7,330	+ 6,730	-11,620	-17,460	
5	37,000	250	+8,780	+20,760	-10,940	-16,070	7
	2,000	120	+1,660	+ 730	- 5,880	-10,870	
	5,000	Ambient	+ 500	No Reading	- 500	- 640	
	10,000	Ambient	+1,260	+ 1,360	- 1,350	- 270	
	20,000	Ambient	+2,840	+ 3,000	- 3,120	- 3,930	
	30,000	Ambient	+4,400	+ 3,180	- 4,820	- 6,110	
	36,000	Ambient	+5,380	+ 5,600	- 5,810	- 7,450	
	37,000	Ambient	+5,550	+ 5,750	- 5,950	- 7,680	
	38,000	Ambient	+5,720	+ 5,950	- 6,080	- 7,860	
6	38,000	250	+7,620	+22,400	- 5,940	-16,300	8
	38,000	120	+6,160	+ 7,210	- 6,920	- 8,000	
7	38,000	250	+7,660	+18,890	- 6,270	- 5,920	9
	38,000	120	+6,240	+ 5,850	- 7,070	- 8,260	
8	38,000	250	+7,690	+11,180	- 6,400	- 6,940	10
	38,000	120	+6,340	+ 5,610	- 7,210	- 8,540	
9	38,000	250	+7,790	+10,690	- 6,640	- 7,180	11
	38,000	120	+6,310	+ 5,110	- 7,310	- 8,940	
	39,000	120	+6,340	+ 4,750	- 7,340	- 9,090	
10	39,000	250	+7,900	+ 9,350	- 6,790	- 7,830	12
	39,000	120	+6,580	+ 5,180	- 7,810	- 9,370	
11	39,000	250	+8,010	+ 9,470	- 7,330	- 8,340	13
	39,000	120	+6,670	+ 5,050	- 7,950	- 9,970	
12	39,000	250	+8,140	+ 8,650	- 7,520	- 8,810	14
	39,000	120	+6,740	+ 5,000	- 8,340	-10,510	

TEST DATA

SPECIMEN B-11 (Continued)

SYMMETRICAL HEATING

Heat Cycle	Load (Pounds)	Control Temp. (°F)	MICROSTRAIN				Elapsed Time (Min.)
			Extenso-meter #2	Extenso-meter #3	Extenso-meter #4	Extenso-meter #5	
13	39,000	250	+8,210	+ 8,060	- 7,880	- 9,500	16
	39,000	120	+6,810	+ 5,120	- 8,761	-10,970	
14	39,000	250	+8,510	+ 7,360	- 8,370	-10,090	19
	39,000	120	+6,910	+ 4,450	- 9,410	-12,380	
15	39,000	250	+8,370	+ 8,260	- 8,730	-11,120	20
	39,000	120	+6,950	+ 5,080	- 9,480	-12,660	
16	39,000	250	+8,440	+ 8,090	- 8,900	-11,440	21
	39,000	120	+6,960	+ 4,170	- 9,690	-12,920	
17	39,000	250	+8,540	+ 5,880	- 9,390	-11,690	22
	39,000	120	+7,180	+ 280	- 9,970	-13,220	
18	39,000	250	+8,500	+ 3,470	- 9,300	-12,060	23
	39,000	120	+6,970	- 840	-10,030	-13,740	
19	39,000	250	+8,610	+ 2,340	- 9,440	-12,330	24
	39,000	120	+7,120	- 600	-10,280	-13,860	
20	40,000	250	+8,910	+ 4,350	-10,210	-12,980	25
	40,000	120	+7,470	+ 840	-11,500	-14,580	
21	40,000	250	+9,150	+ 3,910	-11,570	-13,410	26
	40,000	120	+7,620	+ 1,290	-12,710	-15,310	
22	40,000	250	+9,060	+ 3,080	-12,670	-14,440	27
	40,000	120	+7,930	+ 1,920	-13,520	-15,580	
23	40,000	250	+9,220	+ 3,740	-13,920	-15,090	28
	40,000	120	+7,900	+ 1,900	-14,510	-16,340	
	5,000	Ambient	+ 470	+ 550	- 490	- 670	
	10,000	Ambient	+1,220	+ 1,360	- 1,390	- 1,830	
	20,000	Ambient	+2,740	+ 3,070	- 3,300	- 4,060	
	30,000	Ambient	+4,280	+ 4,700	- 4,960	- 6,200	
	38,000	Ambient	+5,520	+ 6,040	- 6,230	- 7,980	
	39,000	Ambient	+5,690	+ 6,240	- 6,360	- 8,180	
	40,000	Ambient	+5,870	+ 6,400	- 6,500	- 8,440	
24	40,000	250	+8,210	+13,720	- 5,960	- 7,010	29
	40,000	120	+6,470	+ 7,420	- 6,950	- 8,990	
25	40,000	250	+8,310	+15,200	- 6,300	- 7,730	30
	40,000	120	+6,780	+ 9,780	- 7,160	- 9,340	
26	40,000	250	+8,600	+17,110	- 6,390	- 8,560	32
	40,000	120	+6,920	+ 7,320	- 7,620	-10,000	
27	40,000	250	+8,620	+16,250	- 6,680	- 9,300	33
	40,000	120	+6,990	+ 7,068	- 7,640	-11,850	
28	41,000	250	Failure	Failure	Failure	Failure	

TEST DATA

SPECIMEN B-12

SYMMETRICAL HEATING

Temperature: 450°F

Heat Cycle	Load (Pounds)	Control Temp. (°F)	MICROSTRAIN				Elapsed Time (Min.)
			Extenso-meter #2	Extenso-meter #3	Extenso-meter #4	Extenso-meter #5	
	2,000	Ambient	-	-	-	-	
	2,000	450	+ 4,260	+ 3,890	+ 680	+ 5,440	
	2,000	450	+ 4,370	+ 5,090	+ 530	+ 5,440	30
	5,000	450	+ 4,960	+ 5,630	- 450	+ 5,150	
	10,000	450	+ 6,070	+ 6,660	- 1,290	+ 4,180	
	15,000	450	+ 7,060	+ 7,840	- 2,140	+ 2,960	
	17,000	450	+ 7,660	+ 8,580	- 2,980	+ 2,430	
	18,000	450	+ 7,940	+ 8,950	- 3,530	+ 2,150	
	19,000	450	+ 8,350	+ 9,410	- 3,710	+ 1,830	
	20,000	450	+ 8,640	+10,020	- 4,280	+ 1,130	
	21,000	450	+ 9,010	+10,750	- 5,230	+ 690	
	22,000	450	+ 9,620	+11,260	- 6,220	0	
1	22,500	450	+10,140	+12,030	- 7,200	- 570	61
	22,500	120	+ 6,520		- 8,040	- 5,710	
2	22,500	450	+10,850		- 8,040	- 1,720	63
	22,500	120	+ 6,840		- 9,240	- 6,650	
3	22,500	450	+11,700		- 9,310	- 2,720	66
	22,500	120	+ 7,660		-10,220	- 8,010	
4	22,500	450	+12,480		-11,000	- 4,220	71
	22,500	120	+ 8,370		-11,360	- 9,400	
5	22,500	450	+12,940		-12,260	- 5,010	74
	22,500	120	+ 8,940		-12,670	-10,000	
6	22,500	450	+13,430		-13,320	- 6,010	76
	22,500	120	+ 9,430		-13,740	-11,090	
7	22,500	450	+13,790		-13,900	- 6,980	
	18,000	450	+13,220		-13,670	- 6,080	
	15,000	450	+12,690		-13,290	- 5,190	
	10,000	450	+11,740		-12,120	- 4,030	
	5,000	450	+10,570		-10,720	- 2,820	
	2,000	450	+ 9,860		- 9,840	- 2,030	84

TEST DATA

SPECIMEN B-13

SYMMETRICAL HEATING

Temperature 250°F

Heat Cycle	Load (Pounds)	Control Temp. (°F)	MICROSTRAIN				Elapsed Time (Min.)
			Extenso-meter #2	Extenso-meter #3	Extenso-meter #4	Extenso-meter #5	
	2,000	Ambient	-	-	-	-	
	5,000	Ambient	+ 670	+ 500	- 530	- 370	
	10,000	Ambient	+ 1,660	+ 1,230	- 1,270	- 1,260	
	15,000	Ambient	+ 2,580	+ 1,980	- 2,000	- 1,870	
	20,000	Ambient	+ 3,500	+ 2,810	- 2,930	- 2,720	
	25,000	Ambient	+ 4,500	+ 3,620	- 3,800	- 3,580	
	30,000	Ambient	+ 5,690	+ 4,390	- 5,060	- 4,650	
	31,000	Ambient	+ 5,910	+ 4,540	- 5,340	- 4,880	
	32,000	Ambient	+ 6,200	+ 4,710	- 5,650	- 5,190	
	33,000	Ambient	+ 6,340	+ 4,910	- 6,020	- 5,480	
	34,000	Ambient	+ 6,680	+ 5,120	- 6,410	- 5,790	
	35,000	Ambient	+ 6,990	+ 5,270	- 6,890	- 6,250	
	36,000	Ambient	+ 7,250	+ 5,460	- 7,370	- 6,480	
	37,000	Ambient	+ 7,550	+ 5,670	- 8,110	- 6,880	
	38,000	Ambient	+ 7,870	+ 5,830	- 8,540	- 7,340	
	39,000	Ambient	+ 8,180	+ 6,030	- 9,390	- 7,910	
	40,000	Ambient	+ 8,580	+ 6,280	-10,410	- 8,580	
	41,000	Ambient	+ 8,890	+ 6,520	-11,560	- 9,440	
	42,000	Ambient	+ 9,010	+ 6,730	-12,620	-10,900	
1	35,000	250	-26,760	+13,720	-22,830	-12,860	0

TEST DATA

SPECIMEN B-14

UNSYMMETRICAL HEATING - COMPRESSION COVER HOT

Temperature: 450°F

Heat Cycle	Load (Pounds)	Control Temp. (°F)	MICROSTRAIN				Elapsed Time (Min.)
			Extenso-meter #2	Extenso-meter #3	Extenso-meter #4	Extenso-meter #5	
	2,000	Ambient	-	-	-	-	
	2,000	450	-	-	-	-	
	5,000	450	+ 480	+ 700	- 560	- 530	
	10,000	450	+1,300	+ 1,990	- 1,560	- 1,420	
	15,000	450	+2,100	+ 3,930	- 2,700	- 2,460	
	20,000	450	+2,920	+ 4,920	- 4,230	- 4,030	
	21,000	450	+3,160	+ 5,050	- 4,710	- 4,460	
	22,000	450	+3,380	+ 5,500	- 5,250	- 4,960	
	23,000	450	+3,590	+ 5,790	- 5,880	- 5,490	
	24,000	450	+3,840	+ 6,130	- 6,640	- 6,100	
	25,000	450	+4,040	+ 6,140	- 7,450	- 6,680	
	26,000	450	+4,330	+ 4,320	- 8,720	- 7,470	
	27,000	450	+4,620	+ 3,230	- 9,990	- 8,400	
	27,500	450	+4,790	+ 3,460	-11,110	- 9,400	
	28,000	450	+4,960	+ 3,370	-11,740	- 9,970	
1	28,500	450	+5,110	+ 3,110	-12,490	-10,830	66
	28,500	120	+3,990	+ 1,680	-12,970	-15,150	
2	28,500	450	+4,510	+ 1,540	-12,380	-12,120	69
	28,500	120	+3,940	+ 1,700	-13,520	-15,980	
3	28,500	450	+4,690	+ 1,540	-12,830	-12,760	71
	28,500	120	+4,040	+ 1,680	-14,160	-16,380	
4	28,500	450	+4,480	+ 1,540	-13,110	-13,160	73
	28,500	Ambient	+3,590	+ 1,960	-13,920	-17,560	
5	28,500	450	+4,440	+ 1,650	-13,280	-13,550	75
	28,500	120	+4,030	+ 1,890	-14,770	-16,980	
6	28,500	450	+4,980	+ 1,630	-14,510	-14,050	78
	28,500	120	+4,270	+ 1,800	-15,710	-16,130	
7	28,500	450	+4,950	+ 1,650	-15,050	-14,510	
	20,000	450	+3,800	+ 170	-14,510	-12,880	
	10,000	450	+3,520	- 1,220	-12,800	-10,470	
	5,000	450	+1,290	- 1,800	-11,560	- 9,190	
	2,000	450	+ 720	- 2,520	-10,620	- 8,260	88

TEST DATA

SPECIMEN B-15

UNSYMMETRICAL HEATING - - TENSION COVER HOT

Temperature 450°F

Heat Cycle	Load (Pounds)	Control Temp. (°F)	MICROSTRAIN				Elapsed Time (Min.)
			Extenso-meter #2	Extenso-meter #3	Extenso-meter #4	Extenso-meter #5	
	2,000	Ambient	-	-	-	-	
	2,000	450	-	-	-	-	
	5,000	450	+ 670	+ 560	- 530	- 500	
	10,000	450	+ 1,630	+ 1,680	-1,360	-1,330	
	15,000	450	+ 2,550	+ 2,830	-2,280	-2,230	
	20,000	450	+ 4,110	+ 4,010	-3,140	-3,050	
	25,000	450	+ 6,270	+ 5,910	-4,360	-4,210	
	26,000	450	+ 7,920	+ 6,700	-4,810	-4,470	
	27,000	450	+ 8,960	+ 7,740	-5,290	-4,890	
	28,000	450	+11,020	+ 8,980	-5,650	-5,170	
1	28,000	450	+14,210	+11,140	-6,060	-5,650	66
	28,000	120	+ 9,920	+ 9,310	-5,720	-6,770	
2	28,000	450	+15,060	+12,020	-6,050	-6,080	69
	28,000	120	+10,620	+ 9,650	-5,880	-6,800	
	28,000	Ambient	+ 9,810	+10,420	-5,770	-7,370	
3	28,000	450	+15,620	+12,090	-6,090	-6,200	71
	28,000	80	+10,840	+10,100	-5,940	-7,210	
4	28,000	450	+16,310	+12,380	-6,230	-6,110	74
	28,000	95	+11,920	+10,210	-6,060	-7,080	
5	28,000	450	+17,050	+12,810	-6,290	-6,110	77
	28,000	115	+12,650	+10,560	-6,170	-7,100	
6	28,000	450	+17,620	+13,110	-6,300	-6,220	79
	28,000	110	+13,010	+11,120	-6,160	-7,250	
7	28,000	450	+18,160	+13,450	-6,360	-6,250	
	20,000	450	+16,880	+11,820	-4,810	-4,680	
	10,000	450	+14,720	+ 9,540	-2,790	-2,620	
	5,000	450	+13,650	+ 8,400	-1,830	-1,650	
	2,000	450	+12,810	+ 7,570	-1,270	-1,090	89

TEST DATA

SPECIMEN B-16

SYMMETRICAL HEATING

Temperature: 450°F

Heat Cycle	Load (Pounds)	Control Temp. (°F)	MICROSTRAIN Extenso-meter #2	Extenso-meter #3	Extenso-meter #4	Extenso-meter #5	Elapsed Time (Min.)
	2,000	Ambient	-	-	-	-	
	5,000	Ambient	- 340	- 450	+ 510	+ 520	
	10,000	Ambient	-1,010	-1,150	+ 1,320	+ 1,230	
	12,000	Ambient	-1,330	-1 430	+ 1,630	+ 1,550	
	14,000	Ambient	-1,630	-1,710	+ 1,930	+ 1,830	
	15,500	Ambient	-1,840	-1,960	+ 2,170	+ 2,020	
1	15,500	450	+1,190		+ 3,990	+ 9,940	6
	15,500	120	-3,040		+ 2,840	+ 3,160	
2	15,500	450	+ 310		+ 3,990	+ 9,140	12
	15,500	120	-3,040		+ 2,840	+ 3,360	
3	15,500	450	+ 60		+ 4,160	+ 9,490	18
	15,500	120	-3,040		+ 2,840	+ 3,720	
4	15,500	450	+ 160		+ 4,290	+ 9,240	24
	15,500	120	-3,040		+ 2,870	+ 3,690	
5	15,500	450	+ 60		+ 4,160	+ 9,560	30
	15,500	120	-3,150		+ 2,980	+ 3,690	
6	15,500	450	- 60		+ 4,230	+ 9,700	36
	15,500	120	-3,090		+ 2,980	+ 3,834	
7	15,500	450	- 110		+ 4,280	+ 9,560	
	2,000	450	+2,890		+ 1,410	+ 7,130	45
	5,000	450	- 440		+ 600	+ 530	
	10,000	450	-1,180		+ 1,550	+ 1,470	
	15,500	450	-2,280		+ 2,570	+ 2,550	
	16,000	450	-2,410		+ 2,780	+ 2,760	
8	16,500	450	-2,370		+ 2,910	+ 2,860	57
	16,500	120	-5,660		+ 1,880	- 3,050	
9	16,500	450	-2,280		+ 3,090	+ 3,290	63
	16,500	120	-5,790		+ 1,970	- 2,580	
10	16,500	450	-2,430		+ 3,180	+ 3,290	69
	16,500	120	-5,820		+ 1,970	- 670	
11	16,500	450	-2,570		+ 3,250	+ 3,480	
	17,000	450	-2,680		+ 3,380	+ 3,620	
	17,500	450	-2,820		+ 3,490	+ 3,730	
	2,000	450	- 130		+ 250	+ 690	81
	5,000	450	- 410		+ 550	+ 540	
	10,000	450	-1,250		+ 1,410	+ 1,570	
	15,000	450	-2,160		+ 2,590	+ 2,590	
	17,500	450	-2,840		+ 3,280	+ 3,320	
12	18,000	450	-3,110		+ 3,380	+ 3,450	94
	18,000	120	-6,670		+ 2,150	+ 2,380	
13	18,000	450	-3,460		+ 3,600	+ 3,430	100
	18,000	120	-6,980		+ 2,350	- 2,680	

TEST DATA

SPECIMEN B-16 (Continued)

SYMMETRICAL HEATING

Heat Cycle	Load (Pounds)	Control Temp. (°F)	MICROSTRAIN				Elapsed Time (Min.)
			Extenso-meter #2	Extenso-meter #3	Extenso-meter #4	Extenso-meter #5	
14	18,000	450	-3,550		+3,660	+ 3,690	106
	18,000	120	-7,060		+2,390	- 2,150	
15	18,000	450	-3,660		+3,760	+ 3,690	112
	18,000	120	-7,190		+2,500	- 2,150	
	18,000	450	-3,670		+3,860	+ 3,590	
	18,500	450	-4,000		+3,920	+ 3,730	
16	19,000	450	-4,010		+4,040	+ 4,030	120
	19,000	120	-7,420		+2,810	- 1,570	
17	19,000	450	-4,230		+4,360	+ 4,290	126
	19,000	120	-7,670		+3,000	- 1,390	
18	19,000	450	-4,540		+4,530	+ 4,340	132
	19,000	120	-7,840		+3,190	- 1,120	
19	19,000	450	-4,540		+4,630	+ 4,420	
	2,000	450	-1,300		+ 700	+ 1,520	141

APPENDIX B

PHOTOGRAPHS

Figure B.1

Extensometer and Calibration Jig

Figure B.2

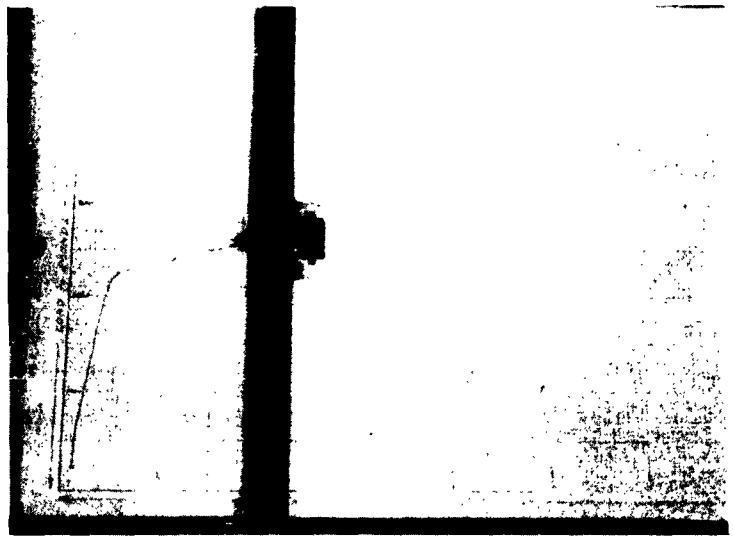

X-Y Plotter Showing Load-Strain
Curve for Typical Tension Coupon

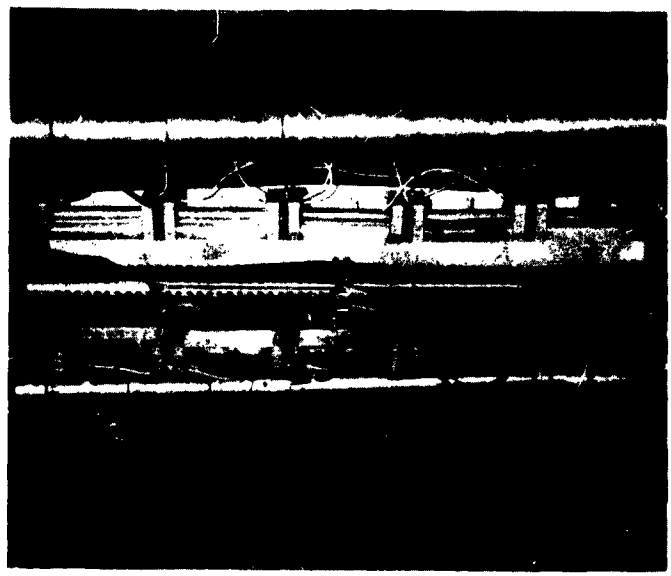

Figure B.4 Typical Test Setup For Long Column Elevated Temperature Test

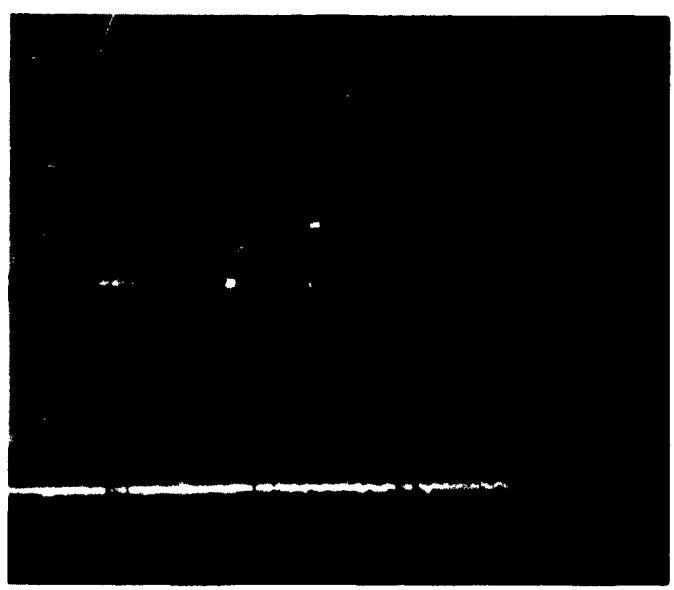

Figure B.3 Typical Test Setup For Tension Coupon Test at Ambient Temperature

Figure B.5

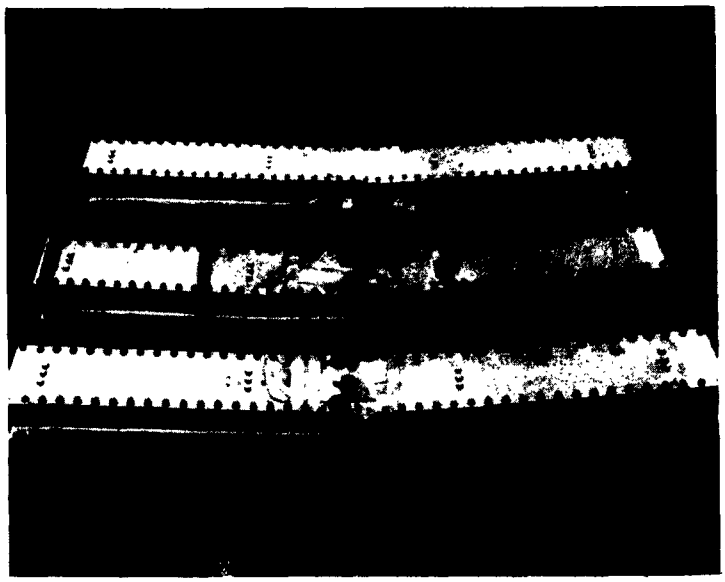

Three Bending Beams Loaded to Failure
at Elevated Temperature

Figure B.6

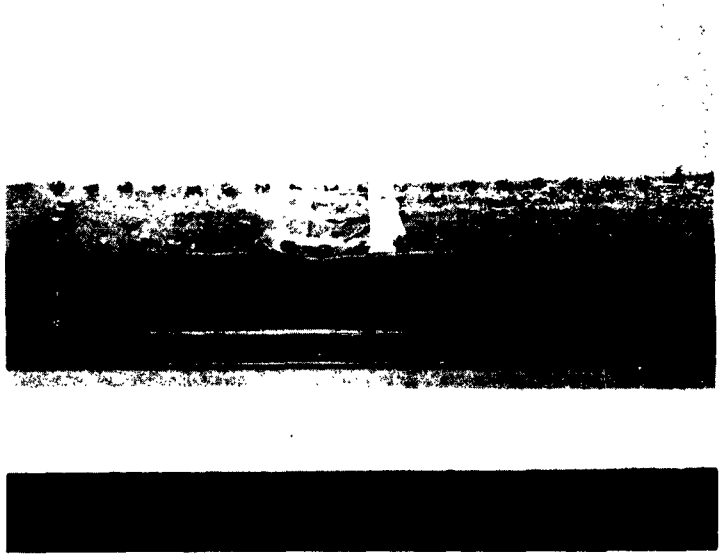

Typical Crippling Failure of Bending
Beam at Ambient Temperature

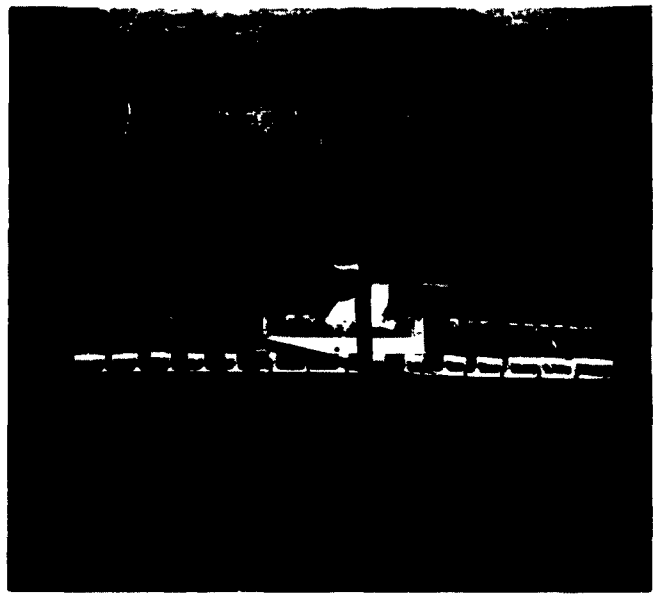

Figure B.8 Typical Setup of Bending Beam During Elevated Temperature Test

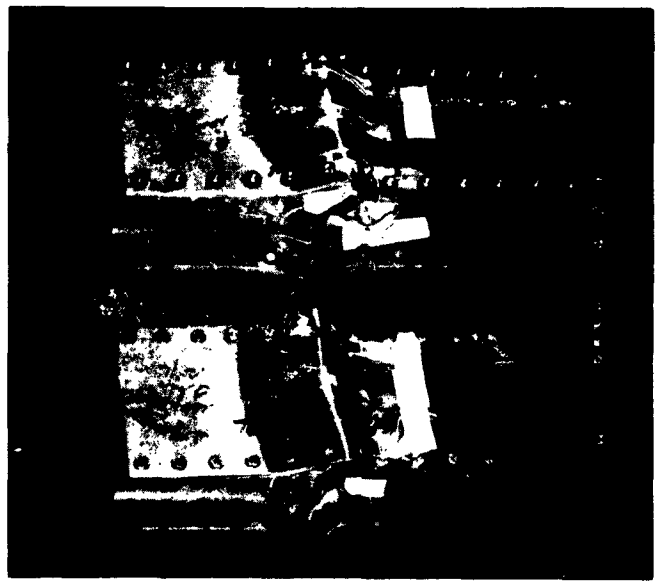

Figure B.7 Short Columns After Failure at Ambient Temperature

UNCLASSIFIED